What controls the reservoir quality of andesitic arc derived volcano clastic sandstone reservoirs: An example from the Mohakatino Formation, Taranaki Basin, New Zealand

GEORGE RUPERT MAGUIRE LODWICK

What controls the reservoir quality of andesitic arc derived volcaniclastic sandstone reservoirs: An example from the Mohakatino Formation, Taranaki Basin, New Zealand

George R. M. Lodwick

Thesis presented for the degree of Master of Science by Research

Under the supervision of Dr Stuart Jones, Dr Peter Kamp and Prof. Jon Gluyas

Department of Earth Sciences

Durham University

2016-2018

Abstract

The mid-Miocene Mohakatino Formation of the Taranaki Basin, New Zealand, is a submarine fan succession sourced dominantly from an offshore, submarine andesitic arc. It is composed of volcaniclastic sandstones, siltstones and mudstones, characterised by a prominent andesitic detritus. The Mohakatino Formation acts as the reservoir rock for the sub-commercial, tight oil producing Kora Field in the Northern Taranaki Basin, New Zealand. This formed due to a combination of proximal tuffs on the flanks of the Kora Volcano and sector collapse of the eastern flank of the volcano within the Mohakatino Volcanic Centre off the west coast of the North Island, and this mass wasting material was deposited distally along the present day Awakino coastline.

The hydrocarbons present in the Kora Field are the product of the thermal maturation of the Late Paleocene Waipawa Formation kerogen, and matured by the residual heat of the Kora volcano. While the Mohakatino Formation does not have significant quantities of hydrocarbons present, the sandstones do have high porosity and permeability with potential that the Mohakatino Formation could have acted as commercially viable reservoir rock in the proximal regions to the Kora volcano. In the medial to distal reaches of the submarine fan systems the reservoir quality for the Mohakatino Formation is of poorer quality and is controlled by sedimentary processes and breakdown of the more volatile and friable components of the andesitic volcaniclastics due to transportation process of the submarine high density turbidity currents.

The reservoir quality is preserved in these proximal regions by early stage authigenic clay precipitation from the breakdown of volcanic and hypabyssal rock fragments which prevented quartz overgrowths and later stage pore filling clay formation. Pore filling calcite that forms in shallow marine rocks was prevented from precipitating by the acidic nature of the proximal rocks, preserving the reservoir quality. Furthermore, rapid burial of the proximal Mohakatino Formation by ~2 km over ~2 Ma by the Giant Foresets Formation contributed to sealing the pore network to create a closed system, occluding the porosity, and which allowed for the reactive materials to be broken down and the resulting authigenic minerals to be retained in the rock. While these factors combined preserved some of the reservoir quality, relative to typical clastic sandstone reservoirs the reservoir quality is still low. The proximal deposits are found to have relatively coarser grain sizes due to their increased weight and density causing them to fall out of water column and be deposited first, and together combined to give relatively good primary porosity. The turbidity currents and tuffs at their furthest extent had lost the majority of their energy and coarsest material, and so when they reached what is now the now Awakino Coastline the deposited material was of a relatively fine grainsize and better sorted than that of proximal. These combined features led to reduced primary porosity and therefore a decreased reservoir quality of the distal Mohakatino Formation rocks from their inception, and is therefore a key control on the potential for these rocks to act as a reservoir.

Table of Contents

List of Figures

Chapter 1

Chapter 2

Chapter 3

Chapter 4

Chapter 5

List of Tables

Chapter 1

Chapter 3

Chapter 4

Glossary of Terms

ϕ: Porosity

BOPD: Barrels of oil per day

BSE: Backscattered electrons

CALI: Calliper reading

CEPL: Porosity loss by cementation

COPL: Porosity loss by compaction

EDX: Energy dispersive x-ray detector

EMB: Eastern mobile belt

GR: Gamma ray log

HRF: Hypabyssal rock fragments

IGV: Intergranular volume

Lf: Lithofacies

MTZ: Median transition zone

MVC: Mohakatino volcanic centre

NPHT: Neutron log

RHOB: Bulk density log

SEM: Scanning electron microscope

SWC: Sidewall coring

TCF: Trillions of cubic feet

WSP: Western stable platform

XRD: X-ray defraction

Acknowledgements

This thesis would not have been possible without the support and guidance of many people in my life who, to various degrees, were invested in this project.

Firstly, I must acknowledge the supervisors I have had for this project, Dr Stuart Jones, Dr Peter Kamp, Dr Jon Gluyas and Dr Adrien Pittari. While having not only provided their world class knowledge and expertise on the subject matter for this project, the time they gave me and their unending patience was more than generous and this combined support gave me the energy and direction I needed to successfully conclude this project. I must additionally thank Dr Stuart Jones as he had the misfortune for me to be given a desk in front of his office allowing me to query him at any time of day. Stuart proved to be an invaluable asset for this project, and there is no doubt that without his expertise as both an academic and a teacher I would have failed, and I will always be indebted to you for your help.

The University of Durham and the Department of Earth Sciences has been my home for four years and provided me with the finest teaching, training and experience I could have ever asked for. Without the outstanding staff, facilities and equipment provided by the university and the department then this project may have not been possible, so thank you for this opportunity.

Due to the travel aspect of this project, financial contributions were key to helping this project succeed. Dr Stuart Jones and University College, Durham must be thanked for their financial support that helped meet some of the costs towards the fieldwork portion of the project, and also Chevron for sponsoring my place at the at the AAPG Asia-Pacific GTW in Oamaru. The opportunity to do this was one of the highlights of my academic career, and so the AAPG must be acknowledged and thanked for the interest they took in this project and my work.

During the year that I worked on this project there were a number of dizzying highs and crushing lows and through all of these moments I was surrounded by my friends who celebrated with me and helped me past the difficult times. In particular, I must say a big thank you to Emily Power: your support and affection was the only thing that kept me sane at times and this work would have never been possible without you. Those of you from the department, thank you for keeping me focused and motivated with tea and support during the long hours at the desks. My housemates Cat, Kit and Sarah, you're all troopers for having listened to my nonsense for so long, along with your support, dinners and bad TV, you have been a great help throughout these years.

I must finally acknowledge the incredible and unwavering support of my family, Jeremy, Anne and Ted, who helped me think through the problems and keep things in perspective when I felt I was in too deep. The belief they have in me was all I needed to get me through this project and all I will ever need in to the future.

Chapter 1

Introduction

1.1 Research Rational

The Taranaki Basin is currently the only sedimentary basin in New Zealand with active hydrocarbon production, with the majority of the petroleum reserves constrained to a few large fields (e.g. Maui, Kupe, and Pohokura) and the remainder in small fields. One of these smaller fields is the Kora Field and the reservoir rocks here are comprised of the mid-Miocene Mohakatino Formation, a series of sandstones and siltstones characterised by a prominent andesitic detritus deposited on the flanks of the Kora volcano, part of an offshore, submarine andesitic arc. Sub-commercial oil discoveries in the Kora-1 well that penetrates the Mohakatino Formation has highlighted the potential of volcaniclastic reservoirs. Prior studies (Bergman et al., 1992; Thrasher et al., 2002; Schumaker et al 2014) have highlighted the potential for significant accumulations of hydrocarbons within the Northern Graben, northern Taranaki Basin, and with the most prospective reservoirs considered to be the more deeply buried Mohakatino Formation along the axis of the graben.

1.2 Aim of Study

The aim of this research is to document the spatial and temporal variability of reservoir quality of the Miocene volcaniclastic Mohakatino Formation. This research will focus solely on the Mohakatino Formation comprising gravel, sandstone and mudstone derived from the submerged chain of stratovolcanoes (ca. 15-6.5Ma) of the Kora andesitic volcano in the Northern Graben. The foraminiferal assemblages within the Mohakatino Formation suggest deposition occurred in the lower bathyal water depths (>1500m) with depositional facies composed of both sediment gravity flow deposits and suspension sedimentation of volcanic debris through the water column within a basin floor fan or fan apron (e.g. King et al., 1993; 2011). The variation in facies is critical to the understanding of the potential reservoir quality combined with the difference between proximal deposits near the Kora volcano to those located more distally and known as the North Awakino mass-transport deposits exposed long the North Taranaki coastline.

Specific objectives to be completed during this research include:

1. To identify the occurrence and distribution of cement types and their influence on porosity and permeability within the Mohakatino Formation.
2. To determine the spatial distribution of grain size values and their correlation with porosity and cementation for the mass transport, sediment gravity flows and basin floor fan deposits.

3. To investigate the facies control on reservoir quality of volcaniclastic samples. Is there a change in reservoir quality during the proximal to distal transition?

In order to investigate these lithological and diagenetic features, various analytical and field techniques were undertaken.

1.3 Focus of Study

The Northern Graben of the Taranaki Basin has a different geological history from the rest of the surrounding basin and has been largely under explored, especially along the deeper portion of the basin axis. Volcanism has formed a major contributing component of the development of the Northern Graben from the Miocene to Recent (Ballance, 1976; Bergman, et al., 1992; Giba et al., 2010; 2013). The volcanism within the Northern Graben is correlated with the initiation of extension both in location and in timing (Giba, et al., 2010; 2013). The volcanic structures in the Northern Graben formed because of the westward subducting Pacific Plate underneath the Australian Plate (Bergman, et al., 1992; King & Thrasher, 1996; Seebeck, et al., 2014). The volcanic features within the Northern Graben are mainly comprised of submarine, strata volcanoes and are referred to as the Mohakatino Volcanic Centre (MVC) (King & Thrasher, 1996), and it is thought this volcanic centre was produced through back arc processes within the Northern Graben (King, 1990; Bergman, et al., 1992). From the Kora wells (Kora-1A, 2, 3, 4), Bergman, et al., (1992), have shown that the andesites of Kora are normal calc-alkalic indicative of intra-arc basin processes, and this can also be assumed for the rest of the Mohakatino Volcanic Centre. This has been interpreted to mean that more than one arc may have been present during this time (Balance, 1975; King & Thrasher, 1996. Perhaps most significantly is the sub-economic oil discovery in the Kora-1/1A well which was drilled into the flanks of the Miocene andesitic Kora volcano, originally targeting the Eocene Tangaroa Formation sandstones within the large dome structure associated with the volcano (GNS PBE, 2013). Drill stem tests of the Tangaroa Formation produced small quantities of oil, but during this investigation of the Tangaroa Formation significant hydrocarbon indications were encountered in the upper region of the Miocene volcaniclastics of the Mohakatino Formation which flowed 1,168 bopd on test, resulting in the plugging of Kora-1 well and the Kora-1A side-track being drilled into the Mohakatino Formation to evaluate potential (GNS PBE, 2013). Long term production produced an average flow rate of 668 bopd in 1988 and eventually the formation was concluded to have poor reservoir quality due to the formation being tight and thermally altered. The Mohakatino Formation has therefore proven its significance as a potential reservoir in the northern Taranaki Basin.

While volcanism is normally considered to be detrimental to hydrocarbon generation it appears in the Northern Graben to have a positive impact, forcing maturation and directing migration as well as controlling the deposition of the reservoir rocks. The Miocene Mohakatino Formation is an example

of this as it is a direct result of sector collapse of the submarine Kora volcano to the east/southeast depositing blankets of pyroclastic material on the volcano's flanks (Shumaker, 2016). The volcanism can also have an influence on the diagenesis of the rocks derived from the volcanic material, with reactive volcanic rock fragments breaking down to produce pore filling or grain lining cements and clays that can have positive or negative influences on the reservoir quality (Berger et al, 2001).

1.4 Wider Rational

1.4.1 Global Energy Trend

In 2009 the Organisation of the Petroleum Exporting Countries (OPEC) and the International Energy Agency (IEA) forecast that by 2030 the total demand for fossil fuels worldwide will have increased to between 42% and 45% over the 2007 levels respectively (Zou, 2013). In recent years the hydrocarbon industry has started exploring for more unconventional sources as many of the conventional hydrocarbon reserves reach the mid-stage of their development where production is beginning to peak. In some regions of the world the scale of the investment, exploration, and production has led to such a radical change in the regional economy the shift is being characterised as an energy revolution (Dreyer & Stang, 2013). This term is used in this context after seeing the affects that the shale gas boom had in the United States since 2007. Between 2007 and 2011, natural gas imports to the US decreased from 16.5% to 11%, the primary natural gas consumption increased to 26% from 11%, the US energy mix accelerated the long term trend towards gas and renewables primarily replacing oil and coal, and in 2012 the US achieved its lowest CO_2 emissions in 20 years (Dreyer & Stang, 2013). Unconventional gas now accounts for around 50% of the total gas production in the USA (Zou, 2013). This trend and its impact on the business climate in the United States is used as an indication of how regionally sourced unconventionals can revitalise and restructure a national energy economy while also meeting targets for environmental sustainability. In Figure 1.1 the development of unconventional petroleum resources in the United States has clearly changed the US domestic market.

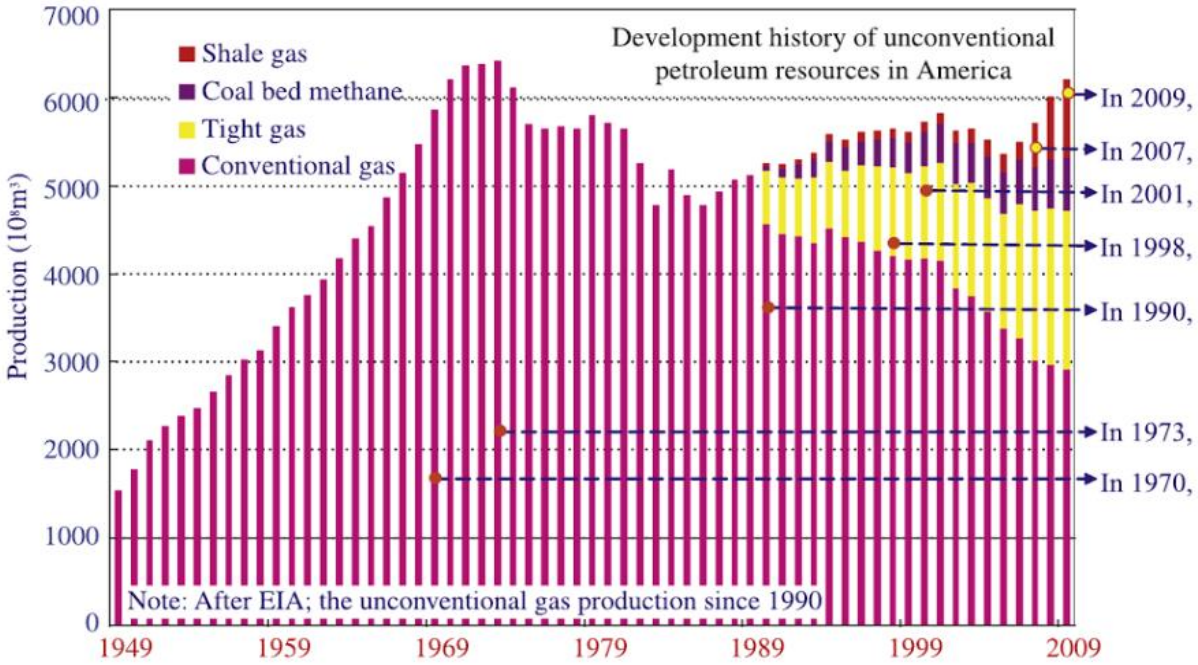

Figure 1.1: Development history of unconventional petroleum resources in the United States. From the late 1980's to 2009, while the overall production of unconventional petroleum increases, conventional gas (which was the exclusive resource until 1989) decreased and the gap was filled with by shale gas, tight gas and coal bed methane. Zou, 2013

A decline in conventional sources alongside an increase in unconventionals, leading to an overall increase in gas production rather than a decline that was occurring before the wider development of unconventional hydrocarbon resources. This fundamental change is not only constrained to the US unconventional gas, with significant advancements made in exploration and production in the Canadian tar sands/oil sandstone and the Venezuelan heavy oil resources (where the resources are enormous but are yet to be exploited), but neither of these have had quite the change in their energy make up that the United States has seen.

In contrast to many countries China is seeing its gap between its petroleum supply and demand increasing and over the last decade has launched a major realignment and focus upon unconventional exploration. In particular, large scale fracturing technologies to develop giant tight gas basins like the Sulige of the Ordos Basin and Xujiahe Formation of Sichuan Basins have been significant changes yielded a new understanding of tight gas reservoirs (Zou, 2013).

The USGS and the US Department of Energy assesses the volume of global unconventional oil resources (including shale oil, bitumen and heavy oil) at $4495x10^8$ t, equal to that of conventional resources, and unconventional gas resources (including gas hydrate, shale gas, CBM and tight sandstone gas) at $3922x10^{12}$ m^3, 8.3 times the volume of conventional gas resources, making these resources crucial for the future of energy security (Zou, 2013). With potential reserves of this size and the recent improvements in exploration and development techniques driven by high oil prices between 2003-2013, peaking at $140 per barrel in 2008, it is clear to see that it is only a matter of time and investment before these unconventionals start to shoulder more of the increasing global energy demand. Another indication for the growth of these unconventional petroleum resources is the petroleum resources triangle from Zou (2013) (Fig. 1.2). This demonstrates the conventional hydrocarbons have the lowest global volume, are the highest grade of hydrocarbon available but require the lowest level of technology to extract, and so make up the apex of the triangle. They are then followed by the middle transitional area where you find the unconventional resources that have been discussed before and also further in this chapter, which have a significantly larger volume than conventionals but have a lower grade and require a more sophisticated level of technology. At the base the enriched natural gas hydrates are found that have the poorest quality and are the most difficult to exploit. Figure 1.2 is relevant because as the top of the triangle/conventionals are used up we must begin to move into the middle of the triangle and exploit more of the unconventionals so as to meet global demand.

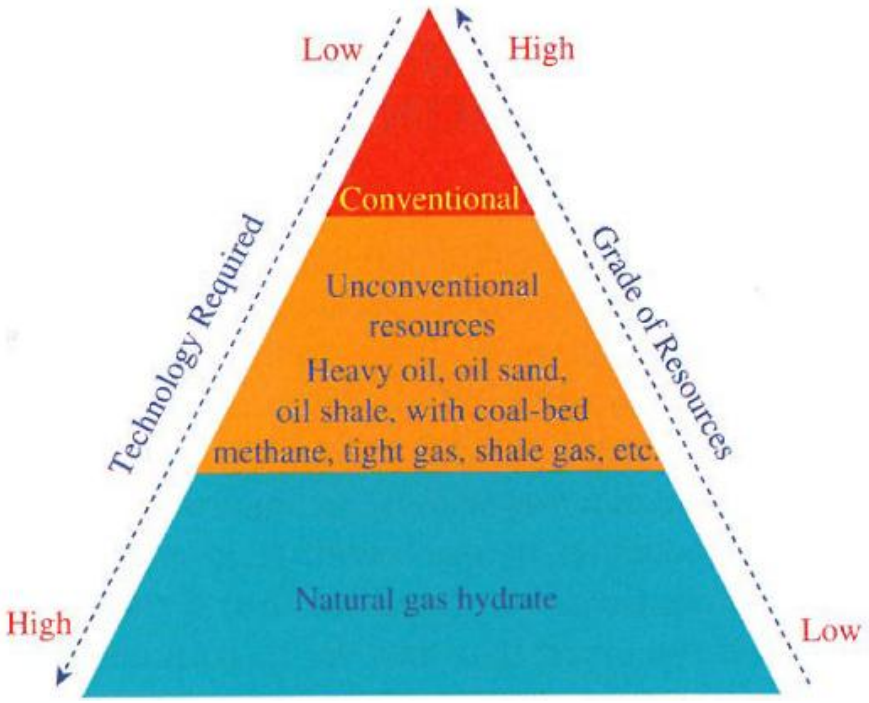

Figure 1.2: Petroleum resource triangle. Zou, 2013.

1.4.2 Conventional vs Unconventional Reserves

Although widely used phrases, conventional and unconventional do not make it completely clear what the difference between the two sources is. Unconventional hydrocarbons are defined by Zou (2013) as continuous or sub-continuous accumulations of petroleum resources for which commercial production is not achievable through conventional techniques and economic extraction in not possible without the use of techniques or technology that improves the reservoir permeability or fluid viscosity. The primary characteristics include:

- An absence of clear seal or trap.
- Large distribution of oil and gas
- Matrix reservoirs of low permeability
- Abnormal pressure.
- Proximity to source rocks.

The primary sources of unconventional oil and gas include shale gas and tight sandstone oil and gas (Zou, 2013). Shale gas is natural gas that is trapped within shale-rich formations and extracted primarily through horizontal drilling and multi-fracking to create maximum borehole surface area in contact with the shale. Shale gas has only become important recently because in conventional hydrocarbon theory organic rich shale were considered to have poor flow rates and technology didn't exist to improve them flow rates and so it was rarely and poorly developed. However, innovations such as multistage hydraulic fracturing of multilevels have allowed for commercial recovery of shale gas, as seen in North America. Tight sandstone oil and gas are hydrocarbons preserved in tight-sandstone reservoirs that are only of commercial significance after they have undergone stimulation. Tight gas is produced from reservoir rocks that have such low permeability (<0.1 mD matrix permeability and <10% matrix porosity) that they require massive hydraulic fracturing for the well to produce at economic levels. Tight oil refers to the crude oil that occurs in silty fine sandstone and tight carbonate reservoirs.

Conventional hydrocarbon reserves are concentrations of oil and gas that occur in isolated accumulations, in rock formations usually with high porosities and permeabilities, and found below impermeable rock formations. These accumulations are developed using vertical well bores and use minimal stimulation, and fall into several categories based on the trapping mechanism of the hydrocarbons:

- Structural traps.
- Dome structures
- Stratigraphic traps.
- A combination of the above.

Table 1.1 breaks down the different features of hydrocarbon accumulations and then compares them between convention and unconventional processes, giving a simplified comparison between these two forms of accumulation, and then also classifying which of these features is convention or unconventional in volcaniclastic reserves. From the evidence above, can it be said that volcaniclastics are conventional or unconventional hydrocarbon reserves? The answer is that they have all the features of a conventional reservoir, but they have such complex features and behaviour that cannot be constrained for all volcaniclastics across the world they cannot be considered either a definitive conventional or unconventional. For the purpose of this study they will be considered to be a type of reservoir in their own and referred to as a non-conventional play (Clark, 2014).

1.4.3 Volcaniclastic Reservoirs: A New Revolution

While volcanic hydrocarbon reservoirs are not a new frontier of hydrocarbon exploration (Primmer et al, 1997) they are becoming an increasingly investigated field, with discoveries in more than 300 basins across 20 countries and regions (See Figure 1.3), with Cretaceous and Cenozoic volcanic rocks contributing around 70% of total global volcanic reservoir preservation (Liu et al. 2012). These volcanic reservoirs can vary in their style and formation, and are controlled by the volcanotectonic and paleogeographic setting, eruptive and depositional mechanisms, composition, age, diagenesis, thermal and burial history of the regional volcano and its associated sediments (e.g. Mathisen & Mcpherson, 1991). Of these volcanic reservoirs, the reservoirs formed of volcaniclastics are the focus of this study. For the purpose of this study, volcaniclastics are defined as clastic rocks characterised by a significant volcanic rock component.

	Conventional vs Unconventional Accumulations		
Features	Unconventional	Conventional	Volcaniclastic Reserves
Distribution	Widespread, continuous distribution at the slope and basin centre	Discontinuous distribution	Conventional
Reservoir	Large-scale, tight reservoirs characterised by low permeability/fluid flow	Conventional reservoirs characterised by good porosity and permeability	Conventional
Configuration of source rocks and reservoirs	Source rocks and reservoirs in one	Complicated, any configurations	Conventional
Trap	No obvious definition, open trap	Obvious definition, closed trap	Conventional
Migration	Primary migration or secondary migration over short distance	Secondary migration over long distance	Conventional
Accumulation	Buoyancy is limited	Buoyancy is the main force	Conventional
Percolation	Non-Darcy flow	Darcy flow	Conventional
Fluid relationship	No uniform fluid or pressure systems, hydrocarbon saturation varies greatly	Uniform fluid contacts	Conventional
Resource assessment	Low resource abundance, and resource is based on well production	Resource is based on trap parameters	Conventional
Development technology	Special technologies, i.e. hydraulic fracturing	Conventional technologies	Conventional

Table 1.1: Comparison between the features of conventional and unconventional petroleum accumulations, and which of these applies to the various features of volcaniclastic reserves. Table redrawn from Zou, 2013

Figure 1.3: Distribution of hydrocarbon-bearing igneous rocks. Farooqui, 2009.

Volcaniclastics are defined as undisturbed deposits of clastic volcanic material, but if the material is reworked and redeposited it is known as volcaniclastic sediment (Arndt, 2011). These reservoirs formed through explosive, effusive, extrusive and subvolcanic processes according to Liu et al (2012), and these reservoirs are present in either autoclastic (mechanical brakeage during magma movement), pyroclastic (magmatic explosion), hydroclastic (water-magma interactions) or epiclastic (Sedimentary erosion, transport, and deposition) deposits (Mathisen & Mcpherson, 1991) (Ólavsdóttir et al. 2015). Autoclastic and hydroclastic deposits are primarily linked to volcanic flows which are poor hydrocarbon reservoirs, while pyroclastic and epiclastic deposits tend to have higher reservoir quality (Mathisen & Mcpherson, 1991).

The reservoir quality of a rock is defined by its hydrocarbon storage capacity and deliverability, and the two primarily controls are the hydrocarbon stage capacity characterised by effective porosity (and reservoir size) and deliverability as a function of permeability. Volcaniclastics have long been defined by their reservoir quality being less consistent due to their heterogeneity, in comparison to conventional sandstones. This is due to high proportions of volcanic rock fragments and minerals that alter to low permeability clays that fill the pore spaces or coat the grains of the rock (Stagpoole & Funnell, 2001), while the conventional clastic sandstones are almost all quartz and are chemically inert (Clark, 2014) meaning that poor filling, low permeability clays are less likely to form. According to Clark (2014), this diagenetic history of volcaniclastic sandstones has a number of influencing factors: depositional environment, detrital mineralogy, grain size, pore-water chemistry, temperature, pressure and burial history. This is a large number of variables that can influence a reservoir of unstable, heterogenetic material, and Table 1.2 demonstrates how all these factors influence reservoir quality of volcaniclastics reservoirs depending on the depositional setting.

Factors	Characteristics			Mohakatino Formation, Kora Field
Composition	Vitric	Feldsapathic	Lithic	**Feldsapathic**
Volcaniclastic facies types	Pyroclastic fall	Pyroclastic flow (ignimbrite)	Epiclastic sediment	**Epiclastic**
Volcaniclastic facies distribution	Widespread	Localised		**Widespread**
Sedimentary environment	Marine (early carbonate common)	Non-marine (early carbonate common)		**Marine**
Reworking	No	Yes		**Yes**
Burial history	Shallow	Deep (uplifted, fractured)		**Shallow**
Compaction	Minimal (inhibited by cement)	Maximum		**Minimal**
Hydrogeology (fluid flow)	Slow fluid flow	Fast fluid flow		**Slow**
Thermal history	Low	High		**High**
Geochemistry (pore waters)	Inorganic pore water reactions	Organic pore water reactions		**Organic**
Porosity change	Cementation	Dissolution		**Cementation**

Table 1.2: The relationship between the factors controlling the properties of volcaniclastic sandstone reservoirs, the various characteristics of these factors, and which of these characteristics are found in the Mohakatino Formation investigated in the Kora Field. The characteristics most favourable for reservoir development are highlighted in green, and those which are detrimental in red. Redrawn from Mathisen & Mcpherson, 1991.

Volcaniclastics have been found to have reservoir quality good enough to be of interest for hydrocarbon exploration across the planet in various geological locations. One such location such as the Serie Tobífera of the Austral Basin, Argentina, with the quench fractured glasses and non-welded ignimbrites having the highest reservoir quality of the ignimbrites, epiclastics and rhyolitic lavas (Sruoga et al. 2004; Sruoga & Rubinstein, 2007). Rhyolitic and flood tuff that make up the Lower Cretaceous Yingcheng Formation of the Qingshen gas field, Songliao Basin, NE China (Feng, 2008; Zou, 2013). The Miocene Tepoztlán Formation, Central Mexico and consists of pyroclastic rocks, mass flow and fluvial deposits and all part of the Transmexican Volcanic Belt (Lenhardt & Götz, 2011). The Sawan gas field, Pakistan acts as a natural gas reservoir with volcaniclastic, feldsapathic litharenites sandstones of the Cretaceous Lower Goru Formation (Berger et al., 2009). Epiclastic and pyroclastic volcaniclastic reservoirs within the Paleocene and Eocene strata in the western Shetland Basin (Ólavsdóttir et al., 2015). Andesite characterised sandstones and siltstones are indicative of the Miocene Mohakatino Formation, Taranaki Basin, New Zealand (Armstrong et al. 1996; Bergman et al., 1992; Stagpoole & Funnell, 2011; King & Thrasher, 1996). These range from large gas fields to small, uneconomic oil fields, but all demonstrate the qualities required for reservoirs despite the influence of volcanic material on the reservoir rocks.

1.5. Methods of Study

1.5.1 Fieldwork

This study investigated the presence of the Mohakatino Formation and its relationship with the surrounding formations across six coastal outcrop locations in the Awakino region on the North Island of New Zealand, with the locations chosen based on the work done in the same region by Shumaker (2016) looking at the Mohakatino.

At each field location a series of common field techniques were conducted as part of the fieldwork section of this study. Field Sketches were made at each location and photographs were also taken at notable outcrops, allowing for facies relationships and the behaviour of the outcrop to be studied at greater depth. Observations were made regarding bed thickness and geometry, grain size and sedimentary structures and features so as to identify the various formations and their corresponding lithofacies. Stratigraphic sections through sedimentary rock sequences were made at four representative locations for the whole region (Awakino Heads, Mokau River, Waikawau Cliffs and Piopio Station). It was not necessary to take more stratigraphic sections of the locations as there have already been studies which have undertaken significant stratigraphic analysis of the region (Sharman, 2014). Rocks were logged at a centimetre scale and samples were taken from these locations as well.

A total of 25 representative rock samples of the Mohakatino Formation were collected from across all major locations (see Appendix II), as well as the overlying Mount Messenger Formation and the underlying Mangarara and Manganui Formations. Samples were collected from the Lf1a, Lf1b, Lf2 and Lf3a lithofacies that make up the Mohakatino Formation, but not the Lf3b and Lf4 because the Lf3b was not accessible anywhere in this study for sampling and Lf4 is comprised of siltstone and not appropriate as a reservoir rock for the Mohakatino and therefore of no use. The number of rock samples that were able to be taken back from the field was limited due to available weight and space and some locations could not be sampled/thin sectioned due to poor lithification. Due to these problems only 10 thin sections samples of the Mohakatino were eventually produced.

1.5.2 Optical Analysis

Thin Sections

Eleven standard size polished thin sections and one large format polished thin sections were loaned from the GNS, and this was the maximum number of thin sections available from the offshore wells in the study area. These were all made from the Mohakatino Formation present in the wells. Of the twelve thin sections, eight were stained blue for porosity using blue epoxy resin, and the remaining four were not.

For studying the onshore region, sixteen standard size polished thin sections were made from samples that were taken from locations in the study area (See Appendix I for sample numbers and locations). Twelve of these samples were from the various lithofacies that make up the Mohakatino Formation, while the other four were the Manganui, Mangarara and Mount Messenger Formations.

Petrography

All thin sections were examined using a polarising microscope and were characterised according to grain size, texture, sorting, mineralogy, visible porosity and alteration. Key features throughout the samples were highlighted and captured on photomicrographs at a variety of scales. Point counting was undertaken on all thin sections to achieve this using an ID818 Stepping Stage and Petroglite Point Counting Software. The thin sections were divided by multiple vertical and horizontal transects to give an even and representative coverage, and across these transects the samples were analysed for 300 points using a step size of 2 mm. While giving a representative and quantifiable analysis of the samples, there were a number of inherent problems with this technique. First of all, it is difficult to step a consistent step size when dealing with heterogeneity between and within each thin section, and so the default step size was kept for the study. Second, there is great difficulty in distinguishing the mineral phases, in particular the clay minerals, and this led to reduced accuracy of the point counting data. The resulting data (i.e. visual porosity, mineral percentages) was then used for further petrographic analysis, such as intergranular volume (IGV) (Paxton et al., 2002), total cement volume (C), porosity lost by mechanical compaction (COPL) and porosity loss by cementation (CEPL) (Lundegard, 1992)

1.5.3 Scanning Electron Microscope (SEM)

The SEM was used to examine samples at very high magnifications (up to 10,000x) and determine the authigenic minerals and their structures, grain boundaries, grain coating and pore filling minerals, all of which is helpful in determining the diagenetic history of the rock. The SEM works by using a high power electron beam fired through two or more electromagnetic lenses targeted at the sample surface and then the electrons can interact with the sample in three ways (all information from Clark, 2014): (1) secondary electrons (SE) are produced by the beam causing the loosely bounded electrons in the sample surface to become excited and eject, and a collection of these gives topographic information about the sample surface. (2) Backscattered electrons (BSE) are primary beam electrons that are scattered from within the sample, and the number of these detected relates to the atomic number of the phase they've interacted with, therefore providing information on the chemical composition. (3) X-rays are formed when the electron beam excites an electron in an inner shell causing it to move to an outer shell. When a high energy outer shell moves back to replace the inner electron an X-ray is emitted, and the process is dependent on the atomic number and the collected X-rays give information on the chemical composition.

SEM/SEM-EDS analysis of onshore thin sections was done using a Hitachi SU-70 field emission gun scanning electron microscope (SEM) and equipped with an energy-dispersive x-ray detector (EDX). Scanning electron microscope analyses of thin sections was conducted at 15 keV (Kilo Electron Volts) acceleration voltage, and an AWD (analytical working distance) of 15mm. SEM-EDX was used for rapid identification of chemical species (i.e. chlorite Fe/Mg- ratio) and concentration/frequency in the samples, and images of the occurrence of the individual elements were captured. Information and data processed using Aztec Chemical Analysis systems. All SEM/SEM-EDX work and equipment provided by and completed at Durham University. Due to time constraints related to the nature of the project it was only possible to analyse four of the ten available onshore samples (Samples 2, 6, 8 and 11) were analysed using these techniques.

When preparing the offshore samples there was an immediate problem and this was that they all had cover slips and so this made them unsuitable for SEM work. Thin sections therefore had to have their cover slips removed so as to give a clear, unobstructed view of the sample. Another problem was that wells such as Kora-1A that have more thin sections available than others, and so while this gave the opportunity to choose samples from some wells, other wells such as Kora-2 and Kora-3 only had one sample available for SEM analysis. See Appendix I for the samples that were available for SEM. Another problem with the offshore samples was that due to conflicts with booking times and availability of staff, the offshore samples were not able to be analysed using the Hitachi SU-70, and the only available SEM was the Hitachi TM-1000 Tabletop Microscope, which is still able to take high magnification images but with poorer resolution and cannot perform EDX analysis of the samples so all minerals and cements seen in the images had to be identified manually.

1.6 Thesis Organisation

Chapter 2 has one simple aim and that is to give a chronological and structured breakdown of the all the features of the Taranaki basin that are relevant to this project. It begins by giving a full geological development of the Taranaki basin, from the Late Cretaceous rifting of the Tasman Sea to the Pleistocene back arc phase, and also providing a breakdown of the general geology. From here the chapter starts to explore the features of the Taranaki that are relevant to the study, including the Mohakatino Volcanic Centre (MVC), Kora Volcano, and the onshore fieldwork area. This chapter does not attempt to address any of the aims or questions of this project, but rather give a clear picture of the Taranaki Basin's setting and where all the different features are located in time and space.

The primary goal of **Chapters 3 & 4** is to present all of the data of this study but to split the chapter into an onshore and offshore section, allowing the spatial differences of the Mohakatino Formation to be clearly defined. **Chapter 3** will be analysing all the data found in the proximal, offshore samples, comprising of the well logs, photo micrographs and SEM images of thin sections, and associated

drilling data, and then working with this data to identify trends in the important fields such as petrography, grain size, porosity, permeability, clays and cements, and burial history. **Chapter 4** will follow the same the structure, but covering the distal, onshore fieldwork that was conducted. This will consist of an overview of how the fieldwork was planned and conducted, the associated lithofacies and their locations, before then presenting the petrographic data in the same format as the previous section.

Chapter 5 is where the results and conclusions of Chapters 3 and 4 are brought together and examined in a more detailed discussion and synthesis. The main problem tackled by this chapter is what causes the variation in reservoir quality between the Mohakatino rocks found in offshore wells and those found as outcrops onshore, as we are seeing strikingly different trends in the petrography and optical data. The spatial-temporal differences between proximal and distal position of the samples must be considered when thinking about these mass transport deposits and will be crucial in the depositional composition of the Mohakatino. As well as the data from this study, other research will be taken into account here for trying to understand how these mass transport deposits behave and now the volcanic component influences the diagenesis. The chapter closes with a selection of the most important conclusions about the study.

Chapter 2

The Geological History and Evolution of the Mohakatino Formation, Northern Taranaki Basin, New Zealand.

2.1 Introduction

The Taranaki Basin is a roughly 100,000 km^2, Cretaceous-Cenozoic sedimentary basin that has undergone a complex and multiphase basin history located on the western margin of New Zealand. The Taranaki Basin initiated during the Late Cretaceous time, when the New Zealand subcontinent rifted from Gondwana (Eastern Australia) and therefore developed into a passive margin setting (King and Thrasher, 1992, 1996; King 2000) The fledgling modern Australian-Pacific plate boundary subsequently propagated through the New Zealand region from middle Miocene time (King 2000). Convergence in the north started around late Eocene time (Bache et al., 2012) and was manifested in the Taranaki Basin as emplacement of the west-verging Taranaki thrust fault, which displaced basement more than 7km vertically (Fig. 2.1 & 2.2; King and Thrasher, 1996; Stagpoole and Nicol, 2008). During the Miocene the Northern Basin acted as a depocentre for predominantly bathyal sediments (>1500m), and defined by uplifted basement to the east and southeast (Herangi-Patea-Tongaporutu submarine highs) and by a submarine andesitic volcanic arc to the west (Figs 2.1 and 2.2; Nodder et al., 1990b; King and Thrasher, 1992; King et al., 1993, 2007a, 2007b). Within the basin there is a collection of 20 andesitic, submarine volcanoes that make up the Mohakatino Volcanic Centre (MVC) that have been active from 16-2 Ma (Giba et al., 2013), and was formed from the westward subduction of the Pacific Plate below the Australian Plate along the Hikurangi margin, 400 km east of the volcanic arc (Fig. 2.1 A) (Shumaker, 2016). After the volcanism ceased around 2 Ma, this andesitic arc was buried by Plio-Pleistocene continental slope and shelf sediments from the south east at a rate of up to 700m Ma^{-1} known as the Giant Foresets (Stagpoole and Funnell, 2001). The Kora volcano, found at the southern end of the MVC is the subject of the offshore section of this study (Fig. 2.2). Onlapping on to the flanks of the Kora volcano are an upward-shallowing succession of the basin floor (bathyal) to upper continental slope sediments that was formed over ~2Ma during the late Miocene (King and Thrasher, 1996). This succession is made up the Manganui Formation (deep marine mudstone) at the base, topped by the Mangarara Formation (lenticular packages of coarse bioclastic sandstone and conglomerate), a submarine fan succession (Mohakatino Formation) that was sourced from the MVC (Fig. 2.2 and 2.3; Shumaker, 2016). The Mohakatino Formation has been identified offshore in the Kora-1/1A, -2, and -3 wells drilled into the flanks of the Kora Volcano as well as Kahawai-1 (Fig. 2.1 B). The Mohakatino Formation comprises volcaniclastic gravel, sandstone and mudstone derived from the submerged chain of stratovolcanoes (ca. 15-6.5Ma) to the north and west (King and Thrasher, 1996; Giba et al., 2013). It was deposited in lower bathyal water

depths (>1500m), and composed of both sediment gravity flow deposits and suspension sedimentation of volcanic debris through the water column within a basin floor fan or fan apron setting (e.g. Utley, 1987; Nodder et al., 1990b; King et al., 1993, 2011). The Mohakatino Formation submarine fan succession extends east all the way to the Taranaki coast and is exposed for 30 km of the coastline from the Mokau River to the Waikawau Cliffs (Fig. 2.2). The Taranaki coastal sections lie to the east of the Taranaki Fault and any significant movement on the fault is thought to have ended by early Miocene time and unlikely to have influenced sedimentation (Stagpoole and Nicol, 2008). The Mohakatino Formation is overlain by the Mount Messenger, Urenui and Kiore Formations that record a pronounced progradation of the continental slope to the north and west from ca. 10.5 to 9 Ma (Fig. 2.2 and 2.3; King et al., 1993, 1994; Browne and Slatt, 2002; Arnot et al 2007a, 2007b; Browne et al., 2000; King et al., 2007a, 2007b, 2007c; Maier, 2012; Masalimova, 2013.

This chapter aims to provide a geological synthesis of the complex and multiphase Taranaki Basin history. There is particular emphasis on the Northern Graben and Mohakatino Formation as encountered flanking the Kora stratovolcano and spectacularly exposed for ~11km along the northern Taranaki coastline of New Zealand, referred to here as the North Awakino mass-transport deposit (NAMTD). The petrography and burial history of the Mohakatino Formation will be discussed in greater detail in Chapters 3 and 4.

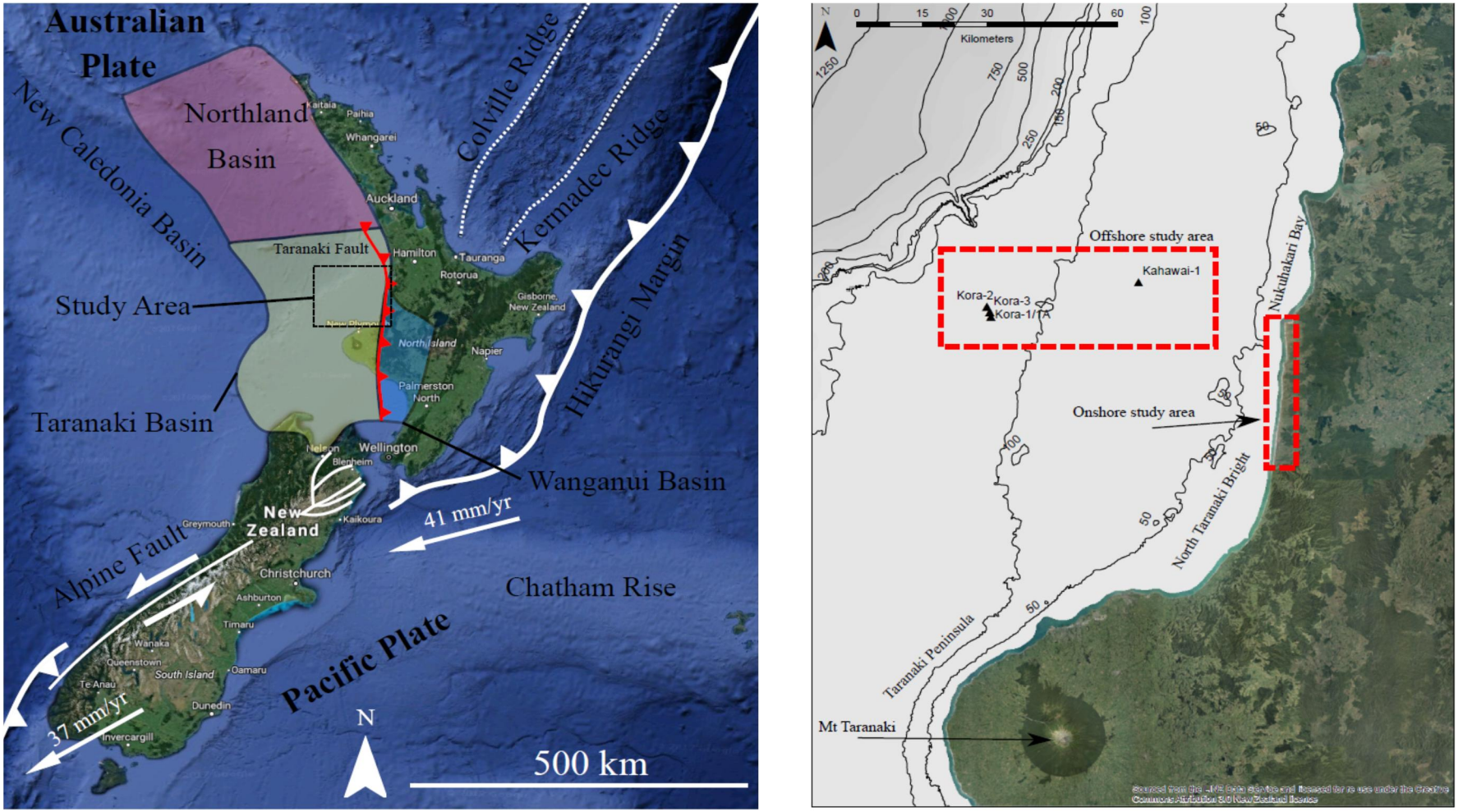

Figure 2.1: The position of the study area with regional context. A, Left) New Zealand's plate tectonic setting along the Australian – Pacific Boundary showing the study area and major tectonic elements of the region. Basemap taken from Google Maps. Major features redrawn from Reilly et al. 2015. B, Right) Magnified regional map of the study area. Onshore and offshore study areas highlighted as well as major coastal features and sea floor bathymetry. Offshore wells can be seen to sit on the continental shelf. Map data sourced from ArcGIS online database.

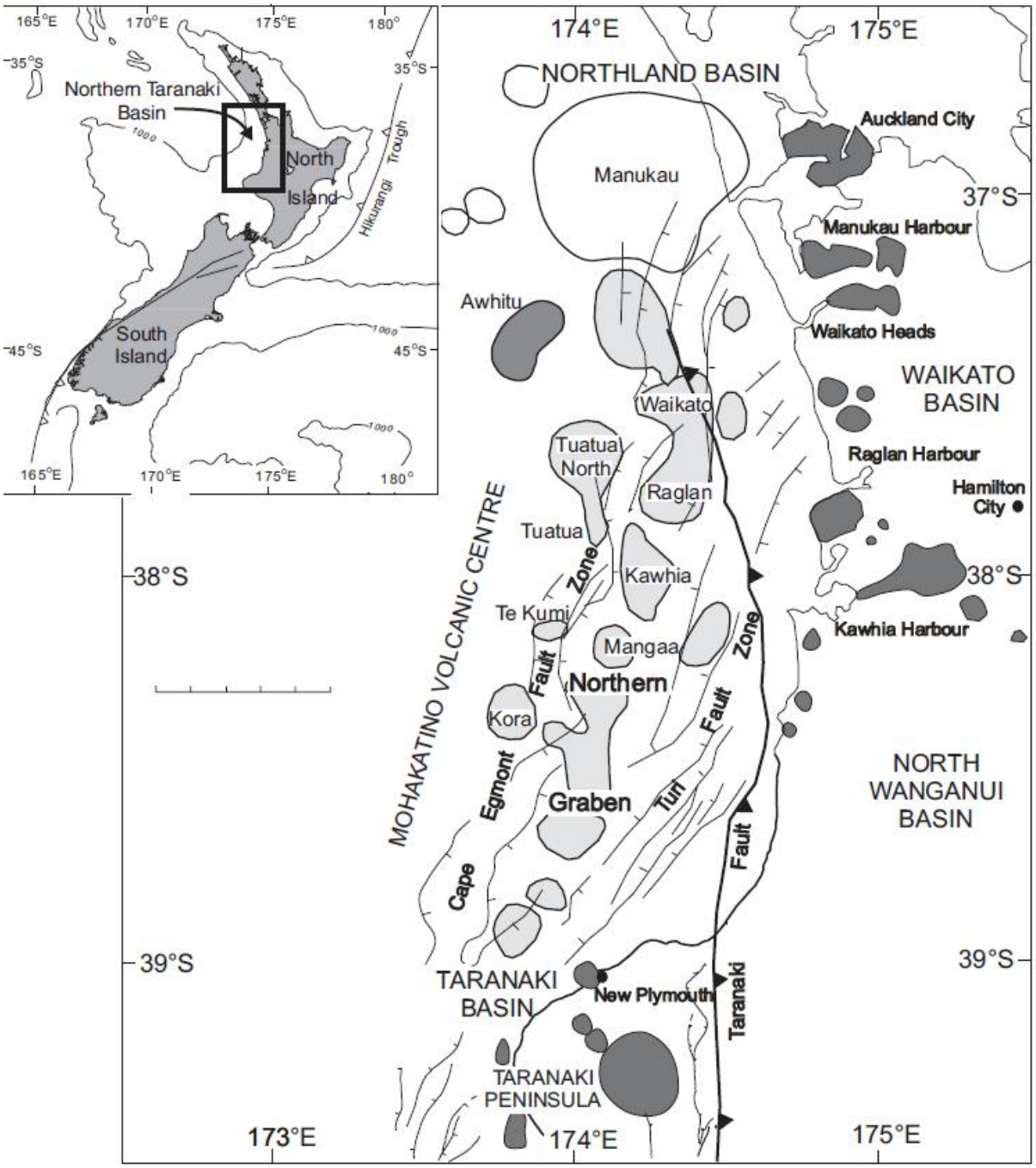

Figure 2.2: A map of the northern Taranaki Basin and the adjacent area showing the Mohakatino Volcanic Centre (MVC) (light shading) formed of Miocene andesitic arc volcanoes. Older volcanic centres (no shading) are the Northland andesitic arc volcanoes; younger volcanic centres (dark shading) andesitic arc volcanoes and basaltic volcanic cones. Major structural features of the Neogene are shown. The position of the Kora volcano within the Cape Egmont Fault Zone, the MVC and the Northern Graben are shown in relation to the North Island. Stagpoole and Funnell, 2001.

2.2 Detailed Geological Development of the Taranaki Basin

The history of the Taranaki Basin can be broken down into three main phases of development according to King and Thrasher (1996), with each phase being dictated by the plate boundary kinematics that are associated with movement and interactions of the Pacific and Australian plates. **The first phase covers the early basin history (Cretaceous – Palaeocene)**, the intra-continental rifting that caused the opening of the Tasman Sea during Gondwanan break up. **The second phase (Eocene – Early Oligocene)** is characterised by the lack of tectonic activity and post rifting thermal contraction and regional subsidence. Finally, **the late basin phase (Oligocene - Recent)** saw the evolution of the Australian – Pacific convergent plate boundary through New Zealand. This led to the evolution of the basin's two tectonic setting: the active margin known as the Eastern Mobile Belt, and the passive margin known as the Western Stable Platform. The stratigraphy that makes up the Taranaki Basin is demonstrated in Figure 2.3 and gives a temporal framework for wider discussion in this chapter. For a clearer expression of the basin's evolution and architecture described in the text, Figure 2.4 A-G gives a paleogeographic breakdown of these features and events.

2.2.1 First Phase (Cretaceous – Paleocene)

The Taranaki Basin's formation begins with the separation of Zealandia from Gondwana during the Late Cretaceous (85-60 Ma) (Figure 2.4, A), and this breakaway led to the formation of the Tasman sea as an intra-plate rift that would eventually become the Taranaki rift, and subsequently the Taranaki Basin (Kroeger et al. 2012). However, prior to the actual separation from Gondwana, there is an earlier period known as the Zealandia rift phase around 105 Ma in the Urutawan (mid Cretaceous), where there was a development of NW to WNW trending half grabens up to 83 Ma in the Haumurian (Late Cretaceous), which preceded and formed parallel to the Tasman Sea spreading centres (Strogen et al. 2017). Strogen et al (2017) define this period of syn-rift from primarily terrestrial (ca. 105 - 95 Ma) to a marine transgressive system (ca. 95 - 83 Ma). This phase is acknowledged to have predated the opening of the Tasman Sea and in turn the break up and separation of Zealandia from Gondwana. Following this, uplift and erosion in the southern Taranaki Basin occurred through 83-80 Ma in the Early Haumurian, and the sedimentation from this formed an unconformity in the southern Taranaki Basin and the deposition of the 'Taranaki Delta' in the Deepwater Taranaki Basin. The Taranaki Delta is a thick (up to 2.5 km) prograding unit of Early Haumurian aged sequence with little normal faulting, aside from small displacements that are thought to be formed through sediment compaction (Strogen et al. 2017). After this brief hiatus a second rift event known as the West Coast – Taranaki rift phase occurred from the Late Haumurian - Teurian (ca. 80 – 55 Ma), and this is a collection of NE extensional half grabens that are observed in central Zealandia/southern Taranaki (Strogen et al. 2017).

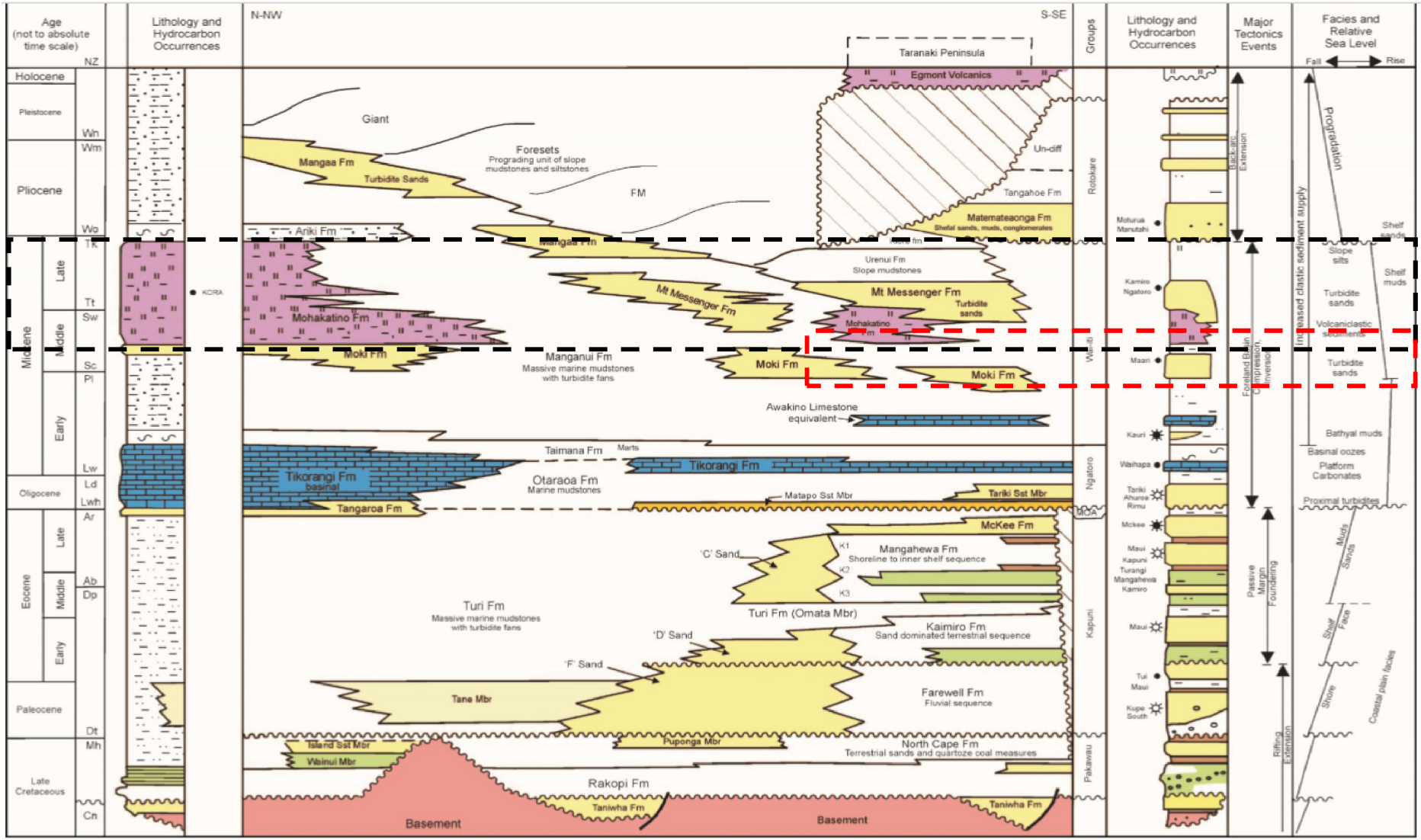

Figure 2.3: Taranaki Basin summary stratigraphic chart. (Not to scale). Regions highlighted in black indicate the position of the Mohakatino Formation within the regional stratigraphic column and those highlighted in red refer to the Mohakatino Formation within the study area from the Lillburnian (SI) (c. 14Ma) to the Kapitean (TK) (ca. 8Ma). Webster et al. 2011.

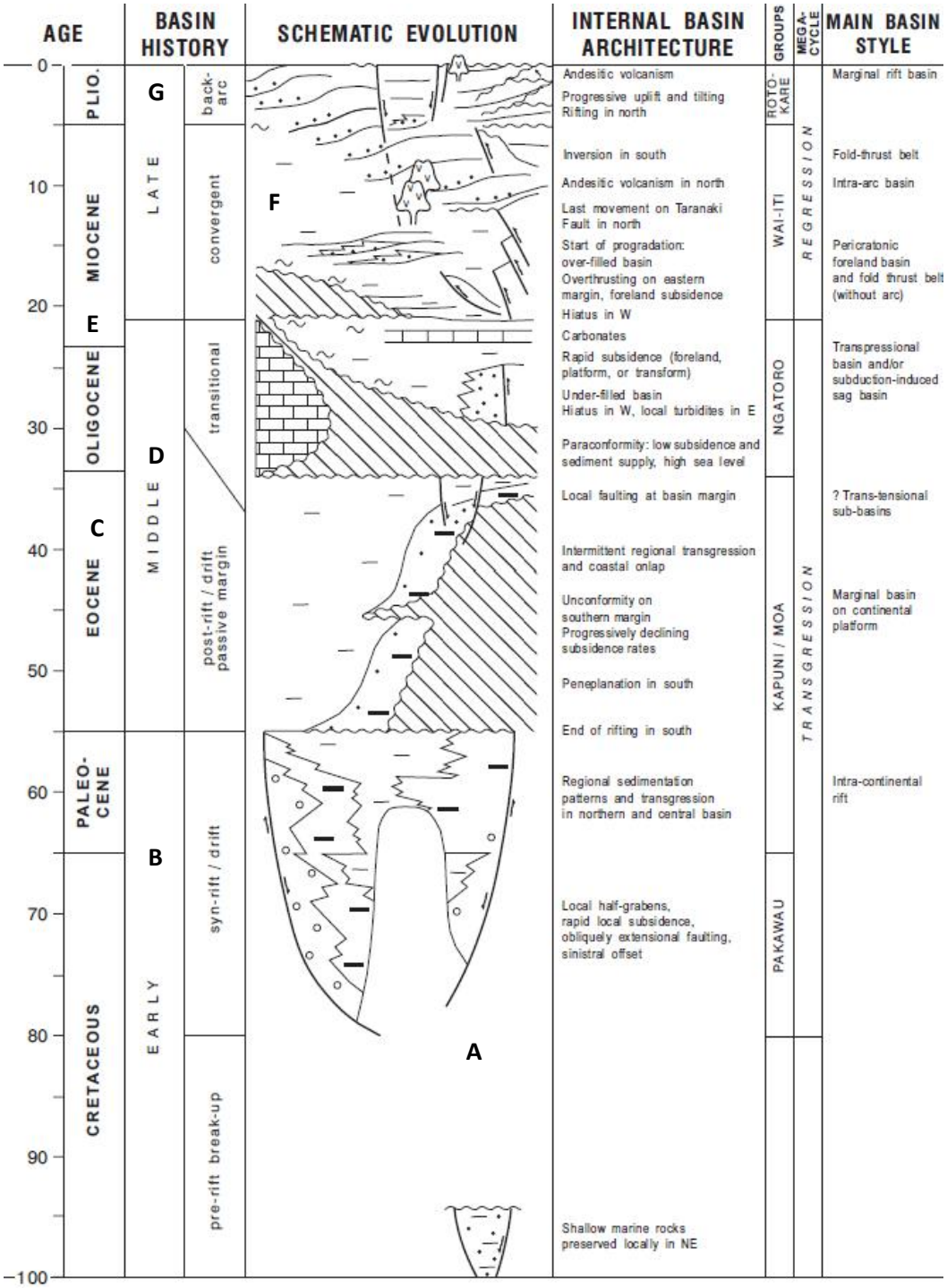

Figure 2.4: Timetable of events and controls in the Taranaki Basin's evolution. Positions A-G represent the position of major or important events during the basin's history, and a description of these events can be found in Section 2.2. King and Thrasher, 1996

These together formed a relatively narrow 500 km belt through central Zealandia as part of the Tasman Sea spreading being involved in the formation of the West Coast Taranaki rift system, and according to Strogen et al. (2017), after reviewing the kinematic data, represents a 'failed rift arm' model where lateral motion along the rift system accommodating differential spreading rates south of Zealandia and coeval opening in the New Caledonia Trough. See Figure 2.5 for a graphic representation of this early breakaway of Zealandia from Gondwana.

Early basin development was distinguished by rapid subsidence and the formation of deep, fault bounded basins (Stagpoole and Funnel, 2001). These filled with organic rich terrestrial and paralic sediments (Stagpoole and Funnel, 2001), the oldest sediments of the Taranaki, and make up the Taniwha Formation of Ngaterian (late-Cretaceous/upper Turonian age (King and Thrasher, 1996). These basin fill sediments are thought to have been deposited during an extensional tectonic regime related to the rifting of the New Caledonia Basin, as well as the north-northeast – south-southwest extension along the Pacific margin of Gondwanaland (King and Thrasher, 1992). A series of fault controlled sub-basins and half grabens make up an obliquely extensional transform system connected to the rifting in the New Caledonia Basin (Strogen et al, 2012). First sedimentation of the Taranaki sub-basins was non-marine, with sand, silt, mud lithologies making up the late Cretaceous succession, and along with the lower carbonaceous mudstone and coal, these represent a mix of different fluviatile and fluviodeltaic facies. King and Thrasher, 1996 stipulate that sub-basin subsidence and sediment infilling were comparatively rapid, with subsidence dictated by high angle bounding normal faults, generally to the west.

2.2.2 Second Phase (Eocene – Early Oligocene)

After the normal fault activity ceased in the late Cretaceous/early Paleocene (Figure 2.4, B), the subsidence within the Taranaki Basin gradually changed to a more regional pattern, and from this point to the mid-Oligocene, subsidence curves begin to show exponential decline in rate with time and in fact start to show a pattern of more post-rift lithospheric cooling and thermal subsidence of continental margins (King and Thrasher, 1996). This period of quiescence was indicative of the second stage of the Taranaki's development. This former rift landscape then became open to the sea to the northwest, allowing the Farewell, Kaimiro and Mangahewa formations to build up in this passive margin through-out the Paleogene (King and Thrasher, 1996). During this period of cooling, the Taranaki started to experience the growth of a number of asymmetric sub-basins clearly caused by faulting on one side and these are generally considered to be normal faults through-out the Eocene, and also developed in neighbouring regions that had subsequently been uplifted by Miocene inversion (King and Thrasher, 1996).

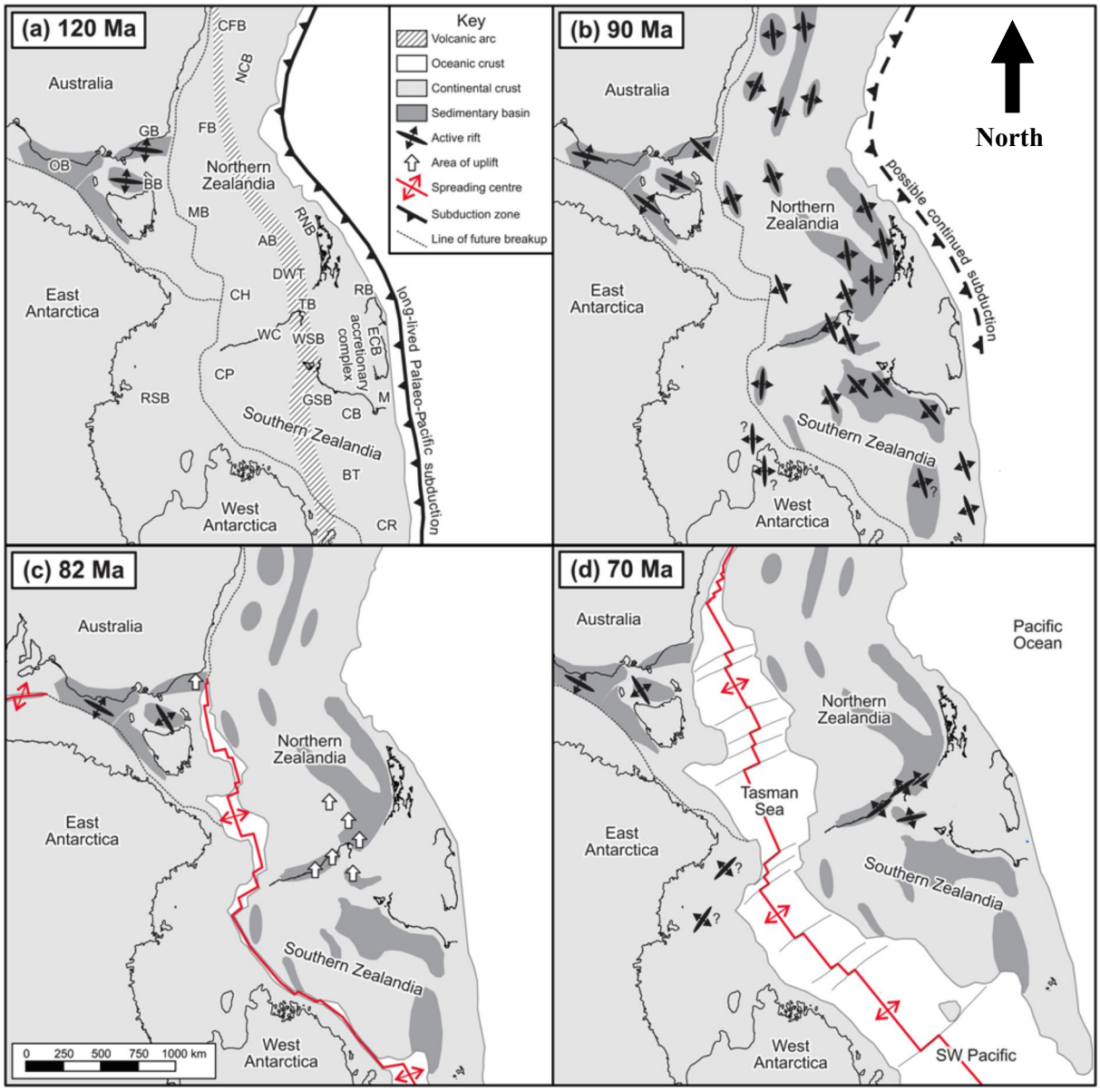

Figure 2.5: Tectonic reconstruction for the Zealandia-Australia-Antarctica region, with East Antarctica fixed. (a) 120 Ma prior to Zealandia rifting at the end of long-lived subduction on the eastern margin of Gondwana, with related arc indicated. Approximate future position of basins shown. (b) 90 Ma showing widespread Zealandia rifting. (c) 82 Ma showing initial seafloor spreading in the Tasman Sea and Southern Ocean with uplift of parts of central Zealandia. (d) 70 Ma showing continuing seafloor spreading and spatially limited West Coast Taranaki rifting in parts of central Zealandia. (Strogen et al. 2017)

This gives the impression that these late Eocene sub-basins were not the result of a simply normal faults uplifting one side of the basin, but rather produced by reverse fault downthrow according to King and Thrasher, 1996, and these reverse faults allow us to infer that the late Eocene was experiencing the early stages of compression across the Taranaki. This compression can be linked to the subduction of the Pacific Plate below the Australian Plate during this 40-35 Ma period (Holt and Stern, 1994). The largest of these faults include the Taranaki Fault, striking NE-SW, are found almost to be vertical, and most likely to have occurred between 30-40 Ma (Reilly et al, 2015) (See Figure 2.4, C). During the late Eocene there was also a significant change in the pole rotation of the Pacific – Australian subduction boundary, moving from a NE – SW trend to a more E – W orientation (Reilly et al. 2015), and by ~3 Ma changing to a SE – NW direction.

After the development of the Taranaki passive margin had come to an end towards the end of the Paleogene, a new phase of swift subsidence began, starting gently at ~35 Ma (Figure 2.4, D) before increasing rapidly after 28 Ma (Runangan – Whaingaroan) (King and Thrasher, 1996). Evidence for this subsidence having occurred comes from Hayward (1990), where his calculated paleodepth, tectonic, corrected and uncorrected subsidence curves all indicate that towards the Mid to Late Whaingaroan stage boundary (30-29 Ma, Late Oligocene) the water depth increased, inferred from foraminiferal assemblages. Greatest levels of subsidence were seen along a NE – SW trend, and combined with the south-eastward migration of the subsidence locus (King and Thrasher, 1994), and these levels of subsidence can be hypothesised to be linked to tectonism, although sediment loading is also a theory that King and Thrasher (1996) have kept as an option for explaining this. Holt et al, (1994), however, postulate that the platform subsidence can be ascribed to the hydrodynamic forces associated with subduction process, with mantle flow initiating subduction of the Pacific Plate and this in turn led to the downward deflection of the Australian Plate. Alongside this subsidence there was also a considerable amount of sedimentation that occurred, which was affected by the rapid subsidence enhancing the marine transgression that was taking place across the basin during this time (King and Thrasher, 1994).

2.2.3 Third Phase (Oligocene - Recent)

The Waitakian (Late Paleogene – early Miocene), ~21-22 Ma (Figure 2.4, E), saw a revival of tectonic activity across the Taranaki's Eastern Margin in the form of a number of parallel thrusts that step basement up to the east, causing a zone of shortening known as the Taranaki Fault Zone (King and Thrasher, 1994). This is a major indicator of the beginning of the third phase of the basin's development. The timing of the thrusting is deduced from the nature and age of the sediments of the eastern basin wells according to King and Thrasher (1994), with an increase of terrigenous detritus at the beginning of the Miocene, oldest rocks found lying over the basement are early Miocene and allochthonous, and the deep water faunas in these sediments show that these rocks were emplaced directly onto the thrust foredeep at bathyal water depths >1500m. The result of this basement overthrusting was to extend the foredeep trough westwards, giving the foreland basin an asymmetric profile, seen in cross-section as a westward-thinning depositional clastic wedge (King and Thrasher, 1996). Another major feature of this period and this region is the Taranaki Fault itself, a west-directed, low angle thrust (King and Thrasher, 1994), hypothesised to be a splay off of the Alpine fault by Knox (1982), but later this theory was improved upon by King (1990), who proposed that, while still related to the Alpine Fault, it was initially derived from a proto-Alpine fault from a transform system through the central North Island in the mid-Oligocene. The convergence at this point in the basin development also saw the creation of the Tarata Thrust Zone, a north-trending belt

of sledrunner-type forethrusts, and their propagation history coincides with that of the Taranaki Fault to the east of this zone (King and Thrasher, 1996).

This period of compression throughout the Miocene is consider by King and Thrasher (1996) as fundamental moment in the basin's history and the result of this action was to lead to the propagation of the subduction zone to southwards to it became positioned to the east of the North Island, and the associated transform zone being rotated clockwise so as to be sub-parallel with the plate vectors (King and Thrasher, 1996). This in turn led to a phase of oblique-slip movement across the south-eastern margin of the pre-existing transform fault, followed by predominantly dextral strike-slip movement of this transform zone, and together these led to the truncation and formation of the Alpine Fault Zone (White and Green, 1986). The formation of the Alpine Fault Zone is important for the Taranaki Basin because as mentioned above it has been hypothesised to have instigated the formation of the Taranaki Fault. The cessation of the contraction/convergence phase across the basin occurred during the Waiauan (~11-13 Ma), marked by a change from uplift to subsidence in the northeast of the basin, and this change is thought to be associated with the onset of Mohakatino volcanism that occurred between the Lillburnian to the Kapitean (15.1-5.33 Ma) (Figure 2.4, F) (King and Thrasher, 1996).

The later period of basin development was characterised by continues plate boundary deformation causing significant extension in eastern regions, such as the Northern and Central Grabens, and crustal downwarp forming the Toru trough/South Wanganui Basin, and these are defined as back-arc basins due to their positioning behind Plio-Pleistocene active magmatic arc or obliquely convergent mountain ranges (King and Thrasher, 1996). This period can also be defined by a large influx of sediment predominantly from the Southern Alps which saw a large amount of uplift from the Opoitian to present (5–0 Ma) (Figure 2.4, G), causing a north-westward progradation of the shelf by contributory channels funnelling sediment off the shelf edge and into the New Caledonia Basin (King and Thrasher, 1994). As these sediments emplaced load across the Western Stable Platform in the form of slope/shelf sedimentary wedge, this led to the subsidence of the platform, and in turn opened up new space along the east of the platform for thick shelf succession to infill (King and Thrasher, 1996).

2.3 Geological Structure of the Taranaki Basin

2.3.1 Basement Rocks

New Zealand's basement geology is split between the early Palaeozoic terranes of the Western Province and the late Palaeozoic-Mesozoic Eastern Province terranes, with a suite of Carboniferous-Cretaceous arc-related igneous rocks known as the Median Tectonic Zone (MTZ) dividing these two regions (See Figure. 2.6) (Sutherland, 1999)

The Western Province is defined as a continental fragment of Gondwana formed of Palaeozoic metasedimentary rocks intruded and metamorphosed by Devonian, Carboniferous and Cretaceous granitoids (Muir et al., 2000). These rocks are split into the Buller and Takaka Terranes (Mortimer, 2004) and only occur offshore in two of the wells (Mortimer et al., 1997) (Figure 2.6). The Eastern Province is comprised of volcanic arc rocks, arc derived sedimentary sequences and accretionary complexes of Permian and Mesozoic age which are relics of convergent margin tectonics (Muir et al., 2000). The majority of the Eastern province is made up of the Torlesse Supergroup, a collection of greywacke sequences derived from Permian (c. 260 Ma) aged plutonic rocks (Muir et al, 2000). The rocks of this region are divided among the Brook Street, Murihiku, Maitai, Caples, Rakaia, Bay of Islands and Pahau Terranes (Mortimer, 2004), and their positions can be seen in Figure 2.6

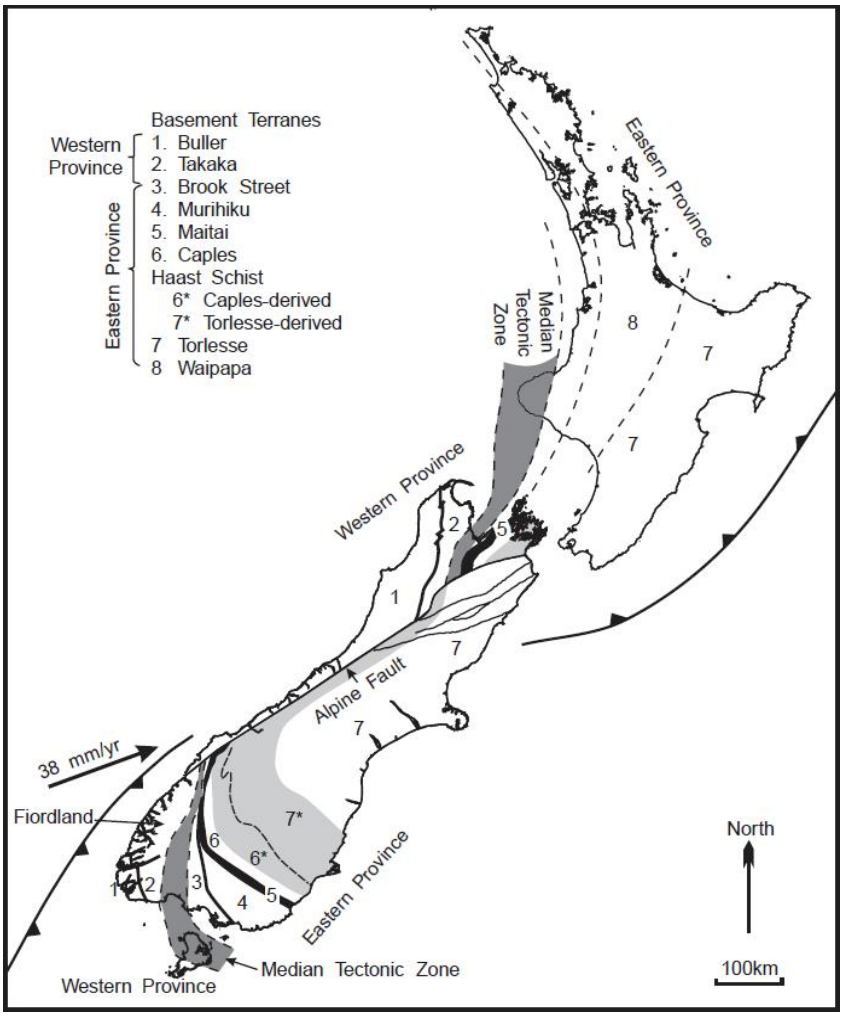

Figure 2.6: Basement terranes of onshore New Zealand. Sutherland et al. 1999

The MTZ is made up of multiple Mesozoic subduction related plutonic, volcanic and sedimentary rocks, dividing the pre-Permian rocks of the Western Province and Permian-Mesozoic accreted metasedimentary rocks of the Eastern Province (King and Thrasher, 1996). These plutonic rocks are primarily calc-alkaline with ages ranging from Mid-Jurassic to Early Cretaceous, although there are

also Carboniferous and Triassic rocks recorded. The origins of the MTZ are hypothesised to be the remnants of a of a long-lived magmatic arc system that developed along the palaeo-Pacific margin. Although not being exposed on the north island, the MTZ lithologies (calc-alkaline plutonic rocks) have been encountered in exploration wells in central Taranaki (Muir et al 2000). The MTZ is also referred to as the Median Batholith by Mortimer (200

4) who defines it as a long lived composite Cordilleran batholith comprising dozens of Devonian to Early Cretaceous gabbroic-granitic subalkaline, I type plutons. These are 1-10 km in size, variably deformed and metamorphosed, and are derived from source rocks of igneous composition.

2.3.2 Onshore Structure

Rocks of the Taranaki Basin are exposed in several locations on the present-day boundaries of the basin on both the North and South Island (Figure 2.7 A and B for positions on the North Island). These Cretaceous – Cenozoic aged rocks are primarily found northwest of Nelson (South Island) and on the west coast of the North Island north of the Taranaki Peninsula (King and Thrasher, 1996). On the South Island, the Late Cretaceous to early Miocene strata is mainly found as part of the north-plunging Wakamarama Anticline, and is lost below the subsurface as you continue north, while also being seen in the Takaka and Aorere valleys, Moutere Depression and Picton (King and Thrasher, 1996). Relevant to this study however is the exposed outcrop along west coast of the North Island. Here the strata of Early to Late Miocene age outcrop is found almost continuously along this section of the coast, and as can be seen in Figure 2.7 A, the Miocene sedimentary rocks extend from the northern side of the Taranaki Peninsula as far north as Nukukakari Bay. These exposed Miocene beds dip roughly 2-4^{o} to the southwest as part of the regional monocline that tilts in to the western region of the South Wanganui Basin, and this coastal exposure also has a number of normal faults trending SW-NE (King and Thrasher, 1996).

To the north are the Permian – Jurassic metasedimentary basement rocks of the Eastern Province, and to the south is the Taranaki Peninsula which is dominated by the 2581 m high andesitic cone of Mount Taranaki composed of radial lava flows at the centre (Figure 2.7 A). This cone is surrounded by a composite ring plain formed of lahar and tephra deposits, minor lavas, alluvium and sand dunes (King and Thrasher, 1996). In Figure 2.7 B, the position of the specific formations is shown, but the area marked as Undifferentiated has been studied in the fieldwork section of this project and by Utley (1987) and has found there is a combination of Mohakatino and Mount Messenger at such small scale that has made this area difficult to differentiate. The onshore structure in this region is studied in greater detail in Chapter 4 as part of the fieldwork for this project.

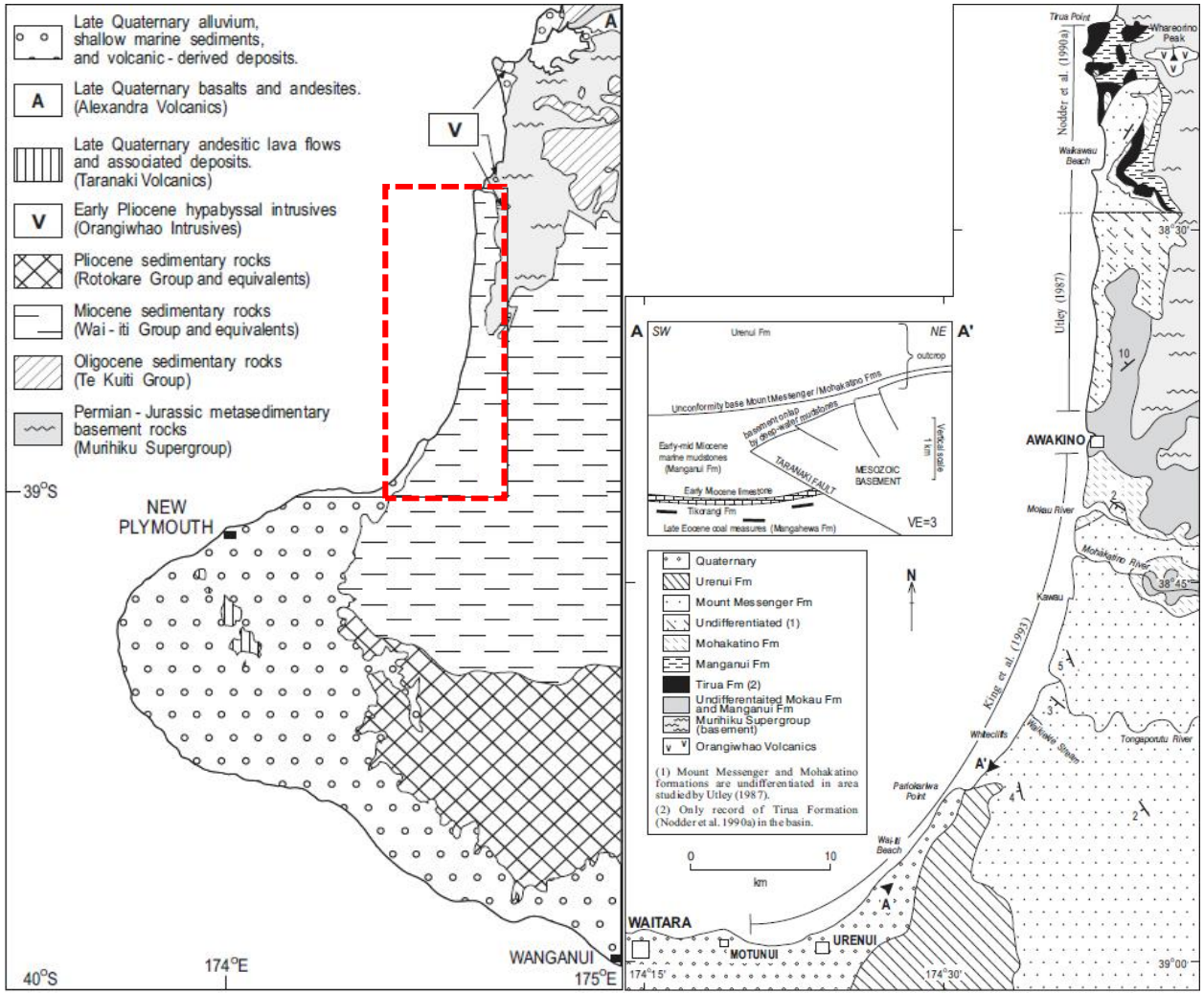

Figure 2.7: A, Left) Simplified outcrop geology of the Taranaki Peninsula and adjacent region. Highlighted area is the region of the Awakino coastline where the Mohakatino Formation outcrops and is the onshore section where fieldwork was conducted. Figure 2.7 B is a more detailed view of this region. B, Right) Simplified outcrop geology of north Taranaki coastal region. Both from King and Thrasher (1996).

2.3.3 Offshore Structure

The Taranaki basin is comprised of two structural regions: The Eastern Mobile Belt (EMB) and the Western Stable Platform (WSP), with the WSP positioned above the Western Province basement rocks and the EMB above the Eastern Province (see Figure 2.6 for positions) and the EMB is the focus of this study. The EMB is an area of interlinked depocentres and structural regions that are the result of Neogene tectonic overprinting of previous basin morphology (King and Thrasher, 1996). The EMB can be sub-divided into two structural sectors which have differing Neogene stress regimes: the northern region and the southern region. The northern sector encompasses the Northern and Central Graben and has experienced 1-3 km of Miocene extension. The southern sector contains the Southern Inversion Zone and the Tarata Thrust Zone and has experienced up to 7 km of contraction. The WSP is considered the antithesis of the EMB by King and Thrasher (1996), as it has been relatively quiescent since the Cretaceous and has a moderately un-faulted, sub-horizontal and regionally subsiding sea floor. The architecture in this part of the basin is made up of Cretaceous-Paleocene relict rift half grabens that are buried by Eocene - Recent progradational basin-fill strata (King and Thrasher, 1996). What is clear from the Northern Graben is that much of the major structural and volcanic development of this region of the basement has occurred in relatively recent geological time. As well as these two primary regions, there are also two sub-provinces that are defined by having less obvious or no-fault control: the MVC and the western extension of the South Wanganui Basin (King and Thrasher, 1996). The South Wanganui Basin, Central Graben, Southern Inversion Zone and Tarata Thrust Zone are not relevant to this study and will therefore not be discussed.

The Northern Graben is as an elongated, extensional feature orientated NNE-SSW, and its boundaries are defined as being the Cape Egmont Fault Zone to the west and the Turi Fault Zone (a collection of subparallel normal faults that progressively step basement and overlying strata down to the northwest) to the east, rather than the Taranaki Fault in the east as it was a relict feature by the time of the Late Miocene (Richardson-Land, 2017). The southern limit is around the offshore northern Taranaki Peninsula while the northern boundary is less well defined as it continues to extend into the Northland Basin, as can be seen in Figure 2.2. These features acted as the controls on the overall sedimentation for the whole graben during the Late Neogene. The Northern Graben itself has a number of faults that are present between east-west boundaries, with the faults in the west downthrown to the east, and then the eastern faults being downthrown to the west forming the graben structure. The faults of the Northern Graben have been identified as of Pliocene age through the relative sediment thickness and differential offset of the Pliocene reflector (King and Thrasher, 1996). The graben's development during the Late Miocene – Early Pliocene was caused by the activation of the Kahawai Fault combined with the extension regime in the northern region of the basin, and together these caused a triangular wedge shape opening wider to the north by 1-3 km over time (Richardson-Land, 2017).

This can be seen in Figure 2.2 where the faults of the Northern Graben are in closer proximity to the south and wider spread to the north. This shape is thought to have been caused by the clockwise rotation of the Australia Plate as part of the Australia-Pacific plate boundary zone (Giba et al., 2010)

The Northern Graben experienced a period of volcanism during the Lillburnian to the Kapitean (15.1-5.33 Ma) and this period of Middle to Late Miocene volcanism is hypothesised to be sourced from the west-directed subduction of the oceanic Pacific Plate below the continental Australian Plate along the Hikurangi margin, roughly 400 km east of the arc, from the geographic position and the andesitic composition of the produced volcanoes. See Figure 2.2 for geographical position in relation to other major features of the northern Taranaki Basin. This region of volcanism forms the MVC, a collection of 20 volcanic cones and multi-vent volcanoes of Miocene age that erupted offshore, covering ~3200 km^2, and with most of these erupting at bathyal depths although some larger comes (>1500 m) have been truncated by erosion and can be inferred to have extended above sea surface (Stagpoole and Funnell, 2001). These volcanoes are made up of calc-alkaline andesites, basaltic andesites, and subordinate basalts (Bergman et al, 1992) occurring primarily between ~14-11Ma, although eruptions occurred up to 7-8 Ma, and occur along a roughly NNW trend along the axis of the Northern Graben (King and Thrasher, 1996). The MVC represents the southernmost extent of a regionally continuous 400 km long belt of andesitic Miocene complexes that occur primarily offshore in the Taranaki and partly onshore Northland (Bergman et al., 1992), and these northern Northland Volcanics differ from the Mohakatino Volcanics in the Taranaki as they are slightly older and larger on average (King and Thrasher, 1994). The north-south difference between the two Mohakatino and Northland volcanic complexes is shown in Figure 2.2 where they are labelled with different shades of grey. The Mohakatino volcanoes offshore have been progressively onlapped and overtopped by Late Miocene to early Pliocene deepwater deposits, and then finally buried by the Plio-Pleistocene Giant Foresets Formation succession up to 4 km thick in some regions, and this burial has preserved many of the volcanoes and their features.

The subsurface structure and sediment thickness of the Taranaki has been characterised on four primary reflectors. These include top seismic basement at the base of the Cretaceous-Cenozoic succession, top Cretaceous, top Eocene and top Miocene (King and Thrasher, 1996). The basin has undergone multiple deformation types and different times, with a large number of faults being generated during the Late Cretaceous rifting and this has led to a very complex pattern of faulting that characterises the subsurface structure. A major feature of the basin is the Taranaki Fault which is found on the eastern edge of the basin, and is a Miocene aged, east dipping, subsurface, reverse fault with an offset of up to 6 km and extends over 600 km across the continental crust of western New Zealand. This fault makes up the western edge of a north trending basement ridge that forms the concealed Patea-Tongaporutu High in the south of the basin and the emergent Herangi Range on the

Awakino coastline (King and Thrasher, 1996). The only onshore faulting in the region is recorded is seen on the northern part of the Taranaki Peninsula with the Inglerwood, Norfolk and Oaonui faults, all striking northeast along the same trend as the Cape Egmont Fault, as well as those within the Central Graben (King and Thrasher, 1996). However, these faults are too far to the south however to have any effect on the study area. Offshore, there is evidence of Late Quaternary faulting, and the main study of these offshore faults has been done on the Cape Egmont Fault Zone and in particular the Cape Egmont Fault itself. Yet again though, this fault zone is not close enough the study area to be expected to have any effect on the strata.

2.4 Stratigraphy

The lithofacies discussed here as part of the stratigraphy are only the Miocene to recent aged sediments that are found in the offshore wells Kora-1/1A,-2, -3, Kahawai-1 (see Figure 2.3 for the stratigraphic sequence and the highlighted region is the section of the basin relevant to this study) and from the onshore section of the study area, and also part of the clastic sequence that the Mohakatino is a part of the overlying Giant Foresets Formation in the offshore region and Mount Messenger Formation are not discussed here as they are outside the scope of this study. The locations of these offshore wells and the onshore section of the study area where the Mohakatino occurs are shown in Figure 2.1.

2.4.1 Manganui Formation

The Manganui Formation was defined by King and Thrasher (1996) as a Miocene aged (Langhian to Clifdenian) (Bernabéu et al. 2010) calcareous, deepwater mudstone, with siltstone as the main secondary lithology that that encompasses all of the Miocene sediments that cannot be conclusively differentiated into separate, distinctive formations. The formation was deposited as a combination of large rates of subsidence in the foredeep and low sediment volume supply during the early Miocene and these led to an increase in the water depth and therefore accommodation space, then infilled by the Manganui at bathyal depths (King and Thrasher, 1996). The Manganui Formation is seen in both the onshore and offshore regions, occurring in the Kora-1/1A well and at Location 1 and 3 in the fieldwork area (See Section 4.2.1). Within Kora-1/1A the Manganui Formation is found over 317 m depth and from the wireline logs it can be identified by a GR reading of around 50 and a relatively consistently low RHOB reading. In the onshore region, the Manganui is found on the shoreline at the Awakino Heads where it occurs as part of a sequence consisting of the Manganui, Mangarara and Mohakatino (in ascending order) as well as part of the same succession slightly further inland mid-way up the slope of Pahaoa Ridge. The extent of the Manganui Formation across the Taranaki Basin can be seen in Figure 2.3 where it is a major unit through-out the basin. However, in the onshore region the Manganui Formation is a more minor unit, appearing at the base of the generalised

stratigraphic sequence for the Awakino coastline in Figure 2.8 where it is the most basal unit and is only up to 100m thick.

2.4.2 Mangarara Formation

The Mangarara Formation is a middle Miocene (Clifdenian to Waiauan), thinly bedded (1-60 m), laterally discontinuous, calcareous (40-90%) facies made up of pure limestone, bioclastic sandstone and conglomerate (Bernabéu et al. 2010). It is interpreted to have been derived from mass transport deposits and occurs within the hemiplegic slope mudstone of the Manganui Formation and is also stratigraphically associated with the redeposited Moki Formation, and then overlain by the Mohakatino Formation (Fig. 2.3). According to Bernabéu et al (2010) the material for the formation is derived partly from an eastern contemporary shelf but primarily the material is made up of skeletal carbonates that come from shoal carbonate facies that are part of the isolated basement highs, such as the Patea-Tongaporutu High. Within the study area the Mangarara lithologies are only seen at the Awakino Heads location and also along the Pahaoa Ridge deposited as part of a submarine channel system. They are part of the same sequence mentioned previously. The Mangarara Formation does not appear in any of the study wells and this is due to the source of the sediments being from the south, in particular regions such as the Patea-Tongaporutu High, and was not able to be transported far enough north to be encountered in the Kora wells. The Mangarara Formation is not significant enough or large enough to be present in a stratigraphic column for a basin wide stratigraphic column (Fig. 2.3), but it can be seen at a more local level in Figure 2.8. Here the Mangarara is simplified as a formation of primarily bioclastic sandstone and occurs in a thin band up to ~20m thick below the Mohakatino Formation and overlaying the Manganui Formation in the simplified stratigraphic sequence for the Awakino coastline.

2.4.3 Mohakatino Formation

The Mohakatino Formation is characterised as Middle to Late Miocene (Lillburnian/c. 14Ma to Kapitean/c. 8Ma) (King and Thrasher, 1996; Strogen 2012; Stagpoole and Funnel, 2001) sandstones and siltstones that have a significant andesitic detritus content, forming the uppermost unit of the submarine fan succession sourced from the MVC (Shumaker, 2016; King and Thrasher, 1996; Bergman et al., 1992), and is found in coastal outcrops on the Awakino coastline and in the wells drilled along the flanks of the Kora volcano (Figure 2.3 for position in the stratigraphic column). This succession is comprised of the deep marine mudstone of the Manganui Formation at the base, overlain by the lenticular packages of course, bioclastic sandstones and conglomerates of the Mangarara Formation, and then followed by the Mohakatino Formation making up the final part of the succession and up to 2 km thick (Shumaker, 2016), and can be seen clearly at Location 1 of this study's fieldwork (See Section 4.2.1). The Mohakatino Formation interfingers and is buried by the

south east derived submarine channel and fan system Mount Messenger Formation at the onshore region of the study area and buried by the Giant Foresets Formation, the Urenui and Kiore Formations offshore. The Mohakatino occurs across the study area, being found in the Kora-1/1A, -2, -3, and Kahawai-1 wells (See Chapter 3), and at a number of locations along the Awakino coastline (See Chapter 4). The Mohakatino Formation is of interest for this study as local hydrocarbon shows in the offshore wells have suggested reservoir potential for these volcaniclastic submarine sediment gravity flow deposits.

The Mohakatino Formation consists of sandstones, siltstones and mudstones, primarily characterised by a prominent andesitic detritus, and these were originally interpreted as re-worked marine and airfall deposits (Utley, 1987; Bergman et al., 1992; King and Thrasher, 1996). However, recent work by Shumaker (2016) has recognised that the andesitic volcaniclastics are made of dominantly hypabyssal volcanic rock fragments and that there is no evidence of vesicular or pumiceous material. The absence of vesicular materials does not indicate eruptive depth of the volcanoes, but rather implies that sector collapse or deep-seated mass wasting on over steepened volcanic flanks, as opposed to ash generating eruptions, dictated the main method of sediment production from the Mohakatino volcanoes. Despite this, anomalous pumice deposits are found throughout the formation, indicating variability in the eruptive style of the MVC, or it could be because of windblown ash or drifting pumice rafts from unrelated submarine or subaerial volcanoes (Shumaker, 2016). The variability of eruptive style as a hypothesis can be further backed up by the presence of high quartz percentages in samples and thin sections, indicating that there have been dacitic eruptions mixed in the andesitic eruptions of the Kora volcanoes.

The depositional process of the Mohakatino is summed up in Figure 2.9 modified from Sharman (2014), and while this diagram was originally used to demonstrate the emplacement of the North Awakino Mass Transport Deposit (NAMTD), it still provides the best schematic representation of the depositional region of the Mohakatino. Here the MVC, which is represented as general stratovolcanoes, can be seen offshore the modern coastline of North Island and those of 16-8Ma age are the source of the Mohakatino submarine fans. The material is hypothesised to have flowed down channels along the middle to lower slope of the continental shelf, having been made actively mobile due to sector collapse/mass wasting. These channels carried the Mohakatino material down the flanks of the volcanoes and further up the shelf slope to the south east/east. The material eventually ran out of energy due to its distal position from the MVC source and the increased gradient of the slope due to the Herangi High in the east (Figure 2.9 B) leading to the Mohakatino submarine fan deposited across the Awakino section of the modern-day coastline and the buried Taranaki fault. The formation of the NAMTD coincides with the uplift of the Herangi bathymetric high (Figure 2.9), and the increased gradient led to the extensive soft sediment deformation and slumping caused by mass-movement

instability that extends for nearly 11 km along the Taranaki coastline. The NAMTD is a Late Miocene (Tortonian/Tongaporutuan, c. 11-7Ma) ~12 km wide and up to 80 m high soft sediment deformation feature (Sharman, 2016). This significant feature was deposited via gravity flow and suspension sedimentation of volcanic debris through the water column as part of as fan apron setting to the east of the MVC onto the continental slope. The NAMTD features prominently at the Piopio Station region of the fieldwork in section 4.2.4. To the south of this depocentre the Mount Messenger Formation prograded to the north and after the deposition of the Mohakatino and then the reverse collapse of some of this material forming the NAMTD, the majority of the distal Mohakatino material is then buried by the Mount Messenger Formation. Figure 2.9 does not show the extent of the proximal deposition and so it is inferred that the proximal material is restricted to the channels and the flanks of the volcano as aprons of volcaniclastic debris on the positive relief of the volcanoes of the MVC such as the Kora volcano, the relief and structure of which can be seen in Figure 2.10. It also does not show the burial of the offshore region, which occurred as rapid sedimentation and progradation of the Giant Foresets Formation during the Plio-Pleistocene.

The Mohakatino Formation is identified in wireline logs from Kora-1, 2, 3 and Kahawai-1 by the low uniform gamma-ray (<50 API), with moderately good porosity (Minimum and maximum values: 2.7-38.4% He; Mean Value: 18.62% He) but poor to moderate permeability (Minimum and maximum values: 0.004-4970 mD; Mean Value: 61.02 mD). Side Wall Coring (SWC), XRD and core analysis by the GNS, New Zealand, as well petrographic, point counting, detailed petrographic analyses, SEM, SEM-EDX analysis undertaken as part of this study has indicated that Mohakatino is composed of quartz andesites. The primary constituent minerals are plagioclase, quartz, hornblende, minor pyroxene as well as a significant hypabyssal and volcanic rock fragments. The mineral composition of the various lithofacies of the Mohakatino Formation varies between distal and proximal regions (Chapters 3 and 4). As well as constraining the mineralogical component of the Mohakatino Formation, analysis has also identified significant variations in porosity and permeability values over small distances. A large proportion of these values indicating potential reservoir quality. Hydrocarbons in the Mohakatino Formation were sourced from the Late Paleocene Waipawa Formation marine source rock (GNS PBE, 2013), one of two source rocks for the northern Taranaki Basin. The other is the Late Cretaceous coals and interbedded shales of the Rakopi and North Cape Formations. These are the principal source rocks for the rest of the Taranaki Basin (Stagpoole and Funnell, 2001). While the Mohakatino does not have commercially viable reserves of hydrocarbons, it does have the source rocks, reservoir characteristics and traps that could act as a hydrocarbon reservoir. The lack of an appropriate seal appears to have allowed oil to seep to the surface. This is one of the fundamental questions of this study and is explored in later chapters. Had an impermeable seal formed across here, would the Mohakatino been able to function as an economic oil field in the offshore region?

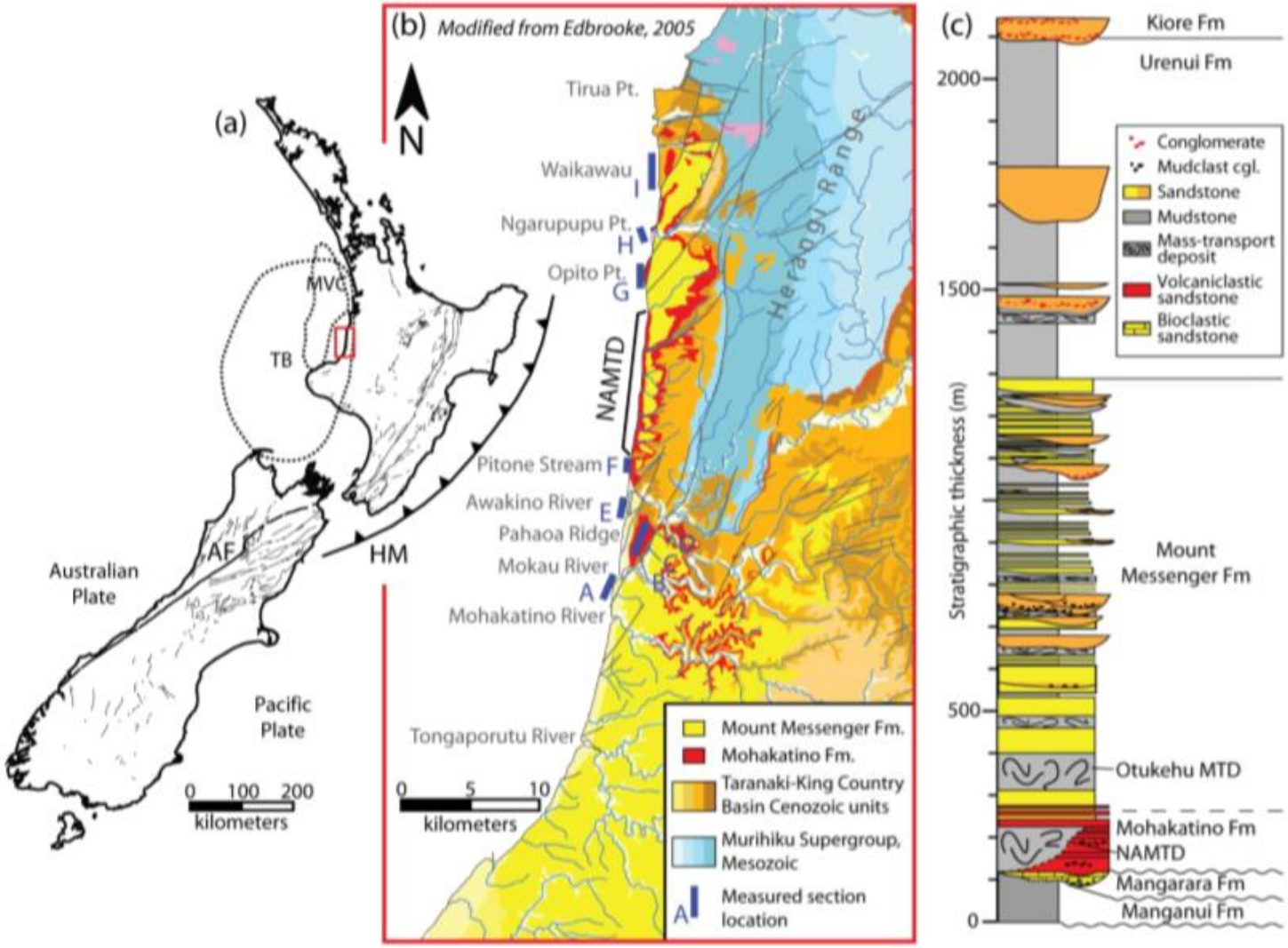

Figure 2.8: (A) Map of the New Zealand coastline showing major onshore faults (AF = Alpine Fault), Hikurangi margin (HM), Taranaki Basin (TB), and Mohakatino Volcanic Centre (MVC). (B) Simplified geologic map of the study area showing the locations of stratigraphic sections from Shumaker, 2016. (C) Simplified stratigraphic column of middle to late Miocene stratigraphy of Awakino coast, Taranaki Basin. Sourced from Shumaker, 2016.

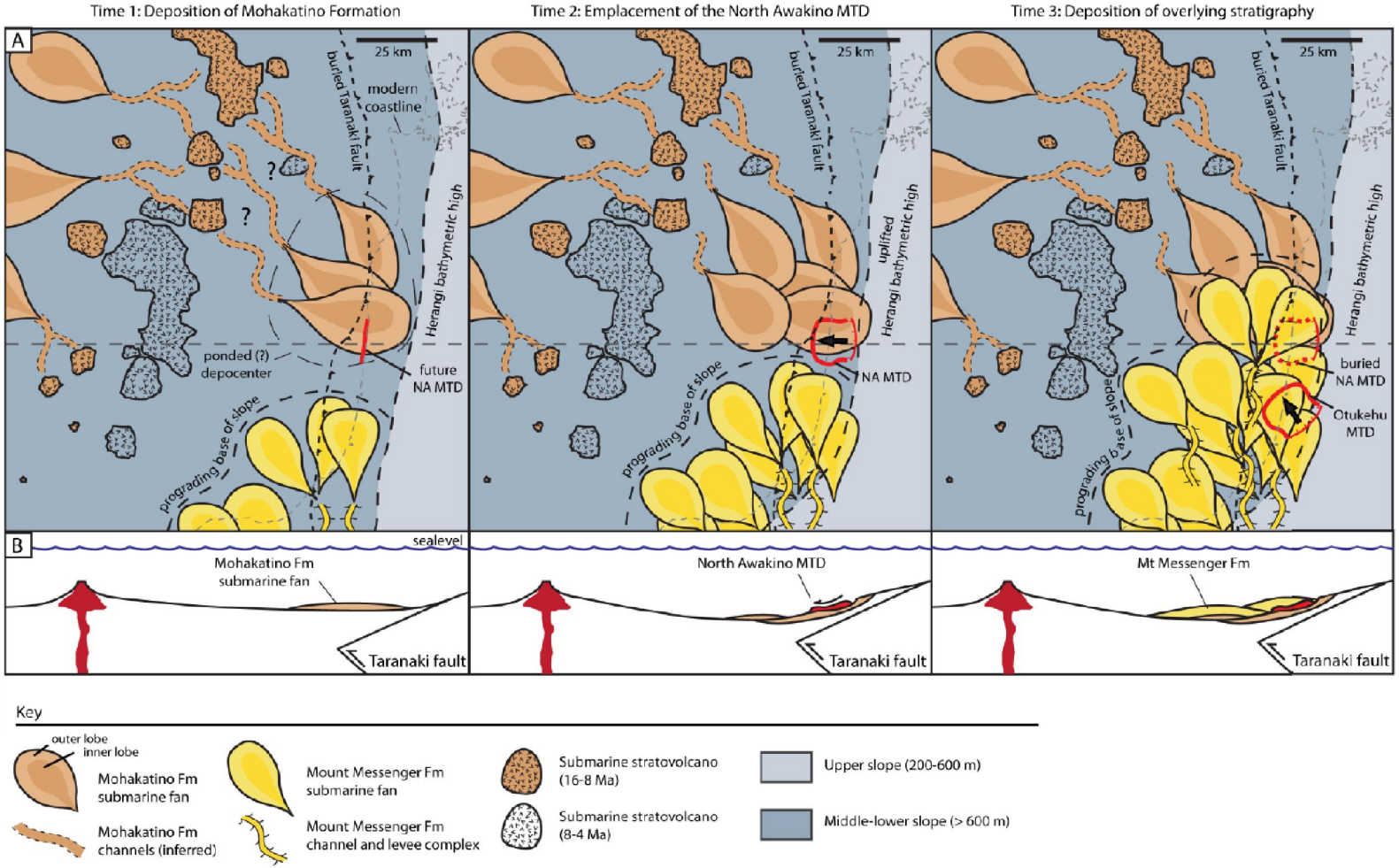

Figure 2.9: Schematic representation of the paleogeography of the north eastern Taranaki Basin and the Mohakatino Formation depositional system during the late Miocene. A) Plan view maps of the region with the stratovolcano/MVC volcano locations, paleobathymetry, Herangi High location, and depositional locations of the Mohakatino and Mount Messenger Formations. B) Schematic cross sections of the region. Locations of cross sections shown as a dashed black line in (A). Sharman, 2014.

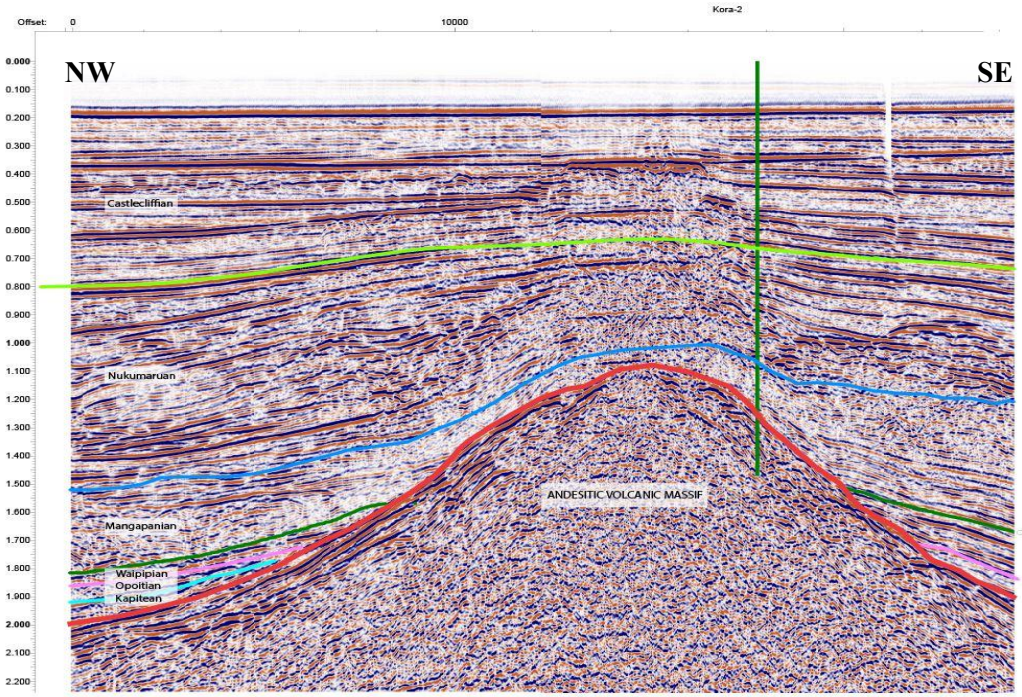

Figure 2.10: A selection of seismic lines across the Kora volcanic structure. New Zealand Geological Units are used to define horizons, the Kora volcano is labelled as the andesitic volcanic massif and shows the doming structure, and the position of Kora-2 penetrating the flank of the volcano to the SE are all shown. Richardson-Land (2017).

2.5 Conclusions

The Mohakatino Formation of the Taranaki Basin, New Zealand is sourced from the submarine Mohakatino Volcanic Centre (MVC). The volcaniclastic sediments deposited on the flanks of these volcanoes are part of a series of low-density turbidity current deposits that form laterally continuous thin-to-medium bedded sandstones and siltstones with a significant andesitic component. The Mohakatino Formation is deposited in a proximal lobe setting around the MVC. This has been investigated around the Kora volcano where the Mohakatino Formation is deposited on the volcano's flanks, with material extending to the Awakino coastline north of the Taranaki Peninsula. The Mohakatino Formation is an example of how submarine volcanoes can be significant sediment sources in tectonically influenced marine settings, and how volcaniclastic sediments have the potential to act as hydrocarbon reservoirs. The NAMTD and sediment gravity flows of the Mohakatino Formation are spectacularly exposed in the coastal cliffs and wave cut platforms of the Taranaki Awakino coast, providing distal examples of sediment gravity flows.

Chapter 3

A Petrographic Study into Reservoir Quality Analysis of the Offshore Mohakatino Formation, Northern Taranaki Basin, New Zealand.

3.1 Introduction

The Taranaki Basin is New Zealand's only petroleum producing basin, with recoverable reserves estimated at 332 million barrels of oil (mboe) and 5.2 trillion cubic feet (TCF) of gas (King and Thrasher, 1996) and the vast majority of these reserves (300 mboe and 5.0 TCF of gas) are found in the five largest fields (Maui, Kapuni, Kupe South, McKee, and Waihapa/Ngaere), while the remainder of the reserves are distributed among several other fields that are too small or have too poor reservoir quality to be economic (King and Thrasher, 1996). The basin is comprised of two structural regions: the active Eastern Mobile Belt (EMB) and the passive Western Stable Platform (WSP), and the EMB is made up of multiple Neogene structural elements including the foreland basin, fold thrust belt, volcanic arc, and back arc extensional graben. All of these Neogene aged structural features of the EMB act as traps with in the fold thrust belt for the previously mentioned hydrocarbons of the Taranaki Basin (See Figure. 2.2).

In the northern sector of the EMB is the Miocene aged Mohakatino Volcanic Centre (MVC), a collection of 20, andesitic arc derived, submarine volcanoes, covering an area of ~3200 km^2 and most were erupted in bathyal water depths and entombed by Pliocene and Pleistocene sediments. These are clearly seen in seismic reflection profiles (Figure 2.7). Rapid subsidence of as much as 4 km since the middle Miocene created a huge depocentre. Voluminous clastic sediment supply from the south and east was deposited as the Giant Foresets Formation, which filled in bathyal water depths to shelf level by the Pleistocene (Stagpoole and Funnell, 2001). Within this collection of volcanoes is the Kora volcano, a 10-12 km diameter and ~1 km thick subsurface volcanic dome complex located on the western margin of the Northern Graben (Figure 2.2). The onset of volcanism in the Mohakatino Volcanic Centre (MVC) began in the early Miocene with intra-basement emplacement followed extrusive submarine volcanic eruptions which peaked between 14 and 11Ma (King and Thrasher, 1997). This phase of volcanism coincided with pronounced tectonism associated with the developing Australian/Pacific plate boundary and migration of the pole of rotation away from New Zealand between 21 and 10 Ma (Walcott 1987*;* Peter Kamp *pers comm*). Mohakatino volcanism finally ceased at approximately 7-8 Ma. Onlapping onto the eastern flanks of this volcano are deposits of the Mohakatino Formation, a collection of Middle to Late Miocene sandstones and siltstones that are characterised by significant andesitic rock detritus and it forms the uppermost unit of a large submarine fan succession as a volcaniclastic formation sourced from the andesitic volcanoes of the MVC (Shumaker, 2016; King and Thrasher, 1996; Bergman et al., 1992). The Mohakatino Formation also occurs onshore along the Awakino coastline of North Island (see Chapter 4 for more details). In

1988, Arco Petroleum NZ commenced a hydrocarbon exploration programme in which a series of wells were drilled around the Kora volcanic complex. In this study the offshore Kora wells (Kora-1/1A, Kora-2, and Kora-3, and also Kahawai-) form the main focus with particular interest in the volcaniclastic Mohakatino Formation and its variable reservoir quality. Volcaniclastic rocks are not usually considered prime hydrocarbon exploration targets, but as the demand for hydrocarbons increases, more complex, non-conventional plays are being targeted in volcanic margin settings. Consequently, it is important to understand the reservoir quality of volcaniclastic rocks. The andesitic volcaniclastics contain a high proportion of mechanically and mineralogically unstable components which generally cause a faster deterioration in reservoir quality upon burial than is found in siliciclastics. The results of the detailed petrographic analysis and mineral distribution in the proximal submarine fan deposits, onlapping on to the Kora volcano are analysed and used to help constrain the primary control on reservoir quality.

3.2 The Mohakatino Formation

The Mohakatino Formation has been previously interpreted as a deep-water submarine fan system. The widely recognised high proportion of hypabyssal rock fragments (intrusive volcanic rocks emplaced at shallow depths (> 2km) in the submarine fan deposits suggests that sector collapse of volcanic flanks of the Kora Volcano was an important sediment-generating mechanism or deep-seated mass wasting on over-steepened volcanic flanks, was an important sediment-generating mechanism.

Petrographic study reveals two distinct compositions in the Mohakatino Formation: i) a plagioclase, pyroxene, and hornblende mineral assemblage expected from an andesitic arc source, with little to no quartz present and ii) a relatively quartz-rich sections and dominated by recycled metamorphic grains. Sand- and gravel-sized clasts from the volcaniclastic facies reveals considerable variety in composition. Crystal-poor rock fragments, typically characterized by large plagioclase crystals in a devitrified groundmass, are interpreted as lavas and ashes (Shumaker, 2016). Crystal-rich rock fragments, exhibiting 30-50% or greater proportion of well-formed crystals, are interpreted as hypabyssal rocks. Hypabyssal rocks represent an intermediate between volcanic and plutonic rocks; they cool moderately slowly, at 1-2 km depth in the crust, resulting in larger crystal sizes and greater proportions of crystals than extrusive volcanic rocks (Winter, 2001). They can be associated with the interiors of the volcanic cones themselves, or with dikes and sills emanating from the volcanic centre.

There is an absence of any recognisable pumice or vesicular tephra (e.g., preserved vesicles or fragmented bubble walls) was noted in the analysed thin sections from the Kora wells in this study and others (Bergman et al, 1992; Maier et al, 2016). Though a depth-dependent control on magma vesiculation has been proposed (e.g., volatile fragmentation depth of Fisher and Schmincke, 1984; or pressure compensation level of Fisher, 1984), explosive, pumice-forming eruptions have been

documented at depths greater than 1 km for rhyolitic, caldera-forming volcanoes (Rotella et al., 2015) and 3 km for basaltic volcanoes (Head and Wilson, 2003; Clague et al., 2009). Magma decompression rates and weight percent of volatiles have also been proposed as key factors in the eruptive behaviour of deep marine volcanoes (Rubin et al., 2012; Cas and Giordano, 2014) that can be attributed for the lack of pumice and vesicular tephra. While these studies could indicate that the MVC did not produce vesicular materials during the period of Mohakatino Formation deposition, there are explanations for these observations: Firstly, that the Kora wells were drilled and their samples taken from the flanks of the cone where non-vesicular materials are dominant, and pumice-rich deposits and tephra are more often deposited on the ring plains; Secondly, large pumice-producing Plinian eruptions are generally not the main eruptive style of andesite stratovolcanoes; Thirdly, the sampling from cores and cuttings on these petroleum wells are not representative of the whole volcanic pile; and finally, vesicular tephra and pumice are especially susceptible to weathering, breaking to form clays for example, and becoming unrecognisable. In summary, the lack of evidence for the vesicular tephra across a limited field of study does mean it was not there necessarily. Thus, the absence of vesicular materials in the Mohakatino Formation does not inform the eruptive depth of the volcanoes or the eruptive style. There is still much more research to be conducted around the Kora volcano to find an answer to this. However, the available evidence does support the interpretation that sector collapse, rather than ash-generating eruptions, was the primary mode of sediment production from the Mohakatino volcanoes. If eruptions were effusive rather than explosive, thermal quenching and fragmentation of lavas may also have been an important mechanism for producing readily transportable clasts, which would be subject to further breakdown and abrasion during transport.

3.2.1 Kora-1A

Kora-1A is a plugged and abandoned offshore hydrocarbon exploration well operated by ARCO Petroleum NZ Inc., found on the SE flank of the submarine Kora volcano off the Awakino coast of North Island, New Zealand (ARCO, 1988a) (Figure 3.0). Drilling was started on 05/02/1988, and abandoned 17/02/1988, reaching a total drilled depth of 3421m AHBRT (ARCO, 1988). A summary of the well's geological features as listed in ARCO (1988a) can be found in Table 3.1. The Mohakatino Formation in the Kora-1A well has four thin sections available for analysis from the GNS (Kora-1A 1798m (1) and (2), 1827.5m and 1901.64m), and their positions in the well are shown in the composite log in Figure 3.1. The average mineral composition for the Kora-1A samples is shown in Figure 3.3 (as calculated as part of this study through point counting), and is also plotted against the averages of the other wells, demonstrating how the primary mineral constituents vary across the study area. There has also be QEMSCAN work that has been done by the GNS on Kora-1A samples. However, this QEMSCAN work is of no use for this study because analysis was undertaken on drill cuttings are not representative of the section, the cuttings were collected from sections of the well

which have not had any other analysis done on them, and they don't overlap with the thin sections available.

3.2.2 Kora-2

Kora-2 is a plugged and abandoned offshore hydrocarbon exploration well operated by ARCO Petroleum NZ Inc., found on the SE flank of the submarine Kora volcano off the Awakino coast of North Island, New Zealand (ARCO, 1988b) (Figure 3.0). Drilling was started on 03/06/1988, and abandoned 25/06/1988, reaching a total drilled depth of 1656m AHBRT (ARCO, 1988b). A summary of the well's geological features, collated from ARCO (1988b), can be found in Table 3.1. Kora-2 has two thin sections (Kora-2 1323.1m and 1330.5m) and their positions are shown in the Kora-2 log (Figure 3.4) as well as the characteristics and features of the Mohakatino Formation in the well. The petrography of the Mohakatino Formation in Kora-2 is established in Figure 3.2 where annotated photomicrographs are plotted against each other, and the average mineral composition from point counting analysis for the Kora-2 samples is shown in Figure 3.3. QEMSCAN analysis has been done on both samples for Kora-2, and these helped provide a clearer picture of the mineralogy of the Mohakatino Formation Kora-2 as well how these mineral constituents interact with each other and where they can be found in the slide samples.

3.2.3 Kora-3

Kora-3 is a plugged and abandoned offshore hydrocarbon exploration well operated by ARCO Petroleum NZ Inc., found on the SE flank of the submarine Kora volcano off the Awakino coast of North Island, New Zealand (ARCO, 1988c) (Figure 3.0). Drilling was started on 02/07/1988, and abandoned 03/08/1988, reaching a total drilled depth of 1934m AHBRT (ARCO, 1988c). A summary of the geological features of the well, collated from ARCO (1988c), can be found in Table 3.1, and a schematic representation of the Mohakatino Formation and its associated features in the well in demonstrated in Figure 3.5. There was only one thin section available for analysis (see Figure 3.2 C) at 1808.55 m depth in the Kora-3 well and so these results cannot be said to be representative of the whole 575 m of Mohakatino Formation shown in the Kora-3 log (Figure 3.5). The point counting analysis of mineral composition done as part of this sample is shown in Figure 3.3. There was no QEMSCAN analysis available from the GNS for this sample slide.

3.2.4 Kahawai-1

Kahawai-1 is a plugged and abandoned offshore hydrocarbon exploration well operated by NZ Oil and Gas Services Ltd (NZOG)., found to the NE of the submarine Kora volcano off the Awakino coast of North Island, New Zealand (NZOG, 1990) (Figure 3.0). Drilling was started on 24/11/1990, and abandoned 28/12/1990, reaching a total drilled depth of 3449m AHBRT (NZOG, 1990). Kahawai-1 has five samples available from the GNS for the Mohakatino Formation (Figure 3.6) used

in petrographic and microscopic analysis. See Figure 3.3 for averaged mineral composition of these Kahawai-1 samples calculated as part of this study. Three of these samples are also used in Figure 3.2 to demonstrate the variation in the samples not just between the wells but also within the Mohakatino Formation for each well. The material seen in each photomicrograph differs drastically from the others, and no pattern can be seen in the grain size or material relative to depth or position in the well. There has not been any QEMSCAN analysis done by the GNS for Kahawai-1

Figure 3.0: Location Map of Kora wells in relation to other hydrocarbon wells and North and South Islands. Kora-2 and 3 are not represented but are within the red circle. King and Thrasher, 1996

	General Well Information		Lithofacies Information						
Well Name	Location (Lat./Long.)	Total Drilled Depth (m AHBRT)	Formations (Interval, m)	Formation Age	Lithology	Additional Features	Depsotional Environment	Reservoir Assessment	Oil Shows
Kora-1A	(-38.3813627) (173.859521)	3421	Giant Foresets Formation (149.6 - 1781m)	Pliocene to Recent	Claystone interbedded with shelly sandstones and siltstones, becoming less shelly with depth.	Divided into two units dependent on the depositional environment: Upper (149.6 - 993m) and Lower (993 - 1781.2m).	Marine inner to middle shelf in Upper Unit and shifts to upper bathyal in Lower Unit.	No reservoir potential.	No oil show.
			Mohakatino Formation (1781.2 - 2581.5m)	Mid to Late Miocene	Series of pyroclastic deposits with an andesitic component. Dominated by plagioclase, hornblende and quartz.	Material sourced from submarine andesitic with some dacitic eruptions, and these provide quartz source	Marine pyroclastic flows deposited along the flanks of the Kora volcano.	Fair to good porosity and permeability throughout.	Good oil shows between 1785 - 1810m and then fair to 1910m.
Kora-2	(-38.3596214) (173.8485239)	1656	Giant Foresets Formation (158.3 - 1290m)	Pliocene to Recent	Claystone (Soft, grey, fossiliferous), siltstone (grey and argillaceous) and trace sandstone (medium to coarse).	Divided into two units dependent on depositional environment: Upper (158.2 - 905m) and Lower (905 - 1290m). Forams, bivalves, gastropods and echinoids are common.	Marine inner to outer shelf in upper unit and then shifting to upper bathyal to inner/middle shelf environment in the lower unit.	Tuff streaks near base of the formation.	None in Upper Unit. Poor to fair oil shows in tuff streaks 1.5m above the Mohakatino Formation
			Mohakatino Formation (1290 - 1656 (TD)	Mid to Late Miocene	Series of pyroclastic deposits with an andesitic component in Upper Unit. Composition and provenance is similar to that of andesitic stratovolcano. Lower Unit is generally crystalline volcanics with plagioclase and hornblende composition.	Divided into two units dependent on lithology: Upper (1290 - 1557m) and Lower (1557 - 1656m).	Marine pyroclastic flows deposited along the flanks of the Kora volcano in Upper Unit. Lower Unit is submairne intrusive volcanics.	Upper Unit sees good porosity and poor permeability in the top few meters. None reservoir potential in the rest of the unit or in the Lower Unit.	Fair to good oil show in top 4m of formation in Upper Unit. None for the formation.
Kora-3	(-38.3712881) (173.8563019)	1934	Giant Foresets Formation (152 - 1774.5m)	Pliocene to Recent	Siltstone (grey, predominantly quartz) interbedded with argillaceous sandstone in the Upper Unit. Predominantly mudstone with calcareous horizons and silty/sandy lenses in Lower Unit	Divided into two units dependent on lithology and depositional environment: Upper (152 - 965m) and Lower (965 - 1774.5m). Up to 10% bioclasts throughout formation, mainly echinoids, bivalves (macrofossils) and foraminifera (microfossils).	Marine inner to middle shelf at top of formation and shifts to upper bathyal at depth.	No reservoir potential.	No oil show.
			Mohakatino Formation (1774.5 - 1934m)	Mid to Late Miocene	Series of pyroclastic deposits with an andesitic component. Upper unit of formation is hard, unaltered tuff, changing to more altered tuff in the middle unit and then less so in the lowest unit	Divided into three units based on amount of alteration to clay and associated log response: Upper (1774.5 - 1807.6m), Middle (1807.6 - 1870m) and Lower Unit (1870 - 1928m)	Marine pyroclastic flows deposited along the flanks of the Kora volcano.	Poor to fair (generally <10%) in Upper Unit, changing to poor due to higher preportion of clay in Middle Unit, and remaining poor to the base.	Fair shows to 1827m and then trace or no oil shows below this depth.

Table 3.1: Summary of lithofacies and their main features. This does not include data from this study's point counting or the data from the GNS. Information collected from well completion reports for each individual well. Sourced from ARCO (1988a), ARCO (1988b), ARCO (1988c), and NZOG (1990). Continued on next page.

Kahawai-1	(-38.3021172) (174.2474147)	3449	Whenuakura (120.4 - 1036m)	Late Pliocene to Pleistocene	Sandstone (grey, medium grained, moderately well sorted) with minor siltstone and silty claystone interbeds	Volcaniclastic material and shell debris found throughout formation. Some microfauna present.	Shelfal paleodepositional setting, moving from inner shelf at 590m to mid shelf at 900m.	Porous and permeable.	No significant hydrocarbons present.
			Giant Foresets Formation (1036 - 1931m)	Early Pliocene to Late Pliocene	Massive , variably silty mudstone with subordinate interbeds of siltstone and sandstone.	Mudstone becomes increasingly more calcareous with depth. Foraminiferal assemblage reveal regressive depositional environment	Mid-shelfal marine deposition up to 1500m and then deep outer shelf below this depth.	No reservoir potential, with low porosity (<5%) and slight permeability.	No oil show
			Volcaniclastic Manganui equivalent (1931 - 2800m)	Mid to Late Miocene	Interbedded andesitic/granitic pyroclastic flows, calcereous mudstones and siltsones.	Interbedded sequence is divided by a more volcaniclastic dominated sequence between 2135 - 2575m. Mudstones resemble strongly the Manganui Formation. Foraminifera are noticble in cuttings. Deep water arenaceous and calcareous benthonic species present, with regularly >80% planktonic percentage.	Deep water, upper to mid bathyal paleodepositional setting.	Limited reservoir potential due to predominance of fine grained clastic material.	No oil show
			Mangaa/Kora volcanic equivalents (2800 - 3449m)	Mid Miocene	Massive volcaniclastic sequence, ranging from tuffaceous siltstones and sandstones to Lapilli Tuffs. Basaltic in nature.	Very high clay mineral percentage (up to 40%)	Open marine environment, no clear depth range but probably in the mid to lower bathyal environment.	Little reservoir potential.	No oil show

Table 3.1 (Continued from previous page): Summary of lithofacies and their main features. This does not include data from this study's point counting or the data from the GNS. Information collected from well completion reports for each individual well. Sourced from ARCO (1988a), ARCO (1988b), ARCO (1988c), and NZOG (1990).

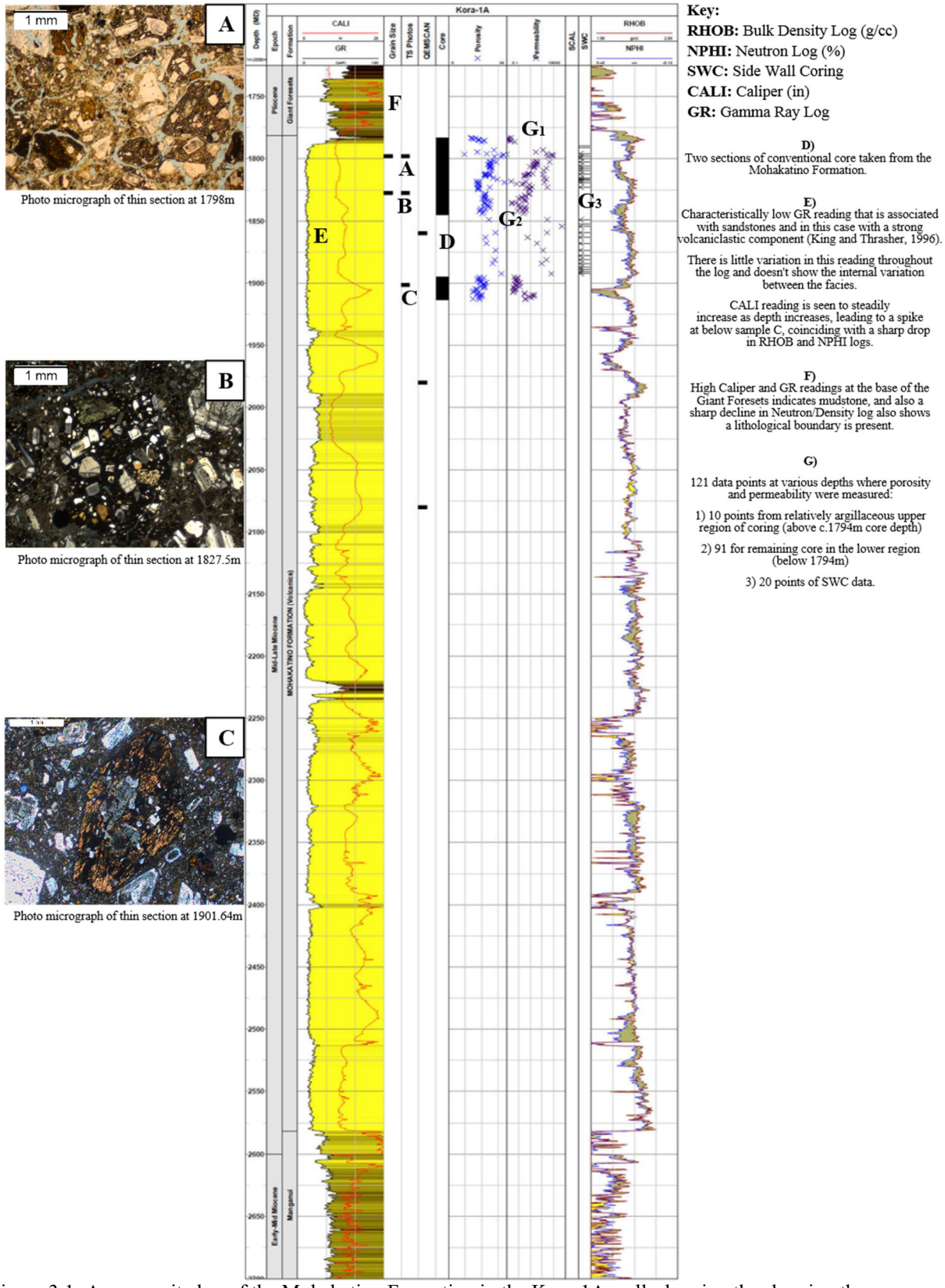

Figure 3.1: A composite log of the Mohakatino Formation in the Kora-1A well, showing the showing the positions of thin sections, QEMSCANS, core samples, porosity and permeability measurements, side wall coring, as well as the regular RHOB, NPHI, CALI and GR readings from wireline logging. Pictures of the thin sections and descriptions of various features have been added. Log sourced from GNS PBE (2013)

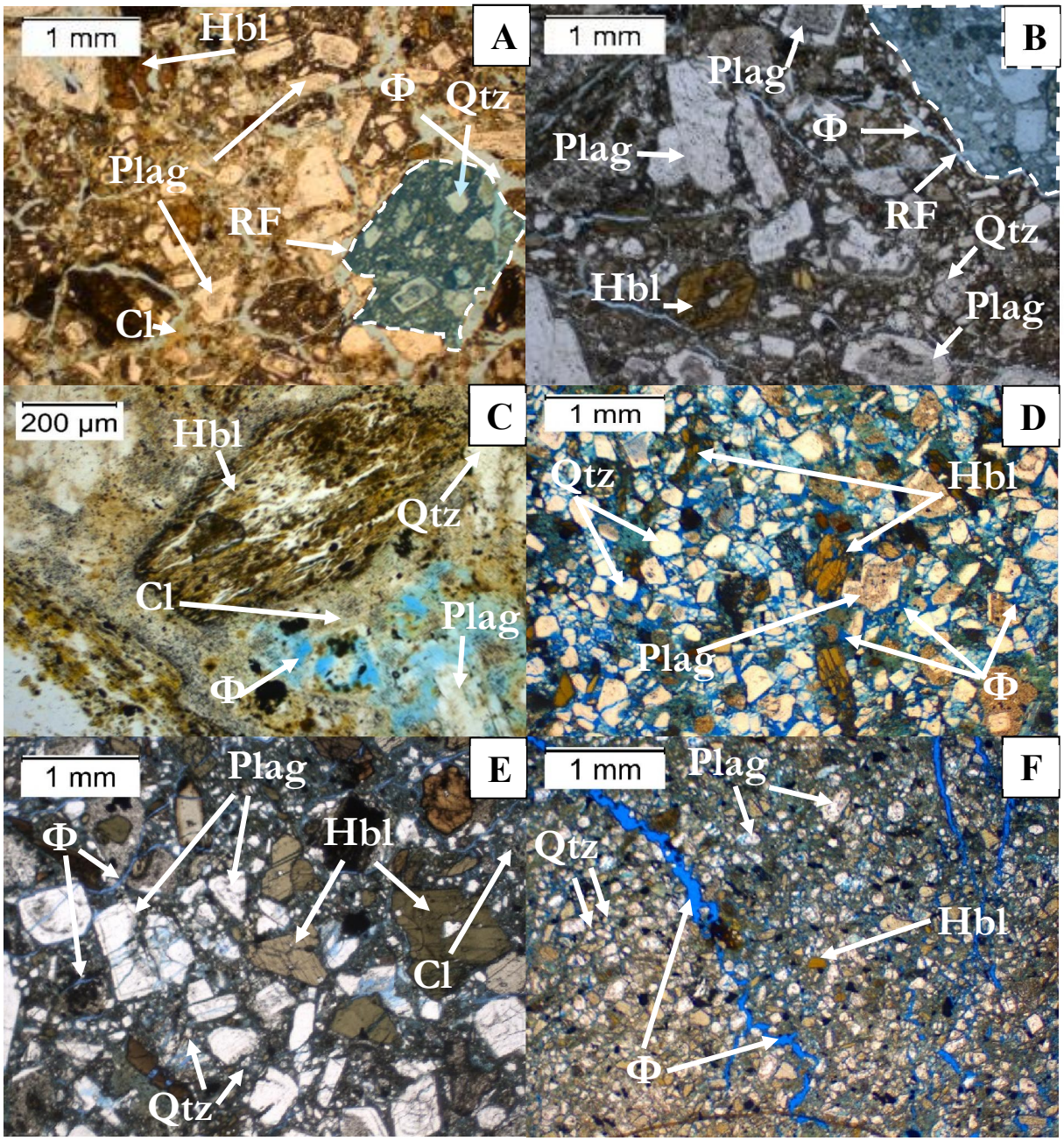

Figure 3.2: Photo micrographs of the general view of thin section samples from A) Kora-1A 1798 m, PPL B) Kora-2 1323.1 m, XPL C) Kora-3 1808 m, PPL D) Kahawai-1 1901.1m, XPL E) Kahawai-1 2049.9 m, XPL F) Kahawai-1 2462.5 m, XPL. Hbl = Hornblende, Qtz = Quartz, Plag = Plagioclase, Cl = Clay mineral (Undifferentiated), RF = Rock fragments, Φ = Porosity (Undifferentiated). Note the boundaries of the rock fragments are depicted with a dashed white line and the internal area is highlighted with transparent blue.

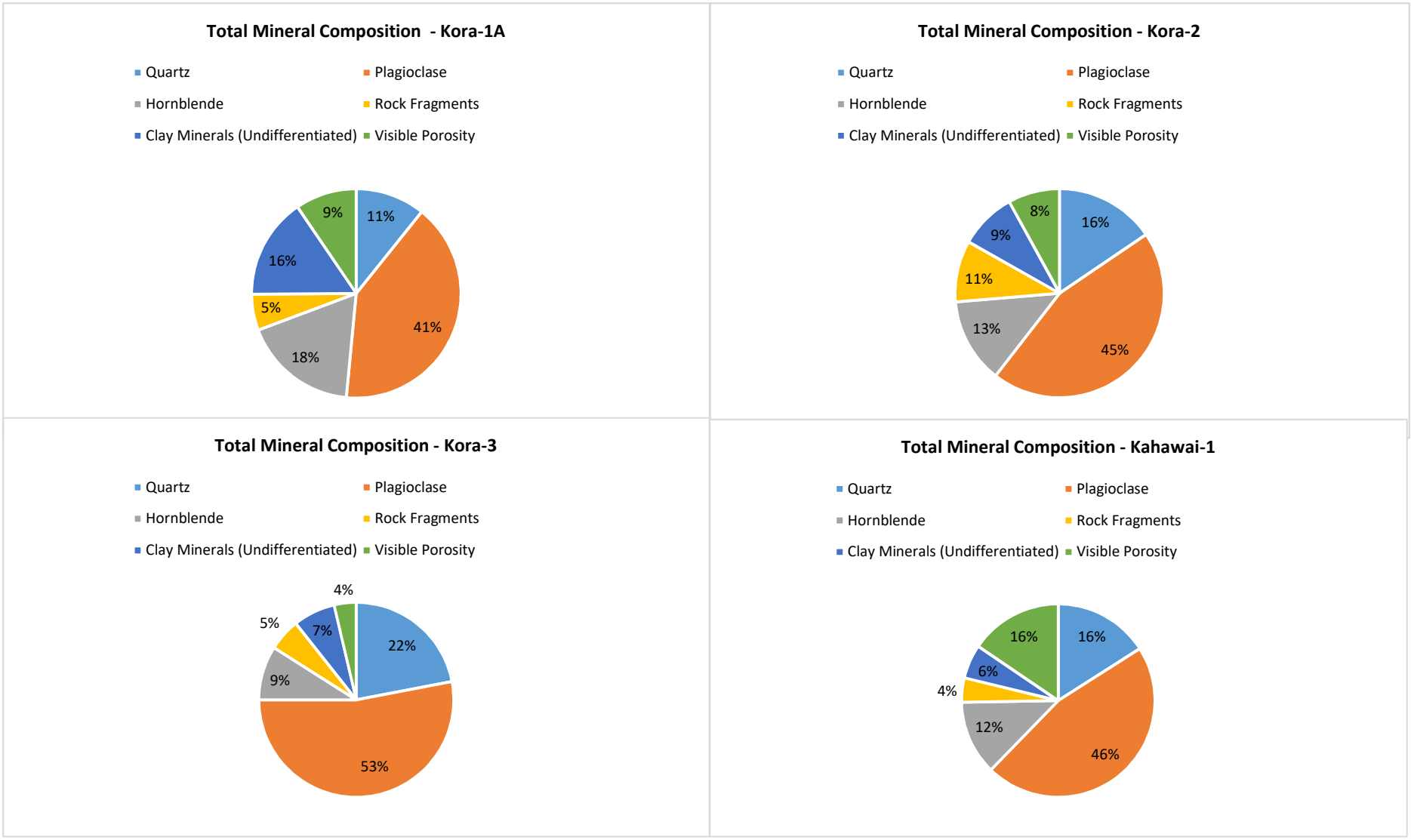

Figure 3.3: The averaged mineral composition for Kora-1A, 2, 3 and Kahawai-1 wells from the point counting analysis. The values next to each section of the chart calculated average percentage for that mineral.

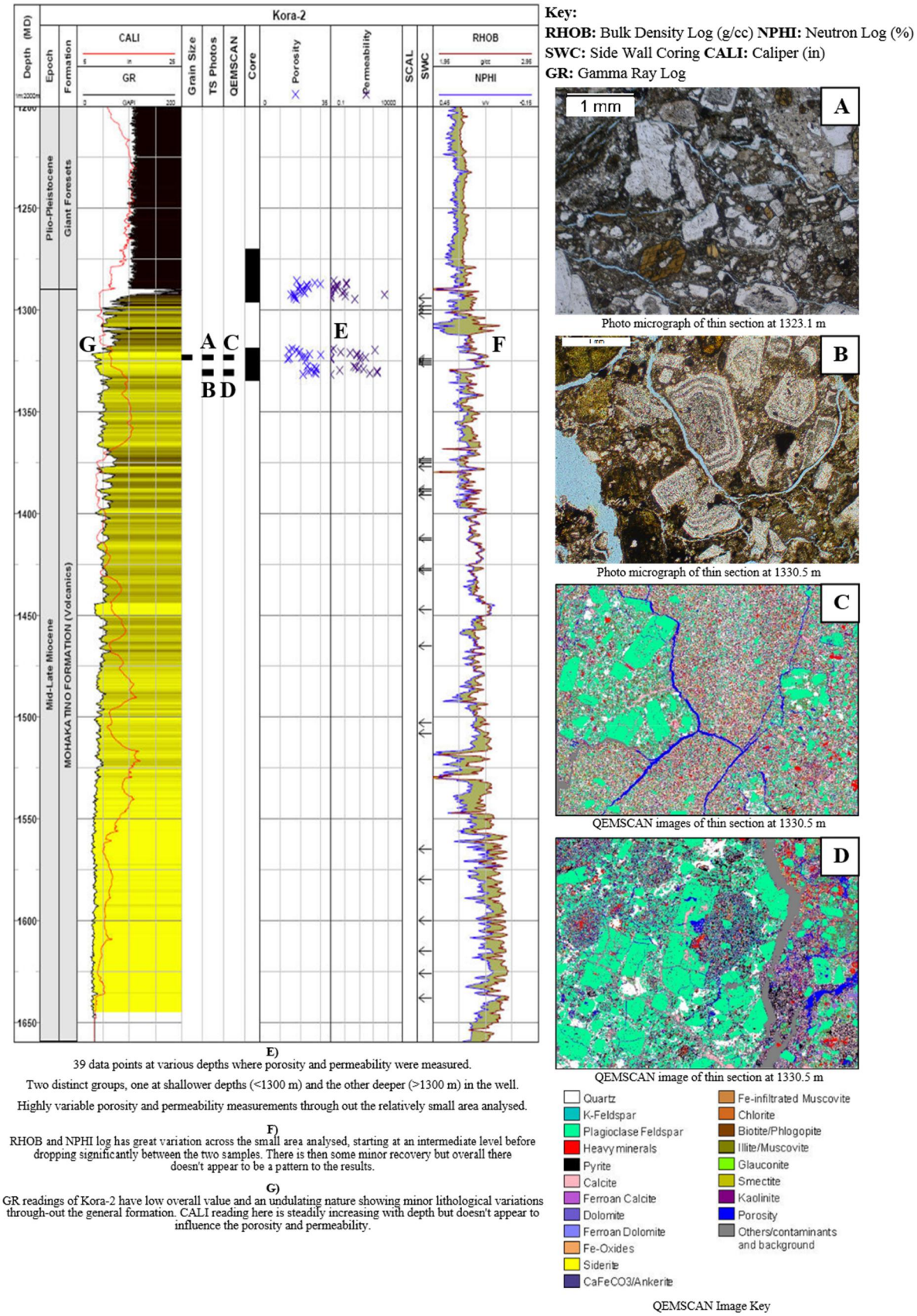

E)
39 data points at various depths where porosity and permeability were measured.
Two distinct groups, one at shallower depths (<1300 m) and the other deeper (>1300 m) in the well.
Highly variable porosity and permeability measurements through out the relatively small area analysed.

F)
RHOB and NPHI log has great variation across the small area analysed, starting at an intermediate level before dropping significantly between the two samples. There is then some minor recovery but overall there doesn't appear to be a pattern to the results.

G)
GR readings of Kora-2 have low overall value and an undulating nature showing minor lithological variations through-out the general formation. CALI reading here is steadily increasing with depth but doesn't appear to influence the porosity and permeability.

Figure 3.4: A composite log of the Mohakatino Formation in the Kora-2 well, showing the showing the positions of thin sections, QEMSCANS, core samples, porosity and permeability measurements, side wall coring, as well as the regular RHOB, NPHI, CALI and GR readings from wireline logging. Pictures of the thin sections and descriptions of various features have been added. Log sourced from GNS PBE (2013)

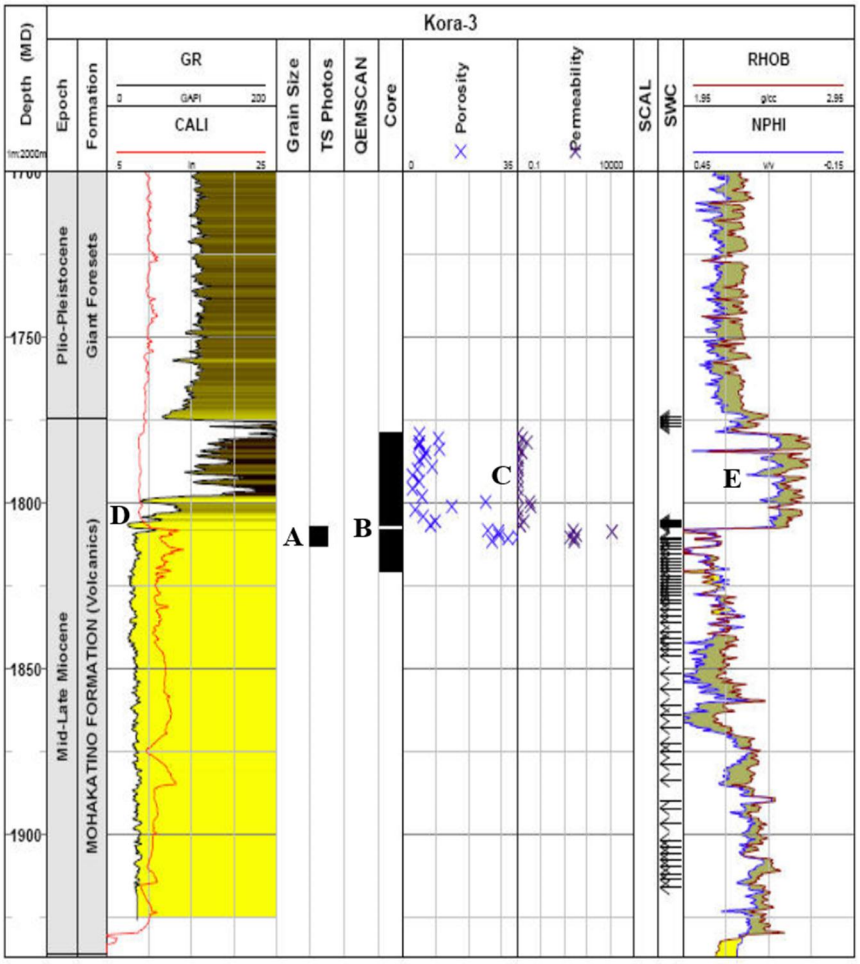

Key:
RHOB: Bulk Density Log (g/cc)
NPHI: Neutron Log (%)
SWC: Side Wall Coring
CALI: Caliper (in)
GR: Gamma Ray Log

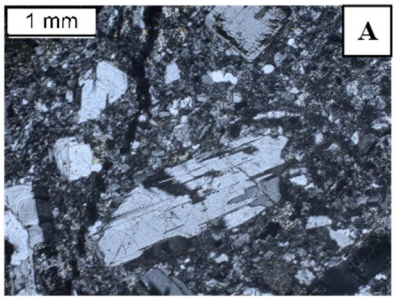

Photo micrograph of thin section at 1808.5m.

B)
Two sections of conventional core taken from the Mohakatino Formation:
The upper is taken from the relatively argillaceous interval at c. 1808m.
The lower core, below 1808 m, from a cleaner, stacked sandstone interval.

C)
26 data points from core analysis from variable depths measureing porosity and permeability: 20 from above 1808 m and 6 below 1808m.
Very low porosity and permeability data through-out the majority of the upper interval.
There is a significant increase in both these values as you move between the intervals and into the underlying sandstones

D)
IThe upper interval has a consistent low CALI reading but the GR reading is significantly higher than the rest of the Mohakatino and has undulating values.
At the bottom of the upper unit the GR unit decreases to indicate the change to sandstone material, the frequency and size of undulations decreases, and the CALI reading starts to increase and become more eratic...

E)
Through-out the upper unit there are high values of RHOB and NPHI with fluctuations of varying sizes in the data.
There is a rapid decrease when the upper unit changes into the lower unit.
In the lower unit there are significantly lower values but still have the undulating nature seen in the other unit..

Figure 3.5: A composite log of the Mohakatino Formation in the Kora-3 well, showing the showing the positions of thin sections, QEMSCANS, core samples, porosity and permeability measurements, side wall coring, as well as the regular RHOB, NPHI, CALI and GR readings from wireline logging. Pictures of the thin sections and descriptions of various features have been added. Log sourced from GNS PBE (2013)

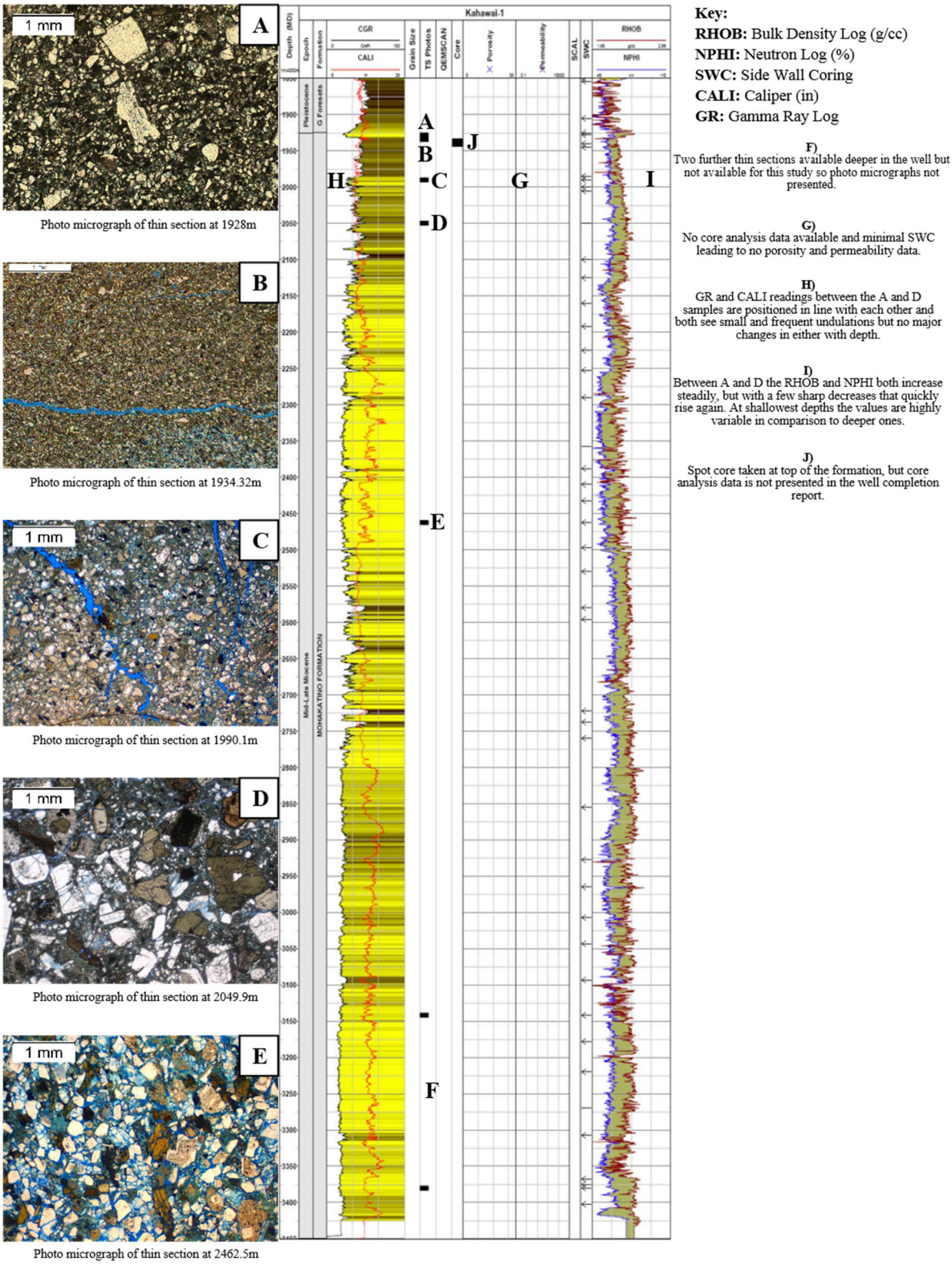

Figure 3.6: A composite log of the Mohakatino Formation in the Kahawai-1 well, showing the showing the positions of thin sections, QEMSCANS, core samples, porosity and permeability measurements, side wall coring, as well as the regular RHOB, NPHI, CALI and GR readings from wireline logging. Pictures of the thin sections and descriptions of various features have been added. Log sourced from GNS PBE (2013)

3.3 Petrography and Diagenesis of the Offshore Mohakatino Formation

3.3.1 Petrography

These samples occur in a compositionally narrow range of >60% feldspars, <20% lithic fragments and <30% quartz (relative to each other), making the general rock type for the Mohakatino Formation arkosic arenites. All of the samples have been averaged and then plotted against each other to generate a QFL plot (Figure 3.7). This shows how these three mineralogical variables differ compared to each other and not including any other minerals. The position of the wells plot on this diagram give an indication of their sedimentological definition.

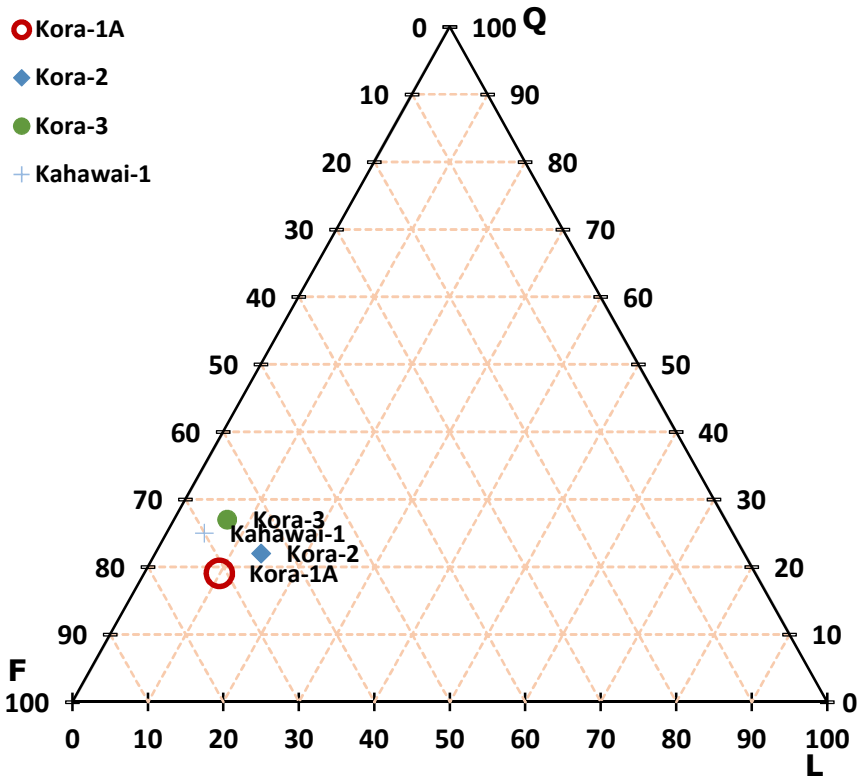

Figure 3.7: QFL plot of the four analysed wells with the data sourced from point counting and averaging the samples. Q = Quartz, F = Feldspars, and L = Rock Fragments

While the Mohakatino Formation is classified as a combination of sandstones and siltstones from the range of grain sizes in the samples (Section 3.3.2), the petrography of the samples is not a typical sandstone. There is a relatively small percentage of quartz grains in all of the samples, with the lowest in Kora-1A (10.67%) and the highest in Kora-3 (22%), and these are significantly than the typical quartz percentages you would expect to see in a reservoir sandstone which are commonly quartzites and sub-arkoses. The defining characteristic of the petrography across all of the samples is the dominance of plagioclase feldspar in all of the samples, ranging between 41% and 53% in Kora-1A and Kora-3 respectively. Figure 3.7 shows this disparity clearly, where out of the three variables of quartz, feldspar and rock fragments all of the wells are nearly three quarters plagioclase. The source

of the plagioclase in the Mohakatino is due to the andesitic composition of the MVC and specifically the Kora volcano where these wells were drilled into the Mohakatino on its flanks. These volcaniclastics are thought to have formed through sector collapse along the side of the volcano, and so the andesitic material has been broken down and then redeposited to form a volcaniclastic sandstone and because the original material was primarily plagioclase this mineral became the primary constituent of the Mohakatino. The hornblende percentages (9% to 18% in Kora-3 and Kora-1A respectively) is also thought to be derived from the andesitic volcanoes of the MVC as well. The undifferentiated clay minerals demonstrate the highest variability of all the material in the samples, with the 16% in Kora-1A to 6% in Kahawai-1, and this variability is difficult to explain from point counting due to not being able to differentiate between the types of clay and also some clays not being visible at all using light microscopes. Further analysis is done using GNS data and SEM analysis of samples in Section 3.3.3 to try and identify the types of clays and cements as well as their behaviours. Refer to Figure 3.3 for the graphic representation of mineral compositions for the wells.

3.3.2 Grain Size Distribution

There is a significant variation in grain size across the samples, ranging from an minimum of very fine sand (3.7 Φ/0.074 mm) in Kahawai-1 (1928 m) to very coarse sand (-0.67 Φ/1.5 mm) in Kora-2 (1323.1 m), and an overall coarse grain size (0.45 Φ/0.8166 mm) average for the Mohakatino Formation across all of the proximal samples. When samples were averaged for each well Kora-1A and 2 were both very coarse sands (-0.275 Φ/1.2 mm and -0.67 Φ/1.5 mm respectively) while the Kora-3 is a medium sand (1.5 Φ/0.3515 mm). This is a significant change in the grain size over the very small distance between Kora-3 and the other wells, and so there is potentially a shift in lithofacies between these two regions. Kahawai-1 has an even finer grain size, classified as a well sorted fine sand, with average grain sizes of 2.1 Φ/0.215 mm, and so while there are variations within the well the overall characteristics show it is potentially a separate lithofacies to the material in the Kora field wells. See Appendix I for the grain size of the samples.

3.3.3 Diagenetic Cements and Grain Coatings

The diagenesis of the Mohakatino Formation has been subject to little research prior to this, but there has been work on the diagenesis of the Taranaki Basin (King & Thrasher, 1996; Higgs et al., 2007; Killops et al., 1994), the Kora volcano (Bergman et al., 1992; Stagpoole & Funnell, 2001), and on igneous influenced reservoirs (Clark, 2014). Cements that are important to reservoir quality according to Stricker (2016) include carbonates, quartz, and K-feldspar dissolution. SEM analysis was used to acquire images to support this data. While cements were identified their coverage was difficult to constrain and also due to the SEM used for the offshore section of this study did not have EDX capability and did not take high-resolution images making mineral and cement identification difficult. Refer back to Section 1.5.2 for explanation in Methods. To help identify and understand coverage of

the main diagenetic cements identified the GNS XRD data was used to supplement the SEM work done during this study. The GNS data identified (through XRD analysis) the main diagenetic cements as authigenic clays, calcite, dolomite, siderite and dawsonite (i.e. carbonates), quartz, Fe oxide, and authigenic opaques (which according to the GNS include pyrite, leucoxene and anatase). See Appendix IV for full table of GNS results.

Quartz Cements

While no quartz cements were identified by the SEM work in this study, the GNS XRD analysis found rare quartz cements in the Kora wells, with no occurrence in Kora-1A and Kora-2, and in Kora-3 it only occurs in the 1811.30 m sample at 0.7%. This significant lack of quartz (i.e. the inhibition of quartz cementation) is most likely derived from the presence of grain coating clays (Worden and Morad, 2000). The quartz overgrowth data for each well sample in Appendix IV supports this theory for the lack of quartz overgrowths because there are significant authigenic clay percentages in every sample other than Kora-3 1811.30 m and these samples have no quartz overgrowths present. In Kora-3 1811.30 m however, there is only trace percentages of authigenic clay (i.e. $\leq$0.1%), and this allows for the creation of quartz overgrowths and explains the trend we see in the samples. These results are therefore too insignificant to be taken into account when analysing reservoir quality.

Carbonate Cements

Like with the quartz cements, carbonates were not identified by this study but the GNS XRD analysis found that carbonate cements occur in much higher volumes than quartz cements in all of the wells (see Appendix IV). In the Kora-1A there is dawsonite as the only carbonate cement, present in the 1901.64 m sample (at 3.3%, shown in Figure 3.8 F) in the form of vermicular dawsonite. In Kora-3 the cement is siderite and is found at 1808.55 m at 1.0%. In contrast Kora-2 has significantly higher carbonate cements and also a greater range of carbonate types present. Kora-2 1323.10 m contains calcite, dolomite and siderite at 4.3%, 2.3% and 0.3% respectively, and 1330.50 m has calcite and dolomite both at 1.0%, giving a well total of 8.9% carbonate cements. The occurrence of these carbonates is thought to be from carbonate material being entrained in the offshore Mohakatino material during deposition in a marine environment. A hypothesis for the lack of carbonate cements in these samples considering they are in a deep marine environment is that due to the acidic nature of the andesitic material being erupted and later becoming part of the Mohakatino breaking down the calcite as it forms in the volcaniclastics (Stuart Jones, pers coms, 2017).

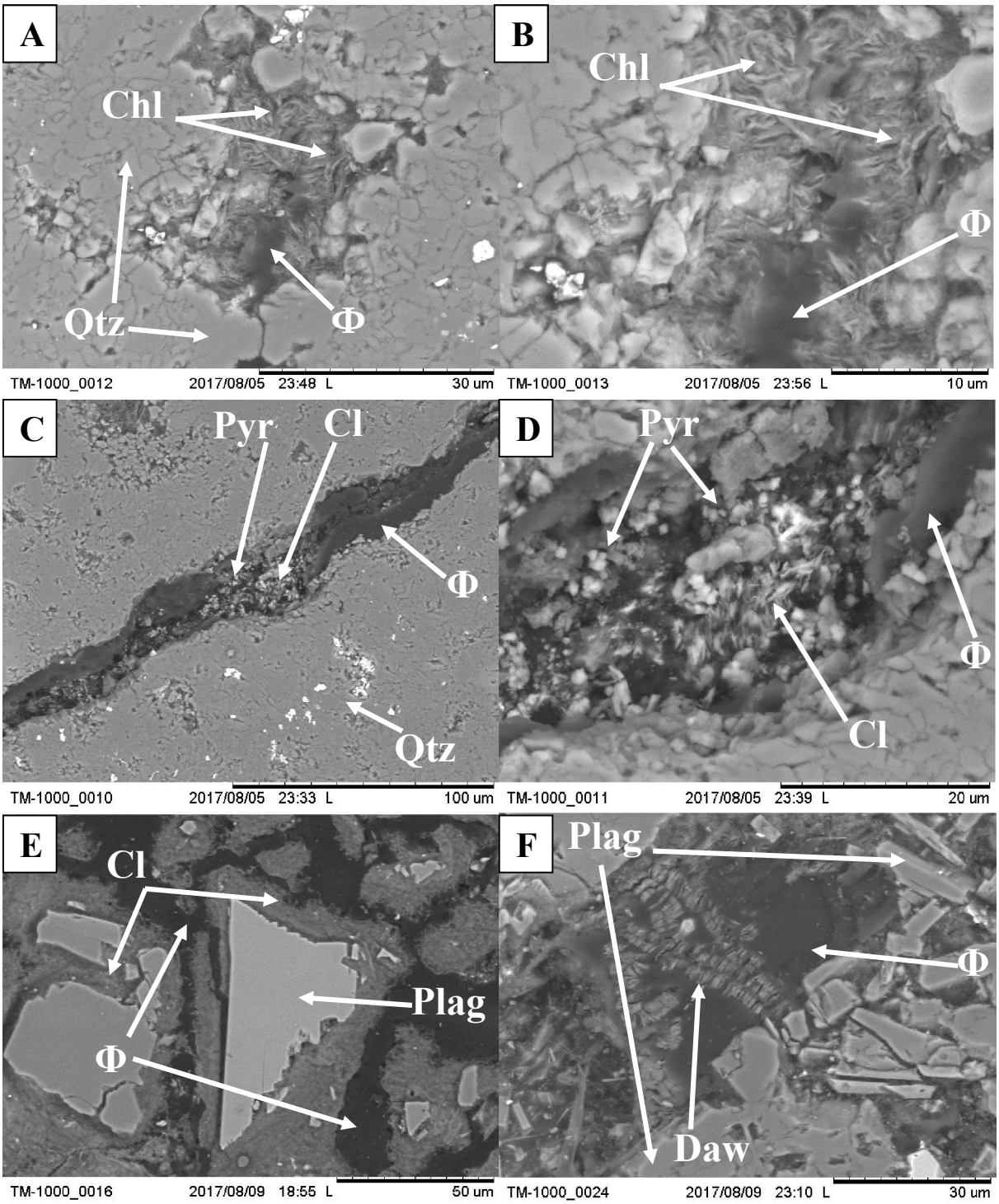

Figure 3.8: SEM images of A) Pore filling chlorite, Kora-3 1808.55m. B) Pore filling chlorite from A at a higher magnification. C) Pore filling indeterminate clay and pyrite, Kora-3 1808.55m. D) Pore filling indeterminate clay and pyrite from C zoomed in. E) Indeterminate clay coating, Kora-1A 1798m F) Vermicular dawsonite, Kora-1A 1901m. Qtz = Quartz, Plag = Plagioclase, Cl = Clay mineral (Undifferentiated), CHL = Chlorite, Pyr = Pyrite, Φ = Porosity (Undifferentiated), Daw = Dawsonite.

Authigenic Opaques

Authigenic opaques are classified by the GNS as pyrite, leucoxene and anatase, and these minerals make up the highest proportion of cements in almost all of the samples from the GNS analysis. The main difference between the authigenic opaques and the other cements is that the opaques occur in every sample, ranging between 2.5% and 5.7% while the other cements only occur in specific samples. The trend of total opaques in each well follows the same trend as the total cements, with the highest percentages in Kora-2, and then decreasing in Kora-1A and the lowest average values in Kora-3.

The opaques have higher percentages compared with the other cements in all samples except Kora-2 1323.10 m, where the calcite cements are higher at 4.3% than the 3.6% opaques. While these authigenic opaques are very difficult to identify using a light microscope, they can be found using SEM analysis. Leucoxene or anatase were not found in any of the analysed samples but pyrite was identified. An example of Pyrite is in Figure 3.8 C and D where SEM imaging was used to identify the cubic pyrite crystals in pore space. These pyrite crystals probably result from volcanic sedimentation and hydrothermal processes. Liu et al (2012) suggested that sulphur rich material sourced from volcanism can increase the sulphur content in an aqueous medium and lead to the formation of pyrite related to kerogen. In the case of volcanic or pyroclastic rocks pyrite can precipitate directly.

Authigenic Clays

Authigenic clay mineral cements occur in all of the samples analysed by point counting and by XRD. From point counting it was not possible to differentiate the clay mineral type, and so any clay identified was marked as undifferentiated authigenic clay (raw data is presented in Appendix I). The Kora-1A samples have the highest volumes of authigenic clays with an average of 15.58% percent across all four samples, with decreasing volumes in Kora-2 and Kora-3, Kahawai-1 having the lowest volumes at 5.59%.

Undifferentiated clays appear in the photo micrographs of Figure 3.8 A and C, where both pore filling and grain coating forms. In Figure 3.8 A and B, the densely packed and laminated features of pore filling chlorite is visible. Figure 3.8 C and D show undifferentiated clay minerals, and they have a similar appearance to previous chlorite minerals. In these samples, the minerals are marked as undifferentiated but there is a possibility that chlorite is part of this undifferentiated mass. Despite the high volumes of clay minerals recorded in the samples that underwent SEM analysis, specific authigenic clay minerals are hard to identify.

The analyses done by the GNS on four of these samples (Kora-1A 1798 m and 1901.64 m, Kora-2 1323.1 m and 1330.5 m, and Kora-3 1808.5 m) prior to this study (data is available in Appendix IV)

has allowed for specific authigenic minerals to be quantified: chlorite and kaolinite/dickite (referred to as kaolinite in this study). This data directly contradicts the point counting analysis, which shows that the lowest percentages of clays are in the Kora-1A samples with values of 5.0 and 2.6% at 1798 m and 1901.64 m respectively. Kora-2 then has the next highest with 8.6% and then Kora-3 with 11%, so these results differ drastically. Chlorite and kaolinite only exist in small quantities, with chlorite present only in the Kora-1A samples, making up 1% of 1798 m and only trace amounts in 1901.64 m. Kaolinite exists in Kora-2 and Kora-3 and not in Kora-1A samples. Kora-3 hold the most kaolinite with 3% and Kora-2 only has 0.6%. Unlike chlorite, kaolinite has not been identified in any of the samples analysed using SEM. The remaining clay percentages are classified as indeterminate clay, making up the majority of the clays in these samples. There is no definition for what the indeterminate clays are but it can be assumed that they are made up of the same minerals mentioned previously.

3.4 Burial History Modelling

The burial history of the Kora-1 well is presented in Figure 3.9 and was generated from 1D modelling conducted by Stagpoole and Funnell (2001) on the well. Present day bottom hole temperatures were used as constraints. There is insufficient data to generate an appropriate burial history model for any of the Kora wells and so the work of Stagpoole and Funnel (2001) has had to be used.

A value of 38 mWm^{-2} was used for heat flow at the base of the 78 km thick post-rift lithosphere for the northern Taranaki Basin, and during deposition surface heat flow varied between 55 and 65 mWm^{-2}, except during the period of volcanism when surface heat flow increased to 90 mWm^{-2} (Stagpoole and Funnell, 2001).

Rapid sedimentation during the Late Cretaceous (75-65 Ma) was the first major event recorded in Kora-1, visible in Figure 3.9 by the raised position of the isotherms, followed then by a long period of slower thermal subsidence from 65 Ma to 25 Ma where the isotherms lowered and then flattened out. After 25 Ma the subsidence rate increased as subduction started to affect the Taranaki Basin. By 14 Ma subduction related volcanism of the MVC had begun, and the sedimentary sequence thickness had exceeded 4000 m. From 14 Ma, the Kora volcanic edifice was emplaced and rapid deposition of the Giant Foresets Formation (~2000 m since 5 Ma) led to the sedimentary succession exceeding 6000 m thick.

This model used a single magmatic intrusion of 900ºC, 900 m thick, instantaneously intruded at top basement depth at 14 Ma. The cooling of the intrusion caused a sharp rise in the temperature of the sediments (Figure 3.9). The temperatures at the top of the Cretaceous horizon at a depth of 3500 m rise to 200ºC for ~100,000 years during the cooling of the intrusion. It took 2-3 Ma before temperatures returned to pre-emplacement levels.

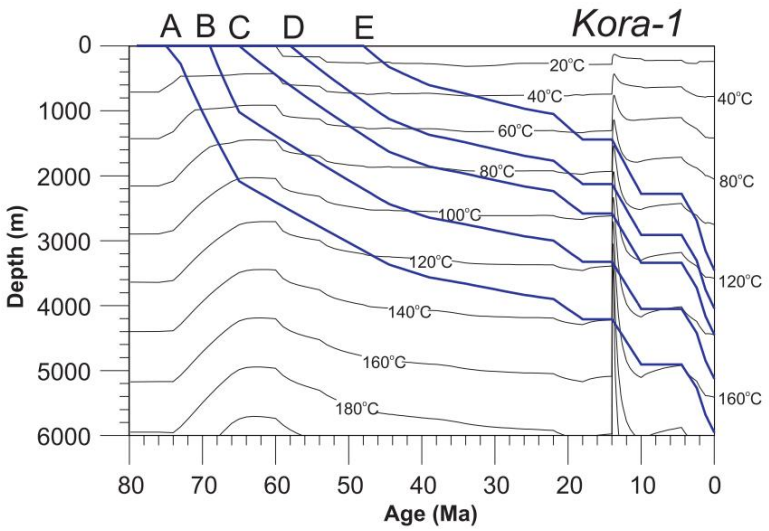

Figure 3.9: Burial history for the Kora field based on Kora-1 exploration well showing the effect of a 900 m thick intrusion injected into the basement at 14 Ma, i.e. the Kora volcano. Depth is shown with respect to the ground surface. Heavy blue lines are tracked horizons showing the depth below sea floor with time. A =top Basement/base Late Cretaceous (75 Ma); B = intra-Late Cretaceous (70 Ma); C = top Cretaceous (65 Ma); D = latest Paleocene (57 Ma); and E = Middle Eocene (48 Ma). Stagpoole and Funnell, 2001.

Stagpoole and Funnell (2001) also applied thermal models with hydrocarbon kinetic parameters to investigate the rate and cumulative amount of hydrocarbon generation and expulsion and to model them for the tracked horizons in Kora-1. The modelling hypothesises that during the period of high heat flow caused by the cooling of the magmatic intrusion, temperatures in the Late Cretaceous Rakopi Formation and North Cape Formation source rocks (lines A, B and C) were high enough to lead to rapid conversion of the majority of the available kerogen into hydrocarbons (Figure 3.10). They also found that some of this generation also occurred in the Early Tertiary/Late Paleocene Waipawa Formation marine shale source rocks higher in the sedimentary section (between lines C and E). As the temperatures returned to the pre-emplacement levels the model predicts that additional generation and expulsion did not occur until the Pliocene (~4 Ma) when the rapid sedimentation of the Giant Foresets Formation caused sufficient depth to re-establish significant hydrocarbon generation. In conclusion, Stagpoole and Funnell's (2001) model identified the Early Tertiary marine source rocks below the volcano as the primary source of hydrocarbon generation (between line C and E, Figure 3.9) while minor generation occurred in the Cretaceous source rocks (between lines A and B) due to the maturity gained and the loss of generative potential during the magmatic events in the Miocene, such as the Kora volcano's formation.

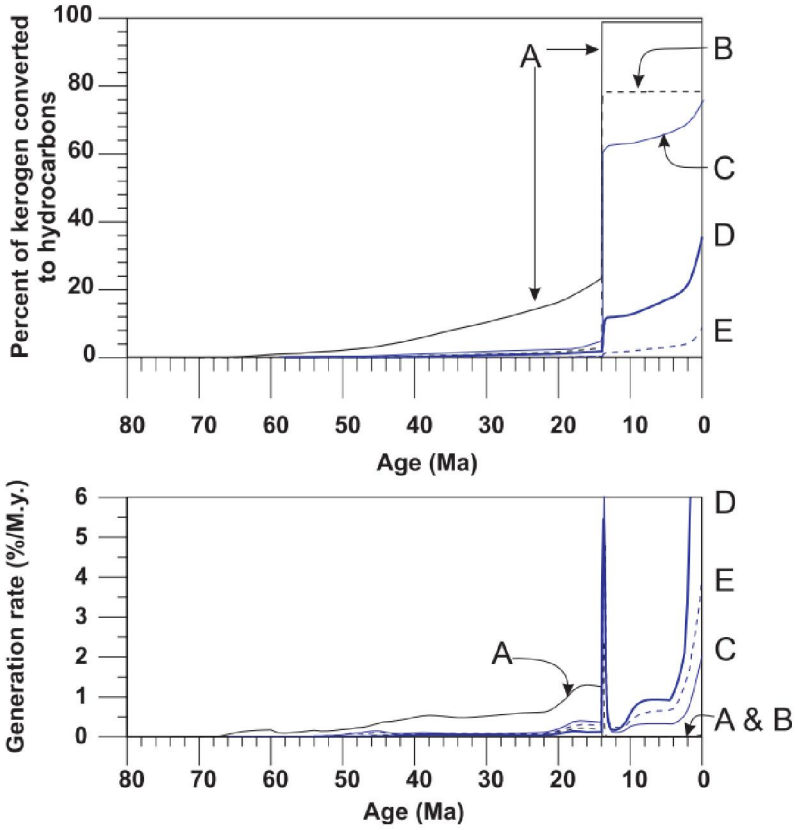

Figure 3.10: Hydrocarbon generation from kerogen based on the burial history and thermal model for Kora-1 exploration well in Figure 3.9. Chart 1 depicts the proportion of kerogen converted to hydrocarbons for tracked intervals (see Figure 3.9 for key). Chart 2 shows the rate at which kerogen is converted to hydrocarbons. Stagpoole and Funnell, 2001.

3.5 Porosity

3.5.1 Previous Studies

Porosity is fundamental to this study as it is one of the key factors that controls the reservoir quality of a rock. There have been extensive studies conducted on porosity of siliciclastic sandstones, but there has been limited work done on the porosity of volcaniclastic rocks. The existence of volcaniclastic reservoirs is possible through the retention of porosity and permeability retained within volcaniclastic rocks during diagenesis (Berger et al., 2009; Clark, 2014; Seeman & Scherer, 1984; Mathisen & McPherson, 2012). Other factors considered for the controlling of porosity include volcanic events and tectonics (Sruoga et al., 2004) and the effect of pore filling zeolite (Iijima, 2001).

3.5.2 Relationship between Porosity and Depth

Optical Porosity

The two Kora-2 samples (found at the shallowest depths) average to 8% optical porosity, the Kora-1A samples average 8.33% (at intermediate depths), and then 15.2% in Kahawai-1 (for the deepest values). The Kora-3 sample does not follow any of these averages with only one available sample. It is sourced from a similar depth to the Kora-1A samples but has a significantly lower value of 3.7%.

While there is a trend in the averaged data the individual samples have highly variable values and these are discussed below.

In the Kora-1A well there is a clear trend of the optical porosity decreasing with depth. At the shallowest depth the porosity is 18% at 1798 m (1) and 12% at 1798 m (2) (both samples averaged to give 15%), before decreasing to 7.7% at 1827.5 m and then falling to 0.3% at 1901.64 m (See Figure 3.11). This gives a total decrease of 17.7% over a change in depth of 103.64 m. Kora-2 however demonstrates a different trend to Kora-1A, which has a >98% decrease in porosity over 103.64 m depth increase, while Kora-2 has an increase in porosity by 5.3% over a much shorter depth increase of 7.4 m. As can be seen in Figure 3.11 there is an increase in optical porosity from 5.3% at 1323.1 m to 10.7% at 1330.5 m. This data is also from much shallower depths, which could have been an influence on these differences. Kora-3 had one sample available so it was not possible to identify the relationship between visual porosity and depth in the well, but it is possible to see how this sample compares to those of different depths from other wells in Figure 3.11. In Kora-3 at 1808.55 m the visual porosity was 3.7%, which is lower Kora-2 that were had greater values at shallower depths, and had significantly lower percentages than those of Kora-1A other than at 1901.64 m. It falls on the trend line for the Kora-1A well and in relation to the Kahawai-1 samples, Kora-3 directly contradicts the trend seen in that well, as they have decreasing porosity with depth and if the Kora-3 sample was part of that data set it would have a far too low optical porosity for its depth.

Kahawai-1 samples are deeper and have it had the most samples available for study. Kahawai-1 results have the highest values with an average visual porosity of 15.2%, compared to 9.7% at Kora-1, 8% at Kora-2 and 3.7% at Kora-3. The results of Kahawai-1, show a clear trend of decreasing optical porosity with increasing depth, falling from 14.3% at 1928 m (a), to 11% at 1934.32 m and then 9.7% at 1990.01 m and 2049.9 m respectively (see Figure 3.11). The anomalous result is found at 1928 m (b) with a result of 26.7%, and has a significantly higher optical porosity than it should at that depth.

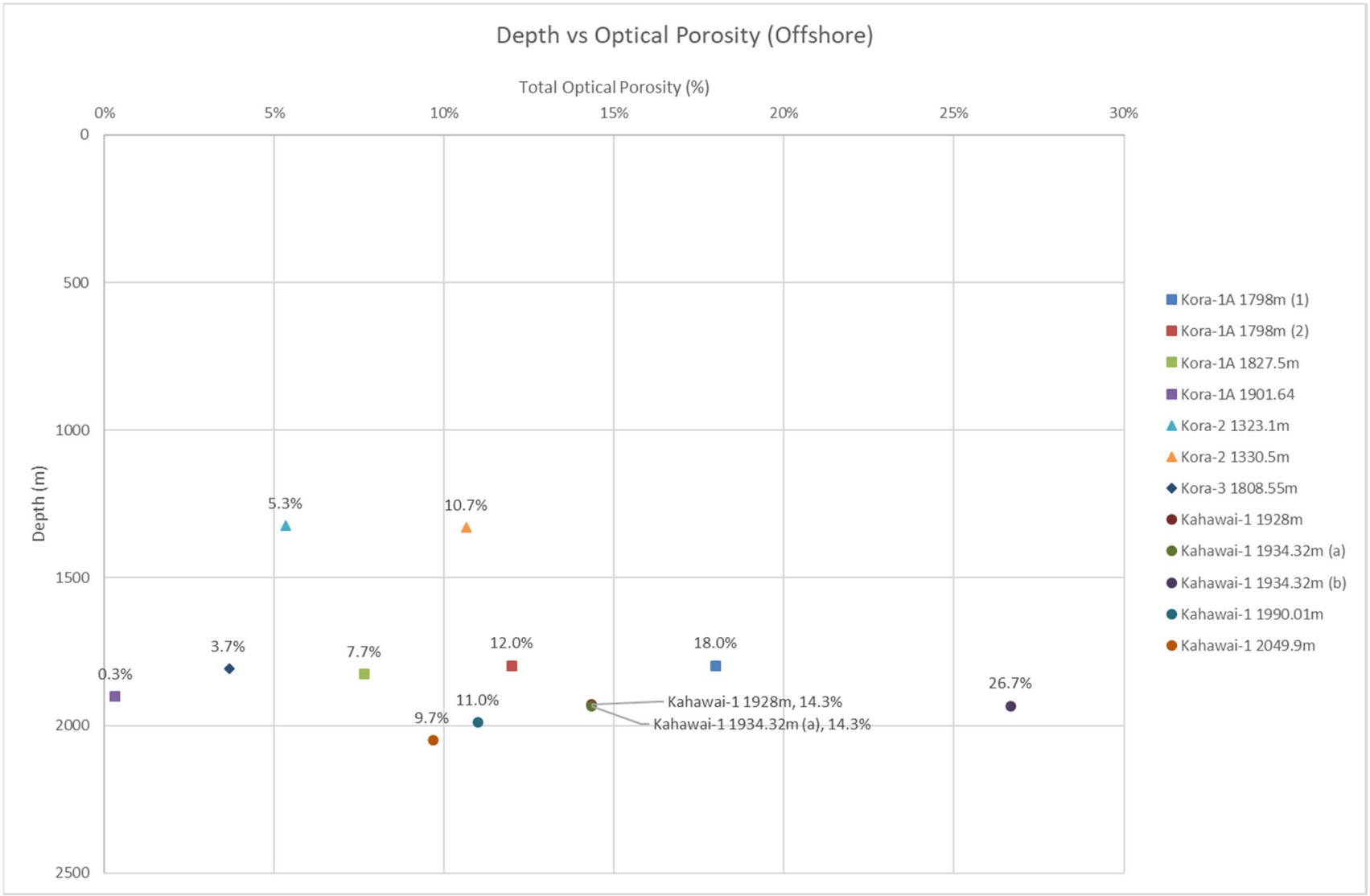

Figure 3.11: A graph of optical porosity plotted against depth, with Kora-1A samples marked with squares, Kora-2 with triangles, Kora-3 with diamonds, and Kahawai-1 with circles. Each sample has their porosity values plotted next to the point.

Helium Porosity

There are 186 helium porosity data points from a range of depths in each well that the GNS has made available, with 121 for Kora-1A, 39 for Kora-2, 26 for Kora-3, and none for Kahawai-1. (Appendix III) (Figure 3.12).

The helium porosity data from the GNS has 121 results from depths ranging between 1856.14 m and 1986 m. These show a great disparity between the highest and lowest porosity values (see Figure 3.12), with the highest value of 35.5% at 1927.3 m and the lowest at 9.5% at 1869.3 m. The majority are between 15% and 25% and porosity decreases as depth increases. For example, the shallow depth results range between 9.5% and 33.1% at 1869.30 m and 1869.80 m, while those at greater depth the results are found between 14.5% and 22.6% at 1980.38 m and 1972.68 m. As well as the graph showing helium porosity vs depth in Figure 3.12, this trend can also be identified in the composite log for the well in Figure 3.1 where there is a visible decrease in porosity with depth. Above 1950 m the majority of the data points are between 17% and 29%, while deeper than 1950 m most of the results are between 14% and 23%, showing a measurable decreasing trend. This shows that as depth increases the rocks exhibit increasingly similar characteristics and a possibly more homogenous composition that would allow for the rocks to all have similar and consolidated values.

There are 39 data points available for Kora-2 (See Appendix III) and this data follows the same trend of increasing porosity with depth, rising by 6.3% over 7.4 m which is very similar to the increase seen with the point counting between these depths. In Figure 3.12, there are two sets of data visible, with an upper set between 1358.60 m and 1366.50 m, and a lower set between 1391 m and 1403.50 m and the position of this data in the well is also shown as part of the composite log in Figure 3.4. Both of these sets of data have a wide range of values, between 15.3% and 29.8% in the upper set and 13.6% and 30% in the lower set, but there isn't a significant change in the porosity as the depth increases between the sets. There does not seem to be any significant trend between porosity and depth from this data, but by averaging the values for the two sets a basic trend is visible. The values of the shallower set average to 20.5% and the deep-set averages to 25.8%, and highlights a trend of increasing porosity with depth (5.36% over 45.9 m) similar in value to that of the point counting data.

Kora-3 has the fewest data points available with 26 measured depths between 1808.55 m and 1811.30 m (see Appendix III) and the data has the widest ranging results over the smallest vertical distance (See Figure 3.12), ranging between the highest value of 38.4% at 1882.20 m to the lowest of 2.7% at 1863.51 m.

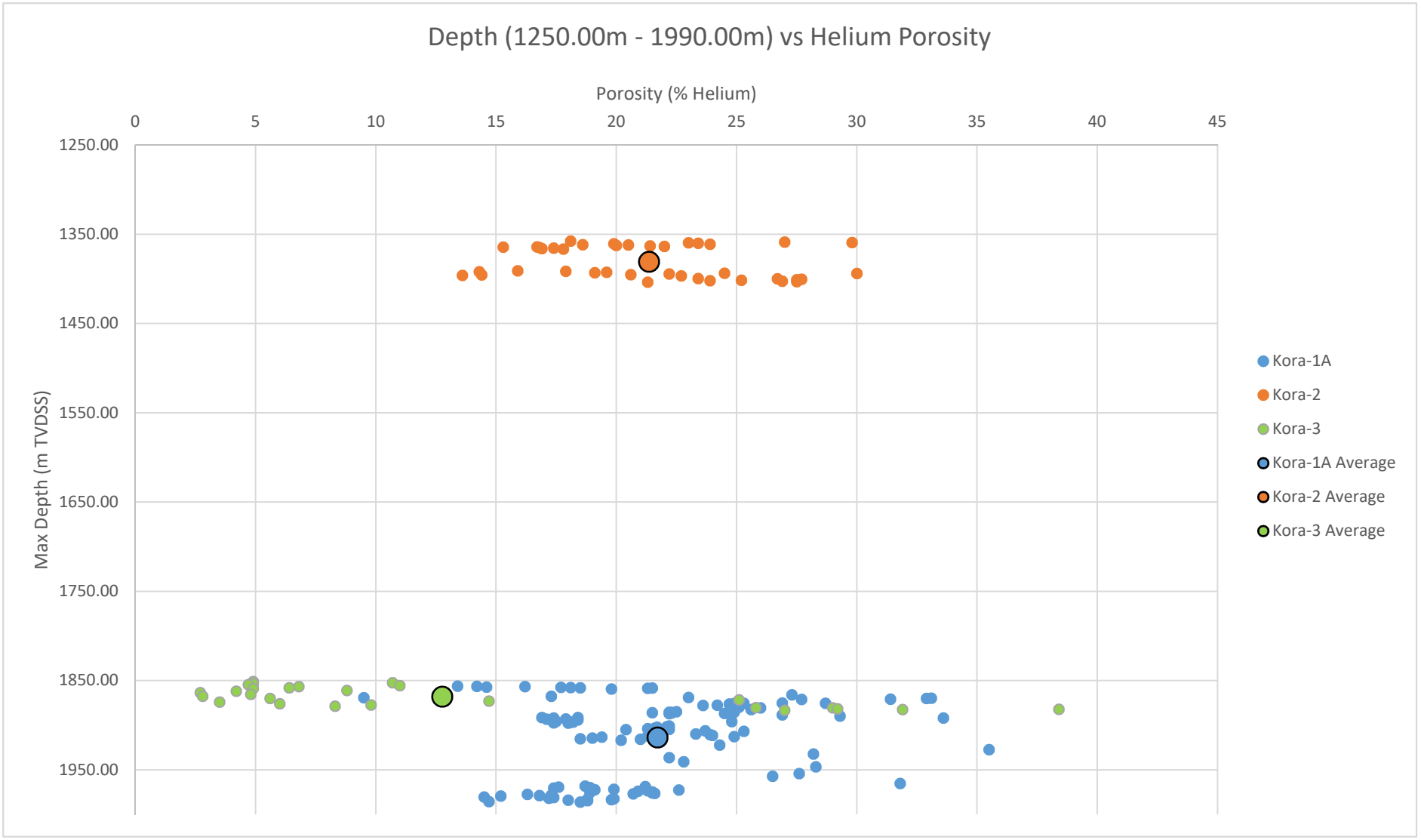

Figure 3.12: A graph of helium porosity plotted against depth, with the y axis shortened to only show results between 1250.00m and 1990.00m.

The data can be placed into two rough groups, one with values between 1851.10 m and 1867.50m and the other from 1867.50 m to 1883.30 m, and representing shallower and deeper regions respectively. The Kora-3 average comes from a bimodal distribution, however, and so this must be considered when reviewing any trends. The shallower region's averaged results have 5.96% and then the deeper region averaged to be 19.56%, clearly showing that even over this short distance of 32.2 m is a trend showing an increase in porosity with depth, as seen in Kora-2. As with the other wells, the position of the porosity data in relation to the other features in the well is shown in the composite log in Figure 3.5.

3.5.3 Relationship between Rock Fragments (RFs) and Optical Porosity

The term rock fragments (RFs) is used to describe both hypabyssal rock fragments (HRF) and volcanic rock fragments (VRF) and the relationship between RF and optical porosity is shown in Figure 3.13. A general trend in the data is that at lower RF percentages there is a greater spread in the optical porosity data, with differences of 26.337% in optical porosity between 4-5% RF compared to 2.334% between 7-8% RF. However, there is no clear distinction of whether the presence of RFs is detrimental or beneficial for porosity.

In Kora-1A the porosity decreases as the RF value increases. This can be seen in Figure 3.13 where optical porosity decreases from 18%, at an RF value of 4.667% at Kora-1A 1798 m (1), to 12% (Kora-1A 1798 m (2)) and then 5.333% (Kora-1A 1827.5 m) with 6% and 7% RF values respectively. This trend does have an anomalous result at 1901.64 m, where the sample has the same RF percentage as Kora-1A 1798 m (1) (4.667%) but has a much lower porosity at 0.33% compared to 18%. Other than this result however, in Kora-1A the RF has a significant influence on the porosity unless another factor can be identified to account for this anomalous result. Coincidently, RF increases as depth increases also while porosity decreases, other than the result at 1901.64 m, and so depth may also influence this trend.

Despite having only two samples available for analysis the trend in Kora-2 shows an increase in optical porosity while RF increases, rising from 7.333% porosity from at 5.333% RF (Kora-2 1323.1 m) to 11.667% porosity at 10.667% RF (Kora-2 1330.5 m). This directly contradicts the results we see from Kora-1A as they follow an increasing porosity with increasing RF trend and also the RF are significantly higher than those of Kora-1A so there is no overlap in any of the data.

With only one sample from Kora-3 is not possible to identify whether there is any trend between these two variables in the well, and in relation to the other samples Kora-3 1808.55 m does not appear to have a similar position in any of the trends of the other samples in Figure 3.13. With a RF of 5.333% it should in theory have an optical porosity roughly between 18% and 12% porosity if it was to follow the other data we are seeing, but actually has a far lower optical porosity than this at 0.33%.

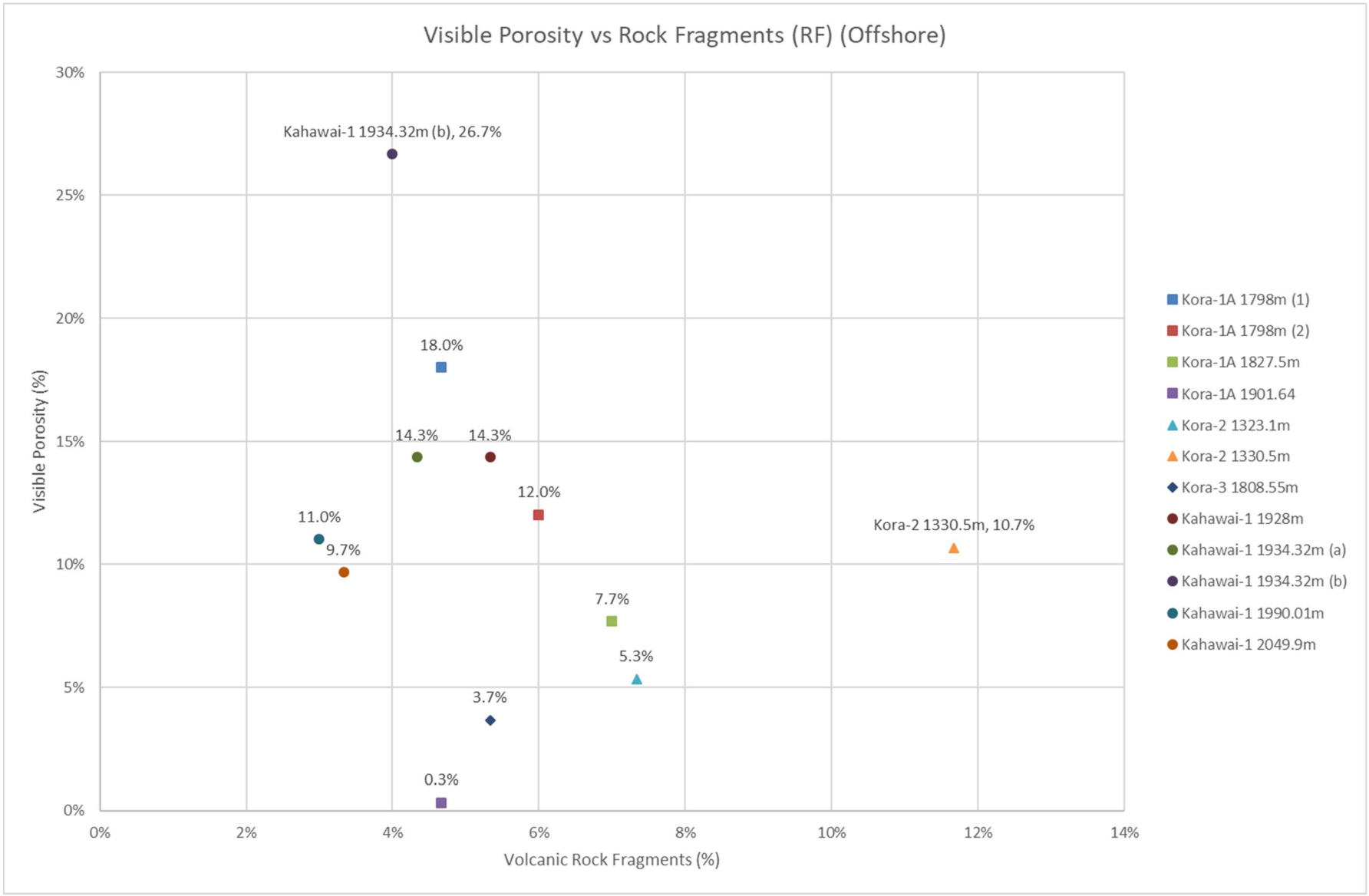

Figure 3.13: A graph of optical porosity plotted against volcanic rock fragment percentage. The values next to each data point is the optical porosity value for that sample.

Kahawai-1 has the most samples for this study and so should give the clearest indication of any trend between these two variables. However, looking at Figure 3.13, there is no clear indication if in Kahawai-1 there is a trend of increasing or decreasing optical porosity with increasing RF. The line of the results at first see decreasing porosity, followed by increasing and then decreasing again before plateauing for the final two results as the RF increases from 11% to 14%.

3.5.4 Relationship between Total Authigenic Clay and Optical Porosity

Total authigenic clay (undifferentiated) is plotted against the optical porosity from the offshore, proximal samples in Figure 3.14. The general trend is that as authigenic clay percentages increases the optical porosity increases as well but the data does not all fall along one trendline. Kora-1A shows no trend of optical porosity being influenced by the increase in authigenic clay in the well. There is an initial decrease in porosity between 1827.5 m and 1901.64 m from 7.667% to 0.33%, but this is then reversed by a sharp increase to 18% at 1798 m (1), and finally decreasing again to 12%. This undulating pattern of results makes it difficult to identify if there is an influence of authigenic clay on optical porosity. Kora-2's two samples don't show any evidence for a whole well trend but in Figure 3.14 we see that there is trend of decreasing porosity from 10.667% at Kora-2 1330.5 m to 5.333% at Kora-2 1323.1 m, with RF results of 7% and 10.667% respectively. The other trend that this data shows that as you increase depth down the well here you also see that authigenic clays decrease while optical porosity increases. When compared with the position of other samples, the Kora-3 sample' (1808.55 m) optical porosity value is >5% lower than other samples for its clay percentage. It is therefore either an anomalous sample or there is a chance of there being no pattern for the relationship between authigenic clay and optical porosity.

Kahawai-1 well data in Figure 3.14 begin with a trend of rapidly increasing porosity from 11% to 26.667% between 0.333% and 5.333% clay for the first three samples, but this trend does not continue as the clay percentage increases. There is a relatively rapid decrease in porosity from 26.667% at Kahawai-1 1934.32 m (b) to 9.667% at Kahawai-1 2049.9 m, followed by another increase to 14.333% at Kahawai-1 1934.32 (a).

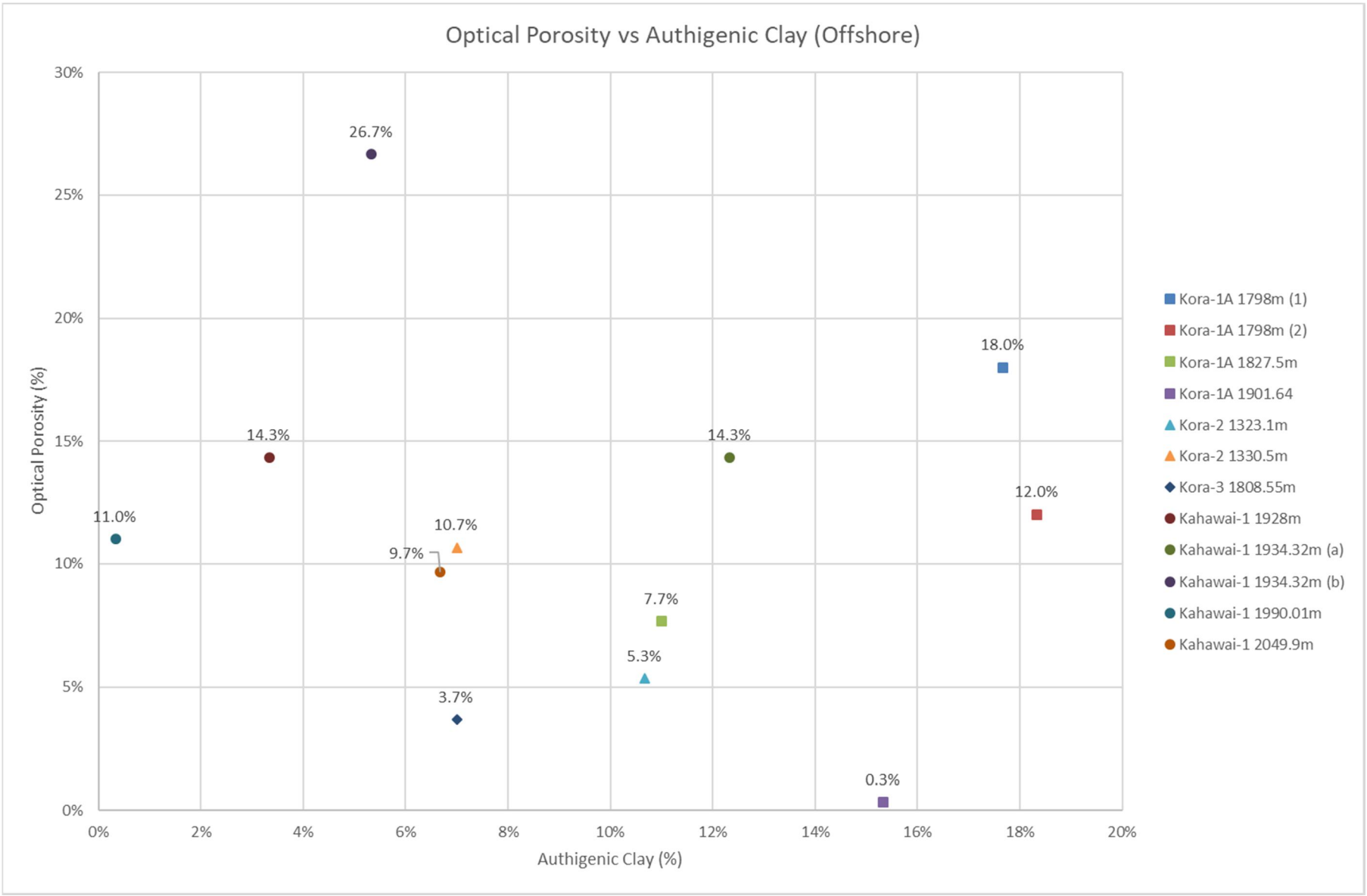

Figure 3.14: A graph of optical porosity plotted against total authigenic clay percentage. The values next to each data point is the optical porosity value for that sample.

3.5.5 Relationship between Average Grain Size and Optical Porosity.

There is a weak trend in the data from the offshore well proximal samples, shown in Figure 3.15, where the weak trend is that as the average grain size in the samples increases the optical porosity decreases. The raw data for all the offshore samples can be found in Appendix I. The Kahawai-1 well samples have the lowest average grain sizes (between 0.07 and 0.297mm) and highest average optical porosity value of 15.2%. These samples are highlighted in Figure 3.15 by a black dashed circle. The Kora-3 sample is an anomalous sample because it has a low average grain size of 0.3515mm and a low optical porosity of 3.667, and this contradicts all the other samples in this region of the figure. However, this is only one sample and from a different well so it can be considered to be anomalous and not an influence on the overall data trend. As the grain size increases the trend line between the well average data points decreases in optical porosity. The Kora-1A well average and the associated samples occur between 1.03 and 1.42mm average grain size and have optical porosities between 0.33 and 18% with an average of 9.499%. These samples are highlighted by the red dashed circle in Figure 3.15. There is a wide range in the values of these samples and no definitive group of data points. Finally, the samples with the highest grain size values are those from the Kora-2 well, between 1.59 and 1.50mm, and these experiences the lowest average optical porosity of 8%. These samples have been highlighted by a blue dashed circle. Like the Kora-1A the samples are spread evenly on either side of the trend line and there is no distinct grouping of data points. It must be acknowledged that this trend is weak, especially with a small data set available, and if this study were to be done again or improved by someone else in the future it would be key to try and source more offshore samples to test. This, however, would be extremely difficult because the well has been plugged and so no new samples can be sourced. The only feasible increase in sample would have to be conducted in conjunction with the GNS who may have more core sections available from the wells that can be sampled to increase the size of the data set.

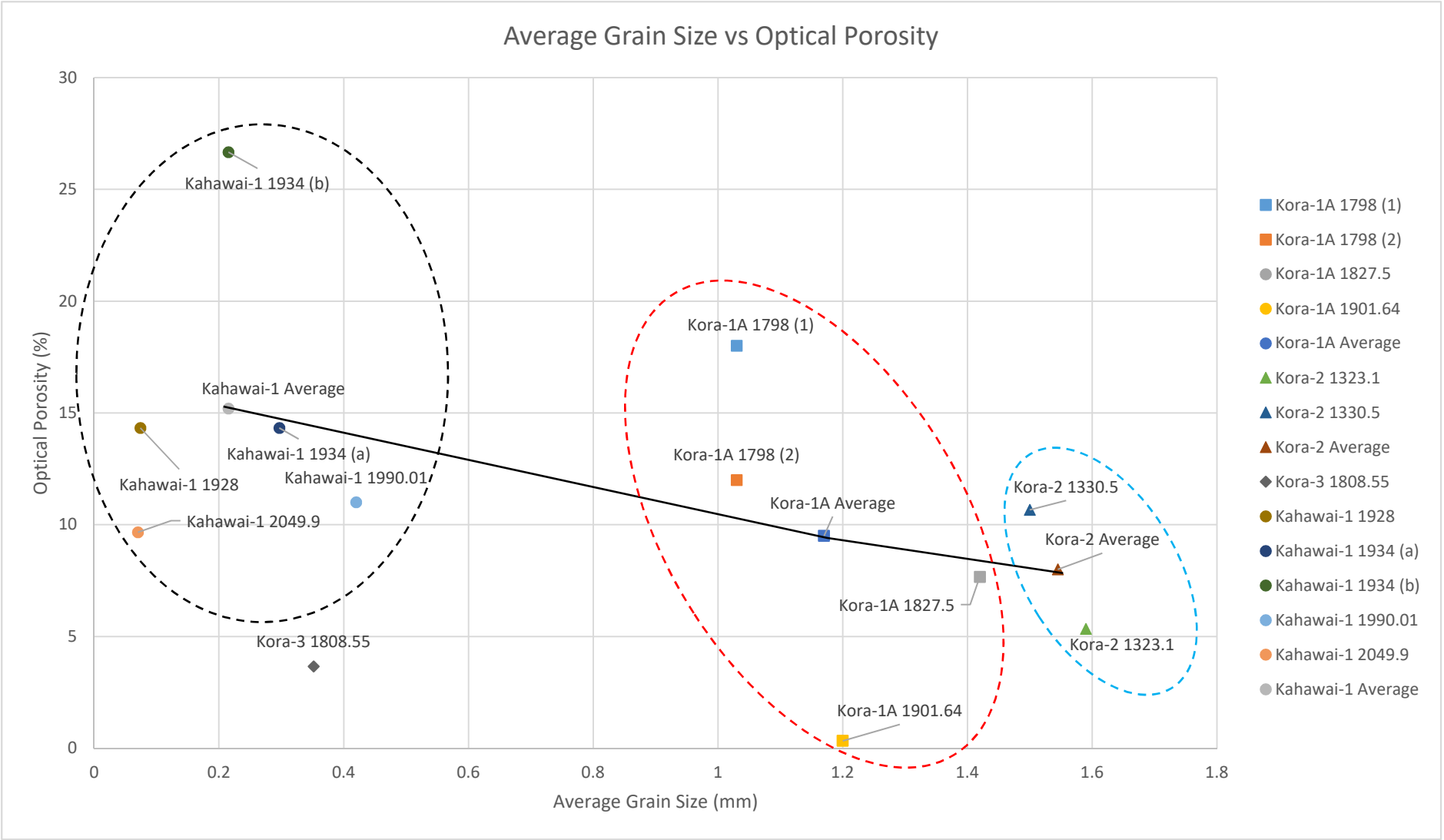

Figure 3.15: A graph of optical porosity plotted against average grain size for individual samples and well averages.

3.6 Permeability

3.6.1 Previous Studies

Permeability is an important factor in determining the reservoir quality of a rock. There has been limited work done on understanding the behaviour and trends of volcaniclastic rock permeability (Seubert, 2015; Mathisen & McPherson, 2012; Sruoga & Rubinstein, 2007; Suroga et al., 2004).

3.6.2 Relationship between Permeability and Depth

Permeability data from GNS is plotted against max depth (m TVDSS) (Figure 3.16). Permeability values (K air) are sourced from the same depths as the porosity data and from the same wells. There are 121 values for Kora-1A, 39 for Kora-2 and 26 for Kora-3. There is a similar spread of permeability data to that of the helium porosity data (Figure 3.12) as depth increases, with great disparity between the highest and lowest values in each well over short depths. The data shows a trend of increasing permeability with depth (Figure 3.16). This is distinct from the porosity results as there was no clear trend of porosity change due to depth between the wells.

In the Kora-1A well the trend is similar to that of the porosity where there are two clear groups of data; a group at shallower depths (roughly between 1856.14 m and 1936.20 m) having a significantly larger spread of data than those as greater depth. The permeability of this group's 86 data points ranges between 4970 mD and 0.005 mD, and the majority of these points can be found between 0.1 and 10 mD, while the remaining 35 values make up the second group that are found between 1936.20 m and 1986.00 m. This second group has a much tighter grouping of values with maximum and minimum values of 639 and 0.342 mD, with a high concentration of these values between 0.342 and 1 mD and then the remaining values dispersed between 1 and 639 mD. The shallower depth group a higher average permeability of 126.24 mD compared to the deeper values that have a decreasing average permeability of 35.449 mD, and so this gives a clear trend of decreasing permeability with depth. This trend can also be seen in the composite log for Kora-1A in Figure 3.1.

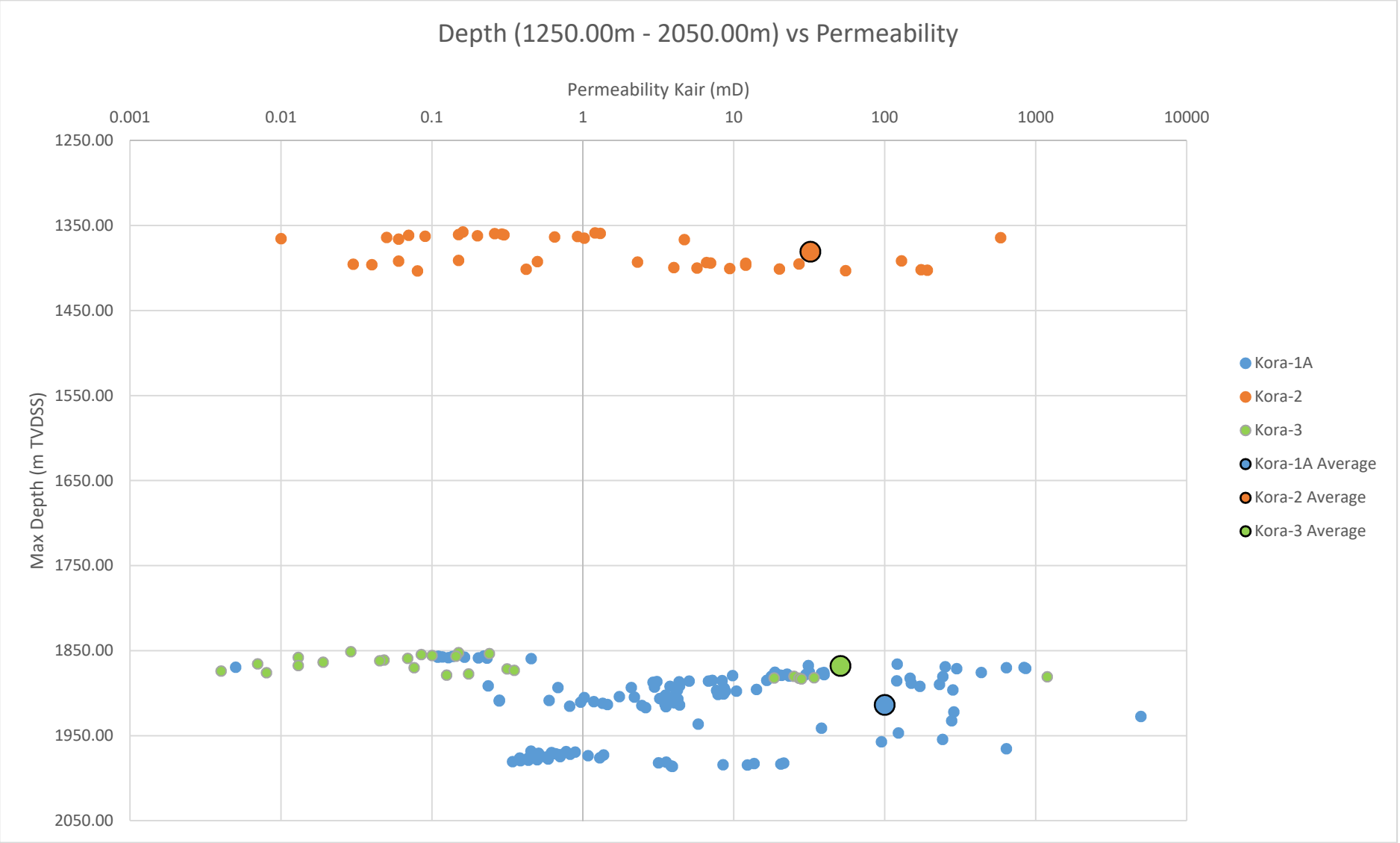

Figure 3.16: A graph of permeability plotted against depth, with the y axis shortened to only show results between 1250.00m and 2050.00m.

In Kora-2, there are two distinct groups of data that are dependent on depth (Figure 3.16). The group at shallower depths (1357.60 m and 1366.50 m) is made up of 18 data points with most found between 0.05 and 1 mD. There are anomalous values between 586 and 0.01 mD, and this is because they are the extreme values of the whole Kora-2 data set. The second group of 21 values is found between 1391.00 m and 1403.50 m, and most are found between 1-100 mD. The deeper group has a much lower average permeability, with an average of 31.3 mD compared to that of 33.2 mD showing a trend of decreasing permeability with increasing depth. This is seen in Kora-1A but with much lower permeability values seen at all levels. See Figure 3.4 for position of the data within the Kora-2 composite log.

Kora-3 permeability data has the same trend as its porosity data (Figure 3.12 and Figure 3.16). The data can be split into two groups dependent on depth. The shallower group (1851.10 m and 1878.68 m) in Kora-3 is the largest, between 0.01 and 1 mD, with an average result is 0.101 mD. The second group has an average permeability of 220.42 mD, but less than 2m deeper than the first group. So, there is a trend of increasing permeability with increasing depth, differing from the other two wells, but over a significantly shorter distance and with the fewest data points.

3.7 Relationship between Helium Porosity and Permeability

The combined 186 data points for porosity and permeability values for the Kora-1, -2 and -3 wells mentioned previous sections are combined in Figure 3.17 A where permeability is plotted against porosity. In this figure the combined data shows a clear trend of increasing permeability with increased porosity, with the lowest value points mainly derived from the Kora-3 well, the intermediate values a combination of Kora-1A and 2, while the highest porosity and permeability data points are from Kora-1A and 3. The values for each well have been averaged out and they show that Kora-3 has a significantly lower porosity and permeability value for the well as a whole, and gives an indication that it has the poorest reservoir quality. While Kora-1A and 2 have similar porosity values Kora-2 has lower permeability on average, and so this shows that from the raw porosity and permeability data Kora-1A has the highest reservoir quality. One distinct trend across all of the data is that none of the material in any the wells has consistent reservoir quality, as there is a large spread of data and no consistent region of values in any of the wells.

Figure 3.17: A collection of graphs where porosity is plotted against permeability for each well and for all the wells plotted together. A) A graph of helium porosity plotted against permeability for Kora-1A, Kora-2 and Kora-3 wells. B) A graph of helium porosity plotted against permeability for the Kora-1A well. C) A graph of helium porosity plotted against permeability for the Kora-2 well. D) A graph of helium porosity plotted against permeability for the Kora-3 well. All of these graphs have a linear trend line to supplement them, and this provides a an additional feature by which the difference between the average values at each end of the graph can be judged. It is also key to note that the graphs are logarithmic.

In Figure 3.17 A the Kora-1A is the most prominent of the three wells due to the number of data points and also the spread of the data across the centre of the graph, but it is difficult to identify the specific trend of the individual well. The Kora-1A data demonstrates a trend of permeability increasing rapidly over smaller increases in porosity (Figure 3.17 B). Where the data for the well is plotted showing alone, a rapid increase in permeability over a short initial increase in porosity before the gradient of the trendline becomes gentler and the permeability increases at a significantly lower rate at the highest porosities. The data in this well has a large range from a highest porosity and permeability value of 35.5% and 4970 mD respectively to as low as 9.5% and 0.005 mD, and most of the data is found between 15% and 25% porosity but has wide ranging permeabilities (39.6 mD to 0.109 mD). Kora-1A has the highest average porosities and permeabilities of all their wells and from these two factors it can be considered to have the highest reservoir quality.

Kora-2 is the only of the three wells to have a trend of decreasing permeability with increasing porosity, (Figure 3.17 C). This trend line shows a distinct difference to the other graphs, showing that the average permeability is decreasing as the porosity increases. Kora-2 also demonstrates a trend in the data where at lower porosities (at around 15%) there are the extreme values of high and low permeability (586 mD to 0.01 mD), and then as the porosity increases the permeability values move away from the extremes to values of 7 mD and 1.3 mD at around 30% porosity. The wide range and lack of a central collection of values means the Kora-2 well does not have consistent reservoir quality and is therefore difficult to understand.

The data for Kora-3 in Figure 3.17 D, has a similar trendline that seen in Kora-1A, with increasing permeability with porosity, but the average values are much lower and so while the rapid increase at lower porosities is the same the initial porosity for Kora-3 is around 5% as a pose to Kora-1A which is around 20%. In this figure we also see that Kora-3 has its values clearly segregated into two groups, with the majority of results with <15% porosity, and then 7 >25% porosity in the second group and no intermediate results. The trend line shows that while there is a distinct, low permeably group at low porosity, there is a relatively sharp increase in the middle data points before plateauing with the higher permeability/high porosity data points raising the trend line. While Kora-3 has the poorest reservoir quality results it also has some of the best, making the overall reservoir quality of the well difficult to constrain.

3.8 Intergranular Volume (IGV)

The intergranular volume (IGV), or minus-cement porosity, is the sum of intergranular pore space, intergranular cement and depositional matrix (Paxton et al., 2002), and decreases with burial depth due to mechanical and chemical compaction (Sticker, 2016). All data for calculating IGV is sourced from the point counting used in this study.

3.9 Porosity Loss by Compaction (COPL) vs Cementation (CEPL)

The trend of plotting porosity loss by compaction (COPL) against porosity loss by cementation (CEPL) is referred to as an intergranular volume (IGV) compaction curve, and this helps to establish the potential extent/limits of, and the interaction between, mechanical grain compaction and cementation in sandstones (Paxton et al., 2002). According to Paxton et al., 2002, porosity-depth curves can be very misleading when predicting reservoir quality in basins where the sandstones vary regionally and stratigraphically in terms of grain compaction, grain size/sorting, and volume of depositional matrix. Therefore, the benefit of using the technique of IGV curves in this study is that they are designed for sedimentologically and stratigraphically complex regions such as the Taranaki Basin and specifically the Mohakatino Formation, and can give a more realistic idea of porosity loss than a simple porosity-depth curve.

Total cement volume is used to help calculate the porosity losses caused by mechanical compaction (COPL) and cementation (CEPL) (Lundegard, 1992). This is achieved using the equations from Lundegard (1992) below:

$$COPL = P_i - \left(\frac{(100 - P_i)P_{mc}}{100 - P_{mc}}\right)$$

$$CEPL = (P_i - COPL)\left(\frac{C}{P_{mc}}\right)$$

Where P_i is the initial or depositional porosity and P_{mc} is the intergranular volume/minus cement porosity calculated by the sum of total optical porosity, P_o, and volume pore filling cement, C. The results of COPL vs CEPL (Table 3.2) are only valid if certain conditions are met according to Stricker (2016): the assumed initial porosity must be correct; the amount of cement must be negligible or known; and the amount of framework mass exported by grain dissolution must be negligible or known. Initial/depositional porosity for the Mohakatino Formation is estimated to be in the region of 40%.

This number is used because the Mohakatino Formation does not have a recorded or estimated initial porosity, while classic reservoir sandstones generally have a 40-42% surface porosity when deposited (Paxton et al., 2002). This number is also supported by Galloway (1979), who found that arc derived volcanic sandstones of the Bristol, Gulf of Alaska, Queen Charlotte, and Grays Harbour-Chehalis basins of the northeast Pacific had initial porosities ranging up to 40%.

	C	P_o	IGV	COPL	CEPL
Well/Sample	**[%]**	**[%]**	**[%]**	**[%]**	**[%]**
Kora-1A 1798 (1)	17.667	18	35.667	6.735268	16.47708
Kora-1A 1798 (2)	18.333	12	30.333	13.87601	15.78911
Kora-1A 1827.5	11	7.667	18.667	26.22921	8.114787
Kora-1A 1901.64	15.333	0.33	15.663	28.85685	10.90838
Kora-1A Average	**15.58325**	**9.49925**	**25.0825**	**19.9119**	**12.48033**
Kora-2 1323.1	10.667	5.333	8	34.78261	6.956739
Kora-2 1330.5	7	10.667	8.8335	34.18635	4.606955
Kora-2 Average	**8.8335**	**8**	**8.41675**	**34.48584**	**5.787194**
Kora-3 1808.55	7	3.667	5.3335	36.61961	4.436628
Kora-3 Average	**7**	**3.667**	**5.3335**	**36.61961**	**4.436628**
Kahawai-1 1928	3.333	14.333	8.883	34.1506	2.194761
Kahawai-1 1934 (a)	12.333	14.333	9.1665	33.94508	8.146554
Kahawai-1 1934 (b)	5.333	26.667	16	28.57143	3.809286
Kahawai-1 1990.01	0.333	11	5.6665	36.39587	0.211802
Kahawai-1 2049.9	6.667	9.667	8.167	34.66401	4.35595
Kahawai-1 Average	**5.5998**	**15.2**	**9.5766**	**33.64549**	**3.71572**

Table 3.2: Data used to calculate COPL and CEPL (Offshore) and then used to generate Figure 3.19. C = volume pore filling cement, P_o = sum of total optical porosity, IGV = intergranular volume, COPL = porosity loss by compaction, CEPL = porosity lost by cementation.

The raw data from Table 3.2 are plotted in Figure 3.18 and here the distribution of porosity loss by compaction against cementation can be clearly seen. In Figure 3.18 10 out of 14 wells/well averages have greater than 25% COPL and less than 10% CEPL, as well as one sample (Kora-1A 1901.64m) with over 25% COPL and less than 15% CEPL and the Kora-1A average with 20% COPL and below 15% CEPL. These samples and the well averages therefore have had their porosity loss influenced by compaction rather than cementation. The averages of Kora-2, Kora-3 and Kahawai-1 can be found clearly in the concentration of data points in the top left of the graph, indicating these well were influenced by COPL, while Kora-1A Average, although still experiencing COPL has lower results due to anomalous results influencing the position.

The samples that have experienced porosity loss from cementation are Kora-1A 1798m (1) and (2), with COPL results below 10% and 15% respectively and CEPL results above 15% each. These two results can be considered anomalous because they come from the same depth of the same well and so cannot be representative of the region or the well. They are also the only two samples to exhibit this trend in the data and if all the other wells and their samples are behaving in one way and this one region of Kora-1A is behaving differently, then it can be inferred there have been other influencing factors on these samples. The position of the Kora-1A Average in Figure 3.18 has been altered by these anomalous results because they have drastically lowered the COPL average results and raised the CEPL results in the well.

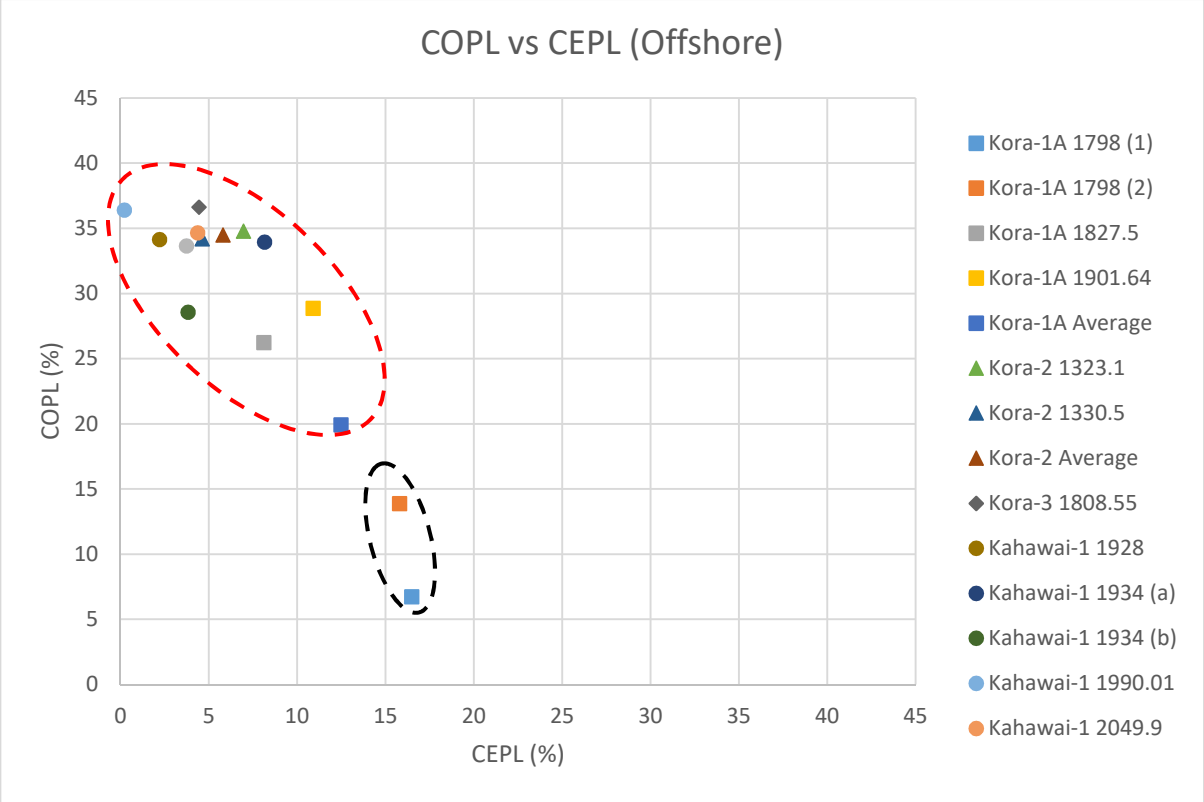

Figure 3.18: A graph of porosity loss by compaction (COPL), with samples affected by this process circled in red, vs cementation (CEPL), and samples affected by this process circled in black.

3.10 Discussion

Mineralogy

The Mohakatino mineral components found in the Kora wells are derived from the mid-late Miocene Kora volcano as part of the MVC and this material was then reconstituted to form the Mohakatino volcaniclastics (King and Thrasher, 1996; Bergman et al., 1992; Stagpoole and Funnell, 2001; Killops et al., 1994). The point counting and petrographic analysis of this study has found that while this is theory is supported by the data there are some irregularities that are not acknowledged, such as the quartz content. Typical andesites have high proportions of plagioclase feldspars and intermediate amounts of amphiboles and micas, with minor pyroxene, quartz and orthoclase, and so it is inferred that these will be the primary minerals of the Mohakatino due to the andesitic source of the MVC/Kora volcano. However, this study found that while plagioclase was the highest mineral component (46.27% averaged across all wells) the second highest was quartz (16.059%) followed by hornblende (13.093%). This is an irregular mineral pattern because quartz should be found as a minor mineral, while the amphibolite hornblende should occur in a higher percentage than it is found. A cause of this is thought to be that, while the dominant eruption type here is andesitic, there is the

possibility of dacitic eruptions occurring as well during the same period and the combined material leads to the higher than expected quartz levels in mainly andesitic volcaniclastics (Adrian Pittari, Pers Coms, 2017). A key feature of the proximal mineralogy of the Mohakatino Formation is that it has been influenced by a number of different factors and events and this has led to an unusual mineralogical makeup of the reservoir sandstones.

Cements and Grain Coatings

The origin of the authigenic clays in these volcaniclastics according to Remy (1994) is that rocks with abundant andesitic rock components, such the Mohakatino, are characterised by early generation of authigenic chloritic mixed-layer clays and lesser quantities of illite-smectite and standalone chlorite. Remy (1994) also found that the compaction and cementation obstructed the majority of macroporosity in the samples with the richest volcanic detritus and this led to the sealing of the rocks and preventing the development of later stage dissolution or authigenic mineral precipitation. This trend is seen in the point counting data, with Kora-1A and 2 having the highest RF percentages and retaining higher levels of porosity. This explains the lack of the other authigenic clays in the GNS analysed samples, and also why the there is such a high proportion of indeterminate clays noted in their work because much of this chlorite is intermixed and harder to identify. From this evidence it can be inferred that the andesitic nature of these Mohakatino samples potentially had an influence in retaining porosity and therefore have a beneficial effect on the reservoir quality.

Compaction and Cementation

The COPL vs CEPL data from Table 3.2 and Figure 3.18 shows that the significant majority of the samples have had their porosity lost through compaction, and this is thought have been influenced, if not caused, by the rapid deposition of the Giant Foresets Formation (see Section 2.2 and 2.3.3) under normal pressure sequences up to 4 km thick in some regions over 2 Ma on top of the Mohakatino Formation (Stagpoole and Funnell, 2001, King and Thrasher, 1996, Hansen and Kamp, 2004). This compaction identified in the COPL vs CEPL plot (Figure 3.18) combined with the minor clay precipitation seen in the point counting data (Appendix IV) and that has been discussed previously in this section, is likely to have occluded most macroporosity in the volcaniclastic Mohakatino Formation, potentially leading to the sealing of the rocks and preventing later stage dissolution and authigenic mineral precipitation (Lundegard, 1992, Remy, 1994).

The results in Figure 3.18 show that compaction is overwhelmingly the primary driver for porosity loss in all of the wells other than two samples in Kora-1A. In Kora-1A the samples at 1798 m (1) and (2) have been influenced mainly by cementation. These two samples have the highest optical porosity values and the highest (undifferentiated) cement percentage. These samples have been influenced by authigenic clay cements in the form of authigenic opaques (4%), chlorite (1% of sample) and Fe Oxide (1%). However, as mentioned previously the majority of the authigenic clays are interpreted as

being undifferentiated (4%) so it is impossible to say if there is another authigenic influence on the samples. As was previously mentioned in Section 3.9 is that these cementations influenced samples must be interpreted as being anomalous because they both occur at the same depth and are therefore not representative of the well as a whole. As well as this, if both samples from the same depth have significantly different results to the rest of the data set and their well then it can be inferred that they have had a localised, anomalous influence on their porosity loss.

Grain Size

When looking at the raw data in Appendix I and the plotted data in Figure 3.15, it may appear that as the grain size increased the optical porosity decreased. However, there is another factor that when paired with grain size could be a more dominant influence on optical porosity and therefore on reservoir quality. In Appendix I, the Kora-1A and Kahawai-1 wells as the depth of the samples increases the average grain size of the samples decreases, although there are some anomalies to this trend such as Kahawai-1 1928. This means that the grain size could have been influenced by depth and how the material was deposited at these different depths, making depth the more influential factor on the optical porosity. There is however no evidence as of yet for the depth of the samples influencing the grain size, so for the time being it can be inferred that as grain size increases in proximal, offshore samples, the optical porosity and the reservoir quality decrease.

Porosity and Permeability

The porosity and permeability data from the sample depths analysed by the GNS was crucial for understanding the trends down each well and across the Kora field as a whole. This data indicates that it is mineral makeup rather than depth that has a greater effect on the porosity and permeability of the Mohakatino Formation.

While permeability values show a slight increase with depth, porosity varies with mineralogy. In both of these variables, it is possible to see that when moving from Kora-2 to Kora-1A they follow a pattern of increasing clay cements and hornblende while the other minerals (plagioclase, quartz and volcanic rock fragments) decrease, and porosity increases with them as well as depth. Kora-3 on the other hand does not follow this trend, which has significantly more plagioclase and quartz while seeing a decrease in porosity and all other variables, and occurring just a bit shallower than Kora-1A. This trend is contradictory to the idea that authigenic clays are detrimental to reservoir quality, the trend of increased porosity with increased authigenic clays seen in the data is a theory that has gained support over time (Heald and Larese, 1974; Thomson, 1979; Galloway, 1979; Pittman 1992; Ehrenberg, 1993; Berger et al., 2009; Taylor et al., 2010; Jiang, 2012; Stricker, 2016). These studies hypothesise that authigenic clays act as a preventative barrier to inhibit secondary quartz cementation/overgrowth, and sands with lower clay volumes will have more authigenic clay. Comparing Kora-1A (the highest average porosity and permeability) and Kora-3 (the lowest), Kora-

1A has almost half the quartz, over twice the amount of clay, and has the highest visible and helium porosity values, and so it can be inferred these clays are behaving in the same way as mentioned above in these studies. This trend is only seen when the samples are collated and averaged for each well, so although we see this general trend this trend is not necessarily true for every individual sample as seen in Figure 3.14. This can also be identified in the COPL vs CEPL plot (Figure 3.18) where the individual samples that have the greatest amount of cementation (all from Kora-1A) have retained the most porosity, while those with lower porosity have undergone greater compaction.

Previous studies of porosity preservation due to clay minerals (Galloway, 1979; and Berger et al, 2009) have found this trend in volcaniclastics. VRF volume has not appeared to have had a detrimental impact on the porosity either, and so it can be inferred that the Mohakatino Formation behaved in a similar way to a regular sandstone. This contradicts the work of Clark (2014), who found that a greater abundance of VRF lowered optical porosity. Clark (2014) focused on how mafic material influenced volcaniclastics, so this difference in the core mineralogy may be responsible for this variation. The ideas of this study are concluded using the mineral data from personally conducted point counting, but the mineral data provided by the GNS is contradictory to this. Their XRD analysis found that depth does not correlate with porosity or mineral data, and they have found the highest volume of clays and cements in samples from Kora-3, decreasing in Kora-2, and with the lowest in Kora-1A. Kora-1A is still found to have the highest individual porosity and permeability values but there are other well samples with higher clays and cements have significantly lower values. The GNS data usefulness therefore remains inconclusive but for the purpose of this study the point counting data will be used as the primary indicator as it is comparable to the point counting work done with the distal samples as presented in the next chapter.

3.11 Conclusions

The greatest challenge for studying the offshore Mohakatino Formation is that there is a limited number of samples available for analysis Porosity retention of the samples may have come from a number of sources, but the mechanical compaction occluding macroporosity working in conjunction with early precipitation of minor volumes of authigenic clays preventing quartz overgrowths and later stage dissolution are the most plausible combination of factors of achieving these porosity levels. This reservoir has not yet undergone significant digenesis, and a greater maturation of this reservoir could have gone in either direction: an increased reservoir quality where porosity could have preserved by mechanical compaction and early authigenic clays; or reservoir quality could be lost when they come to chemical equilibrium from interacting with seawater.

Chapter 4

A Petrographic Study into the Reservoir Quality of the Onshore Mohakatino Formation, Northern Taranaki Basin, New Zealand.

4.1 Introduction

This Chapter moves the focus from the offshore Kora and Kahawai wells to onshore sections of the Mid-Miocene Mohakatino Formation of the northern Taranaki coastline. The ~100 m-thick Mohakatino Formation, crops out for over ~30 km in wave-cut platforms and cliff sections up to 100m high (Figure 4.1). The sedimentary facies of these mass-transport deposits (MTD) along the North Awakino coastline provides a unique insight to observe lateral relationships where cm- to m-scale beds persist in thickness for many kilometers laterally within the coastal sections. The coastal sections allow comparison with the offshore Mohakatino Formation where lateral connectivity and architecture cannot be readily achieved in a subsurface proven volcaniclastic hydrocarbon reservoir. This submarine fan system is unique in the Taranaki Basin for its combination of sediment gravity flow deposits and ash-fall deposits, the dominance of coarse-grained sand to gravel of predominantly volcanic origin from the MVC.

Figure 4.1: A view of the Awakino Coastline towards the south, away from the Waikawau Cliffs, where the Mohakatino Formation outcrops onshore.

This chapter documents petrographic variations in the Mohakatino Formation using key lithofacies and spatial distributions within MTDs that are exposed for over 30 km for ~80 km of the Awakino coastline of North Island, NZ. Key sections along the coast from the Mokau River to the Waikawau Cliffs (Figure 4.2) provides the opportunity to investigate lateral variations in reservoir quality in the

Mohakatino Formation, and determine if reservoir quality is influenced by proximal to distal fining of a volcaniclastic MTDs.

4.1.1 Overview of Fieldwork Area

The Taranaki Basin of the North Island, New Zealand, hosts the remains of the Mohakatino Volcanic Center (MVC), an andesitic, submarine volcanic arc that was active from about 16 to 2 Ma (Giba et al., 2013). The MVC was situated ~40 km west of the nominal eastern margin of the Taranaki Basin, which is defined by the Taranaki Fault (Stagpoole and Nicol, 2008) and the Herangi and Patea-Tongaporutu basement highs, the former of which is now represented by the Herangi Range (Figure 4.2). The MVC is now buried by Pliocene- Pleistocene continental slope and shelf sediments. Sediments sourced from the MVC are preserved in the upper Miocene Mohakatino Formation, variably exposed in cliffs along more than ~30 km of coastline between the Mohakatino River and the Waikawau Cliffs. The distal coastal outcrops of Mohakatino Formation are some 80 km east of the offshore subsurface data sets as penetrated by the Kora and Kahawai wells and represent the distal portions of the MTD.

The Mohakatino Formation is near the base of an upward-shallowing succession of basin floor to upper continental slope sediments that spans a roughly two-million-year period in late Miocene time (Figure. 2.3) and forms the majority of the exposed coastal sections used in this study. It is overlain by the Mount Messenger Formation: a submarine channel and fan system sourced from the south (King et al., 1993, 1994; Masalimova et al., 2015). The Mohakatino Formation is largely found offshore, buried beneath the same Pliocene-Pleistocene sediments that covered the MVC, but long-wavelength unwarping of the central North Island associated with growth of the Taupo Volcanic Center caused localized uplift of the easternmost margin of the Taranaki Basin, ultimately exposing this sedimentary succession in coastal cliffs at sea level (Kamp et al., 2004).

4.1.2 Methodology

This study investigated the presence of the Mohakatino Formation and its relationship with the surrounding formations across six coastal outcrop locations in the Awakino region. A total of XXX metres of stratigraphic section at a cm-scale was measured documenting bed thicknesses, geometry, grain size and sedimentary structures and textures.

Field Locations	Latitude, Longitude
1 -Awakino Heads	(-38.665700, 174.621827)
2 - Awakino Heads	(-38.665425, 174.619387)
3 - Pahaoa Ridge	(-38.663940, 174.628241) to (-38.664254, 174.627558)
4 - Mokau River	(-38.706955, 174.616683)
5 - Piopio Station	(-38.636014, 174.621817)
6 - Piopio Station	(-38.632815, 174.622222)
7 - Piopio Station	(38.627927, 174.622468)
8 - Waikawau Cliffs	(-38.475710, 174.639609)
9 - Waikawau Cliffs	(-38.471579, 174.642043)
10 - Opito Point	(-38.485124, 174.637848)

Table 4.1: Field Locations

Detailed field sketches were made at each location and photographs were also taken at notable outcrops, allowing for facies relationships and in particular the lateral variabilities of beds and lithofacies to be identified. Stratigraphic sections through sedimentary rock sequences were made at representative locations 1, 4, 5, and 8. It was not necessary to take more stratigraphic sections of the locations as there has already been studies which have undertaken significant stratigraphic analysis of the region (Sharman, 2014; Schumaker, 2016). Samples were taken from all key identified locations. A total of 25 representative rock samples of the Mohakatino Formation were collected from across all major locations (see Appendix II), as well as the overlying Mount Messenger Formation and the underlying Mangarara and Manganui Formations. Samples were collected from the lithofacies that make up the Mohakatino Formation.

4.1.3 Lithofacies Descriptions and Depositional Interpretations

When this fieldwork was conducted the work of Shumaker (2016) was used as a guide for identifying the specific lithofacies that make up the Mohakatino Formation at the locations that were surveyed. A summary of Shumaker's (2016) lithofacies descriptions and interpretations is found in Table 4.2, and example photographs of the identified lithofacies from the fieldwork can be found in Figure 4.3.

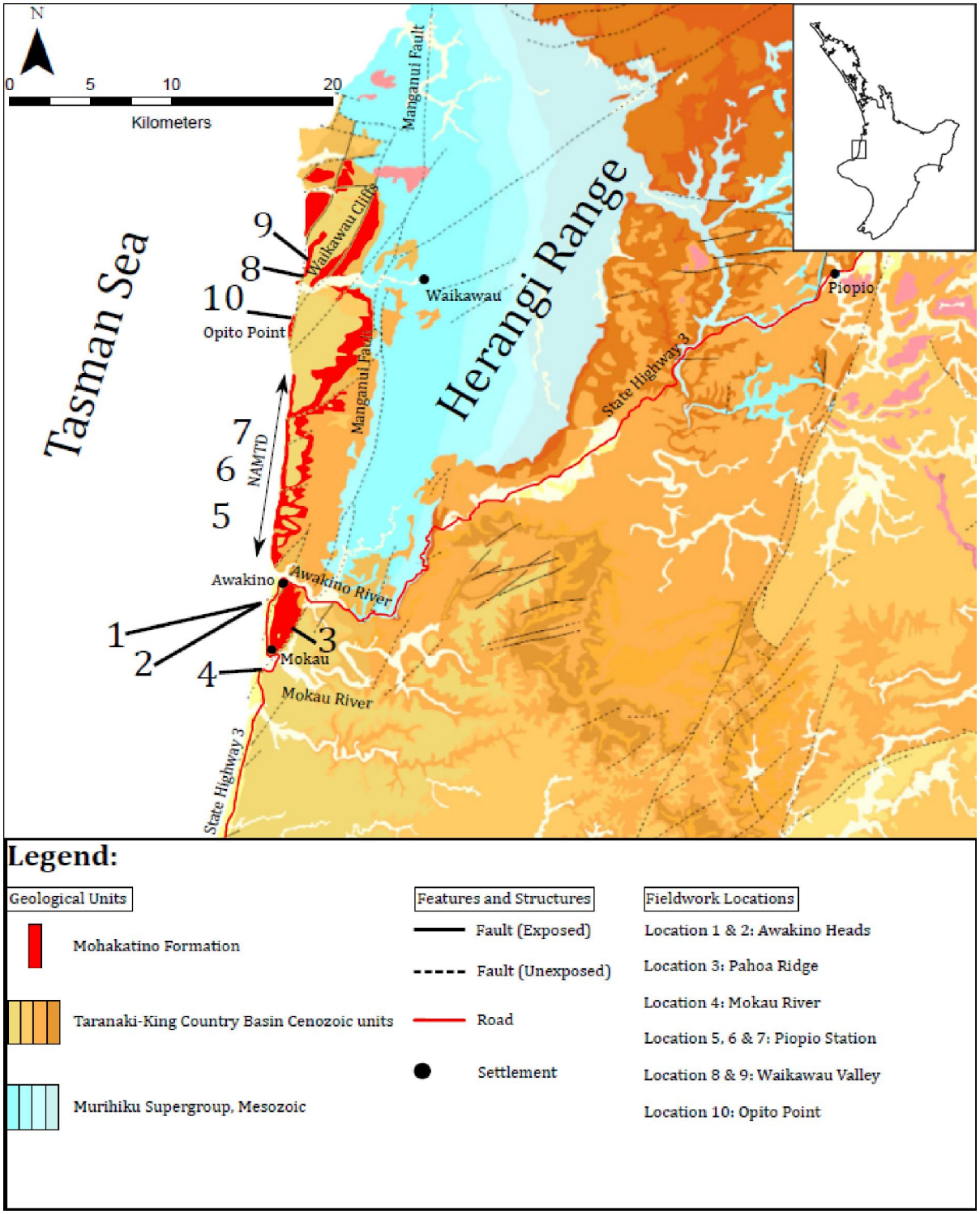

Figure 4.2: Location of study area with structural features, landmarks and local geological units with the inset image showing the position of this area in a regional context. Base map downloaded from ArcGIS Database and was provided by the GNS. Modified from Shumaker, 2016.

Lithofacies	Lithology	Bedding Style	Bedding Thickness	Grain Size Range	Sedimentary Textures	Sedimentary Structures	Lithologic Accessories	Bioturbation	Inferred Depositional Processes
1a	Alternating thin- to medium-bedded sandstone and siltstone	Tabular	1-50 cm	Silt to gravels	Normal to coarse-tail grading, very poorly sorted	Massive	Rare shell debris, rare pebble scale intrabasinal clasts	Minor to moderate; sand-filled burrows common	Waning low-density turbidity current with preferential deposition of Ta Bouma division
1b	Alternating thin- to medium-bedded sandstone and siltstone	Tabular	1-50 cm	Silt to gravels	Normal to coarse-tail grading, very poorly sorted	Planar lamination, ripple lamination	Rare shell debris, rare pebble scale intrabasinal clasts	Minor to moderate; sand-filled burrows common	Waning low-density turbidity current with preferential deposition of Ta-d Bouma divisions
2	Thin to medium-bedded sandstone	Lenticular	2-30 cm	Medium sand to gravels, rare pebbles	Normal grading, moderately well sorted	Low-angle tangential dune cross-stratification, some ripple lamination	None	Minor to absent	Sustained, energetic, erosive turbidity current
3a	Medium- to thick-bedded sandstone and medium-bedded siltstone	Tabular, amalgamated locally, minor basal scour locally	50-600 cm	Silt to pebbles	Normal grading, very poorly sorted	Planar to wavy lamination, ripple lamination, dish structures, dewatering pipes, flame structures	Abundant intrabasinal clasts (pebble to boulder scale), rare shell debris	Minor to moderate; sand-filled burrows common	Collapsing high-density turbidity current
3b	Medium- to thick-bedded sandstone and medium-bedded siltstone	Tabular, amalgamated locally, minor basal scour locally	50-700 cm	Silt to fine sand	Normal grading, well sorted	Planar to wavy lamination, dish structures, dewatering pipes	Locally abundant intrabasinal clasts (pebble to boulder scale)	Burrows present locally	Collapsing high-density turbidity current
4	Siltstone	Tabular	10-100 cm	Silt	Very well sorted	Planar to convolute lamination, ripple lamination	None	Moderate to pervasive	Low-energy, low-density turbidity current

Table 4.2: Summary of lithofacies descriptions and the inferred depositional processes that make up the Mohakatino Formation. From Shumaker (2016).

Figure 4.3: Example field photographs of lithofacies (See next page).

(A) Lf1a thinly bedded deposit demonstrating, coarse-tail graded and structureless bedding. Waikawau Cliffs. GB = Graded Bedding

(B) Lf1b beds shown with a distinct fining upwards trend from gravel at the base to silt at the top. Opito Point. GB = Graded Bedding

(C) Lf1b with structures consisting of ripples and wavy laminations. Mokau River. WL = Wavy Laminations; R = Ripples.

(D) Lf2 cross stratified sandstone, with the black slip faces being made up of concentrations of heavy minerals. Piopio Station. CS = Cross Stratification.

(E) Thick bedded Lf3a deposits made up of fining upward gravelly sandstone with internal horizons of intrabasinal clasts. Waikawau Cliffs. IC = Intrabasinal Clasts

(F) Lf3b dark grey beds with wavy lamination in the upper most bed. Waikawau Cliffs.

(G) Thick to medium bedded Lf4 deposits seen as the blue-grey beds. Waikawau Cliffs.

(H) Lf4 beds with convolute and ripple lamination, and moderate bioturbation through-out the beds. Opito Point. CL = Convolute Laminations. RL = Ripple Laminations.

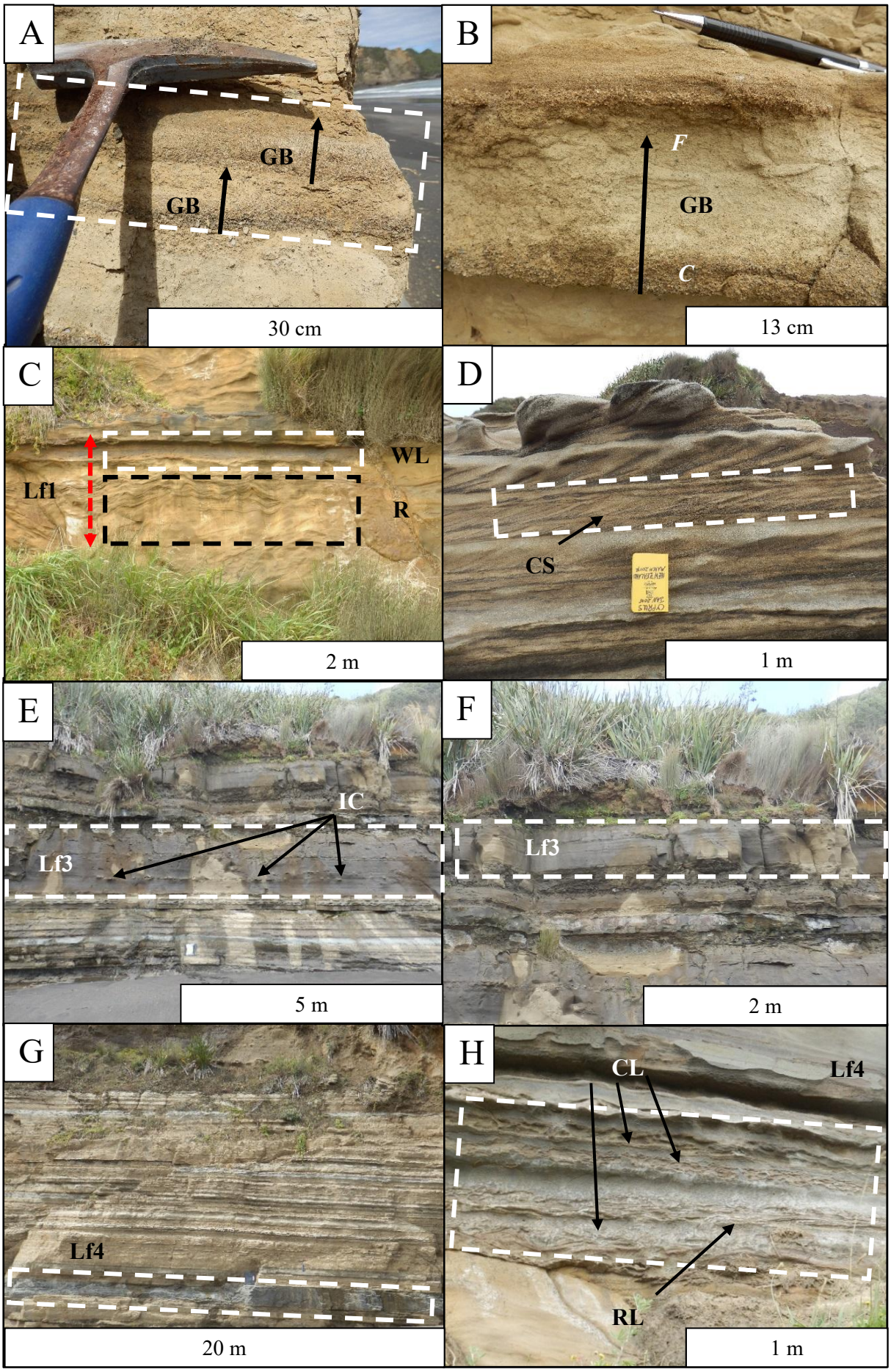
A
GB
GB
30 cm
B
F
GB
C
13 cm
C
WL
Lf1
R
2 m
D
CS
1 m
E
IC
Lf3
5 m
F
Lf3
2 m
G
Lf4
20 m
H
CL
Lf4
RL
1 m

4.2 Field Locations

Locations were chosen due to their accessibility and to allow for the study of how the lithofacies change and how they interact with the other formations in the region (Figure 4.2).

4.2.1 Awakino Heads

The Awakino Heads is a collection of residences 1.6 km south of Awakino village, just off State Highway 3 and adjacent to the Awakino River, and the outcrop here is situated on the area of headland roughly 30 m south of the buildings at the mouth of the Awakino River (Figure 4.2). Here there is a sequence of three sedimentary marine deposits that are exposed over ~30 m and consist of the Manganui, Mangarara and Mohakatino Formations with the Mohakatino Formation being the dominant lithofacies. The largest section of Mohakatino outcrop is summarised by the stratigraphic log in Figure 4.5. The outcrop here is north facing and extends east – west, with Location 1 based at the eastern section of the outcrop inland (-38.665700, 174.621827) and then Location 2 is situated at the western end towards the ocean (-38.665425, 174.619387).

At Location 1 the lower most unit is the Manganui Formation, a massive and structure-less grey mudstone. Overlaying this is a thin, (0.3-0.4 m) laterally discontinuous submarine channel deposit of the Mangarara Formation. This is intermixed with clasts formed of the Manganui and the unit's matrix coming from the Mohakatino Formation. The upper unit of the sequence is the Mohakatino Formation, which extends ~4 m to the top of the outcrop and is composed of centimetre scale parallel beds (~5-30 cm thickness). The beds dip 6ºS and the Manganui and Mangarara Formations pinch out to the west. Location 2 is at the end of the headland (see Figure 4.4 B) and is comprised entirely of the Mohakatino Formation.

The Mohakatino Formation at these locations is comprised of alternating beds that are formed primarily of Lf1a and Lf1b, which are very similar in their characteristics such as bedding styles, thickness, texture bioturbation and depositional processes (see Table 4.2). Other similar features found in both lithofacies include the presence roughly oval shaped, irregularly edged mafic clasts that are preferentially orientated in line with the bedding, and these are interpreted as peperite clasts (Figure 4.4 C). Peperite is defined by Shumaker (2016) as the result of lava intruding into unconsolidated sediment below or at the base of a lava flow, and that in this region there is no evidence for this peperite having formed *in situ* and the origin is upstream of the study area and these clasts were entrained by passing turbidity currents. Shumaker (2016) also stipulated that due to the irregular boarders these clasts were not transported long distances before re-deposition. These lithofacies are differentiated by their sedimentary structures where Lf1a has a distinctly massive structural style to its beds (see Figure 4.4 A), while Lf1b has planar and ripple lamination throughout

the beds (Figure 4.4 B) and this allows the lithofacies to be separated out within the outcrop. While these two lithofacies dominate the outcrop as these locations there are also beds of Lf2 that exist sporadically throughout the outcrop and almost exclusively at Location 2. These are recognised by their lenticular bedding compared to the tabular nature of Lf1a and Lf1b, as well the low angle tangential cross stratification, better sorting and lack of bioturbation (Figure 4.4 D), while their bedding is roughly the same scale at centimetre scale.

A stratigraphic log was made at Location 2 as it was a region that gives a good representation of the Mohakatino in this area of fieldwork. The log is shown in Figure 4.5). The two lithofacies are clearly distinguished by using the laminations of Lf1b and the massive structure of Lf1a, and smaller local features are also present, including peperite clasts, burrows, large phenocrysts and an intrabasinal clast. The alternating sandstone and siltstone nature of these lithofacies is much easier to see using the log as the grain size is hard to distinguish from the photographs The Lf2 beds of the location are not represented here and that was a due to a lack of foresight in choosing the location to conduct the logging, and in hindsight this would have been taken into consideration. As well as the logging done at this section, a sample of Lf1a (Sample 2 (Lf1a)) was taken to be used for petrographic analysis.

Both Lf1a and Lf1b (Table 4.2) are the result of waning, low density energy currents. Lf2 is interpreted as the deposits of sustained, energetic turbidity currents. The Lf1a and Lf1b lithofacies transport over large distances and deposition occurs at the distal ends of the turbidity currents. Lf2 lithofacies indicate deposition from larger, higher energy turbidity current or a turbidity current of the same size has occurred but at a closer proximity to this area and so the turbidity current still proximity to this area and so the turbidity current still has high energy when it is deposits material in this region.

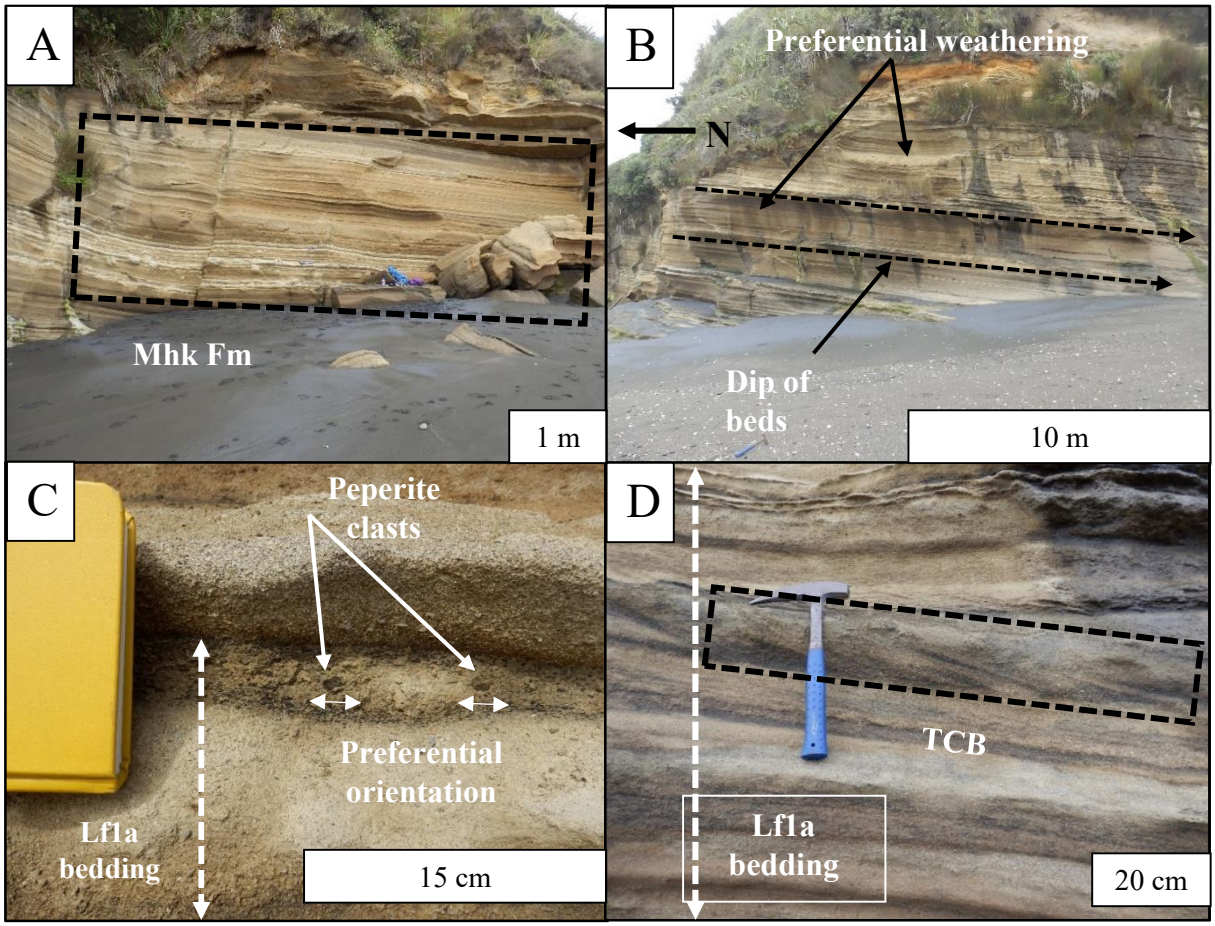

Figure 4.4: Example field photographs of the Mohakatino Formation from Location 2 at the Awakino Heads. A) Location 2 facing south where the outcrop has changed from Location 1 to being formed of only the Mohakatino Formation (Mhk Fm). B) Location 2 facing east showing the Mohakatino Formation, the dip of the beads to the south clearly as well as the bedded nature of the formation's lithofacies and their preferential weathering. C) Preferentially orientated peperite clasts entrained within a Lf1a bed. D) Low angle, tangential cross bedding (TCB) and minor laminations all with mafic compositions with Lf2 beds.

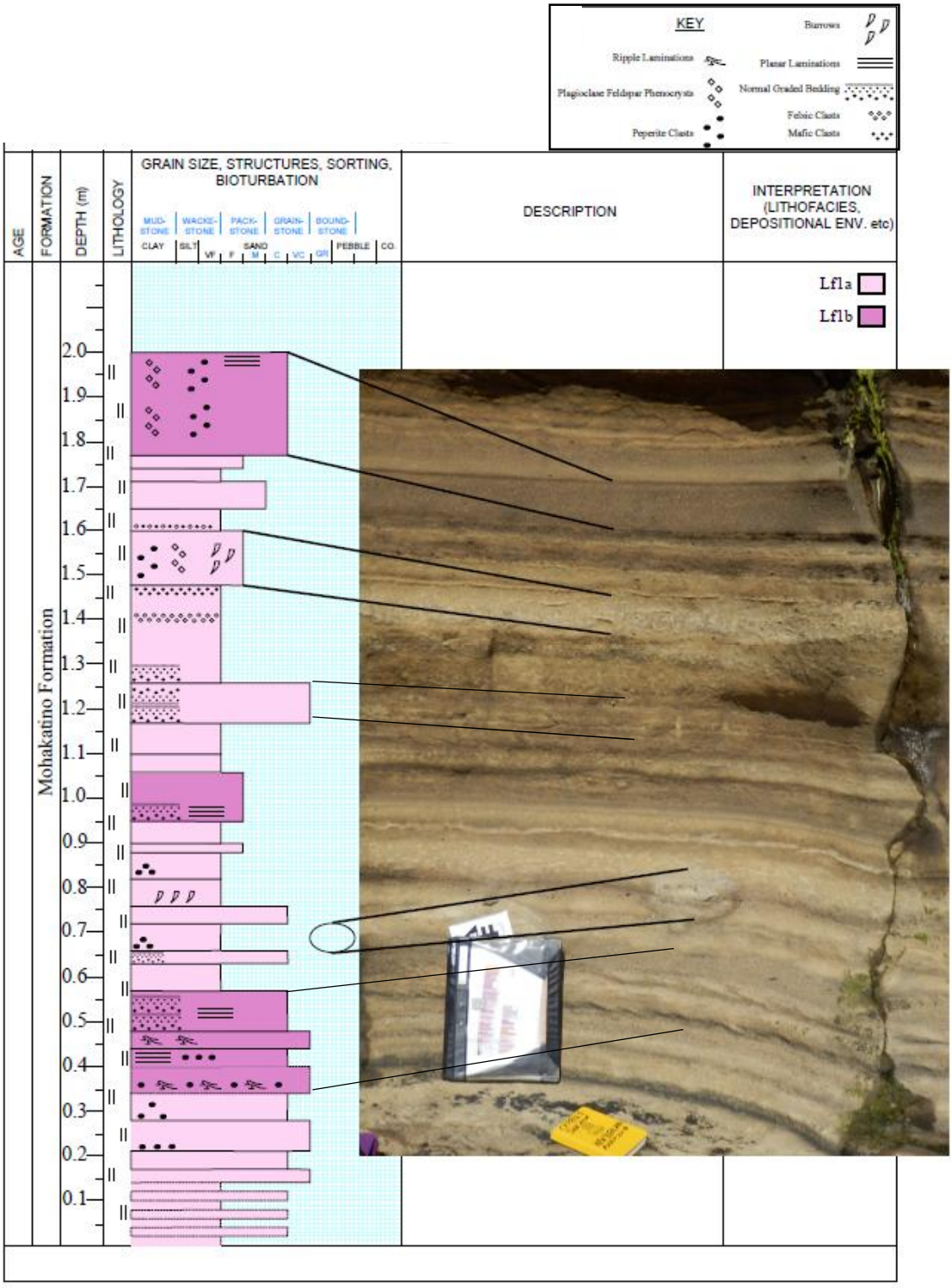

Figure 4.5: A stratigraphic log taken from Location 2 at the Awakino Heads and a corresponding photograph of the analysed section of outcrop.

4.2.2 Pahaoa Ridge

Pahaoa Ridge is situated inland east of Awakino Heads on the East side of State Highway 3 (Figure 4.2). The outcrop is accessible on the western face of the ridge and is reached by following the end of the ridge line up from the side of the highway and then runs along the ridge line (see Figure 4.6 A). Two major rock units make up this ridge and these are the Mohakatino and the Mount Messenger Formations. The Manganui and Mangarara Formations are also present but they cannot be seen at a distance due to their centimetre scale in comparison to the other units and the extent of the vegetation on the ridge. A significant amount of outcrop that was available for analysis in this region that was not surveyed, and this is due to the steep gradient, unstable footing, and working independently, all together making very little of this ridge possible to access without taking unnecessary risks. It is possible to infer that the outcrop (~15 m further up the ridge from the surveyed region) is made up of the Mount Messenger Formation, as it has been found previously the Mount Messenger Formation overlays the Mohakatino Formation as you move up the ridge (Shumaker, 2016).

Location 3 extends across the ridge from the northern end (-38.663940, 174.628241) to the southern end (-38.664254, 174.627558) of the accessible outcrop seen in Figure 4.6 A. The Mohakatino Formation forms this section of the ridge and severely weathered. The rocks demonstrate similar characteristics to Lf1a at Awakino Heads, and the Mohakatino Formation here is comprised exclusively of Lf1a (Figure 4.6 B) where the alternating beds at centimetre scale are visible, have a massive structure to them, graded bedding in places and beds of poorly sorted gravel. A sample of this Lf1a (Sample 6 (Lf1a)) was taken. Other similar features to those at Location 1 and 2 are the bedding measurements with an average planar measurement of 058/12/SSE, indicating the same southward dipping nature of the rocks and that the Mohakatino should disappear below sea level somewhere south of this location These features continue across the ridge outcrop to the south (see Figure 4.6 C), however half way along the ridge, the Manganui and Mangarara Formations appear in thin, laterally restricted packages, while the Mohakatino forms the uppermost layer. Weathering has masked almost all features. The environment of deposition for this area is inferred to be the same as that of the Awakino Heads.

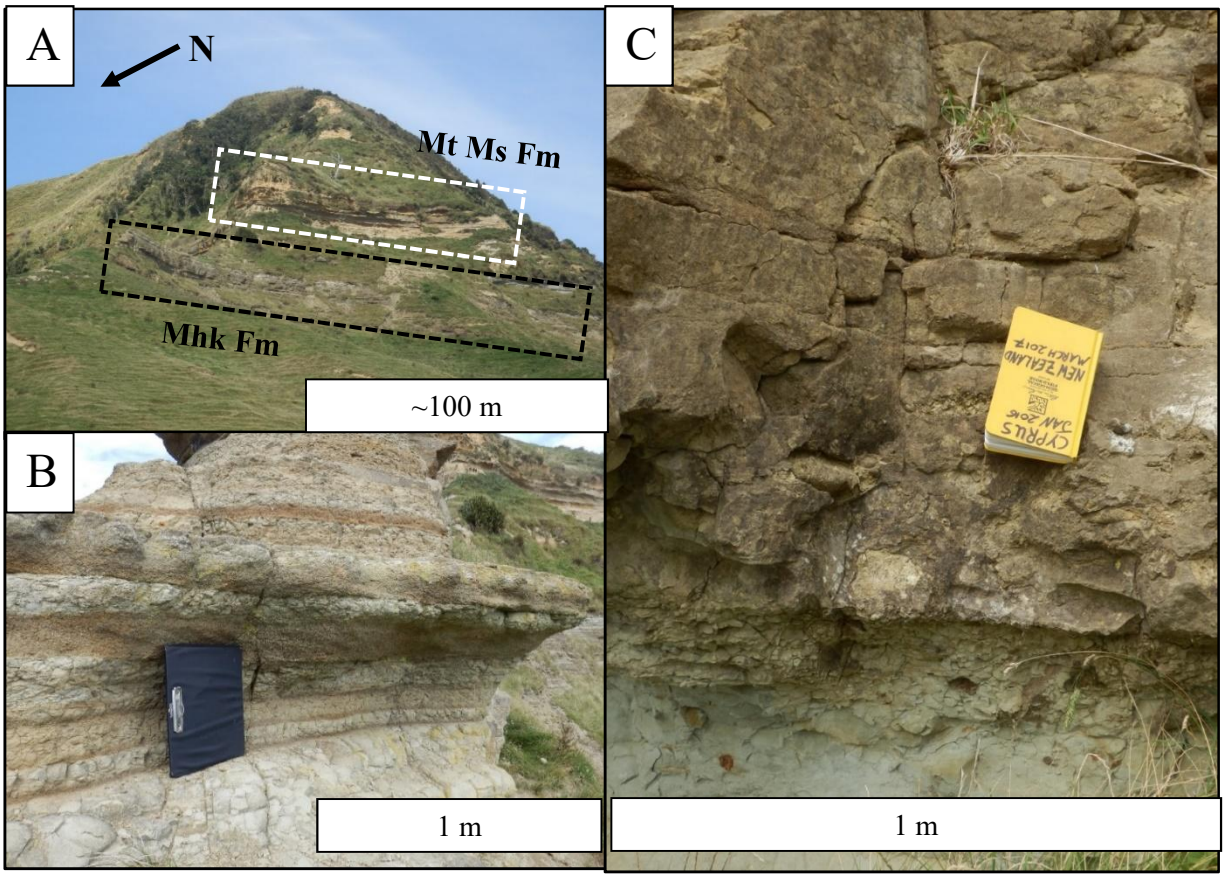

Figure 4.6: Example field photographs of the Mohakatino Formation at Location 3 on Pahaoa Ridge. A) A view of Pahaoa Ridge taken from the base of the ridge on the side of State Highway 3. Lower section of the outcrop is the Mohakatino Formation, with the Mount Messenger (Mt Ms Fm) seen further up the ridge. B) North end of the outcrop, showing heavily weathered Lf1a and Lf1b bedding of the Mohakatino Formation. C) The southern end of the outcrop, large, featureless and highly weathered Lf1a Mohakatino outcrop.

4.2.3 Mokau River

The Mokau River fieldwork was conducted on the southern side of the Mokau River, on the south bank of the river (see Figure 4.2 for position in the region). The outcrop is ~25m high and extends ~100 m east to west Location 4 is found on the most inland section of this extent of outcrop (-38.706955, 174.616683). This location is anomalous for the region because at Location 2 the Mohakatino was dipping towards the south and decreasing in height with distance. The explanation for this large outcrop is that to the south of the Mokau river there is a normal fault that uplifted the subsurface Mohakatino Formation to the surface from beneath the Mount Messenger Formation.

At Location 4 the Mohakatino Formation forms the lowest 20 m of the cliff while the uppermost 5 m is comprised of the Mount Messenger Formation (see Figure 4.7 A). To the south the Mount Messenger Formation increases to ~10 m thick, while the Mohakatino remains roughly the same thickness. The Mohakatino Formation at this location is similar to Location 3 at the Pahaoa Ridge as it is formed mainly of Lf1a (Figure 4.7 B) but at Location 4 there are some thin beds of Lf1b identified at random points throughout the outcrop. An example of a Lf1b bed can be seen in the stratigraphic log for Location 4 (Figure 4.8), and also the photograph of a specific peperite supporting

bed (Figure 4.7 D). A sample of Lf1a (Sample 7) was taken for petrographic analysis. The beds are the same as previous locations (Table 4.2). Additional features include 2-3 cm coarse grained infilled burrows seen at the base of some of the beds (Figure 4.7 C), with the coarser material coming from the graded bedding in these beds. There are also a few small peperite clasts in the very thin, coarse grained beds (Figure 4.8). These lithofacies indicate that the Mohakatino Formation here was deposited from waning, low density turbidity currents and due to the close proximity to the same lithofacies at the Awakino Heads and Pahaoa Ridge they could all have potentially been deposited together.

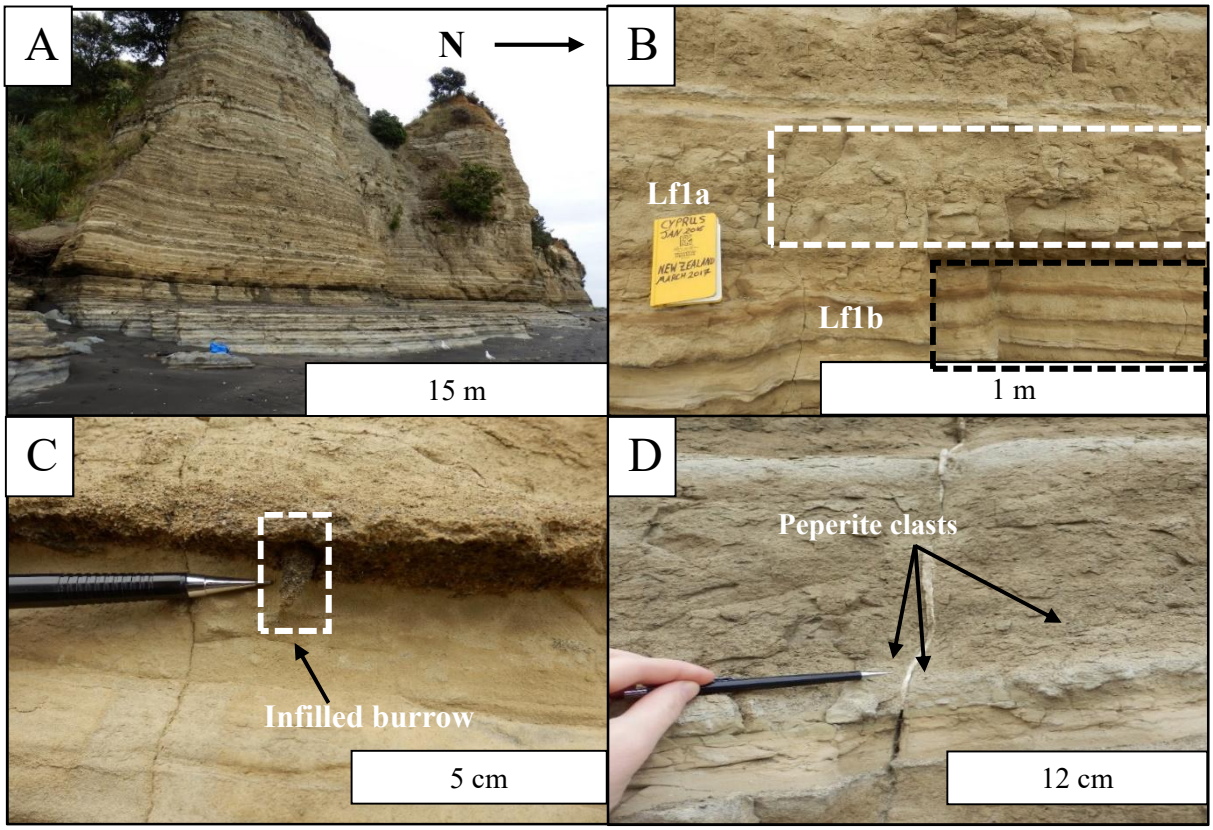

Figure 4.7: Example field photographs of the Mohakatino Formation at Location 4 on the south side of the Mokau River. A) A general view of the outcrop at Location 4 facing to the south. Outcrop seen to be made multiple beds that are primarily of Lf1a composition and features, with a few beds of Lf1b present. B) Representative view of the Lf1a and Lf1b beds that make up the outcrop at the Mokau River. Lf1b is seen at the bottom of the photograph and is distinguished by the lamination features, while the majority of the outcrop in the image is Lf1a. C) A burrow infilled with coarse grained material from the base of an L1fa bed which has gravel sized material at the base. D) Peperite clasts contained within a Lf1a bed. Peperite is found just above the pencil as black, mafic looking clasts.

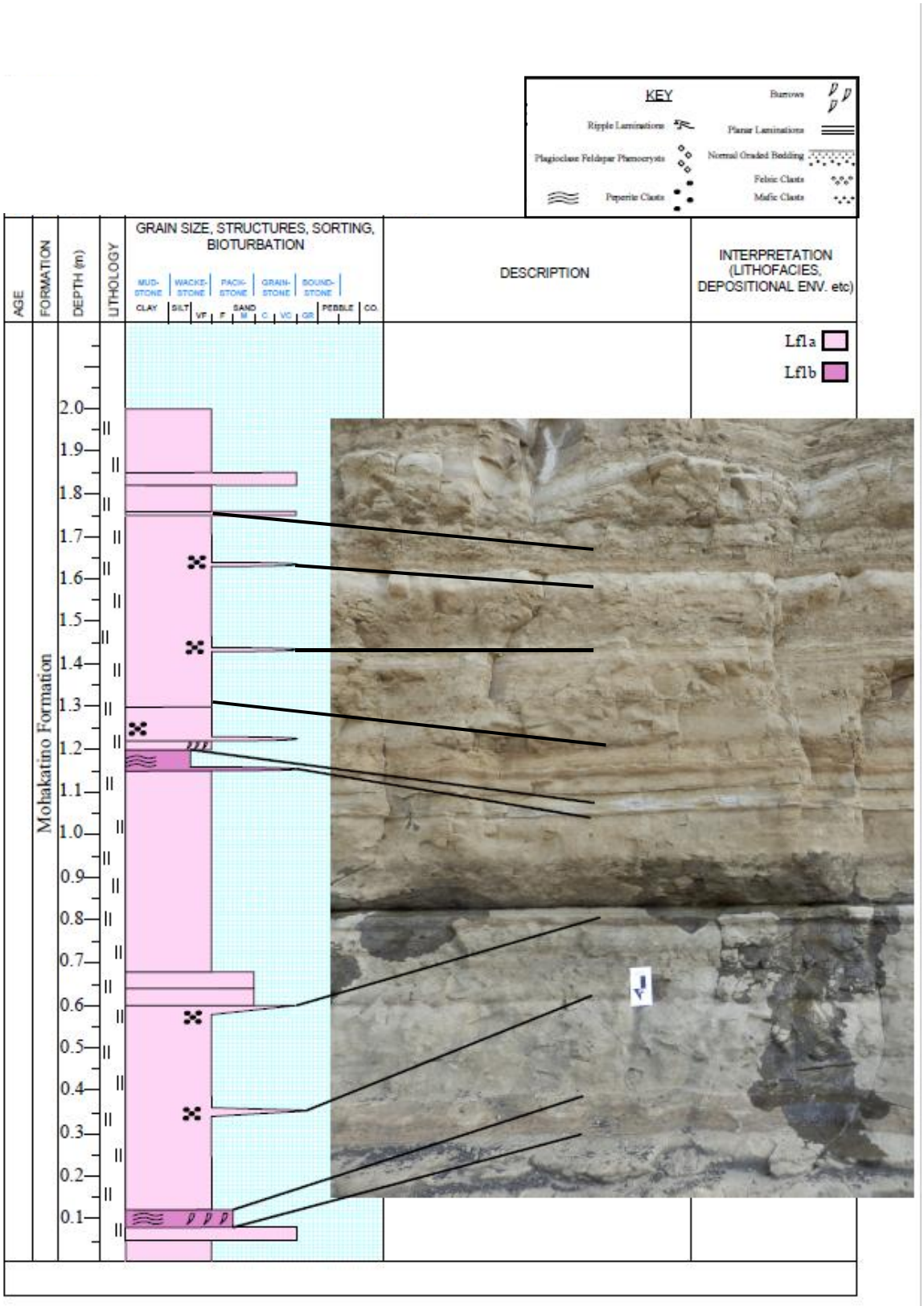

Figure 4.8: A stratigraphic log taken from Location 4 at the Mokau River and a corresponding photograph of the analysed section of outcrop.

4.2.4 Piopio Station

The region of the fieldwork area referred to here as Piopio Station is found on the north side of the Awakino River, down Fraser Smith Road until the road reaches the Pitone Stream just before the Piopio Station buildings, at which point the stream is followed to the beach and the 900m of coastline to the north is the assessed region of fieldwork (-38.636014, 174.621817 to -38.627927, 174.622468). The region is referred to as Piopio Station after the nearest farm, and includes Locations 5, 6 and 7. The outcrop is low lying, constrained to the coastline and comprised of the Mohakatino Formation.

The clearest change from other locations is the shift in the dip direction, which has changed from the S/SE to the NW and with an average planar bedding measurement of 53/17/NW (Figure 4.9 A). This demonstrates a change in the deformation seen to the south. Moving north the beds are dipping below the beach surface and the outcrop becoming lost, but this now to the north rather than the south. Another difference is that the dominant lithofacies is Lf2 and is characterised by low angle tangential cross stratification at Location 5 (-38.636014, 174.621817) (Figure 4.9 B and C). While being the dominant lithofacies for this part of the region, there are also beds of Lf1a and Lf1b that occur at infrequent intervals through-out the outcrop. Lf1a bed are distinct due to their characteristic massive nature while Lf1b demonstrates planar lamination not found in the other lithofacies (Figure 4.10).

Following the outcrop north along the beach away from Location 5 towards Location 6, the outcrop undulates above and below the surface of the beach. There is also a change in the dominant lithofacies, with Lf2 becoming rarer and the dominant lithofacies being once again Lf1a with minor Lf1b (Figure 4.9 D). There is a distinct change in the structural style of the area, to small, outcrop scale anticlines (Figure 4.9 E) and synclines (Figure 4.9 F). This region of local deformation and structure that is not seen in any of the other locations is explained by Sharman (2014) who interprets all of this as being part of the North Awakino Mass Transport Deposit (NAMTD). The NAMTD is defined as a roughly 11km submarine soft sediment mass-movement characterised by extensive deformation along the coastline between Pitone and Paparahai Streams, and the southern end of this interval was analysed at the Piopio Station section of the fieldwork area (Sharman, 2014).

Location 7 (38.627927, 174.622468), has been affected to a lesser extent by deformation. At this location the deformation seen previously is less obvious (Figure 4.9 G), with the bedding parallel, regular and continuing to dip towards the south while being formed exclusively of Lf1a (Sample 10). Despite the differences to the outcrops described to the south, Location 7 is within the boundaries of the NAMTD (Sharman, 2014) and so is inferred to have experienced similar deposition to Locations 5 and 6. There is evidence within the Lf1a beds of soft sediment deformation in the usually massive/structureless Lf1a material (Figure 4.9 H), and this supports the interpretation of the NAMTD (Sharman, 2014).

Figure 4.9: Example field photographs of the Mohakatino Formation at Locations 5, 6 and 7 along the Piopio Station section (See next page).

A) A general view of Location 5 next to the mouth of the Pitone Stream facing to the east. The bedding can be seen to be dipping to the north and some of the cross bedding and laminations can be seen across the surface. Bedding at this Location is exclusively Lf2.

B) A face on view of the Lf2 beds, demonstrating the tangential cross stratification and the lenticular bedding that makes it clearly identifiable.

C) A contextual view of the cross bedding in the Lf2 beds facing to the north.

D) The southern end of Location 6, at the central section of the Piopio Station section, where the dip direction has reversed and the bedding now dips towards the south and the beds are rise out of the ground forming outcrop.

E) Anticline structure in the Lf2 beds at Location 6.

F) Syncline structure in the Lf2 beds at Location 6.

G) General view of Location 7 at the most northern end of the Piopio Station section. Beds here continue to dip to the south.

H) Soft sediment deformation seen within a Lf2 bed at Location 7.

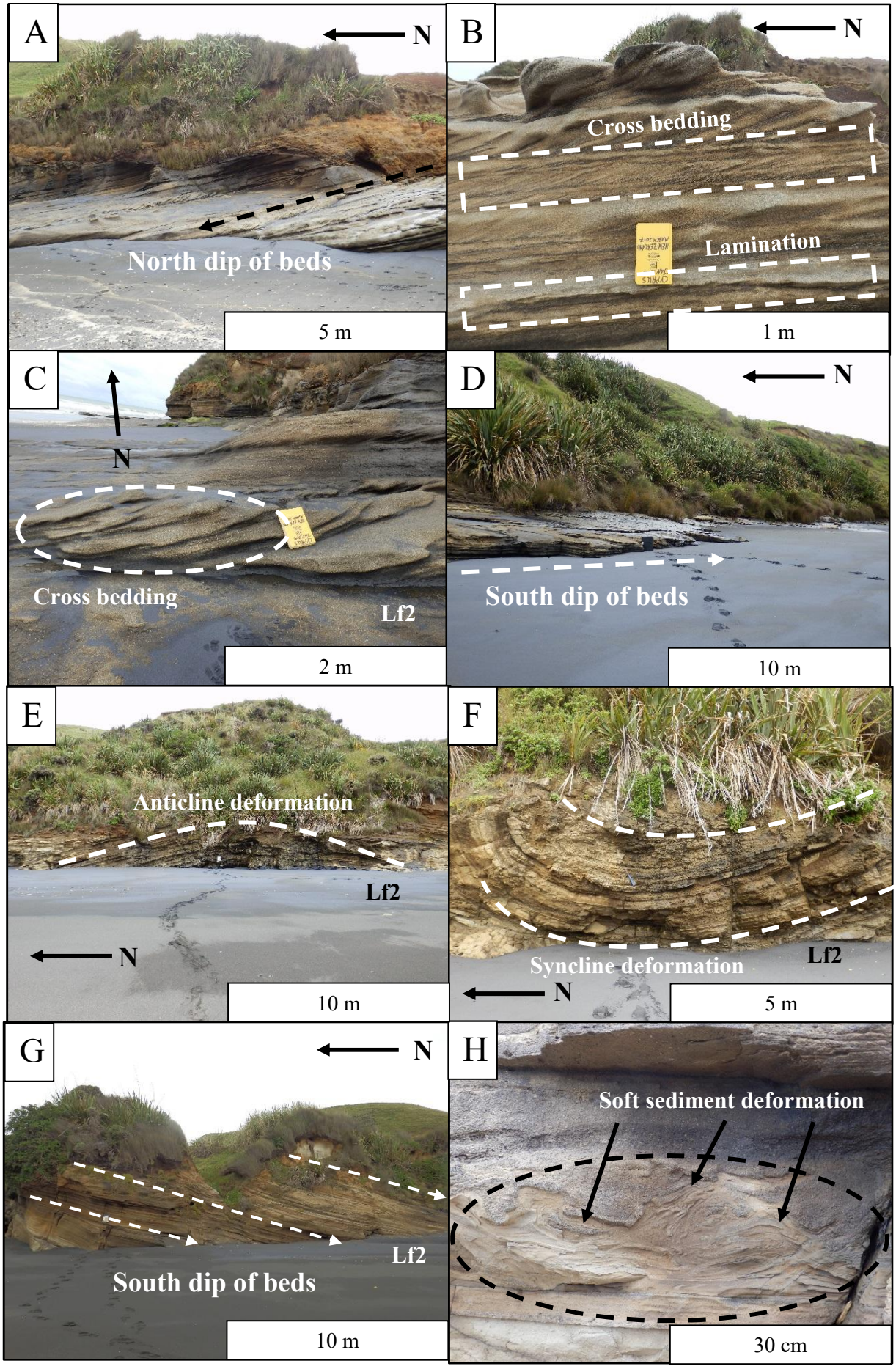
A
N
North dip of beds
5 m
B
N
Cross bedding
Lamination
1 m
C
N
Cross bedding
Lf2
2 m
D
N
South dip of beds
10 m
E
Anticline deformation
Lf2
N
10 m
F
Lf2
Syncline deformation
N
5 m
G
N
Lf2
South dip of beds
10 m
H
Soft sediment deformation
30 cm

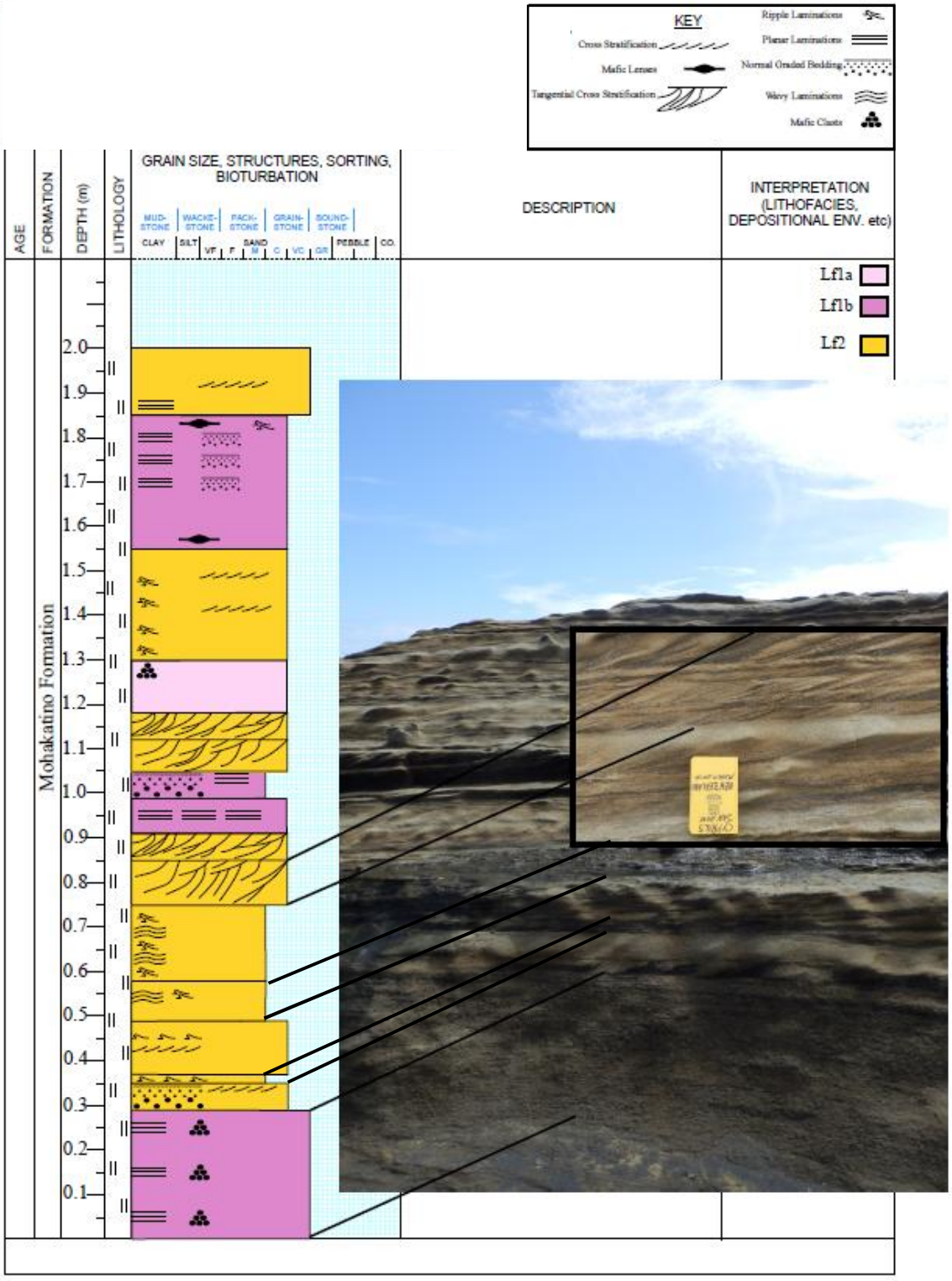

Figure 4.10: A stratigraphic log taken from Location 5 at Piopio Station and a corresponding photograph of the analysed section of outcrop. The inset photo gives a clearer view of the of the Lf2 beds in this log.

4.2.5 Waikawau Cliffs

The Waikawau Cliffs and beach is the most northern region of the fieldwork area, accessible by exiting State Highway 3 onto Manganui Road and following this road north to the village of Waikawau and then turning left onto Waikawau Road that leads down the Waikawau Valley. At the end of the road on the inland side of the cliffs, there is a stock tunnel that provides access to the Waikawau Cliffs and beach, and the exit onto the beach where Location 8 is positioned (-38.475710, 174.639609). Roughly 700 m of the ~80m high cliff outcrops to the north of this location were surveyed, including Location 9 (-38.471579, 174.642043). The Waikawau cliffs are composed of both the Mohakatino Formation from the base and then the uppermost few meters of the cliffs are made up of the Mount Messenger Formation, and this trend continues from Location 8 to Location 9.

Location 8 is situated next to the entrance to the stock tunnel on the coastal side of the Waikawau Cliffs and is roughly 5 m high. The Mohakatino Formation is composed of alternating beds of sandstone to siltstone (Lf1a and Lf1b) which are differentiated by the absence or presence of laminations. Overlying these is a bed of Lf3a (Figure 4.11 A and 4.12). Lf3a is distinct due to its thickness of 50-600 cm and the presence of intrabasinal pebbles and boulders. At Location 8 they appear in the Lf3a to be entrained at the same relative position within the bed and form a band across the surface of the outcrop (Figure 4.11 A). The internal structure of these clasts appears to be formed of multiple infilled burrows (Figure 4.11 B). Lf4 is present at the base of the outcrop (Figure 4.11 A), and occurr as a single band, standing out due to its dark grey colour and the very well sorted sand.

Moving further north, the Location 9 outcrop continues to rise out of the ground and increases in height to ~80 m (Figure 4.11 C). The same beds seen at Location 8 can be traced along the outcrop to the north and they rise to the top of the cliffs (Figure 4.11 D). Location 9 has all of the same lithofacies identified at Location 8 and some of the of the same beds have continued across the outcrop and are still present in Location 9, most noticeably the Lf3a bed that can still be clearly seen across the upper section of the outcrop (Figure 4.11 E). Looking further north along the beach, the trend seen between Location 8 and 9 continues making up the rest of the Waikawau Cliffs, as seen in Figure 4.11 F. A sample of Lf1a is taken at this location (Sample 15 Lf1a)

The combination of all these lithofacies (Lf1a, Lf1b, Lf3a and Lf4) shows that at these locations there are multiple turbidity currents of various styles and from various distances flowed across the area. The majority of the Lf1a and Lf1b beds indicate most of the material here has a similar source and are on the more distal end of deposition. The Lf3a and Lf4 beds have very limited occurrence show that the material and circumstances that came to form these beds was much rarer. There is only one, large bed of Lf3a that was potentially sourced from a nearby volcanic sector collapse, causing the emplacement of this massive bed. The Lf4 bed is an indication of a low energy, low density turbidity current, and this is possibly the most distal portion of the turbidity current, giving rise to the siltstone.

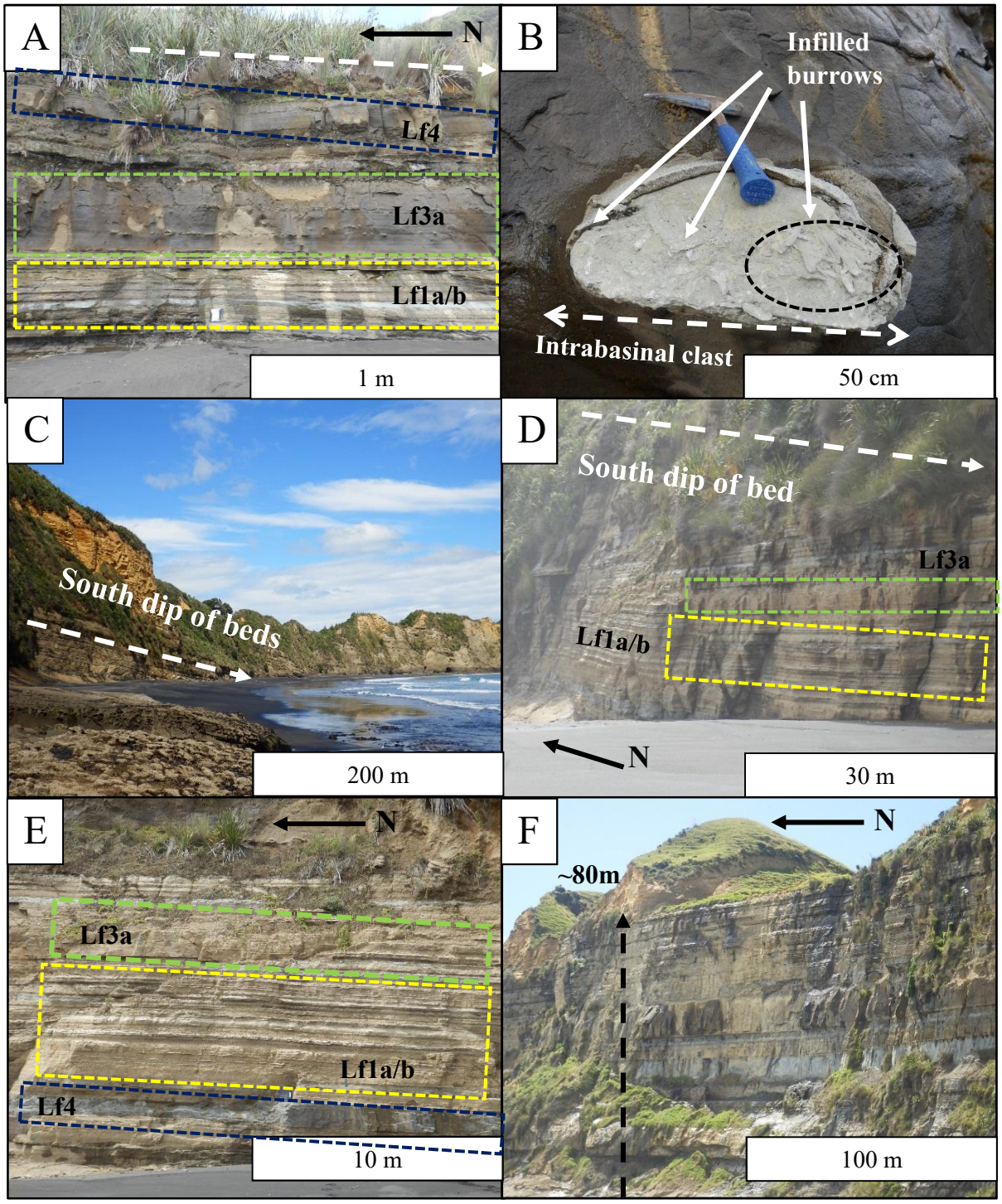

Figure 4.11: Example field photographs of the Mohakatino Formation at Location 8 and 9 along the Waikawau Cliffs. A) Location 8 next to the stock tunnel at the southern end of the Waikawau Cliffs. Lithofacies Lf1a, Lf1b (Yellow highlighted region), Lf3a (Green highlighted region) and Lf4 (Purple highlighted region) are all demonstrated here and the south dip of the beds. White dashed line indicates dip of beds to the south. B) An internal view of an intrabasinal clast that is emplaced within a Lf3a bed. C) A view of the Waikawau Cliffs towards the south taken from between Location 8 and 9. The south dipping trend of the beds continues from Location 8. D) A view of the Waikawau Cliffs facing to the north taken between Location 8 and 9. The dip angle of the beds can be seen to increase the further along the cliffs to the north and the height of the outcrops increases equally. E) Location 9, ~400m north of Location 8. All of the lithofacies mentioned at Location 8 have continued along the outcrop to this location but their height/position in the outcrop has changed with them shifting higher up the outcrop. Lf3a can been at the very top of the picture while a distinct bed of dark grey Lf4 can be seen around the base of the outcrop. F) A view of the Waikawau Cliffs from Location 9 to the north showing how the bedding of the outcrop eventually flattens out to become almost horizontal.

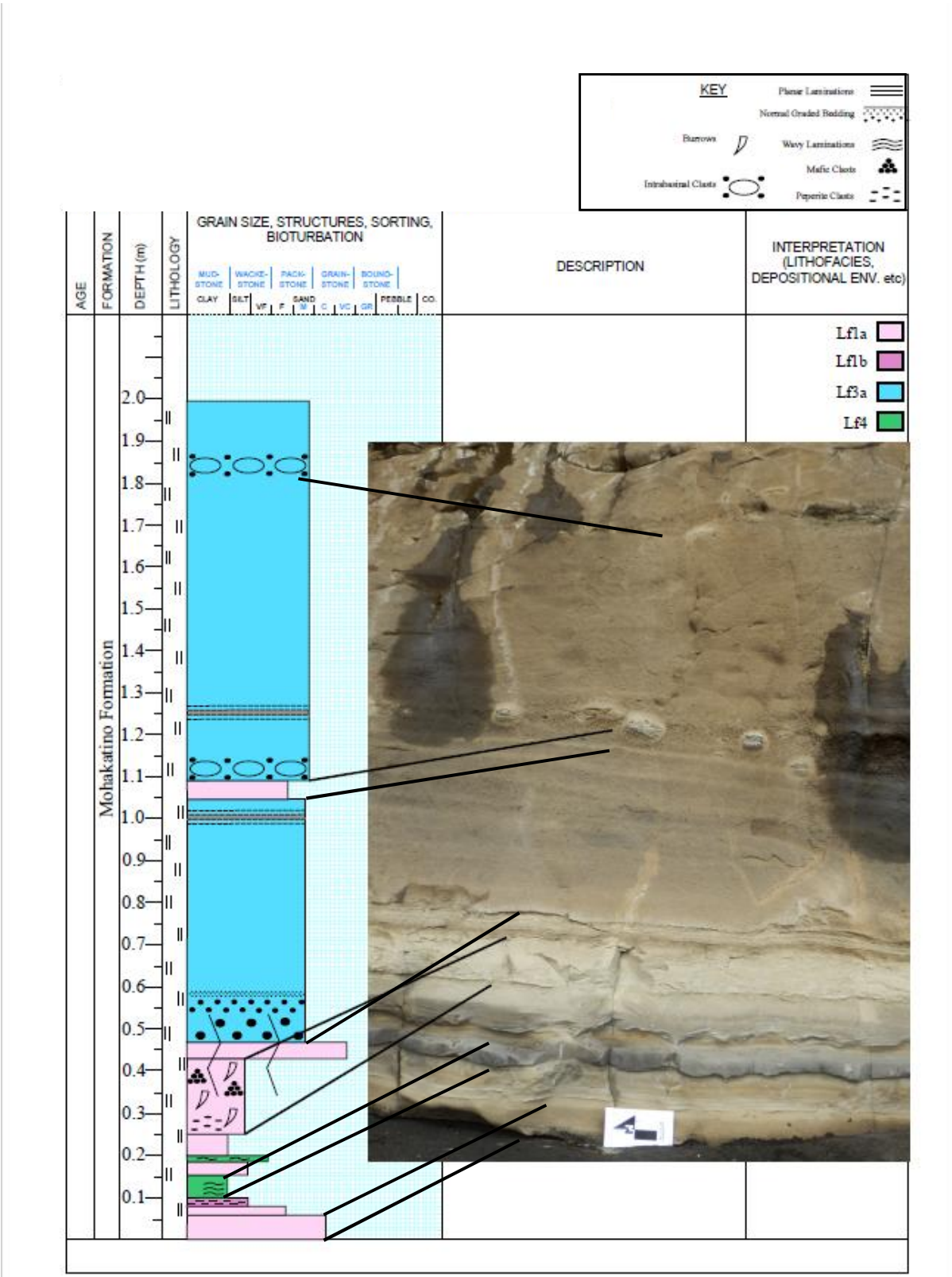

Figure 4.12: A stratigraphic log taken from Location 8 at the Waikawau Cliffs and a corresponding photograph of the analysed section of outcrop.

4.2.6 Opito Point

Location 10 is the final assessed area of the fieldwork and this was conducted at Opito Point (-38.485124, 174.637848), a section of coastline designated after the nearest farm for this study. Opito Point is accessed by taking the same route to the village of Waikawau along Manganui Road, but before entering the village turn off onto Ordish Road on the left and following the road as far as it goes along the Mangawhitikau Stream. At the end of the road a field must be crossed to gain access to the beach before moving south along the coast until reaching the outcrop of the Mohakatino Formation. The outcrop here is ~5 m high and extends ~30 m across the beach (Figure 4.13 A).

Location 10, while having a significant amount of laterally extending outcrop, was difficult to survey due to scree and dunes. It is also weathered and partly covered in vegetation. The largest proportion of the beds are composed of Lf3a (Figure 4.13 B), and interbedded with Lf3a are the beds of Lf1a and Lf1b. Lf1a beds are the thicker of the two lithofacies, with the laminations of Lf1b distinct in the thinner beds (Figure 4.13 C). No samples were taken from this location.

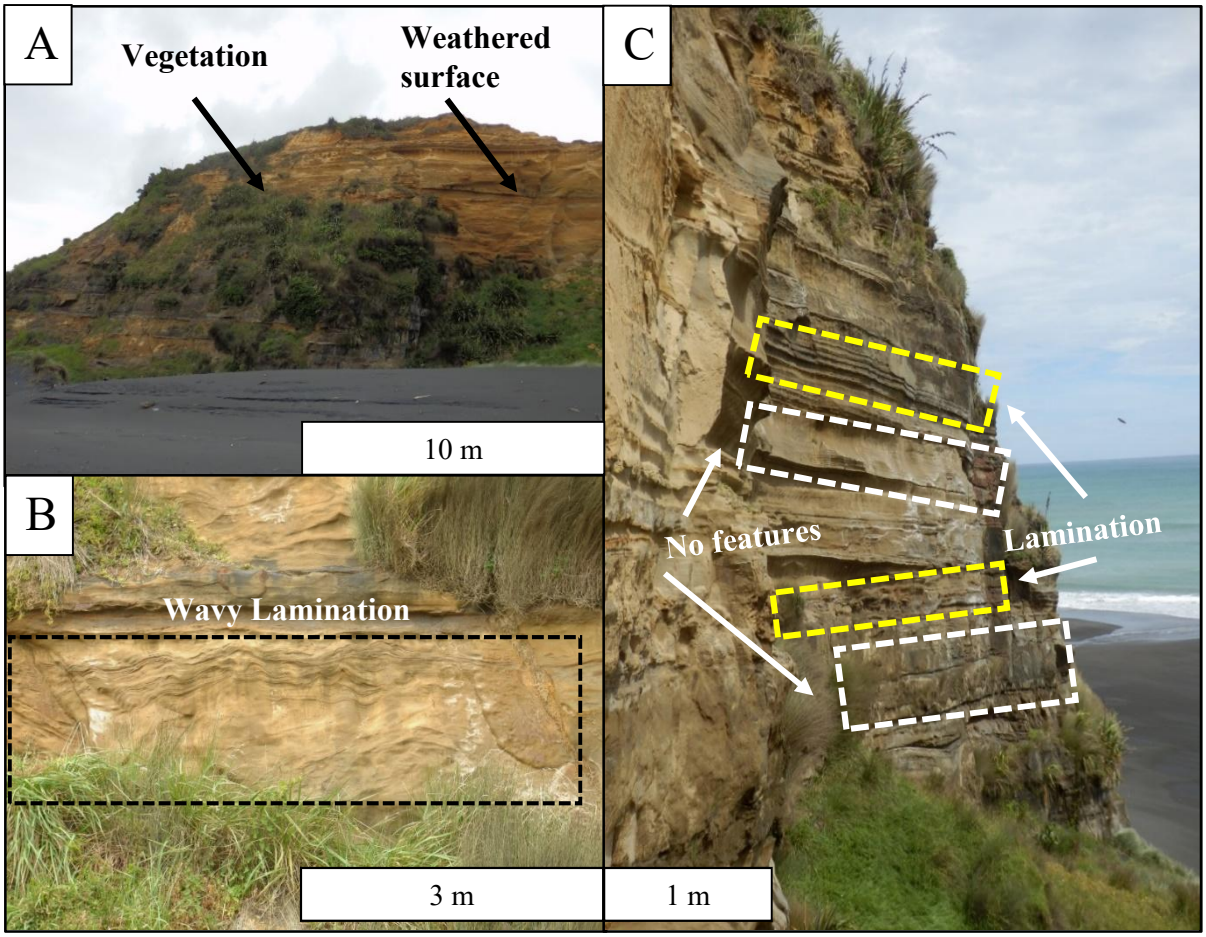

Figure 4.13: Example field photographs of the Mohakatino Formation at Opito Point. A) A general view of Location 10 at Opito Point facing east. The outcrop is heavily weathered, obscured in places by vegetation, and has low lying dunes at the base of the outcrop. B) A Lf3a bed, identified by the wavy lamination and large scale of the bedding, found across the base of the outcrop (Highlighted region). C) A combination of Lf1a and Lf1b beds across the upper section of the outcrop. The Lf1a beds are those that are lacking structure or features (White highlighted region) while the Lf1b have lamination features within the beds (Yellow highlighted region).

4.3 Petrographic Analysis of the Mohakatino Formation – North Taranaki Coastline

In order to achieve the aims and objectives of this part of the study a range of analytical techniques were used. A list of the samples collected and their collection date, location, formation, lithofacies, and their petrographic characteristics can be found in Appendix II.

4.3.1 Optical Analysis

Thin Sections

Sixteen standard size 30 µm polished thin sections were made from field samples. Twelve of these samples were from the Mohakatino Formation, while the other four were from the Manganui, Mangarara and Mount Messenger Formations. Of the 12 Mohakatino thin sections two of these were unable to be analysed under thin section because of a lack of optical clarity.

4.3.2 Petrography of the Mohakatino Onshore Samples

The thin sections of the Mohakatino comprised of Lf1, Lf2 and Lf3a that were sampled from the fieldwork area have similar composition and are only differentiated by sedimentary and bedding structures. The samples are dominated by plagioclase feldspar (>45%) and have common secondary minerals of hornblende (>8%), pyroxene (<1%), and volcanic rock fragments (>1%). Quartz is absent from all of the samples (see also Shumaker, 2016), specifically Lf1, Lf2 and Lf3a lithofacies which were compositionally distinct from Lf3b and Lf4 because the former lacked quartz while the latter contained approximately 25% quartz. The plagioclase feldspar in these samples appear as well-formed crystals and with polysynthetic twinning, and minor Carlsbad twinning (Figure 4.14 A). The second most abundant mineral is hornblende and then there are minor percentages of pyroxene scattered across the samples (10% to 0%), and these minerals occur as both small fragments and large grains. Planktonic foraminifera occur infrequently. In the field there is graded bedding present across many of the beds ranging from coarse grains/pebbles to fine sands and silts, and in Figure 4.14 B a cross section of the coarsest material next to the finest material is demonstrated in Sample 7. This represents the fine sediment at the top of a bed and transitions immediately into coarser material from the bottom of a bed. Although hornblende (>8%) and pyroxene (<1%) are the second and third largest mineral constituents, clay minerals also make up large portions of the material. The sample areas range from 12% in Sample 15 (Lf1a) to 32% in Sample 9 (Lf1a) which is an extremely high abundance for clay minerals. The clay minerals appear as a brown-green mass that either fills pores or lines grains.

Lf1a, Lf2 and Lf3a have similar compositions (Figure 4.15) but there are aesthetic differences between them. Lf1a (Figure 4.14 A) has larger grain sizes (on average >1mm) than the other lithofacies. Sample 8 (Lf2) (Figure 4.14 C) and Sample 11(Lf3a) (Figure 4.14 D) have smaller grain sizes (on average <1mm), and darker groundmass that makes mineral identification more difficult.

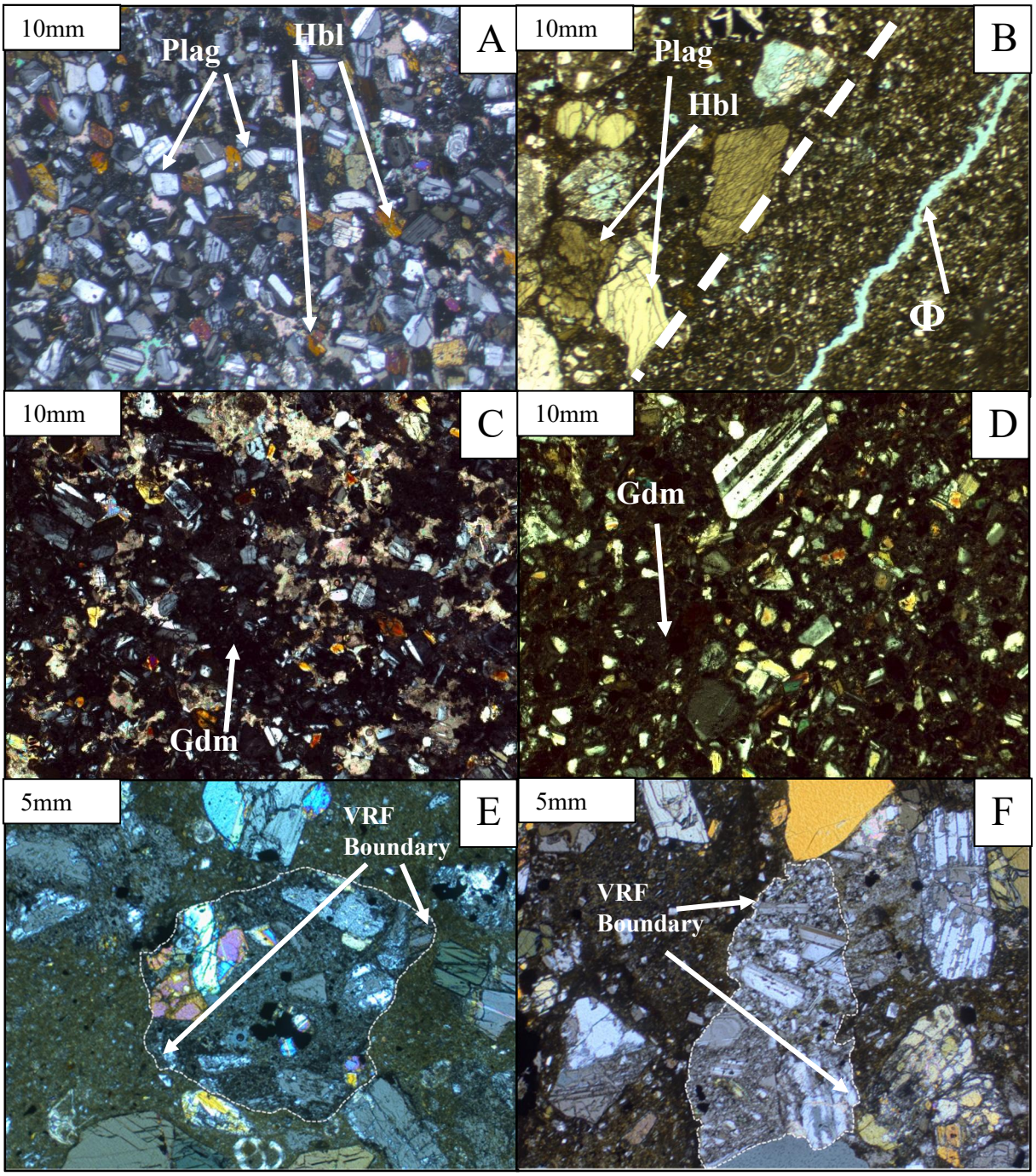

Figure 4.14: Example photomicrographs of the onshore samples of the Mohakatino Formation. All images in XPL unless stated. Scales in top left comer defined in description. A) Sample 2 (Lf1a), showing all minerals that are present within the Mohakatino (plagioclase, hornblende, pyroxene and authigenic clays). B) Sample 7 (Lf1a) (PPL), showing the range of grain sizes within Lf1a beds, coarsest material (top left) separated by white dashed line from finest (bottom right). C) Sample 8 (Lf2), a dark ground mass makes specific grains difficult to identify. D) Sample 11 (Lf3), similar dark to Sample 8 but with a smaller average grain size. E) Slide 9 (Lf1a), Volcanic Rock Fragment (VRF) example with large plagioclase crystals with a dominant devitrified groundmass. F) Slide 7 (Lf1a), Hypabyssal Rock Fragments (HRF), crystal rich with ~50% plagioclase crystals. Plag = Plagioclase, Hbl = Hornblende, VRF = Volcanic Rock Fragments, Gdm = Groundmass, Φ = Porosity.

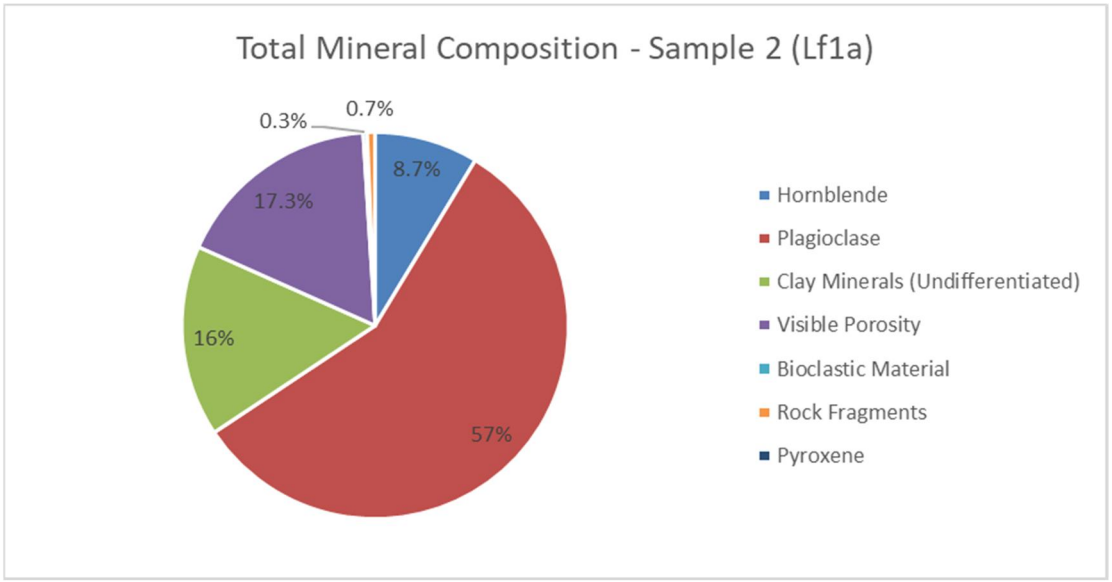

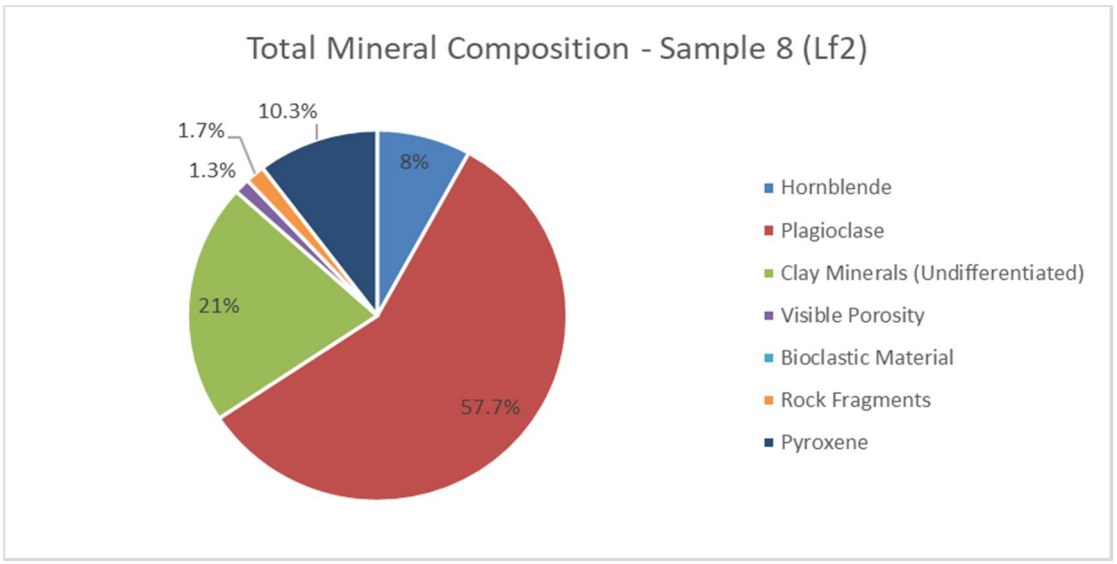

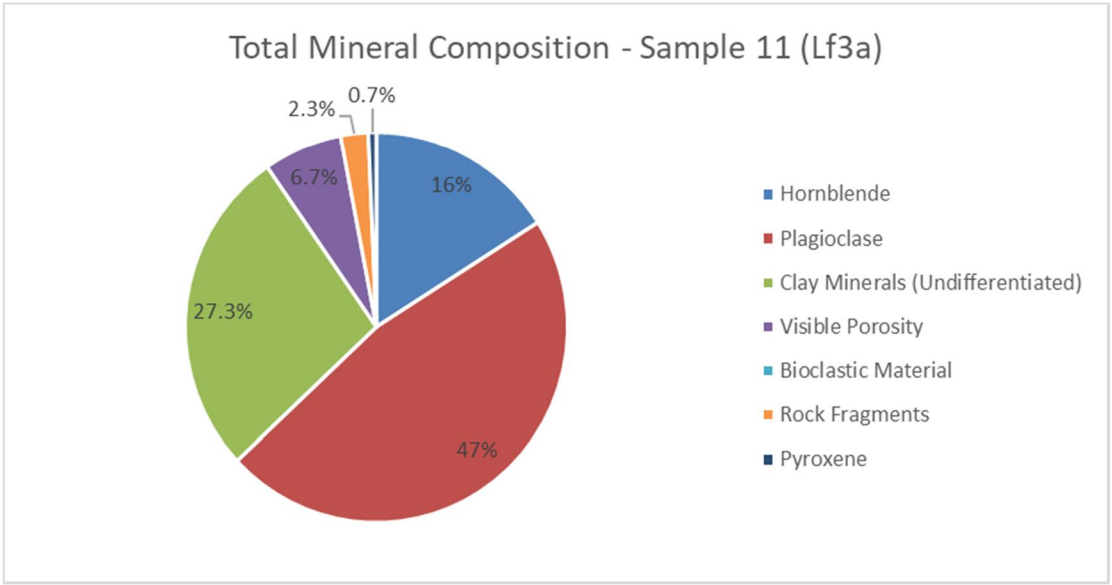

Figure 4.15: Total mineral compositions for Samples 2 (Lf1a), 6 (Lf1a), and 11 (Lf3). Major mineral constituents (plagioclase, hornblende and clay minerals) are similar to each other while the minor mineral phases and optical porosity are the most variable features.

Shumaker (2016) identified two different groups of rock fragments: crystal-rich, with 30% - 50% crystals; or crystal poor with <30% crystal. Both types occur in the distal sample (Figure 4.14 E and F). These have similar compositions, with plagioclase remaining the dominant mineral, with pyroxene and hornblende crystals as secondary mineral, and devitrified groundmass. Shumaker (2016) interprets the crystal poor rocks as being volcanic rocks due to their large plagioclase crystals in a devitrified groundmass, while the crystal rich rocks are hypabyssal rocks. There is a greater proportion of hypabyssal rock fragments in the samples, suggesting that sector collapse/deep-seated mass wasting on over steeped volcanic flanks possibly occurred, making it an important sediment producing process for the MVC (Shumaker, 2016). These groups of rock fragments can potentially be the source of peperite clasts seen in the field, indicating that dike activity and lava flows occurred in this region (Shumaker, 2016).

4.3.3 Grain Size and Porosity Distribution

The Mohakatino Formation shows a wide range of optical porosities calculated through point counting. The highest optical porosity value through-out all of the samples is found in Sample 2 as part of the Lf1a lithofacies at 17.33%, and then throughout all of the other samples with Lf1a compositions the optical porosity does not all appear to have similar values. (Figure 4.16). Sample 14 has an 10.67% and Sample 12 with 9.67% optical porosity, but then the lowest Lf1a percentage is seen in Sample 15 which has fallen to 0.33%, and the other samples are between 1.67% and 6.67%. Across all the samples of this lithofacies, some have medium optical porosity but none have high enough optical porosity to be considered a reservoir rock. The Lf2 type lithofacies is represented in Sample 8 and this lithofacies does not have any optical porosity. This may not be representative of the lithofacies. Sample 11 is composed of Lf3a material from Location 8 and this sample has a low optical porosity value of 6.67%, and while this value is similar to than many of the other samples it is still of no use as a reservoir rock.

The grain size of these samples is just as variable as the optical porosity, with the largest average grain sizes found in the Lf1a facies, but this also has the lowest grain size values (Figure 4.16). These values range between 2.2 mm in Sample 2 as the largest to 0.4 mm in Sample 15, and the average value for all Lf1a samples is 1.4 mm. The Lf2 material in Sample 8 has a mid-ranged grain size value of 1.6 mm which is almost equidistant between the highest and lowest values of the samples On the other hand, the Lf3a material in Sample 11 average grain size of 0.8 mm. Sample 7 has a complex grain size distribution as it has both the coarse grains of the base of a bed and the fine grains of the top of the underlying bed, and therefore the two extremes of a section of graded bedding seen in these Lf1a beds (Figure 4.14 C). The coarser material in this sample was measured to have 3.4 mm average grain size while the more fine-grained material is 1.1 mm, and averaged out these give an overall result for the sample 2.3 mm (Figure 4.14 C).

The average grain size decreases across the study area as you move the Mokau River/Awakino Heads to the northern end at the Waikawau Cliffs (Figure 4.16). The two most southern areas (Awakino Heads and Mokau River) have averages of 2.6 mm and 2.3 mm respectively, while the central locations of Piopio Station combined and averaged are 1.2 mm, and then Waikawau Cliff locations average to 0.9 mm. These results give a clear indication that there has been a shift in the depositional style or processes of the material along the coastline from north – south. The influence of this shift in grain size is seen in the COPL vs CEPL (Figure 4.20) and optical porosity (Figure 4.16) analysis.

4.3.4 Diagenetic Cements and Grain Coatings

The diagenetic cements of the distal samples were originally identified using point counting techniques mentioned previously in the methods sections, but the problem with this technique is that it uses a light microscope which does not have a strong enough magnification to differentiate between the minerals and cements. Extra analysis had to be done on the samples in order to identify what these cements were and this was conducted on Samples 2 (Lf1a), 6 (Lf1a), 8 (Lf2) and 11 (Lf3a). These are the representative samples for the three lithofacies found in the field and the samples with the highest optical porosity. The clays and cements encountered include calcite, chlorite and smectite.

Calcite occurs in Sample 2 (Lf1a) as a pore filling cement where it is interpreted from the data extracted from analysis of Spectrums 4 and 5. In the standard SEM image the two spectrum locations where calcite was identified are in the spaces between grains and these areas are lighter on the grey scale of the backscattered SEM image helping with constraining their locations (see Figure 4.17 A and B). The dominance of calcium in two distinct peaks and the lack of other elements made calcite the clear interpretation

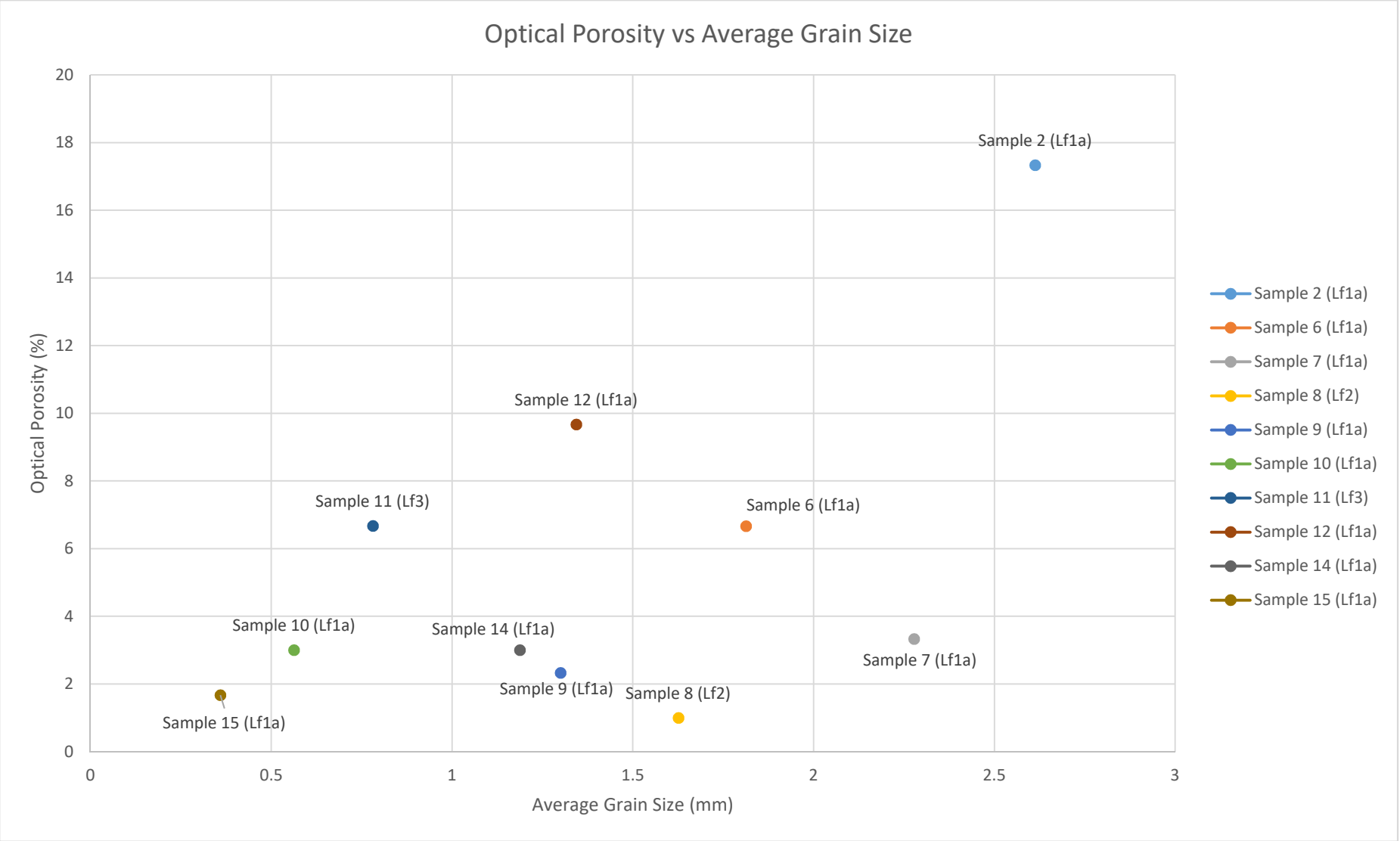

Figure 4.16: A plot of measured optical porosity plotted against average grain size from distal samples. A trend line (orange) between the Lf1a samples has been plotted.

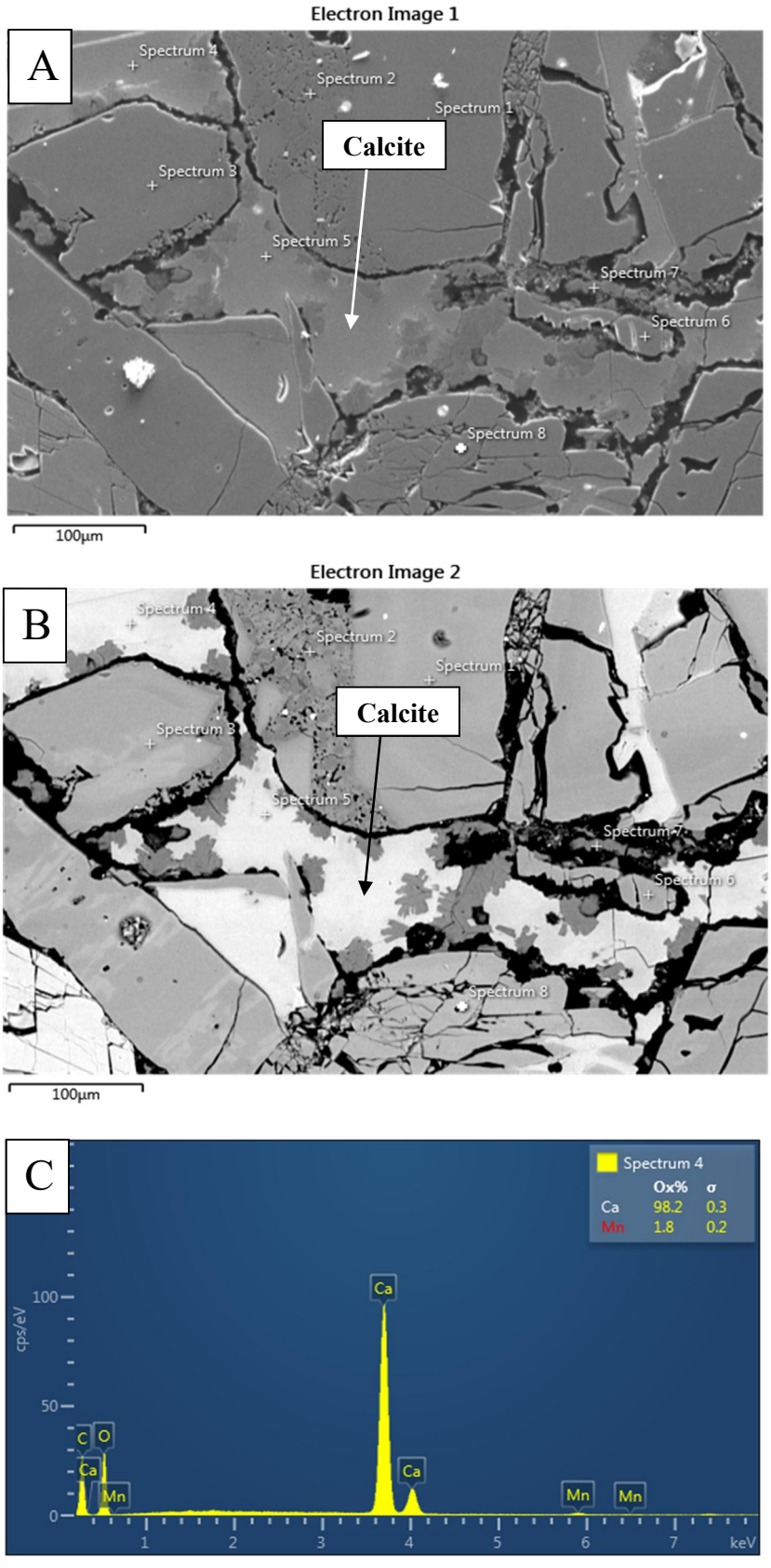

Figure 4.17 Sample 2 SEM images and elemental spectrum data. A) Secondary electron (SE) image of Sample 2 with spectrum data points. B) Back-scattered electron image of Sample 2 with spectrum data points. C) Elemental spectrum data from point 4 indicating calcite.

The calcite is likely to have precipitated in a shallow marine setting in which the Mohakatino here was deposited on the New Zealand continental shelf and because of the distance from the MVC where the acid nature of the volcanoes would have destroyed the calcite (Dr Stuart Jones, Pers Coms 2017).

Chlorite is found in Samples 6, 8 and 11, and like the calcite it occurs in pores (Figure 4.18 A and B). Chlorite has the general habit of platy chlorite with no particular orientation, crystals are <5 μm in diameter and <1 μm thick, although in the image these chlorite crystals aren't particularly clear and only the general shapes can be identified. The true identification of the chlorite was achieved by analysing the data from Spectrums 33 and 34 (see Figure 4.18 C for example Spectrum 33) from Sample 8, where there the major elements of Si, Al, Mg and Fe are clear in the raw data and the height of the troughs. The chlorite is thought to have formed due to the process of VRFs breaking down and altering the feldspar that was originally present in the sample at deposition (Berger et al., 2009). Smectite is found in Sample 8 as pore lining (Figure 4.19). The elemental analysis of this region identified major elements of Si, Al, Fe and Mg but most noticeably a large proportion of K that could be derived from underlying detrital K-feldspar (Welton, 1984).

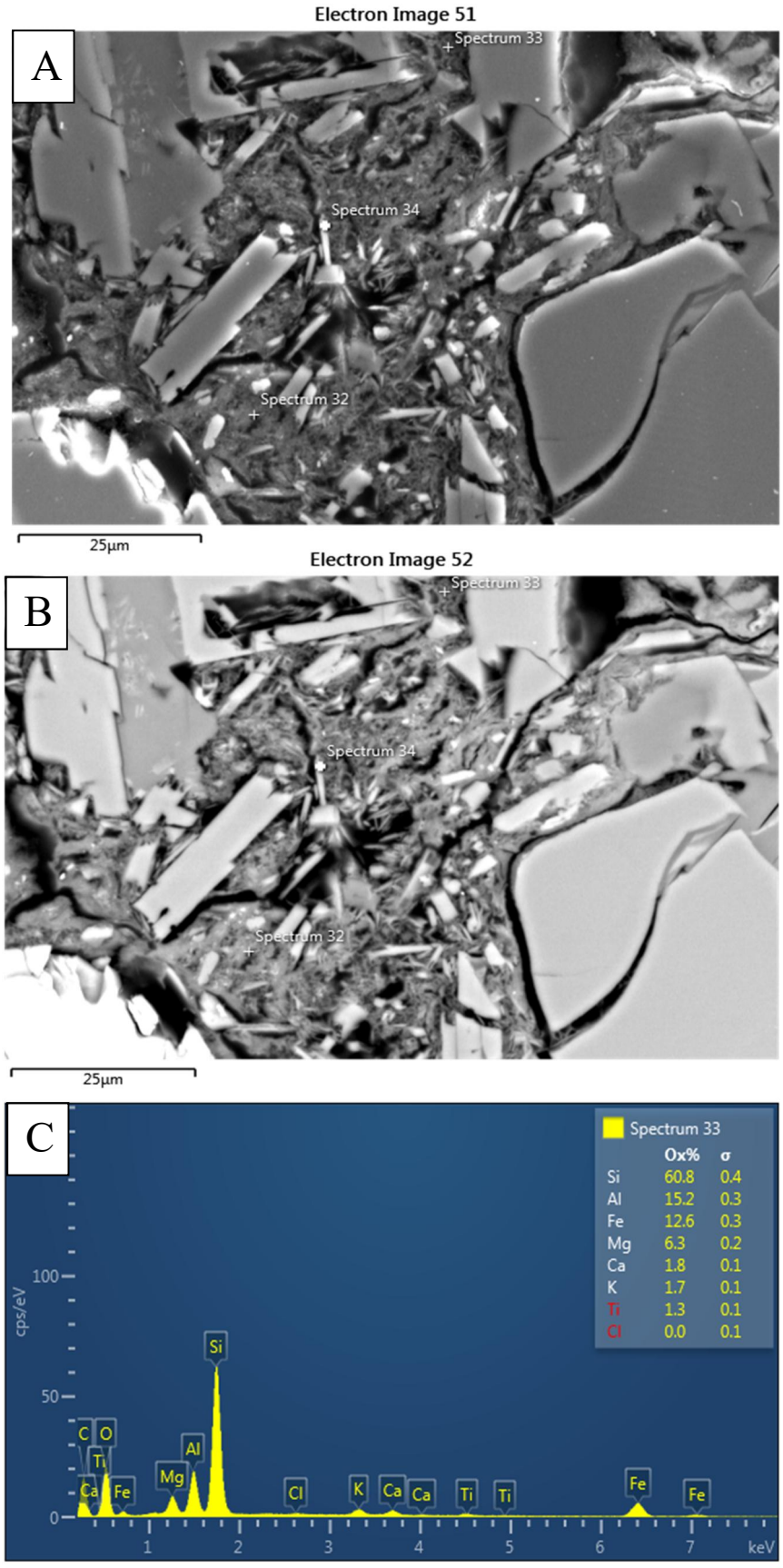

Figure 4.18: Sample 6 SEM images and elemental spectrum data. A) Secondary electron (SE) image of Sample 6 with spectrum data points. B) Back-scattered electron image of Sample 6 with spectrum data points. C) Elemental spectrum data from point 33 indicating chlorite.

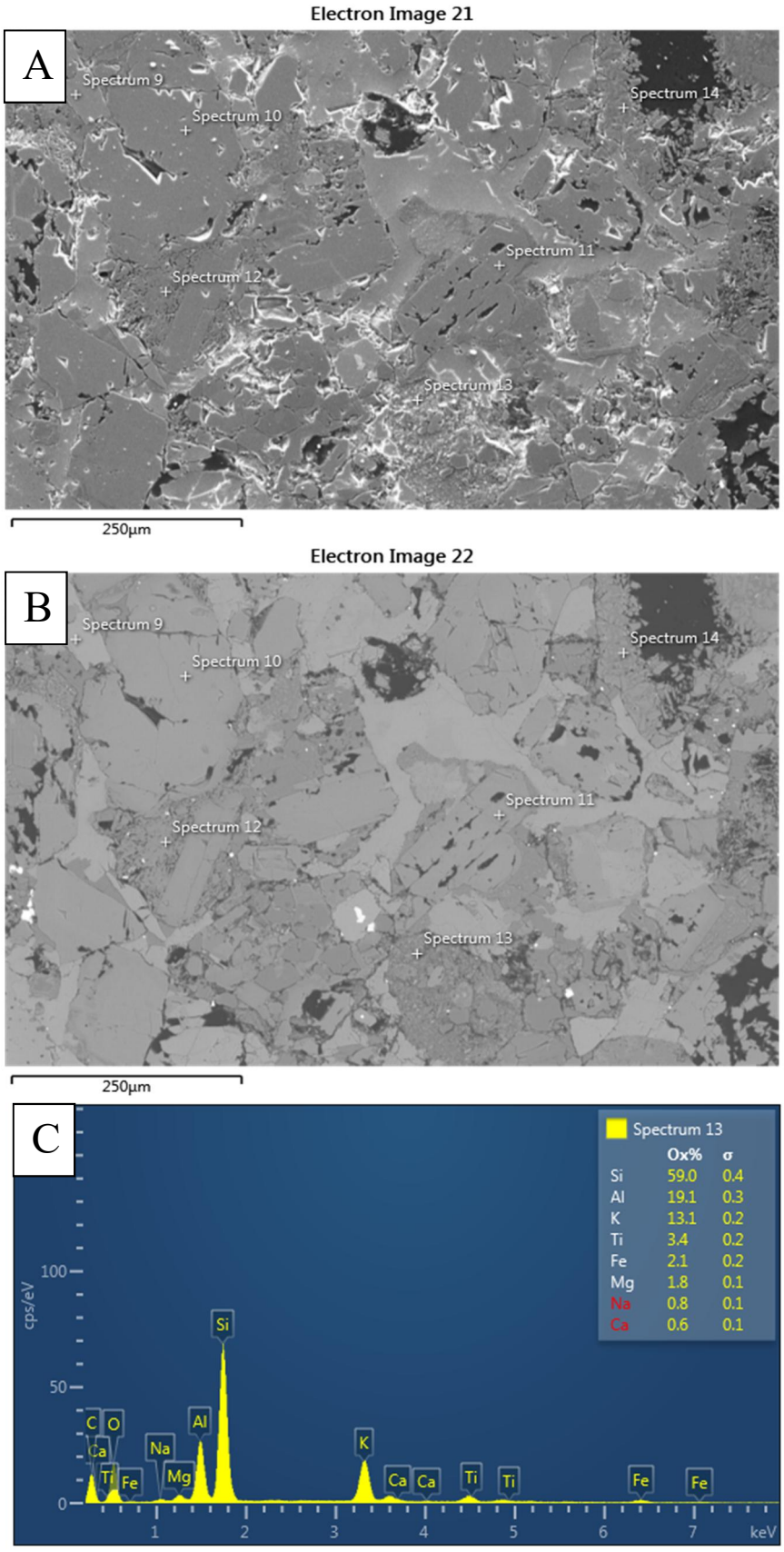

Figure 4.19: Sample 8 SEM images and elemental spectrum data. A) Secondary electron (SE) image of Sample 8 with spectrum data points. B) Back-scattered electron image of Sample 8 with spectrum data points. C) Elemental spectrum data from point 13 indicating smectite.

4.3.5 Porosity

Previous Studies

Shumaker (2016) is the only work done regarding the Mohakatino Formation onshore and included petrographic analysis, but this work was not investigating reservoir quality and there are no porosity measurements taken. Therefore, there is no other previous work by which to compare to this study.

Relationship between Clay Minerals and Porosity

The relationship between optical porosity and the total clay minerals in each of the samples is represented in Figure 4.20. Clay minerals is used as a term for all clays identified across the samples as they are unable to be differentiated between using light microscopes and so cannot be separated during point counting.

There is no overwhelming correlation between optical porosity and clay mineral abundance, but there is a rough trend that indicates that as the abundance of clays minerals increases optical porosity also increases. There are two outliers (Samples 2 and 12) that have significantly higher optical porosity values than other samples with similar clay mineral contents. It is assumed that the reason for the anomalously high optical porosity in these samples is due to the influence factors such as grain size

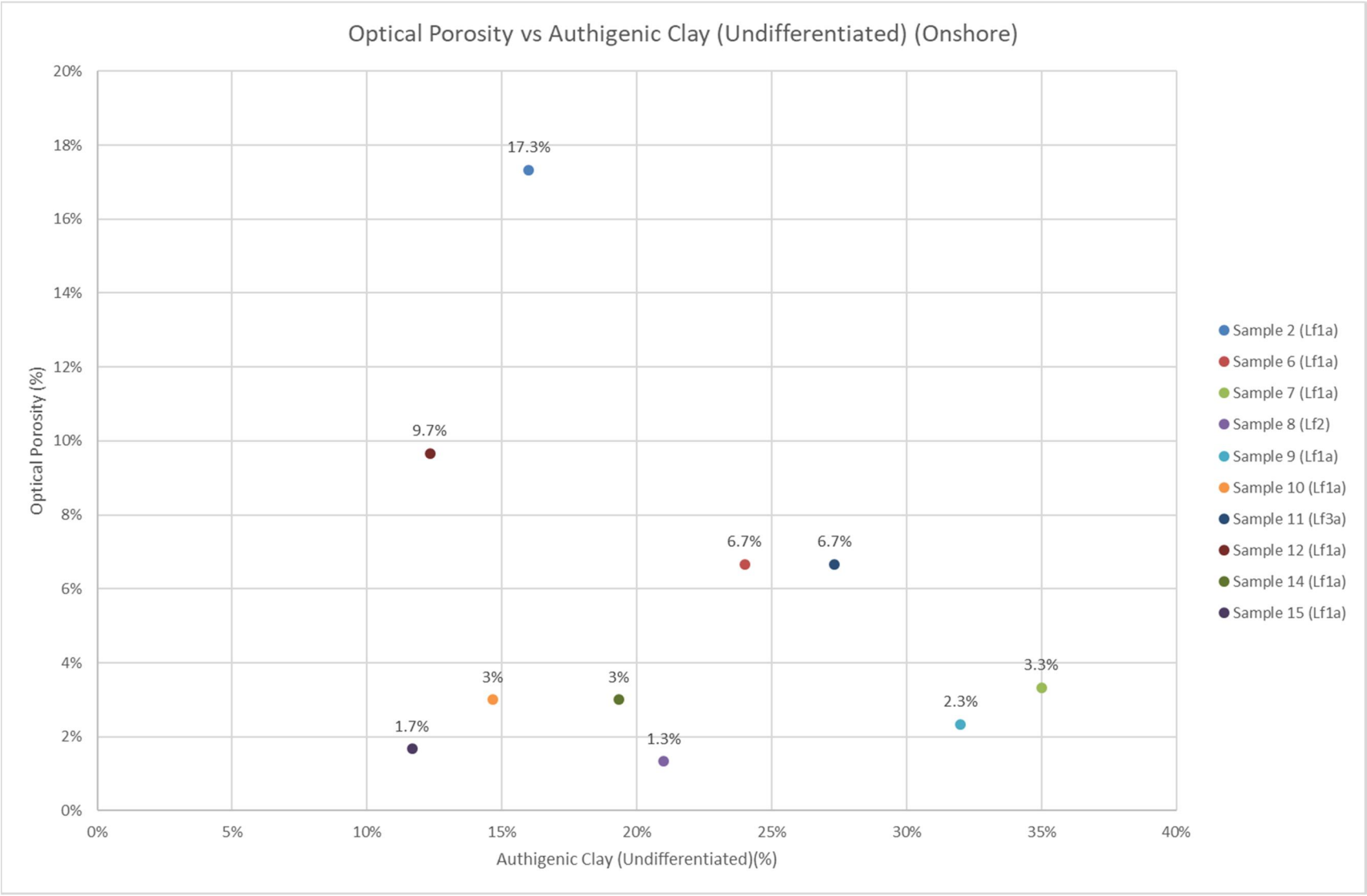

Figure 4.20: A plot of the optical porosity percentage against the authigenic clay percentage calculated through point counting. The values next to each data point is the optical porosity value for that sample.

Relationship between Rock Fragments (RFs) and Porosity

For the purpose of identifying a trend between these two values the term rock fragments (RFs) is used for both hypabyssal rock fragments (HRF) and volcanic rock fragments (VRF) (Figure 4.21). There is a general trend that optical porosity increases as RF percentage increases. This trend is exhibited by Samples 6, 7, 8, 9, and 14. Optical porosities rise from 1% in Sample 8 to 6.7% in Sample 6 over an increase of 7% RFs. Samples 2, 10, 11, 12, and 15 have either significantly higher or lower optical porosity values relative to their RF percentages. For example, Sample 2 has an optical porosity of 17.33% but has a RF percentage of 0.7%, a result that contradicts the other samples. Other samples that have higher optical porosities than their FR value suggests they should be Samples 11 and 12. Half of the samples follow this trend, but the other samples are potentially influenced by other factors as they do not follow this trend. However, none of these other samples present an alternative trend.

4.3.6 Intergranular Volume (IGV)

The intergranular volume (IGV), or minus-cement porosity, is the sum of intergranular pore space, intergranular cement and depositional matrix (Paxton et al., 2002). The IGV decreases with burial depth and reflects the degree of mechanical and chemical compaction (Stricker, 2016). See Appendix II for IGV results.

Porosity Loss by Compaction (COPL) vs Cementation (CEPL)

The trend of plotting porosity loss by compaction (COPL) against porosity loss by cementation (CEPL) is referred to as an intergranular volume (IGV) compaction curve, and this helps to establish the potential extent/limits of, and the interaction between, mechanical grain compaction and cementation in sandstones (Paxton et al., 2002). According to Paxton et al., 2002, porosity-depth curves can be very misleading when predicting reservoir quality in basins where the sandstones vary regionally and stratigraphically in terms of grain compaction, grain size/sorting, and volume of depositional matrix. Therefore, the benefit of using the technique of IGV curves in this study is that they are designed for sedimentologically and stratigraphically complex regions such as the Taranaki Basin and specifically the Mohakatino Formation, and can give a more realistic idea of porosity loss than a simple porosity-depth curve.

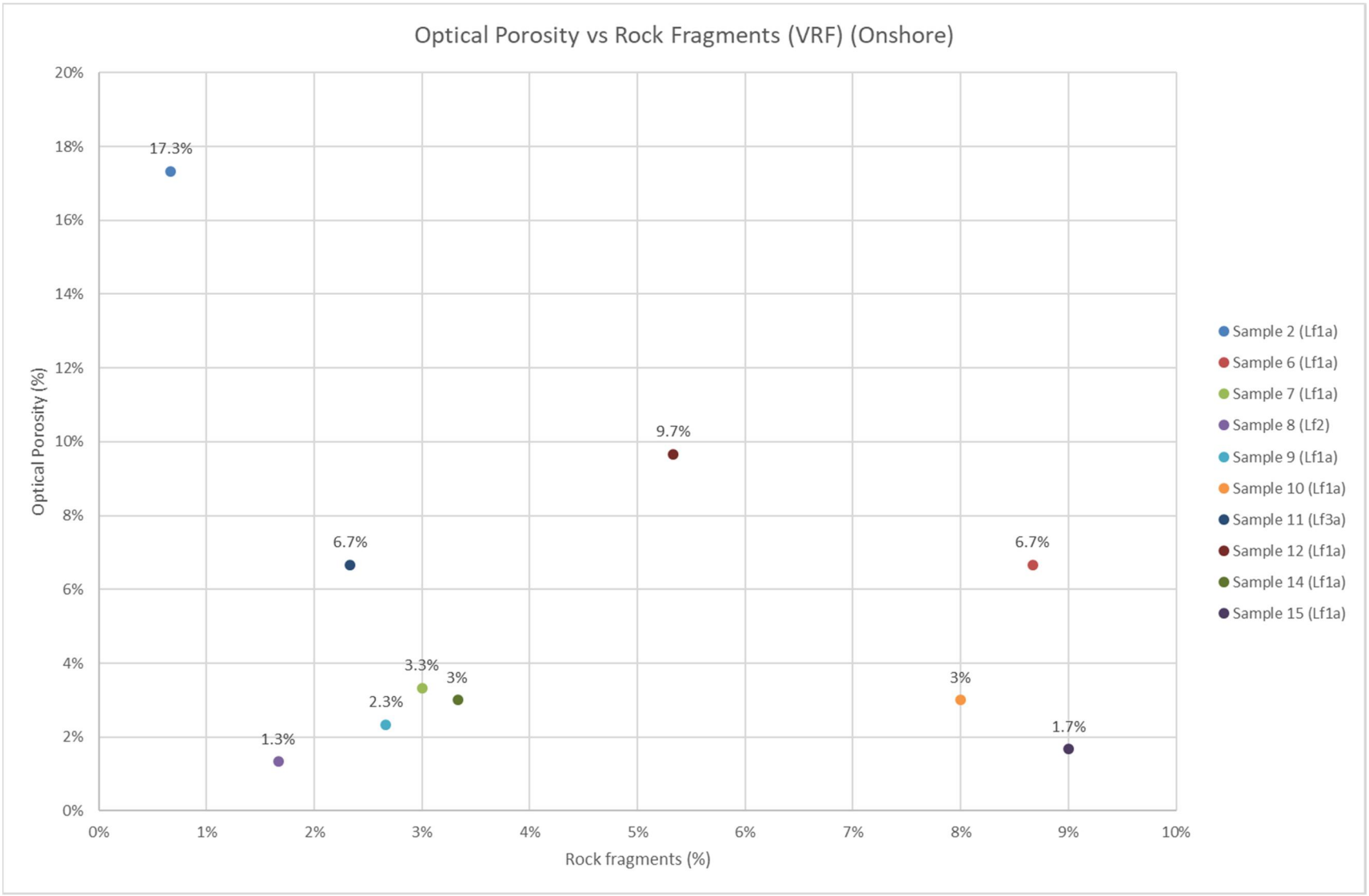

Figure 4.21: A plot of the optical porosity percentage against the rock fragment percentage calculated through point counting. The values next to each data point is the optical porosity value for that sample.

Total cement volume is used to help calculate the porosity losses caused by mechanical compaction (COPL) and cementation (CEPL) (Lundegard, 1992). This is achieved using the equations from Lundegard (1992) below:

$$COPL = P_i - \left(\frac{(100 - P_i)P_{mc}}{100 - P_{mc}}\right)$$

$$CEPL = (P_i - COPL)\left(\frac{C}{P_{mc}}\right)$$

Where P_i is the initial or depositional porosity and P_{mc} is the intergranular volume/minus cement porosity calculated by the sum of total optical porosity, P_o, and volume pore filling cement, C. The results of COPL vs CEPL (Table 4.3) are only valid if certain conditions are met (Stricker, 2016): 1) the assumed initial porosity must be correct; 2) the amount of cement must be negligible or known; 3) the amount of framework mass exported by grain dissolution must be negligible or known. Initial/depositional porosity for the Mohakatino Formation is estimated to be in the region of 40%. This number is used because the Mohakatino Formation does not have a recorded or estimated initial porosity, and the sandstones generally have a 40-42% surface porosity when deposited (Paxton et al., 2002). This number is also supported by Galloway (1979), who found that arc derived volcanic sandstones of the Bristol, Gulf of Alaska, Queen Charlotte, and Grays Harbour-Chehalis basins of the northeast Pacific had initial porosities ranging up to 40%. The COPL and CEPL results are plotted in Figure 4.22.

Sample	C	P_o	IGV	COPL	CEPL
	[%]	[%]	[%]	[%]	[%]
Sample 2 (Lf1a)	16	17.33	33.33	10.004	14.399
Sample 6 (Lf1a)	24	6.667	30.667	13.461	20.769
Sample 7 (Lf1a)	35	3.33	38.33	2.708	34.052
Sample 8 (Lf2)	21	1	22	23.077	16.154
Sample 9 (Lf1a)	32	2.33	34.33	8.634	29.237
Sample 10 (Lf1a)	14.667	3	17.667	27.125	10.689
Sample 11 (Lf3)	27.33	6.67	34	9.091	24.845
Sample 12 (Lf1a)	12.33	9.67	22	23.077	9.485
Sample 14 (Lf1a)	19.333	3	22.333	22.747	14.935
Sample 15 (Lf1a)	11.67	1.67	13.34	30.764	8.079

Table 4.3: Data used to calculate COPL and CEPL (Onshore) and then used to generate Figure 4.22. C = volume pore filling cement, P_o = sum of total optical porosity, IGV = intergranular volume, COPL = porosity loss by compaction, CEPL = porosity lost by cementation

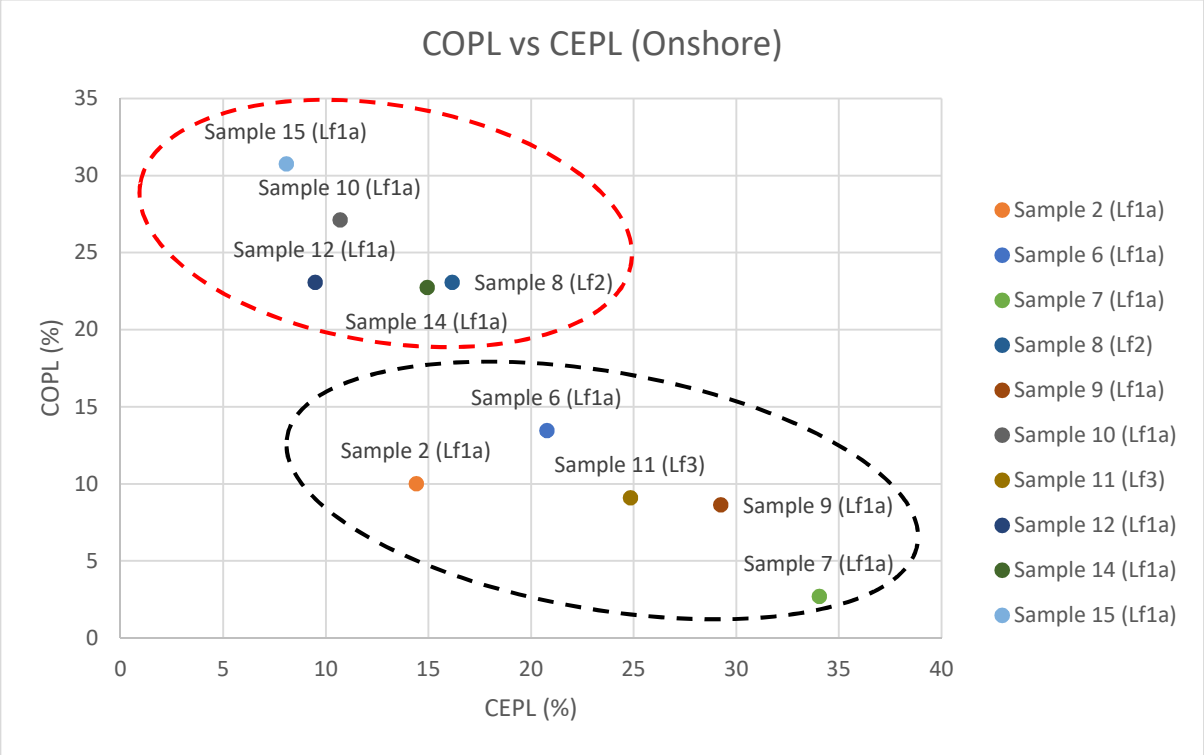

Figure 4.22: A graph of porosity loss by compaction (COPL) vs cementation (CEPL), with the sample name added as a data label. The samples in the red highlighted region are primarily influenced by compaction related porosity loss, and those in the black highlighted region are influenced by cementation related porosity loss.

The results in Figure 4.22 show that there is a wide range of values across the results and the Awakino region does not undergo the same method of porosity loss through-out it but rather has localised processes of compaction or cementation occurring. There are two distinct groups of samples (Figure 4.22) with one group of five in the top left of the graph (Samples 8, 10, 12, 14 and 15) that have are more affected by compaction and then there is the second group of four samples (Samples 6, 7, 9 and 11) that is towards the bottom right of the graph. This second group is therefore more likely to have had its porosity loss influenced by cementation due to their higher CEPL and lower COPL values. While these groups of samples are positioned roughly in the regions of compaction or cementation influence, they are not influenced completely by just one processes. This is because majority of the samples, whether they are dominated by COPL or CEPL, still have significant values of the other process. For example, in the group dominated by COPL, these samples are between 22.7% and 30.7% COPL, yet they still have between 8% and 16% CEPL values, showing the influence of both these processes is present in both samples. This is also seen in the second group of samples. Sample 2 differs from this however because it has almost matching COPL and CEPL results showing that it has almost had its porosity decreased equally by compaction and/or cementation.

4.4 Discussion

4.4.1 Mineralogy

Petrographic analysis demonstrates sample compositions dominated by the plagioclase feldspar. Hornblende and pyroxene mineral percentages fluctuating between samples. This is similar to the offshore/proximal samples (Chapter 3). Quartz is not present in any distal samples, unlike the proximal samples of the Kora Volcano which were relatively quartz rich (9%-22%). This is a typical component derived from an andesitic arc source (Shumaker, 2016). The lack of quartz is strange because the distal turbidites are supposedly sourced from the same material as the proximal deposits. One hypothesis is that the quartz found in the Kora well samples is due to minor dacitic eruptions from the Kora volcano that have combined with the andesitic eruptions (Adrian Pittari, Pers Coms, 2017) to form predominantly andesitic material but with a high quartz content. This could have been a singular event in an isolated region, and so this quartzite-rich material was not part of the turbidity current that flowed away from the MVC/Kora Volcano to form the distal Mohakatino Formation. Another hypothesis is that the quartz grains are denser and heavier than the other minerals that form the proximal Mohakatino Formation, and so while being transported by the turbidity current these dense quartz grains could have been deposited first and not as part of the main body of material deposited to form the distal Mohakatino Formation. However, mafic minerals are generally dense than quartz and so this is unlikely.

While these plagioclase, hornblende and pyroxene minerals make up over 50% of the samples' composition, undifferentiated cements also have a high percentage with between 11% and 32%, making them a significant influence on the reservoir quality of the samples and also a key indicator of their diagenesis. This is a significant difference between proximal and distal regions of the Mohakatino Formation, and could be an indication of why there is variation in reservoir quality between them. The difference in quartz percentage could affect a change in the reservoir quality in the proximal samples by potentially preventing the development of later stage dissolution or authigenic mineral precipitation (Section 3.10). This could have helped retain porosity and improved reservoir quality. The distal samples that do not contain quartz have lower porosity and permeability values, and therefore lower reservoir quality. The lack of quartz promoted dissolution or precipitation of cements that filled pore spaces and decreased the porosity. The samples with the lowest optical porosities generally have the highest volume of cement (Table 4.3 and Figure 4.22).

4.4.2 Cements and Grain Coatings

There are significant volumes of pore-filling cements minerals (chlorite, smectite, etc.) (11% to 33%) contribute to the low optical porosity values (CEPL). The presence of calcite comes from onshore

deposition being a shallower marine environment than that of the MVC and so lacks the acidic material found volcanic centres that would usually destroy this calcite (Dr Stuart Jones, Pers Coms 2017). While it is difficult to determine the dominant cement across the onshore region, it can be hypothesised to be calcite, unlike chlorite which was seen to be the dominant cement through-out the proximal samples in Chapter 3. This conclusion is reached because the lack of acidic material during formation would have allowed the precipitation of calcite before chlorite, and this would have coated the grains and inhibited the precipitation of chlorite (Dr Stuart Jones, Pers Coms 2017). The depositional conditions of this distal region would have allowed the formation of this chlorite if the calcite had been prevented in a similar manner to the proximal region. This contrasts the findings of Chapter 3 and this difference will be addressed in Chapter 5.

As discussed in Chapter 3, Remy (1994) found that compaction and cementation obstructed the majority of macroporosity in the samples with the richest volcanic detritus and this led to the sealing of the rocks and prevented the development of dissolution or authigenic mineral precipitation. This was identified in the proximal samples where the highest optical porosity values were seen in samples which also had the highest RF volumes. However, there is significantly more variation and anomalous results in the distal samples so this result is not as conclusive.

4.4.3 Compaction and Cementation

The COPL vs CEPL data trend (Figure 4.22) shows that there is an equal divide between the samples, with half showing porosity loss by compaction (COPL) and half showing porosity loss by cementation. Additionally, the Lf1a samples that are more influenced by compaction tend to be found in the northern region while the more southern samples have had their porosity lost primarily through cementation. However, Samples 2, 6, 7 and 9 in the southern region are dominated by CEPL, and Samples 10, 12, 14 and 15 are predominantly found ~40km to the north yet are COPL influenced. Grain size may be an influence because CEPL influenced samples also have coarser grained material compared to the northern, and COPL samples are finer grained. Sample 8 and Sample 11 are anomalous to this trend, but there is an explanation for this. Sample 8 was collected from Piopio Station in the south but has higher COPL values than other samples collected in this area, and this is possibly due to it being formed of Lf2, which while being located to the south has a coarser grain size that other Lf1a and Lf1b beds in the area, and so has a different position on the COPL - CEPL plot to the other southern samples. Sample 11 is formed of Lf3a and sourced from the Waikawau Cliffs in the north but is more influenced by cementation, and while this cannot be attributed to grain size it could be due to the different depositional process it has compared to all the other samples influencing the porosity loss

One sample that stands out is Sample 2 and this is because unlike the other samples it has COPL and CEPL values that are the closest to being the same (10% and 14.4% respectively). This means that its

porosity loss has been almost equally influenced by compaction and cementation in porosity loss, but mainly by cementation. Sample 2 has the highest recorded optical porosity (17.3%) and is greater than the next highest sample by 10.7%, and so this means that the combination of both COPL and CEPL may be beneficial to the reservoir quality in these distal samples.

This compaction and cementation data clearly contrast with that of the offshore/proximal samples (See Sections 3.9 and 3.10). Over 85% of the proximal samples are identified as being influenced by COPL compared to 50% in the distal ones, and these COPL influenced proximal samples have higher COPL values as well as a great range of COPL values (Proximal: 20-37%; Distal: 23-31%). The reverse is seen in the CEPL influenced samples, where in the proximal samples only 14% have had CEPL occur compared to 50% of the distal samples. In these CEPL influenced samples, the distal samples have a significantly higher and wider range of CEPL values (14-34%) compared to the proximal (15-17%). The hypothesis for this difference is that because the proximal samples are sourced from a region that underwent rapid, thick burial there had more of a compaction effect at a faster rate than cementation. As well as this, the reduction in pore space by compaction reduces the available space for cement growth. The distal samples did not experience the same rapid burial due to being deposited on a shallower region of the continental shelf and were not buried to the same depth (Stagpoole and Funnell, 2001, King and Thrasher, 1996, Hansen and Kamp, 2004). Thus, there is less porosity lost through compaction, and cementation occurred to a greater degree.

4.4.4 Grain Size

The influence of grain size on the optical porosity and therefore the reservoir quality can be clearly seen in the distal onshore samples of the Mohakatino Formation. Samples with larger average grain sizes generally have larger optical porosity values (Figure 4.16). What must be addressed first is that this data is not conclusive and the figure shows a lot of anomalous results. This has led to the trend line through the Lf1a samples to not be a one of simple proportional increase. Despite this, an increasing trend can be seen, and this directly contradicts what has been seen in Chapter 3 (Section 3.5.5 and 3.10), where in the proximal, offshore samples the optical porosity was seen to decrease as the average grain size increased. The average grain size for all the onshore samples is 1.4mm while the offshore samples is 0.8mm, and the average optical porosity is 5.5% and 10.3% respectively. This direct contradiction makes using grain size as an indicator of reservoir quality control invalid, and unless an explanation for this difference can be found then an alternative factor is responsible for the preservation of porosity.

4.4.5 Distal Depositional Model

An available model to illustrate the transport and depositional processes of the distal Mohakatino Formation is that of Sharman (2014), who hypothesises the occurrence of large scale mass-movement

in the north-eastern Taranaki Basin during the late Miocene, with the source material derived from the submarine volcanic arc of the MVC to the west and its eastern boundary and back stop provided by the Herangi submarine high. The MVC acted as the source of the Mohakatino volcaniclastics and also formed the seafloor topography to the west and north, and so when volcanic cone sector collapse occurred the material flowed down the pre-existing, NNW orientated channels formed during the Mangarara Formation deposition (Sharman, 2014). Hypabyssal rock fragments and peperite clasts support this model. When the volcaniclastics reached the inclined seafloor near the Herangi submarine high the energy was lost from the flows and the Mohakatino Formation was deposited on the western continental slope of New Zealand. Following this deposition, NAMTD reversed direction, and was deposited on the slope it collapsed back towards the MVC over a short distance and was possibly caused by uplift and tilting in last 2 Ma (King and Thrasher, 1996). It is this local uplift, collapse and deformation that is responsible for the structures seen across the Piopio Station region of the fieldwork.

4.5 Conclusions

The Mohakatino Formation of the Taranaki Basin, New Zealand, records deposition of submarine volcano-sourced sediment in a bathyal submarine lobe environment. The dominant sedimentation style was characterized by coarse-grained, mud-poor, low-density turbidity currents that deposited laterally continuous, thin- to medium-bedded sandstone and siltstone at the distal end of the depositional system on what is now the Awakino Coastline of New Zealand. The Mohakatino Formation demonstrates that volcanic complexes can be significant sources of sediment in marine basins in convergent plate tectonic settings. The large volumes of inputted into the system volcaniclastics significantly contributed to sedimentary sequence in the proximal setting close to the MVC. Periods of tectonic instability, volcanic eruption, and sector collapse caused a mass transport deposit that allowed the Mohakatino Formation to flow from the proximal region of deposition around the MVC to the more distal setting along the continental shelf that would become the Awakino coastline. As the mass transport deposit moved towards the North Taranaki coastline and the faulted margin it is obvious down fan fining has played a significant role in controlling reservoir quality. The petrography of these distal turbidity current deposits differs significantly to those of the proximal region.

From the fieldwork and subsequent analysis of the onshore outcrops, the North Taranaki, Awakino coastal sections are dominated by the Mohakatino Formation formed of thin bedded turbidites, differentiated primarily by their bedding thickness and sedimentary structures such as planar lamination, cross-stratification, and various types of lamination. The petrography of these turbidity current deposits is very similar. The petrography of the distal samples varied significantly from that of

the proximal, through the absence of quartz, greater percentages of samples influenced by porosity loss by cementation, larger average grain size, and different pore filling cement types.

Mass transport deposits with significant volcanic components have largely been considered unsuitable hydrocarbon reservoirs. Chapter 4 has demonstrated that the majority of the Mohakatino Formation consists of well mixed deposits of remobilized sediment from volcanic flanks and exhumed material from volcanic interiors. In the coastal section, Mohakatino Formation clastic mud-rich sediments derived from the north represent material eroded from submarine volcanic edifices and re-worked to the distal basin floor. Overall, the Mohakatino Formation onshore samples and all three lithofacies associated with them have not demonstrated any features that would identify them as having the potential to be reservoir rocks. While there were cases of the Mohakatino Formation in the proximal samples having appropriate reservoir quality, there is likely to be a petrographic change between these distal and proximal samples that in turn caused a decrease in reservoir quality.

Chapter 5:

Discussion and Implications of Reservoir Quality in the Miocene Mohakatino Formation, Northern Taranaki Basin, New Zealand.

5.1 Introduction

The Mohakatino Formation has been studied a number of times since it was first identified as a proven hydrocarbon prospect as part of the Kora Field. But while these studies have investigated many aspects of the MVC and the Kora Volcano there has been little work focused on determining the controls on reservoir quality of the Mohakatino Formation in both the proximal and distal regions. Most studies investigated the offshore region of the formation such as the Kora field (Armstrong et al., 1996; Bergman et al., 1992; King & Thrasher, 1996; Stagpoole & Funnell, 2001; Webster et al., 2011) and few have examined the onshore region (Sharman, 2014; Shumaker, 2016). None of these have specifically looked at reservoir quality of the Mohakatino Formation. This provides a unique opportunity for conclusions to be drawn about the reservoir quality of the distal, now onshore Awakino region and how this compares and contrasts to the proximal offshore region around the Kora Volcano.

5.2 Volcanic Sourced Sediments and Key Petrographic Controls

5.2.1 Clay and cement precipitation

In this study it has been identified that the Mohakatino Formation sourced from the Kora Volcano clearly illustrate early authigenic clay cementation, caused by the highly andesitic composition of the Mohakatino volcaniclastics. This prevented clay development that would have significantly reduced porosity and permeability. After the deposition of the volcaniclastic sediments the first two processes were the formation of early carbonate pore fill (calcite) and the precipitation of clay rims and coats (i.e. mixed layer chlorite grain coats) (Figure 5.1). The carbonate pore fill reduces porosity but this is offset by the acidic nature of the MVC material making the region unable to precipitate carbonate cements. The distal onshore outcrops and this study found that the distal material has significantly lower porosity values (5.46% and 10.34% for the onshore and offshore samples respectively) due to pore filling calcite that formed in the shallow marine environment away. The clay rims that formed early in the Mohakatino Formation history allowed for net porosity preservation and combined with relatively shallow depths of burial <2050m has maintained excellent reservoir quality and porosity. The volcaniclastic sediments are deposited in the proximal region of the MVC on the flanks of the Kora Volcano (Figure 5.2, samples A and B) can be seen to be much closer to the volcanic centre and undergone less transport than samples in a more distal setting. These samples (Figure 5.2 E and F) are far from the volcanic centre and deposited on the shallow marine continental shelf of Zealandia,

allowing for the early carbonate pore filling calcite precipitation shown in Figure 5.1 to occur and decrease the primary porosity.

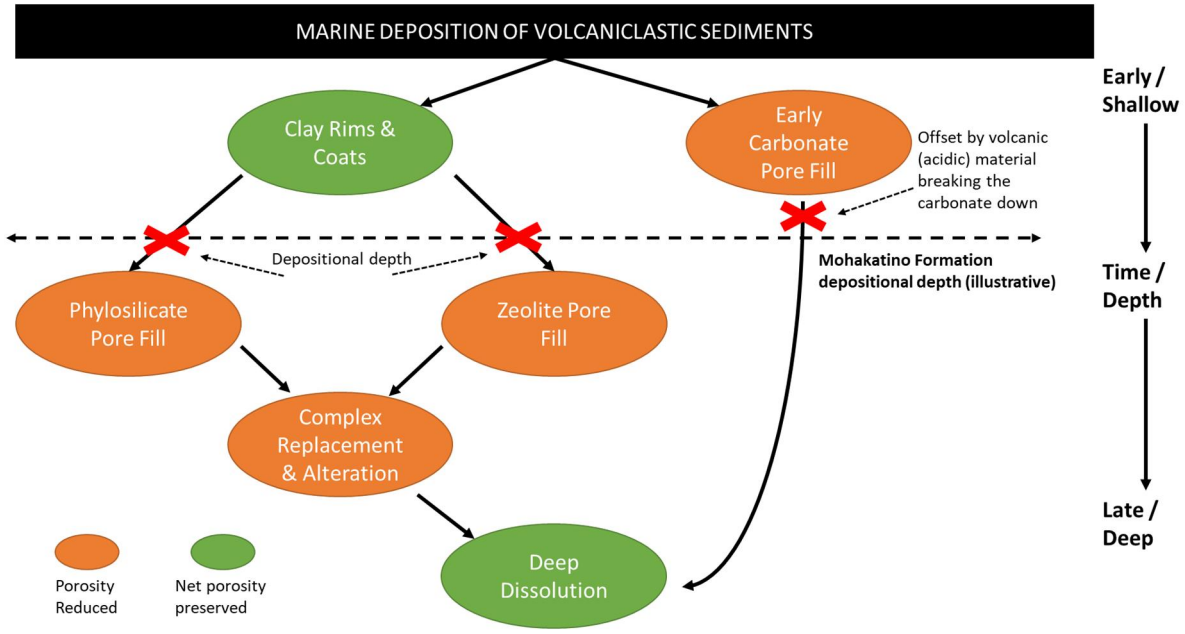

Figure 5.1: A schematic summary of factors controlling the diagenesis of the Mohakatino Formation volcaniclastics, and how depth and time can be highly influential. Based on Mathisen and McPherson, 2012.

The pore filling and pore lining clays in this study have behaved in a similar manner to those identified by Berger et al (2009), whose work found that the alteration and dissolution of the volcanic rock fragments and hypabyssal rock fragments provided a source for chlorite authigenesis. There is found an empirical relationship between the presence of chlorite and inhibition of quartz overgrowths, preserving reservoir quality (Berger et al, 2009). The same occurrence is identifiable in the Mohakatino Formation where authigenic chlorite grain coatings prevented any significant quartz precipitation. Remy (1994) found that the increased proportions of volcanic detritus resulted in greater volumes of authigenic chlorite, mixed layer clays and decreased illite and illite-smectite, and that compaction of these clays could occlude macroporosity in volcaniclastic sediments.

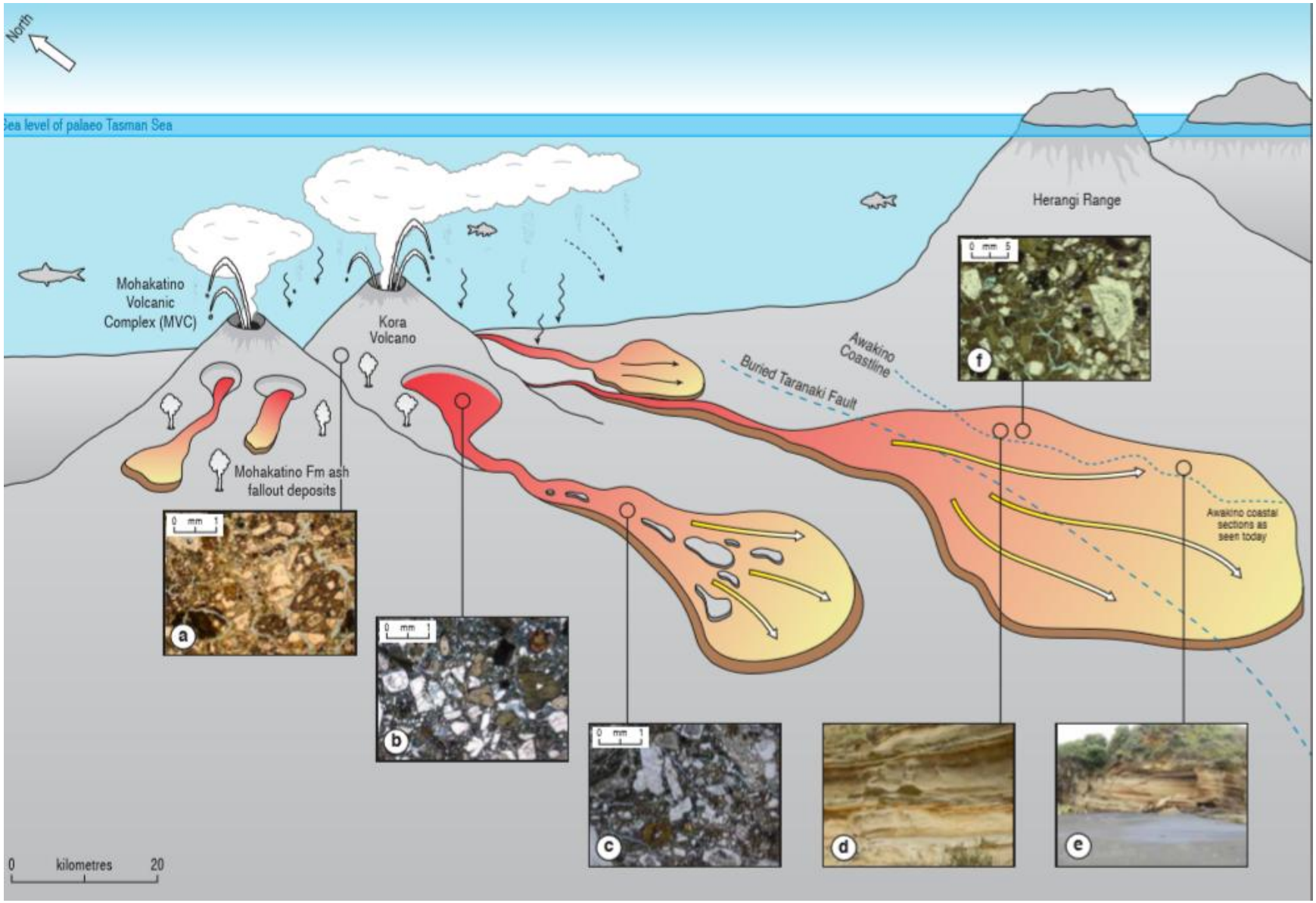

Figure 5.2: See next page for full description of figure.

Figure 5.2: Schematic representation of the Mohakatino Formation petrography and proximal to distal submarine fan system key changes. Mohakatino Volcanic Centre (MVC) and Herangi Range from the north-western and eastern margins of a narrow basin, with main channels oriented axially to the basin trend. a) Volcaniclastic breccia and ash fall deposits on a submarine volcanic flank. Note extensive fracturing and large angular andesitic volcanic grains and rock fragments (from Kora-1 core logs); b) Volcaniclastic breccia in a mass-wasting deposit and less proximal in the MVC. (From Kora 3 core logs); c) High-density turbidity current deposits, possibly channelised. Highly fractured but normal grading from gravel to silt, surrounded to subangular andesitic clasts, sand size grains and some clays (mainly kaolinite). Rare foraminifera can be found. Key feature is the finer grained nature and greater abundance of clay; d) Thin bedded lower density turbidity current deposits at distal margin of a lobe / submarine fan. Interbedded thin fine to medium-grained sandstones and silts, with some bioturbation and rippling; e) Thin-bedded, structureless low-density turbidity current deposits at the distal end of a lobe, with coarse-tail grading of gravel- to silt-sized grains and vertical mixing of sediment in burrows. From Awakino Heads coastal section of the Mohakatino Formation; f) From Pahaoa Ridge, North Awakino coastal section of the Mohakatino Formation.

This compaction of clays was found to prevent later stage dissolution (Berger et al, 2009) or authigenic mineral precipitation and therefore preserving reservoir quality, and the same processes can be extrapolated to the results of this study as the same intermixed chlorite minerals are observed, there is significant volcanic detritus and the Mohakatino Formation was rapidly buried by the Giant Foresets Formation that allowed for the sealing of the rocks and preventing dissolution. A combination of this rapid eruption and burial of volcaniclastic sediments led to ~2 km of Giant Foresets Formation material being deposited over 2 Ma on top of the Mohakatino Formation (see A, B, C and D samples in Figure 5.2). However, while this theory (Berger et al, 2009) has had successful application in other geological regions, taking an empirical approach is not the ultimate answer for porosity and permeability prediction in this setting (Bloch, 1991). It can be conceded that an empirical approach is the only feasible way to tackle reservoir quality prediction, but this technique does not take into account all of the diagenetic processes, and the result is quantitatively inaccurate predictions (Blotch, 1991). So, while this empirical method of study is useful and the best method available, its results must be properly scrutinised and must be acknowledged to not be totally holistic.

The Cretaceous feldspathic litharenite volcaniclastic sandstones of the lower Goru Formation (Berger et al, 2009), Sawan Field, Pakistan, have a similar composition to the Mohakatino Formation, and are likely be similar. The Mohakatino Formation is formed of hypabyssal, andesite derived sandstones and siltstones, closer to the Sawan Field rather than the Rosebank Field in comparison. A reasonable comparison to the Sawan Field can be made and used as a general guide of how the Mohakatino Formation behaves. This is useful because the types of cement and their influence on the Mohakatino Formation remains inconclusive, primarily due to the indeterminate nature many of these cements. Despite the limited data that was achieved in this study, the most influential cement in preserving porosity and permeability was identified as chlorite.

Clark (2014) used a model for predicting the diagenetic evolution of volcaniclastic rocks and determined that while the early stage growth of smectite or chlorite coats prevented compaction of pores, dissolution of mineral phases can cause significant secondary porosity. The clay formation in this study did not end conclusively and so the majority of the porosity was then filled. This was attributed to rapid burial promoting clay development, or an abundance of volcanic clasts that reacted with pore waters. Clark (2014) also acknowledges that these processes can become a negative effect on the reservoir quality, depending on the circumstances. Clark's (2014) basaltic rocks from the Rosebank Field, North Sea, can be relatable to this study, but the more felsic andesitic nature of the Mohakatino Formation may not behave in quite the same manner as the Rosebank Field.

5.2.2 Volcanic Rock Fragments

Sand- and gravel-sized clasts from the volcaniclastic facies are composed of a considerable variety of compositions. Crystal-poor rock fragments, typically characterized by large plagioclase crystals in a devitrified groundmass, are interpreted as lavas and pyroclasts. Crystal-rich rock fragments, exhibiting 30-50% or greater proportion of euhedral crystals are interpreted as hypabyssal rocks. Hypabyssal rocks cool relatively slowly, at 1-2 km depth in the crust, resulting in larger crystal sizes and greater proportion of crystals than extrusive volcanic rocks (Winter, 2001). They can be associated with the interiors of volcanoes, or with dykes and sills emanating from the volcanic center. The dominance of hypabyssal over volcanic rock fragments in the Mohakatino Formation suggests that sector collapse, or deep-seated mass wasting on over-steepened volcanic flanks, was an important sediment-generating mechanism among these volcanoes (Figure 5.2).

The absence of pumice in the study area and lack of evidence for vesicular tephra (e.g., preserved vesicles or fragmented bubble walls) in thin sections and in samples drilled from the volcanoes (e.g. Bergman et al., 1992) indicates that the Mohakatino volcanoes likely did not erupt explosively between 10.65 to 10.39 Ma (Maier et al., 2016). Though a depth-dependent control on magma vesiculation has been proposed (e.g., fragmentation depth. Fisher and Schmincke, 1984; pressure compensation level, Fisher, 1984), explosive, pumice-forming eruptions have been documented at water depths greater than 1 km for other rhyolitic, caldera-forming volcanoes (Rotella et al., 2015) and 3 km for basaltic volcanoes (Head and Wilson, 2003; Clague et al., 2009). Magma decompression rates and weight percent of volatiles are key factors in the eruptive behavior of deep marine volcanoes (Rubin et al., 2012; Cas and Giordano, 2014). Thus, the absence of vesicular materials in the Mohakatino Formation does not inform the eruptive depth of the volcanoes, but does support the interpretation that sector collapse, rather than explosive eruptions, was the primary mode of sediment production from the Mohakatino volcanoes (Fig.5.2). If eruptions were effusive rather than explosive, thermal quenching and fragmentation of lavas may also have been an important mechanism for producing readily transportable clasts, which would be subject to further breakdown and abrasion during transport. Anomalous pumice deposits can be found in the upper Mohakatino Formation and Lower Mount Messenger Formation of the Awakino coastal sections and may indicate variability in the eruptive behavior of the MVC, or may be the product of wind-blown ash or drifting pumice rafts from unrelated submarine or subaerial volcanoes.

When considering the sand and silt particles of the Mohakatino Formation the distribution of the VRF's are of particular importance. Berger et al. (2009) found that chlorite grains coats grew through direct precipitation of pore waters using products derived from VRFs, and these well-developed rims were able to inhibit quartz cementation and preserve porosities up to 20% as well as good permeability in shallow marine environments. This process can be identified in Figure 5.2 where the volcanic input from the MVC and the Kora Volcano in particular can be seen through the explosive

eruptive andesitic volcaniclastic sediments on the flanks of the volcano. The proximal region of the Mohakatino Formation is similar to the Sawan Field (Berger et al, 2009), and the same process of porosity preservation can be inferred here. The rapid burial of the proximal Mohakatino Formation led to the destruction of the pore network and subsequently acting as a closed system. This area affected by the high VRF input and the rapid burial in Figure 5.2 are A, B, C and D, with the volcanic input from the Kora Volcano and the rapid burial from the deposition of the GFF. In this system the pore fluids were able to breakdown the VRFs present in the rock composition and allow for the dissolution of pore lining authigenic minerals (e.g. Clark, 2014; Berger, 2009; Galloway, 1976; and Remy, 1994), which in turn inhibited quartz overgrowths and cementation and potentially preserved porosity. This was possible due to the significant presence of VRFs in the offshore samples (see Appendix I). However, in the distal samples, the percentage of VRFs making up the rock compositions is significantly lower (see Appendix II). This means that there is less reactive material available to be altered by pore fluids and form authigenic, pore-lining minerals. This combined with a lack of rapid, deep burial (see Section 5.3) to produce a closed system means that there is no prevention of later stage authigenic mineral precipitation that would reduce the porosity significantly. This is shown in Figure 5.2 where this distal samples are represented by E and F, and their distance from the source of the volcanic materials means that any VRFs transported by the turbidity currents have been significantly reduced.

5.2.3 Grain Characteristics

The reservoir quality of newly deposited clastic sedimentary rocks in shallow reservoirs is primarily controlled by the depositional environment which exists as a first order control on grain size, sorting, porosity and permeability. This determined characteristics such as grain size, sorting, sphericity, angularity, packing and abundance of matrix minerals. The highest quality reservoir rocks are well-sorted, have well-rounded grains, no matrix material and quasi-homogenous mineralogy. The source of the Mohakatino Formation is the MVC and primarily the Kora Volcano, with volcaniclastic material being deposited along the flanks of the volcano, a short distance from the source. This means there is little time or distance available for the transportation of the volcaniclastics. The proximal Mohakatino volcaniclastic rocks/sediments (See Chapter 3) are composed of very poorly sorted, have wide ranging grain sizes (sand to conglomerate), tightly packed, sub-angular to sub-rounded grains, and with a heterogeneous mineralogy. The regional location of these rocks is shown in Figure 5.2 A - D, which from a petrographic standpoint is not conducive to preserving a good reservoir quality. There are some exceptions to this, such as samples Kahawai-1 1990.1 and Kahawai-1 2462.5 (See Figure 3.6), where the grains are moderately well sorted, the angularity is lower and they are loosely packed. However, despite the grain characteristics of the proximal samples being unsuitable reservoir rocks, there are still specific samples that exhibit high porosity and permeability values which may

indicate good reservoir quality (See Chapter 3 and Appendix I). Overall, w despite the lack of commercial volumes of hydrocarbons, some wells still have good reservoir quality, such as Kora-1A. This is due to their low volume of intergranular matrix. The distal material does not exhibit these positive reservoir quality traits. In Section 4.3.2 the grain characteristics of the distal samples can be seen to be very poorly sorted, tightly packed and sub-angular to sub-rounded, all of which are similar characteristics to the proximal samples. Examples of these samples are also depicted in their regional context in Figure 5.2 E and F. The main difference here is that there is significantly more matrix material between the grains, and the comparison of matrix volumes can be seen in Appendix I and II. The reason for this is discussed previously in Section 5.2.1 and 5.2.2.

The grain characteristics between the proximal and distal samples of the Mohakatino Formation are similar, both regions poorly sorted with highly variable grain sizes, tightly packed, sub-angular to sub-rounded grains, and with a wide-ranging heterogeneous mineralogy. While these are not positive reservoir rock characteristics, in proximal regions they do contribute towards a good to average porosity and permeability in the wells (See Chapter 3 and Appendix I and III). In the distal region, while the reservoir quality may be poor, this can be attributed primarily to the cementation processes (Section 4.4.2 and 5.2.1) which filled a large percentage of the pore space, decreased reservoir quality. There is still the possibility that these rocks may have retained porosity and permeability to act as reservoir rocks, if the influence of the cementation is removed. The conclusion of this thesis is that this would still not have occurred, because the distal region did not encounter the same burial as that of the proximal rocks, and the formation of a closed system would not have been possible.

5.3 Spatial Controls on Reservoir Quality

5.3.1 Burial History

The rapid burial of the Mohakatino Formation by the GFF (mentioned previously in Section 5.2) of ~2 km of sediment over 2 Ma combined with the reactive mineralogy and the thermal influence of the MVC potentially caused the destruction of the formation's pore network at relatively shallow depths and caused the rock to behave like a close system (Clark, 2014). This closed system results in a feedback mechanism with small quantities of water becoming trapped in the pores, and as they cannot exchange with an outside source, these waters become enriched leading to accelerated alteration of VRFs and the formation of pore lining authigenic minerals (e.g. Clark, 2014). Depending on whether the authigenic minerals are beneficial to reservoir quality or not, this rapid burial is an important process in the development of reservoir quality. I conclude that the rapid deposition of the GFF has helped with the preservation of the porosity and permeability of proximal deposit of the Mohakatino Formation. This burial rate did not occur in more distal regions of the Mohakatino Formation, which were buried by the Mount Messenger Formation over a much longer period of time and to a lower

depth. This means that the distal rocks did not behave like a closed system in the same way as the proximal region, and so did not have the accelerated authigenic mineral precipitation. While generally considered detrimental to porosity preservation, these minerals can be considered porosity-preserving (as discussed in Section 5.2) and so the distal region's reservoir quality was at a spatial disadvantage compared to those rocks in a proximal setting.

5.3.2 Compaction vs Cementation

The spatial influence on whether porosity loss was primarily through compaction or cementation is clearly seen in Figure 5.3. Here the proximal samples (green) have significantly higher COPL values than CEPL, and are primarily grouped in the top left quadrant of the graph. The distal samples (black), however, are more widely spaced across the graph, indicating that COPL and CEPL occurred. The proximal samples (rocks, not sediments) experienced relatively consistent porosity loss across the region through compaction mechanisms. On the other hand, the distal material did not experience this regionally homogenous porosity loss. In the samples from this region there has been variation between compaction and cementation influence in porosity loss, with 50% through compaction and 50% through cementation. These samples also have, on average, poorer porosity that the proximal samples. The samples are all derived from the same andesitic arc material from the MVC and the Kora Volcano and so they should all have experienced the same porosity loss processes had they all been deposited in the same region and undergone the same burial history. This difference in burial is concluded to have been influenced by the difference in spatial parameters, and had these regions been closer together, or influenced by the same burial across the whole formation, then the COPL vs CEPL data would likely have looked much more similar. However, it must be acknowledged that there are multiple other factors that can contribute the cementation levels seen in the distal samples.

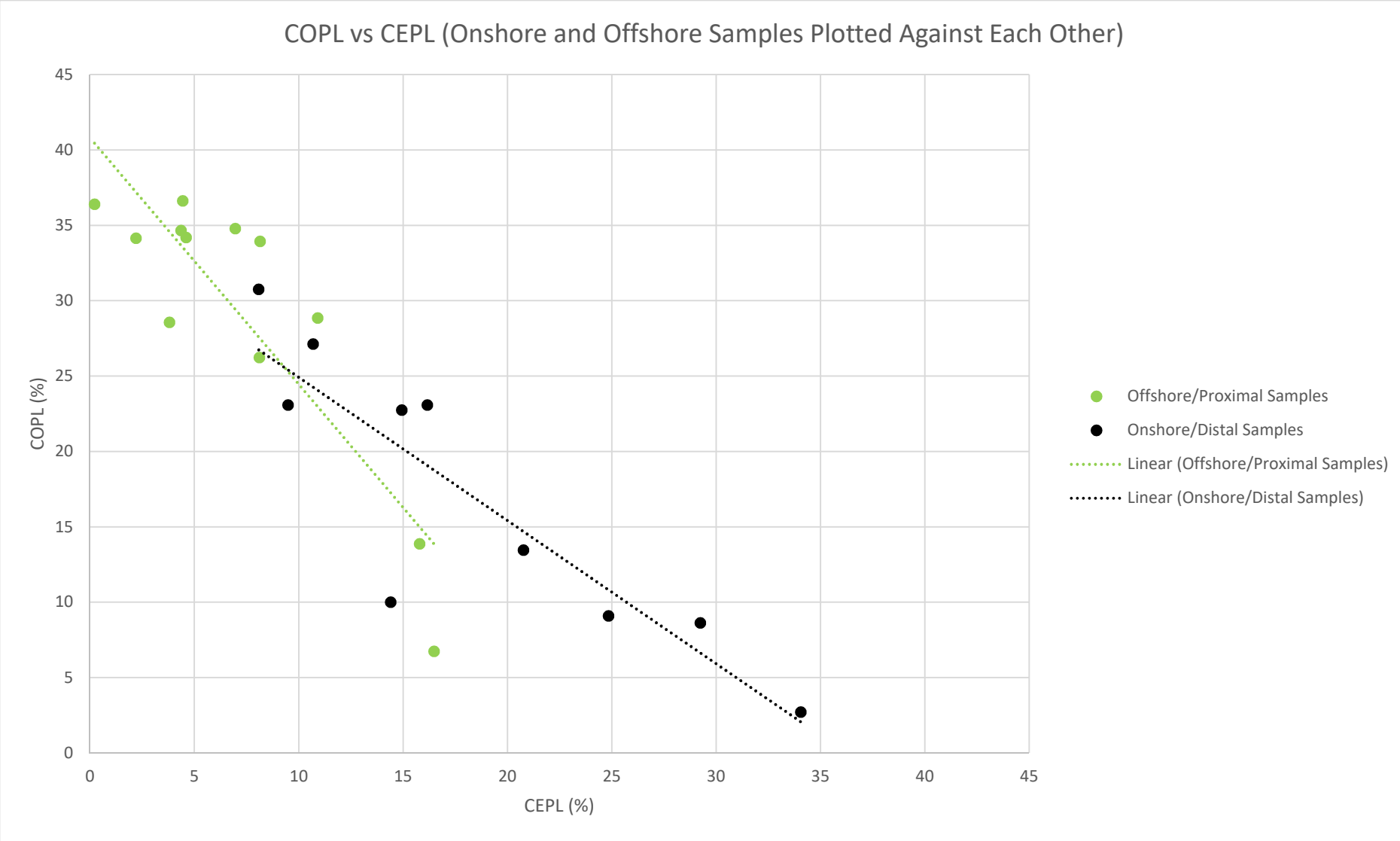

Figure 5.3: A graph plotting porosity loss by compaction (COPL) against porosity loss by cementation (CEPL) for both the proximal offshore samples and distal onshore samples.

5.4 Implication for Reservoir Quality of Volcaniclastic Reservoirs

A key point to consider is that the reservoir quality described here as having anomalous porosity is potentially the higher end of the range of possible outcomes, and that a specific combination of grain size, sorting, composition, early diagenesis, and burial history have acted together to minimize the effects of compaction and cementation and preserve the greatest amount of porosity and permeability at depth considering the conditions (Ajdukiewicz and Lander, 2010). While it is possible to say one well has better reservoir quality than the other, it is not necessarily true to say that it has high reservoir quality in relation to other volcaniclastic reservoirs in the region or around the world. This is one of the greatest limitations of the study and something that must be seriously considered when comparing it to other studies.

The primary implication for the reservoir quality of volcaniclastic reservoirs in general is that they require very specific processes to occur at certain points in the diagenetic process for them to preserve optimal porosity and permeability. For example: plots from point counting data show that volcaniclastic rocks have very poor reservoir quality at depth when they have more than 10% volcanic clasts in the Rosebank Field and Staffa Formation (Clark, 2014); two stage double layers of pore-lining authigenic chlorite inhibiting quartz cementation in the Sawan gas field (Berger et al., 2009); facies controls dictated the porosity and permeability values in the Faroe Island Basalt Group, where rocks of epiclastic origin retained their reservoir quality to a much greater extent than the pyroclastic rocks (Ólavsdóttir et al., 2015); and the degree compaction of the Middle Park Basin, Colorado, is found to occlude macroporosity in the volcaniclastic-rich samples and preventing later stage dissolution or authigenic mineral precipitation (Remy, 1994). All of these different volcaniclastic regions show similar processes occurring in them as the Mohakatino Formation has, and this highlights the variability and heterogeneous nature of porosity and permeability preservation in volcaniclastic rocks. Diagenetic mineral paragenesis is highly dependent on localised mineral composition and this composition can vary considerably between the samples, reservoirs and wells. It is difficult to accurately predict the reservoir quality of volcaniclastic rocks and inherently makes them more challenging than traditional sandstone reservoirs. Identifying one process from this study and trying to apply to other regions would be difficult and unlikely to be applicable, due to the combination of factors required for successful preservation of reservoir quality not guaranteed to be present in most volcaniclastic basins.

The reservoir quality of the Mohakatino Formation had been considered poor due to failed attempts to commercially produce oil from the Kora Field. However, the poor performance of the Mohakatino Formation as a reservoir was more due to the lack of an appropriate seal, and much of any hydrocarbons generated due to the thermal input of the magmatism was lost to the surface very quickly. If there had been the formation of this seal at the appropriate time in the basin's history then

it is likely that in areas of the field such as Kora-1/1A well the Mohakatino could have acted as a hydrocarbon reservoir, although the size and commercial viability of such a reservoir is debatable. This is a key point of this study because there are a number of similar fields to the Kora of the same size and characteristics in both the Taranaki and Northland basins along the MVC (Bergman et al., 1996). Assuming a similar type of volcanism is occurring to produce submarine volcanos and they are depositing similar material to that of the MVC, positive reservoir quality may exist as part of a fully formed petroleum play in this region.

5.5 Implications for Basin Scale Processes in Volcanogenic Dominated Basins

Volcanogenic dominated sedimentary basins require significant volumes of material deposited over the volcaniclastics rapidly and at depth. This provides the compaction that is needed to seal the rocks and form a closed system, as discussed previously in this chapter, and this process will help achieve occluding the porosity and/or allow for the dissolution of volcanic materials to produce the pore lining cements that prevent later stage pore filling authigenic clays from decreasing the porosity. The type of volcanic material produced is a major control on how volcaniclastics are able to form a reservoir rock. If the erupted material is felsic, it can be beneficial (as discussed previously in this study) because in a shallow marine environment it can prevent early stage calcite cement precipitation reducing porosity. If the rocks are mafic then the volcanic clasts, they produce are more reactive and there is a greater chance of authigenic mineral formation which can be considered detrimental or beneficial depending on the depositional system. Unlike traditional hydrocarbon reservoirs, volcaniclastics are more influenced by their mineralogy which can be highly reactive and influenced by changes in pressure, temperature, salinity, compaction or time, and so the basin wide processes that produce this material are a factor that must always be taken into account when investigating volcaniclastics.

An implication from understanding the spatial and temporal controls on reservoir quality of the volcaniclastic sediments of the MVC is that the deeply submerged volcanoes such as the MVC are disconnected from many of the effects of climate and sea level change than are common in many submarine sedimentary processes. The environmental signals from many allocyclic forces may not be detectable in the volcanogenic sedimentary record as seen in the MVC. Warming ocean temperatures and large magnitude sea level falls could influence pore fluid pressure on volcanic flanks, triggering mass wasting events (Leynaud et al., 2009), but changes in precipitation, storm frequency or intensity, shoreline position, and growth or retreat of glaciers would have little to no direct effect on the sediment supply from deeply submerged volcanoes. Local tectonic activity on short timescales ($<10^3$yr) would likely be indistinguishable from volcanic activity (eruption events, mass wasting on flanks), and longer-term regional tectonic signals of uplift or subsidence would potentially correlate with shifts in volcanic activity, particularly for cases like the MVC in which volcanism and tectonism are inherently linked, thereby masking the tectonic vs. volcanic origin of a signal. Thus, for source-to-

sink studies in which a deeply submerged volcanic center plays a role in basin sedimentation, volcanogenic sediment can be expected to record signals of volcanic evolution and autogenic behavior of submarine sediment transport systems, but largely be buffered from climate and sea level fluctuations.

5.6 Conclusions

- The Mohakatino Formation of the Taranaki Basin, New Zealand, records deposition of submarine volcano-sourced sediment in a bathyal submarine lobe environment. The dominant sedimentation style was characterized by coarse-grained, mud-poor, low-density turbidity currents that deposited laterally continuous, thin- to medium-bedded sandstone and siltstone. In the proximal lobe setting, this background sedimentation was punctuated periodically by much larger, higher energy, upstream- erosive flows that entrained rip-up clasts from the basin floor and deposited very thick- bedded, variably amalgamated sandstone and conglomerate.
- Proximity of the offshore samples from this study to the MVC and the Kora Volcano meant that the original material had a high volume of VRFs in the composition and also experienced the thermal influence of the volcanic centre. The VRF content provided the reactive material that could be broken down to form the pore lining authigenic minerals that would prevent later stage authigenic cementation and quartz overgrowths, and lead to the overall preservation of porosity.
- This process was aided by the thermal input from the MVC, which provided additional heat to the processes and stimulated the reactivity and breakdown of the authigenic minerals.
- The rapid burial of the proximal Mohakatino Formation around the Kora volcano by ~2 km of the Giant Foresets Formation over ~2 Ma lead to rapid compaction. This formed a closed system that resulted in a feedback mechanism, allowing the accelerated alteration of VRFs to be contained in the formation and distributed chlorite clay coatings throughout the rocks.
- The distal, onshore samples did not have the thermal influence or the same acidic nature of the rocks. There was limited deterrence for the formation of early carbonate pore fills cements such as calcite, which led to the loss of porosity and the reduction in reservoir quality.
- The distal Mohakatino Formation volcaniclastics exposed along the Awakino coastline of North Island, New Zealand, were buried to a shallower depth (~1km) than contemporaneous volcaniclastics proximal to the MVC which experienced rapid, deep burial. The early onset of carbonate cements and the finer grained distal turbidite volcaniclastics distal to the Kora volcano experienced significantly reduced porosity and therefore decreased reservoir quality.
- While there were a number of factors such as composition and calcite formation that were detrimental to the retention of reservoir quality, there are still a number of external influencing factors, such as thermal input, burial and compaction, and appropriate cementation that prompted the appropriate reactions and processes required to retain the limited porosity and permeability of these rocks and allow the proximal regions of the Mohakatino Formation to act as reservoir rocks.

5.7 Future Work

Further work could be done to improve this study by collecting more data from the offshore and onshore regions of the study area. As can be seen throughout this thesis, there is a small sample set of rocks collected from the onshore region during the fieldwork and thin section slides from the offshore wells. While these limited samples were unavoidable due to time and logistical problems, a simple way to improve this work in the future would be to collect more samples of the necessary rocks and outcrops from the onshore region, and then request the GNS for the opportunity to have access to more data or thin sections for the offshore study. This increase would allow for the results to be more holistic and conclusive.

A problem encountered through this study was the complex nature of the grains that made up these rocks and the cements that bound them together and filled the pore spaces. While they were studied using optical microscopy, SEM and SEM-XRD analysis, the type of analysis used was inconsistent and this was again down to time and logistical problems. For future work all analysis of all samples should be done with optical microscopy and SEM-EDX analysis, allowing for the more conclusive identification of cements, porosity and permeability. This would also allow for less reliance on third party data which can potentially lead to inconsistencies.

Volcanic reservoirs which have commercially viable hydrocarbon resources do exist in the Taranaki Basin, most notably in the Maui and Kupe Fields, and so there is good reason to suspect there are more such fields to be found. Further areas of study that might produce volcanic reservoirs similar to the Kora Field would possibly be the complexes more deeply buried in the axis of the northern Taranaki Basin (Bergman et al, 1992) and towards the Northland Basin, where the development of a suitable seal is possible and the thermally mature Pakawau source rocks to feed these reservoirs.

References

ARCO/ARCO Petroleum NZ Inc., 1988a. Final well report, Kora-1/Kora-1A. PPL 38447. *Ministry of Economic Development*, *New Zealand.* Unpublished Petroleum Report PR 1374.

ARCO/ARCO Petroleum NZ Inc., 1988b. Final well report, Kora-2. PPL 38447. *Ministry of Economic Development*, *New Zealand.* Unpublished Petroleum Report PR 1439.

ARCO/ARCO Petroleum NZ Inc., 1988c. Final well report, Kora-3. PPL 38447. *Ministry of Economic Development*, *New Zealand.* Unpublished Petroleum Report PR 1441.

Armstrong, P., Chapman, D., Funnel, R., Allis, R. and Kamp, P., 1996. Thermal modelling and hydrocarbon generation in an active-margin basin: Taranaki Basin, New Zealand. *AAPG Bulletin.* Vol. 80, pp. 1216-1241.

Arndt, N., 2011. Volcaniclastic sediment. In *Encyclopaedia of Astrobiology.* (pp. 1756-1753). Springer Berlin Heidelberg.

Arnot, M.J., King, P.R., Browne, G.H. and Helle, K. 2007b. Channelized, innermost, basin floor fan morphologies, Mount Messenger Formation, Waikiekie South beach and inland, New Zealand. In: Nielsen, T.H., Shew, R.D., Steffens, G.S. and Studlick, J.R.J. (Eds), Atlas of deep-water outcrops. *AAPG Studies in Geology*. Vol. 56, Chapter 60 (7p).

Ajdukiewicz, J.M. and Lander, R.H., 2010. Sandstone reservoir quality prediction: The state of the art. *AAPG bulletin*, Vol 94(8), pp.1083-1091.

Bache, F., Sutherland, R., Stagpoole, V., Herzer, R., Collot, J., and Rouillard, P., 2012. Stratigraphy of the southern Norfolk Ridge and the Reinga Basin: A record of initiation of the Tonga-Kermadec-Northland subduction in the southwest Pacific. *Earth and Planetary Science Letters.* Vols 321-322, pp. 41-53.

Ballance, P.F. 1976. Evolution of the upper Cenozoic magmatic arc and plate boundary in northern New Zealand. *Earth and planetary science letters*. Vol. 28, pp. 356–370

Berger, A., Gier, S., and Krois, P., 2009. Porosity-preserving chlorite cements in shallow-marine volcaniclastic sandstones: Evidence from cretaceous sandstones of the Sawan gas field, Pakistan. *AAPG Bulletin.* Vol. 93, pp. 595-615.

Bergman, S. C., Talbot, J. P., and Thompson, P. R., 1992. The Kora Miocene andesite submarine stratovolcano hydrocarbon reservoir, Taranaki Basin, New Zealand. *1991 New Zealand Oil Exploration Conference Proceedings*. New Zealand Ministry of Commerce, Wellington. 178-206.

Bernabéu, A., Vonk, A., Nelson, C., and Kamp, P., 2009. Mangarara Formation: exhumed remnants of a middle Miocene temperate carbonate, submarine channel fan system on the eastern margin of the Taranaki Basin, New Zealand. *New Zealand Journal of Geology and Geophysics.* Vol. 52, pp, 73-93.

Bloch, S., 1991. Empirical prediction of porosity and permeability in sandstones. *AAPG Bulletin.* Vol. 75, pp. 1145-1160.

Browne, G., and Slatt, R., 2002. Outcrop and behind outcrop characterisation of a late Miocene slope fan system, Mt Messenger Formation, New Zealand. *AAPG Bulletin.* Vol 86, pp. 841-862.

Browne, G., Slatt, R., and King, P., 2000. Contrasting styles of basin floor fan deposition: Mount Messenger Formation, New Zealand. *AAPG Memoir.* Vol. 72, pp. 143-151.

Clague, D.A., Paduan, J.B. and Davis, A.S., 2009. Widespread strombolian eruptions of mid-ocean ridge basalt. *Journal of Volcanology and Geothermal Research*. Vol. 180(2), pp. 171-188.

Cas, R.A. and Giordano, G., 2014. Submarine volcanism: a review of the constraints, processes and products, and relevance to the Cabo de Gata volcanic succession. *Italian Journal of Geosciences*. Vol. 133(3), pp. 362-377.

Clark, Samantha Jean., 2014. Constraining diagenetic timings, processes and reservoir quality in igneous-affected basins. Durham PhD Thesis, Durham University. Available at Durham E-Thesis Online: http://ethesis.dur.ac.uk/10827/

Dreyer, I. and Stang, G., 2013. The shale gas 'revolution': Challenges and implications for the EU. *EUISS Brief Issue*. Vol. 11.

Ehrenberg, S., 1993. Preservation of anomalously high porosity in deeply buried sandstones by grain-coating chlorite: Examples from the Norwegian continental shelf. *AAPG Bulletin.* Vol. 77, pp. 1260-1286.

Farooqui, M., 2009. Evaluating volcanic reservoirs. *Oilfield Review Schlumberger.* Vol. 21, pp. 36-47.

Feng, Z.Q., 2008. Volcanic rocks as prolific gas reservoir: a case study from the Qingshen gas field in the Songliao Basin, NE China. *Marine and Petroleum Geology.* Vol. 25, pp. 416-432.

Fisher, R.V., 1984. Submarine volcaniclastic rocks. In: Kokelaar, B.P., and Howells, M.F. (eds) Marginal basin geology - volcanic and associated sedimentary and tectonic processes in modern and ancient marginal basins. *Spec Pub Geol Soc London.* Vol. 16, pp. 5–27.

Fisher, R.V. and Schmincke, H.U., 1984. Submarine volcaniclastic rocks. In *Pyroclastic Rocks*. Berlin, Heidelberg.

Galloway, W., E., 1979. Diagenetic control of reservoir quality in arc-derived sandstones: Implications for petroleum exploration. *SEPM Special Publication.* Vol. 26, pp. 251-262.

Giba, M., Nicol, A., and Walsh, J., 2010. Evolution of faulting and volcanism in a back-arc basin and its implications for subduction processes. *Tectonics.* Vol. 29, pp. 1-18.

Giba, M., Walsh, J., Nicol, A., Mouslopoulou, V., and Seebeck, H., 2013. Investigation of the spatio-temporal relationship between normal faulting and arc volcanism on million-year time scales. *Journal of the Geological Society, London.* Vol. 170. pp, 951-962.

GNS Science Petroleum Basin Explorer. 2013. *Kora Oil Discovery*. [ONLINE] Available at: https://data.gns.cri.nz/pbe/index.html. [Accessed 21 September 2017].

Hayward, B., 1990. Uses of foraminiferal data in analysis of Taranaki Basin, New Zealand. *Journal of Foraminiferal Research.* Vol. 20, pp. 71-83.

Head III, J.W. and Wilson, L., 2003. Deep submarine pyroclastic eruptions: theory and predicted landforms and deposits. *Journal of Volcanology and Geothermal Research*. Vol. 121(3-4), pp. 155-193.

Heald, M., T., and Larese, R., E., 1974. Influence of coatings on quartz cementation. *Journal of Sedimentary Petrology.* Vol. 44, pp. 1269-1274.

Higgs, K., Zwingmann, H., Reyes, A., and Funnell, R., 2007. Diagenesis, porosity evolution, and petroleum emplacement in tight gas reservoirs, Taranaki Basin, New Zealand. *Journal of Sedimentary Research.* Vol. 77, pp. 1003-1025.

Holt, W., and Stern, T., 1994. Subduction, platform subsidence, and foreland thrust loading: The late Tertiary development of Taranaki Basin, New Zealand. *Tectonics.* Vol. 13, pp. 1068-1092.

Iijima, A., 2001. Zeolites in petroleum and natural gas reservoirs. *Reviews in mineralogy and geochemistry,* Vol. 45, pp. 347-402.

Jiang, S., 2012. Clay minerals from the perspective of oil and gas exploration. *Clay Minerals in Nature – Their Characterisation, Modification and Application.* InTech.

Kamp, P.J., Vonk, A.J., Bland, K.J., Hansen, R.J., Hendy, A.J., McIntyre, A.P., Ngatai, M., Cartwright, S.J., Hayton, S. and Nelson, C.S., 2004. Neogene stratigraphic architecture and tectonic evolution of Wanganui, King Country, and eastern Taranaki Basins, New Zealand. *New Zealand Journal of Geology and Geophysics.* Vol. 47(4), pp. 625-644.

King, P., 1990. Polyphase evolution of the Taranaki Basin, New Zealand: changes in sedimentary and structural style. *1990 New Zealand Oil Exploration Conference Proceedings. Wellington, Ministry of Commerce.* pp. 135-150.

King, P.R., Browne, G.H., Arnot, M.J., and Crundwell, M.P., 2007a. A 2-D, oblique-dip outcrop transects through a third-order, progradational, deep-water clastic succession, Urenui-Mount Messenger Formations, New Zealand, in Nilsen, T.H., et al., eds. *Atlas of deep-water outcrops*: *American Association of Petroleum Geologists Studies in Geology.* Vol. 56, CD-ROM, 42 p.

King, P.R., Browne, G.H., Arnot, M.J., Slatt, R.M., Helle, K., and Stromsoyen, I., 2007b. A 2-D oblique-dip outcrop transect through an entire third-order, progradational, deep-water clastic succession (Late Miocene Mount Messenger–Urenui Formations), Taranaki Basin, New Zealand, in Nilsen, T.H., et al., eds. *Atlas of deepwater outcrops: American Association of Petroleum Geologists Studies in Geology*. Vol. 56, pp. 238–240.

King, P.R., Browne, G.H., Arnot, M.J., and Stromsoyen, I., 2007c, Slope feeder channels, Urenui Formation, Wai-it and Mimi Beaches, New Zealand, in Nilsen, T.H., et al., eds., *Atlas of deep-water outcrops: American Association of Petroleum Geologists Studies in Geology.* Vol. 56, pp. 262–264.

King, P.R., Browne, G.H., Slatt, R.M. 1994. Sequence architecture of exposed Late Miocene basin floor fan and channel-levee complexes (Mount Messenger Formation), Taranaki Basin, New Zealand. In Weimer, P., Bouma, A.H., Perkins, B.F. (eds) Submarine fans and turbidite systems: sequence stratigraphy, reservoir architecture and production characteristics Gulf of Mexico and international: 177–192. Gulf Coast Section, *Society of Economic Paleontologists and Mineralogists Foundation, Houston.*

King, P., Scott, G., and Robinson, P., 1993. Description, correlation and depositional history of Miocene sediments outcropping along North Taranaki coast. *Institute of Geological and Nuclear Sciences monograph 5.* Institute of Geological and Nuclear Sciences Ltd, Lower Hutt.

King, P., and Thrasher, G., 1992. Post-Eocene Development of the Taranaki Basin, New Zealand. Convergent Overprint of a Passive Margin. *DSIR Geology and Geophysics of Continental Margin.* Pp. 93-118.

King, P., and Thrasher, G., 1996. *Cretaceous Cenozoic geology and petroleum systems of the Taranaki Basin, New Zealand.* Vol. 2. Institute of Geological & Nuclear Sciences.

Killops, S., Woodhouse, A., Weston, R., and Cook, R., 1994. A geochemical appraisal of oil generation in the Taranaki Basin, New Zealand. *AAPG Bulletin.* Vol. 78, pp. 1560-1585.

Knox, G., 1982. Taranaki Basin, structural style and tectonic setting. *New Zealand Journal of Geology and Geophysics.* Vol. 25, pp. 125-140.

Kroeger, K., Funnell, R., Nicol, A., Fohrmann, M., Bland, K., and King, P., 2012. 3D crustal-scale heat-flow regimes at a developing active margin (Taranaki Basin, New Zealand). *Tectonophysics.* Vol. 591, pp. 175-193.

Lenhardt, N. and Götz, A., 2011. Volcanic settings and their reservoir potential: An outcrop analogue study on the Miocene Tepoztlán Formation, Central Mexico. *Journal of Volcanology and Geothermal Research.* Vol. 204, pp. 66-75.

Leynaud, D., Mienert, J. and Vanneste, M., 2009. Submarine mass movements on glaciated and non-glaciated European continental margins: a review of triggering mechanisms and preconditions to failure. *Marine and Petroleum Geology*, *26*(5), pp.618-632.

Liu, J., Wang, P., Zhang, Y., Bian, W., Huang, Y., Tang, H. and Chen, X., 2012. Volcanic rock hosted natural hydrocarbon resources: a review. In *Updates in Volcanology-New Advances in Understanding Volcanic Systems.* InTech.

Lundgard, P., 1992. Sandstone porosity loss – A "big picture" view of the importance of compaction. *Journal of Sedimentary Petrology.* Vol. 62, pp. 250-260.

Maier, K.L., 2012, Depositional architecture of deep-water slope systems: Examples from the Quaternary Lucia Chica channel system, offshore central California and the Upper Miocene Urenui Formation, New Zealand [Ph.D. thesis]: *Stanford, California, Stanford University*. 412 p.

Maier, K.L., Crundwell, M.P., Coble, M.A., King, P.R., and Graham S.A., 2016. Refined depositional history and dating of the Tongaporutuan reference section, north Taranaki, New Zealand: new volcanic ash U–Pb zircon ages, biostratigraphy and sedimentation rates. *New Zealand Journal of Geology and Geophysics*. Vol. 59:2, pp. 313-329

Masalimova, L., 2013, Stratigraphic architecture and flow dynamics of deep-water turbidite deposits: The Miocene Lower Mount Messenger Formation in the Taranaki Basin in New Zealand, and the Oligocene Puchkirchen Formation in the Molasse Basin in Austria [Ph.D. thesis]: *Stanford, California, Stanford University.* 193 p.

Mathisen, M., and Mcpherson, J., 1991. Volcaniclastic deposits: implications for hydrocarbon exploration. *SEPM Special Publication.* Vol. 45, pp. 27-36.

Mortimer, N., 2004. New Zealand's Geological Foundations. *Gondwana Research.* Vol. 7, pp. 261-272.

Mortimer, N., Tulloch, A., and Ireland, T., 1997. Basement geology of Taranaki and Wanganui Basins, New Zealand. *New Zealand Journal of Geology and Geophysics.* Vol. 40, pp. 223-236.

Muir, R., Bradshaw, J., Weaver, S., and Laird, M., 2000. The influence of basement structure on the evolution of the Taranaki Basin, New Zealand. *Journal of the Geological Society, London.* Vol. 157, pp. 1179-1185.

Nodder, S.D., Nelson, C.S., and Kamp, P.J.J., 1990b, Massemplaced siliciclastic-volcaniclastic-carbonate sediments in Middle Miocene shelf-to-slope environments at Waikawau, northern Taranaki, and some implications for Taranaki Basin development: *New Zealand Journal of Geology and Geophysics.* Vol. 33, pp. 599–615. doi: 10 .1080 /00288306 .1990 .10421378

NZOG/NZ Oil & Gas Services Ltd, 1990. Kahawai-1 well completion report. PPL 38451. *Ministry of Economic Development*, *New Zealand.* Unpublished Petroleum Report PR 1878.

Ólavsdóttir, J., Andersen, M.S. and Boldreel, L.O., 2015. Reservoir quality of intrabasalt volcaniclastic units onshore Faroe Islands, North Atlantic Igneous Province, northeast Atlantic. *AAPG Bulletin*, Vol. 99, pp.467-497.

Paxton, S., Szabo, J., Ajdukiewicz, J., and Klimentidis, R., 2002. Construction of an intergranular volume compaction curve for evaluating and predicting compaction and porosity loss in rigid-grain sandstone reservoirs. *AAPG Bulletin.* Vol. 86, pp. 2047-2067.

Pittman, E.D., 1992. Relationship of porosity and permeability to various parameters derived from mercury injection-capillary pressure curves for sandstone. *AAPG bulletin*. Vol. 76, pp.191-198.

Primmer, T.J., C.A. Cade, J. Evans, J.G. Gluyas, M.S. Hopkins, N.H. Oxtoby, P.C. Smalley, E.A. Warren, and R.H. Worden, 1997, Global patterns in sand- stone diagenesis: their application to reservoir quality prediction for petroleum exploration, in J.A. Kupecz, J. Gluyas, and S. Bloch, eds., Reservoir quality prediction in sandstones and carbonates: AAPG Memoir 69, p. 61-77.

Richardson Land, Jessica. 2017. Late Cenozoic development of north Taranaki Basin, New Zealand: A seismic investigation. MScR Thesis, University of Waikato.

Reilly, C., Nicol, A., Walsh, J., and Seebeck, H., 2015. Evolution of faulting and plate boundary deformation in the Southern Taranaki Basin, New Zealand. *Tectonophysics.* Vol. 651, pp. 1-18.

Remy, R., 1994. Porosity reduction and major controls on diagenesis of Cretaceous-Paleocene volcaniclastic and arkosic sandstone, Middle Park Basin, Colorado. *Journal of Sedimentary Research.* Vol. A64, pp. 797-806.

Rotella, M.D., Wilson, C.J., Barker, S.J., Schipper, C.I., Wright, I.C. and Wysoczanski, R.J., 2015. Dynamics of deep submarine silicic explosive eruptions in the Kermadec arc, as reflected in pumice vesicularity textures. *Journal of Volcanology and Geothermal Research*. Vol. 301, pp. 314-332.

Rubin, K.H., Soule, S.A., Chadwick Jr, W.W., Fornari, D.J., Clague, D.A., Embley, R.W., Baker, E.T., Perfit, M.R., Caress, D.W. and Dziak, R.P., 2012. Volcanic eruptions in the deep sea. *Oceanography*. Vol. 25(1), pp. 142-157.

Stagpoole, V. and Funnell, R., 2001. Arc magmatism and hydrocarbon generation in the northern Taranaki Basin, New Zealand. *Petroleum Geoscience*. Vol. 7, pp.255-267.

Stagpoole, V., and Nicol, A., 2008. Regional structure and kinematic history of a large subduction back thrust: Taranaki Fault, New Zealand. *Journal of Geophysical research:* Solid Earth. Vol 113, Issue B1.

Seebeck, H., Nicol, A., Giba, M., Pettinga, J., Walsh, J.J., 2014. Geometry of the subducting Pacific plate since 20 Ma, Hikurangi margin, New Zealand. *J. Geol. Soc.* Vol. 171, pp. 131-143.

Seeman, U., and Scherer, M., 1984. Volcaniclastics as potential hydrocarbon reservoirs. *Clay Minerals*. Vol. 9, pp. 547-470.

Seubert, B., 2015. Volcaniclastic Petroleum Systems – Theory and Examples from Indonesia. *Indonesian Petroleum Systems – Thirty-Ninth Annual Conventional & Exhibition.*

Sharman, Glen. 2014. Provenance, paleogeography, and mass-movement of deep-water depositional systems in arc-adjacent basins: The Cretaceous-Paleogene California forearc and Upper Miocene Mohakatino Formation New Zealand. PhD Thesis, Stanford University.

Shumaker, Lauren., 2016. Sedimentology, Seismic Geomorphology, and Provenance Investigations of Deep-Water Deposits: Taranaki Basin, New Zealand. PhD thesis, Stanford University, United States of America.

Sruoga, P., Rubinstein, N. and Hinterwimmer, G., 2004. Porosity and permeability in volcanic rocks: a case study on the Serie Tobífera, South Patagonia, Argentina. *Journal of Volcanology and Geothermal Research*, Vol. 132, pp.31-43.

Sruoga, P. and Rubinstein, N., 2007. Processes controlling porosity and permeability in volcanic reservoirs from the Austral and Neuquén basins, Argentina. *AAPG bulletin*, Vol. *91,* pp.115-129.

Stricker, Stephan, 2016. Influence of fluid pressure on the diagenesis of clastic sediments. Durham thesis, Durham University.

Strogen, D., Seebeck, H., Nicol, A., and King, P., 2017. Two-phase Cretaceous-Paleocene rifting in the taranaki Basin region, New Zealand; implication for Gondwana break-up. *Journal of the Geological Society of London.* Vol. 174, pp. 929.

Sutherland, R., 1999. Basement geology and tectonic development of the greater New Zealand region: an interpretation from regional magnetic data. *Tectonophysics.* Vol. 308, pp. 341-362.

Taylor, T.R., Giles, M.R., Hathon, L.A., Diggs, T.N., Braunsdorf, N.R., Birbiglia, G.V., Kittridge, M.G., Macaulay, C.I. and Espejo, I.S., 2010. Sandstone diagenesis and reservoir quality prediction: Models, myths, and reality. *AAPG bulletin*. Vol. 94, pp.1093-1132.

Thomson, A., 1979, Preservation of porosity in the deep Woodbine/Tuscaloosa trend, Louisiana: *Journal of Petroleum Technology*, Vol. 34, pp. 396–403.

Utley, J., 1987. The Middle to Late Miocene Mohakatino Group in the coastal Herangi region, northern Taranaki, New Zealand: Punctuated sedimentation in continental slope-slope basin environments. Unpublished M.Sc. thesis, University of Waikato, Hamilton, New Zealand.

Webster, M., O'Conner, S., Pindar, B., and Swarbrick, R., 2011. Overpressures in the Taranaki Basin: Distribution, causes, and implications for exploration. *AAPG Bulletin.* Vol. 95, pp. 339-370.

Welton, J., E., 1984. SEM Petrology Atlas. 2nd edn, The American Association of Petroleum Geologists, USA. ISBN: 1-58861-214-7.

White, S., and Green, P., 1986. Tectonic development of the Alpine fault zone, New Zealand: A fission-track study. *Geology.* Vol. 14, pp. 124-127.

Winter, John D., 2001. *An Introduction to Igneous and Metamorphic Petrology*. Prentice Hall.

Worden, R.H. and Morad, S., 2000. *Quartz cementation in sandstones*. Wiley-Blackwell.

Zou, C., 2013. *Unconventional petroleum geology*. Elsevier.

Appendix I: Offshore Sample Data

Kora-1A

Sample	Depth	GS	Optical Porosity	IGV	COPL	CEPL	Q	F	L	C	SEM
	[m]	[mm]	[%]	[%]	[%]	[%]	[%]	[%]	[%]	[%]	Y/N
Kora-1A 1798 (1)	1798	1.03	18	35.667	6.735268	16.47708	9.667	37	4.667	17.667	Y
Kora-1A 1798 (2)	1798	1.03	12	30.333	13.87601	15.78911	9.33	34	6	18.333	N
Kora-1A 1827.5	1827	1.42	7.667	18.667	26.22921	8.114787	10.667	42	7	11	N
Kora-1A 1901.64	1901.64	1.2	0.33	15.663	28.85685	10.90838	13.333	50	4.667	15.333	Y
Well Average	-	1.17	9.49925	25.0825	19.9119	12.48033	10.74925	40.75	5.5835	15.58325	-

Kora-2

Sample	Depth	GS	Optical Porosity	IGV	COPL	CEPL	Q	F	L	C	SEM
	[m]	[mm]	[%]	[%]	[%]	[%]	[%]	[%]	[%]	[%]	Y/N
Kora-2 1323.1	1323.1	1.59	5.333	8	34.78261	6.956739	15	46.333	7.333	10.667	Y/N
Kora-2 1330.5	1330.5	1.5	10.667	8.8335	34.18635	4.606955	16	43.667	11.667	7	N
Well Average	-	1.545	8	8.41675	34.48584	5.787194	15.5	45	9.5	8.8335	

Kora-3

Sample	Depth	GS	Optical Porosity	IGV	COPL	CEPL	Q	F	L	C	SEM
	[m]	[mm]	[%]	[%]	[%]	[%]	[%]	[%]	[%]	[%]	Y/N
Kora-3 1808.55	1808.55	0.3515	3.667	5.3335	36.61961	4.436628	22	53	5.333	7	Y
Well Average	-	0.3515	3.667	5.3335	36.61961	4.436628	22	53	5.333	7	-

Kahawai-1

Sample	Depth	GS	Optical Porosity	IGV	COPL	CEPL	Q	F	L	C	SEM
	[m]	[mm]	[%]	[%]	[%]	[%]	[%]	[%]	[%]	[%]	Y/N
Kahawai-1 1928	1928	0.074	14.333	8.883	34.1506	2.194761	18.333	44.667	5.333	3.333	N
Kahawai-1 1934 (a)	1934	0.297	14.333	9.1665	33.94508	8.146554	12	47	4.333	12.333	N
Kahawai-1 1934 (b)	1934	0.215	26.667	16	28.57143	3.809286	12	37.667	4	5.333	N
Kahawai-1 1990.01	1990.01	0.42	11	5.6665	36.39587	0.211802	20.333	53	3	0.333	N
Kahawai-1 2049.9	2049.9	0.07	9.667	8.167	34.66401	4.35595	15.667	44.667	3.333	6.667	N
Well Average	-	0.2152	15.2	9.5766	33.64549	3.71572	15.6666	45.4002	3.9998	5.5998	-

Appendix II: Onshore Sample Data

Sample	Location Number	Location Name	Lithofacies	GS	Optical Porosity	IGV	COPL	CEPL	Q	F	L	AC	SEM
	-	-	-	[mm]	[%]	[%]	[%]	[%]	[%]	[%]	[%]	[%]	Y/N
1	1	Awakino Heads	Mgu Fm	-	1	-	-	-	0	27.33	2.67	23.33	-
2	2	Awakino Heads	Mhk Fm (Lf1a)	2.613	17.33	33.33	10.0045	14.39928	0	57	0.67	16	Y
3	3	Pahaoa Ridge	Mt Mgn Fm	-	19	-	-	-	0	41.333	0.333	37	-
4	3	Pahaoa Ridge	Mgu Fm	-	7.333	-	-	-	0	47.333	8.333	31.333	-
5	3	Pahaoa Ridge	Mga Fm	-	-	-	-	-	-	-	-	-	-
6	3	Pahaoa Ridge	Mhk Fm (Lf1a)	1.813	6.667	30.667	13.46112	20.76933	0	42	8.67	24	Y
7	4	Mokau River	Mhk Fm (Lf1a)	2.278	3.33	38.33	2.707962	34.05221	0	50.33	3	35	N
8	5	Piopio Station (South)	Mhk Fm (Lf2)	1.626	1	22	23.07692	16.15385	0	57.67	1.67	21	Y
9	6	Piopio Station (Central)	Mhk Fm (Lf1a)	1.3	2.33	34.33	8.634079	29.23709	0	50	2.67	32	N
10	7	Piopio Station (North)	Mhk Fm (Lf1a)	0.563	3	17.667	27.12521	10.68855	0	60.333	8	14.667	N
11	8	Waikawau Cliffs	Mhk Fm (Lf3a)	0.781	6.67	34	9.090909	24.84545	0	47	2.33	27.33	Y
12	9	Waikawau Cliffs	Mhk Fm (Lf1a)	1.344	9.67	22	23.07692	9.484615	0	59.33	5.33	12.33	N
13	9	Waikawau Cliffs	Mhk Fm (Lf1a)	-	-	-	-	-	-	-	-	-	N
14	8	Waikawau Cliffs	Mhk Fm (Lf1a)	1.188	3	22.333	22.74711	14.9353	0	64	3.333	19.333	N
15	8	Waikawau Cliffs	Mhk Fm (Lf1a)	0.359	1.67	13.34	30.7639	8.079852	0	58.33	9	11.67	N
16	10	Opito Point	Mhk Fm (Lf1a)	-	-	-	-	-	-	-	-	-	-

Appendix III: GNS Porosity and Permeability Data

Kora-1A		
Max Depth (m TVDSS)	Porosity (% Helium)	Permeability Kair (mD)
1856.14	13.4	0.221
1856.41	14.2	0.11
1856.65	16.2	0.137
1857.21	14.6	0.117
1857.61	17.7	0.164
1857.74	18.1	0.109
1858.12	18.5	0.128
1858.36	21.5	0.203
1858.70	21.3	0.231
1859.45	19.8	0.454
1865.90	27.3	121
1867.52	17.3	31.1
1869.00	23	251
1869.30	9.5	0.005
1869.80	33.1	838
1870.10	32.9	640
1870.90	31.4	857
1871.20	27.7	299
1875.06	26.9	31.6
1875.42	25.3	18.7
1875.50	28.7	435
1875.62	24.9	39.5
1876.33	24.7	38
1877.46	24.2	22.5
1877.83	23.6	30
1878.01	25	39.6
1878.43	24.9	19.8
1879.00	24.8	20.7
1879.40	24.8	9.81
1879.72	25.1	23.3
1880.10	24.9	17.7
1880.50	26	242
1882.50	25.6	147
1884.82	22.5	7.19
1885.02	24.8	16.5
1885.30	22.2	8.35
1885.40	24.9	120
1885.66	22.3	6.79
1885.86	21.5	5.05
1886.23	22.3	3.09
1886.70	24.5	4.33
1887.15	22.2	2.91
1888.40	26.9	150

1889.70	29.3	230
1891.27	16.9	0.236
1891.45	18.4	4.36
1891.90	17.4	3.77
1891.90	33.6	171
1892.88	17.9	2.98
1893.22	17.1	0.684
1893.40	17.4	2.09
1894.09	18.4	8.64
1895.69	17.5	14.1
1896.00	24.8	282
1896.40	18.1	4.23
1896.59	18.2	7.68
1897.42	17.4	8.79
1897.60	18	10.4
1900.92	22.2	8.55
1901.54	22.1	7.84
1902.30	21.7	3.52
1903.17	21.6	4.03
1903.90	21.3	1.74
1904.60	22.2	2.19
1905.00	20.4	1.02
1905.66	21.9	3.53
1906.37	23.7	3.23
1906.90	25.3	4.26
1908.12	21.4	0.28
1908.60	21.9	0.597
1909.15	21.6	0.279
1909.78	23.3	1.18
1910.58	23.9	0.966
1911.32	24	4.03
1911.90	21.3	1.35
1912.64	24.9	3.49
1913.23	19.4	1.45
1913.97	21.8	4.37
1914.34	19	2.45
1915.12	18.5	0.815
1915.81	21	3.55
1916.93	20.2	2.6
1922.10	24.3	287
1927.30	35.5	4970
1932.30	28.2	277
1936.20	22.2	5.8
1941.00	22.8	38
1946.70	28.3	123

1954.20	27.6	241
1957.20	26.5	95
1965.30	31.8	639
1968.12	18.7	0.452
1968.68	21.2	0.772
1969.25	17.6	0.887
1969.83	18.9	0.618
1970.50	17.4	0.508
1971.15	18.9	0.658
1971.70	19.9	0.823
1972.32	19.1	0.7
1972.68	22.6	1.37
1973.33	21.3	1.08
1973.93	20.9	0.489
1974.64	21.5	0.705
1975.15	18.9	0.568
1975.88	21.5	1.29
1976.30	21.6	0.381
1976.85	20.7	0.43
1977.45	16.3	0.588
1978.15	17.3	0.497
1978.85	16.8	0.435
1979.45	15.2	0.385
1980.38	14.5	0.342
1981.00	17.4	3.56
1981.75	17.2	3.17
1982.28	19.9	21.4
1982.70	18.8	13.6
1983.32	19.8	20.5
1984.03	18	8.47
1984.52	18.8	12.3
1985.52	14.7	3.84
1986.00	18.5	3.91

Kora-2		
Max Depth (m TVDSS)	Porosity (% Helium)	Permeability Kair (mD)
1357.60	18.1	0.16
1358.60	27	1.2
1359.10	29.8	1.3
1359.50	23	0.26
1360.00	23.4	0.29
1360.50	19.9	0.15
1361.00	23.9	0.3
1361.60	18.6	0.07
1362.00	20.5	0.2
1362.50	20	0.09
1363.00	21.4	0.92
1363.50	22	0.65
1364.00	16.7	0.05
1364.40	15.3	586
1364.90	16.8	1.02
1365.40	17.4	0.01
1366.00	16.9	0.06
1366.50	17.8	4.7
1391.00	15.9	0.15
1391.50	17.9	129
1391.90	14.3	0.06
1392.50	19.6	0.5
1393.00	19.1	2.3
1393.50	24.5	6.6
1394.00	30	7
1394.50	22.2	12
1395.10	20.6	27
1395.60	14.4	0.03
1396.00	13.6	0.04
1396.60	22.7	12
1399.50	23.4	4
1399.90	26.7	5.7
1400.50	27.7	9.4
1401.00	27.5	20
1401.50	25.2	0.42
1402.00	23.9	174
1402.50	26.9	191
1403.00	27.5	55
1403.50	21.3	0.08

Kora-3

Max Depth (m TVDSS)	Porosity (% Helium)	Permeability Kair (mD)
1851.10	4.9	0.029
1852.41	10.7	0.15
1853.50	4.9	0.24
1854.60	4.7	0.085
1855.60	11	0.1
1856.61	6.8	0.144
1858.00	6.4	0.013
1858.90	4.9	0.069
1861.00	8.8	0.048
1861.84	4.2	0.045
1863.51	2.7	0.019
1865.45	4.8	0.007
1867.50	2.8	0.013
1870.00	5.6	0.076
1871.50	25.1	0.314
1873.00	14.7	0.351
1873.96	3.5	0.004
1875.92	6	0.008
1877.38	9.8	0.175
1878.68	8.3	0.125
1880.22	25.8	25
1880.55	29	1190
1881.70	29.2	34
1882.20	38.4	18.5
1882.50	31.9	27
1883.30	27	28

Appendix IV: GNS Offshore Sample Data

GENERAL SAMPLE INFORMATION	**Well Name**		**Kora-1A**	**Kora-1A**	**Kora-2**	**Kora-2**	**Kora-3**
	Sample Depth (m AH)		1798.00	1901.64	1323.10	1330.50	1808.55
	Formation		Mhk Fm	Mhk Fm	Mhk Fm	Mhk Fm	Mhk Fm
CORE ANALYSIS	Measured Porosity (%)		31.4	18.8	20.6	26.9	29
	Permeability (mD)		1032.00	13.6	27.00	191	1190
TEXTURE	Principal Mean Grain Size (phi)		-0.041	nd	-0.672	nd	nd
	Principal Grain Size (class)		vcL	nd	vcU	nd	nd
	Sorting (phi std dev)		0.689	nd	0.851	nd	nd
	Sorting (class)		MG	nd	MP	nd	nd
SUMMARY TOTALS (%)	**Total Grains**		64.5	72.6	62.9	68.5	79.0
	Total Matrix		22.0	16.0	17.7	11.3	5.5
	Rock Flour						
	Total Authigenic Clays		5.0	2.6	8.6	11.7	11.0
	Total Cement		5.0	8.6	10.5	7.3	4.0
	Total Hydrocarbons						
	Total Macropores (> 16um)		3.0	Tr		1.0	
	Counted Micropores (< 16um)						
MACROPORES (%)	**Total Macropores (> 16um)**		3.0	Tr		1.0	
	Intergranular Macropores		1.0				
	Grain Dissolution (or Mouldic/intraparticle) Macropores		1.0	Tr		0.7	
	Grain Fracture Pores						
	Total Hybrid Macropores						
	Hybrid Macropores	IG	0.5				
		GD	0.5			0.3	
COUNTED MICROPORES (%)	**Counted Micropores (< 16um)**						
	Intergranular Micropores						
	Other Counted Micropores						
MATRIX (%)	**Total Matrix**		22.0	16.0	17.7	11.3	5.5
	Detrital Clay						

	Pseudomatrix						
	Carbonate Mud						
	Recrystallised tuffaceous matrix		22.0	16.0	17.7	11.3	5.5
GRAINS (%)	**Total Grains**		64.5	72.6	62.9	68.5	79.0
GRAINS (%)	**Quartz**	**Total Quartz**	6.0	9.3	12.7	5.3	16.5
		Monocrystalline Quartz	5.0	6.7	9.0	4.3	12.0
		Polycrystalline Quartz		0.3	0.7	0.7	3.0
		Inclusion-rich Quartz	1.0	2.3	3.0	0.3	1.5
	Feldspar	**Total Feldspar**	36.0	39.0	23.3	31.7	39.5
		K-feldspar				0.7	
		Plagioclase	36.0	39.0	23.3	31.0	39.5
	Lithic Fragments	**Lithic Fragments**	5.0	1.6	2.9	1.9	3.5
		Metamorphic					2.5
		Plutonics: Q-Fdsp		0.7	1.0	0.3	0.5
		Plutonics: Q-deg			0.3		
		Plutonics: Other		0.3			
		Plutonics: Fdsp-Fdsp	0.5	0.3		0.3	0.5
		Volcanic	4.5	0.3	1.3	1.3	
		Chert					
		Sandstone/Siltstone					
		Siltstone/Mudstone			0.3		
	Mica	**Total Mica**	Tr	0.7	0.3	0.3	0.5
		Muscovite		0.7		0.3	0.5
		Biotite	Tr	Tr	0.3	Tr	
		Chlorite					
	Other Grains	**Total Other Grains**	17.5	22.0	23.7	29.3	19.0
		Degraded Grains	8.0	9.3	12.7	11.3	18.0
		Total Heavy Minerals	9.5	12.7	11.0	18.0	1.0
		Organic/Plant Material					

		Mudstone Intraclasts/Clay Pellets					
		Carbonate Intraclasts					
		Skeletal Carbonate					
		Phosphate					
		Glauconite					
AUTHIGENIC CLAYS (%)	**Total Authigenic Clay**		5.0	2.6	8.6	11.7	11.0
	Chlorite	Total Chlorite	1.0	Tr		0.7	
		Intergranular	0.5	Tr		0.7	
		Grain Coating/Pore Lining	0.5				
		Secondary Pore Fill/Grain Replacement	Tr	Tr		Tr	
AUTHIGENIC CLAYS (%)	Kaolinite/Dickite	Total Kaolinite/Dickite			0.6	0.3	3.0
		Intergranular					
		Secondary Pore Fill/Grain Replacement			0.3	0.3	3.0
		Kaolinitised Mica			0.3		
	Fine Kaolin	Total Fine Kaolin					
		Intergranular					
		Secondary Pore Fill/Grain Replacement					
	Slightly Illitised Kaolinite/Chlorite	Total Illitised Kaolinite					
		Intergranular					
		Secondary Pore Fill/Grain Replacement					
	Coarsely Crystalline Illite	Total Coarse Illite					
		Intergranular					
		Secondary Pore Fill/Grain Replacement					
	Mixed Layer/Indeterminate Clay	Total Mixed Layer/Indeterminate Clay	4.0	2.6	8.0	10.7	8.0
		Intergranular	2.0	1.3	1.0	1.0	0.5
		Grain Coating/Pore Lining					0.5
		Grain Replacement	2.0	1.3	7.0	9.7	7.0
OTHER AUTHIGENIC MINERALS (%)	**Total Cement**		5.0	8.6	10.5	7.3	4.0
	Quartz	**Total Quartz Overgrowths**					

		Intergranular					
		Secondary Pore Fill					
	Feldspar	**Total Feldspar Overgrowths**					
		Intergranular					
		Secondary Pore Fill					
	Calcite	**Total Calcite**			4.3	1.0	
		Intergranular				Tr	
		Grain Replacement/Secondary Pore Fill			4.3	1.0	
		Fracture Fill					
	Dolomite/Ankerite	**Total Dolomite**			2.3	1.0	0.5
		Intergranular			0.3	0.3	
		Grain Replacement/Secondary Pore Fill			2.0	0.7	0.5
		Fracture Fill					
OTHER AUTHIGENIC MINERALS (%)	**Siderite**	**Total Siderite**			0.3		1.0
		Intergranular/Grain Coating					
		Grain Replacement			0.3		1.0
	Authigenic Opaques	**Total Authigenic Opaques**	4.0	5.3	3.6	5.3	2.5
		Intergranular/Grain Coating	0.5		0.3	0.3	
		Grain Replacement	3.5	5.3	3.3	5.0	2.5
	Fe Oxide/Hydroxide	**Total Oxide/Hydroxide**	1.0	Tr		Tr	
		Grain Coating/Pore Lining					
		Grain/Mud Replacement	1.0	Tr		Tr	
	Dawsonite	**Total Dawsonite**		3.3			
		Grain Coating/Pore Lining					
		Grain/Mud Replacement		3.3			
RESIDUAL HYDROCARBON (%)		**Total Residual Hydrocarbons**					
		Grain Coating/Pore Lining					
		Clay Staining					